Synthesis of Novel Polyol Structures for Polyurethanes and other Thermosets

Zur Erlangung des akademischen Grades eines

DOKTORS DER NATURWISSENSCHAFTEN

(Dr. rer. nat.)

von der KIT-Fakultät für Chemie und Biowissenschaften

des Karlsruher Instituts für Technologie (KIT)

genehmigte

DISSERTATION

von

M. Sc. Michael Rhein

aus Eberbach

1. Referent: Prof. Dr. Michael A. R. Meier
2. Referent: Prof. Dr. Joachim Podlech

Tag der mündlichen Prüfung: 28.04.2022

Für meine Eltern,

Klaus und Helga Rhein.

„Ich lege mich jetzt erstmal drei Tage in die Eistonne“

P. Mertesacker

Declaration of Authorship

Die vorliegende Arbeit wurde von Dezember 2018 bis März 2022 unter Anleitung von Prof. Dr. Michael A. R. Meier am Karlsruher Institut für Technologie (KIT) angefertigt.

Hiermit versichere ich, dass ich die Arbeit selbständig angefertigt, nur die angegebenen Quellen und Hilfsmittel benutzt und mich keiner unzulässigen Hilfe Dritter bedient habe. Insbesondere habe ich wörtlich oder sinngemäß aus anderen Werken übernommene Inhalte als solche kenntlich gemacht. Die Satzung des Karlsruher Instituts für Technologie (KIT) zur Sicherung wissenschaftlicher Praxis habe ich beachtet. Des Weiteren erkläre ich, dass ich mich derzeit in keinem laufenden Promotionsverfahren befinde und auch keine vorausgegangenen Promotionsversuche unternommen habe. Die elektronische Version der Arbeit stimmt mit der schriftlichen Version überein und die Primärdaten sind gemäß Abs. A (6) der Regeln zur Sicherung guter wissenschaftlicher Praxis des KIT beim Institut abgegeben und archiviert.

Karlsruhe, 16.03.2021

_____

Michael Rhein

I. Danksagung

Ich möchte mich an dieser Stelle bei all denjenigen Personen bedanken, welche mir diesen Weg ermöglicht und einen wesentlichen Beitrag zum Gelingen dieser Arbeit geleistet haben.

Zunächst möchte ich mich bei dir, Mike, für die Aufnahme in deinen Arbeitskreis, dein entgegengebrachtes Vertrauen und deine Unterstützung während meiner ganzen Promotion bedanken. Danke für deine immer offenstehende Bürotür, welche auch symbolisch für unser sehr angenehmes Arbeitsverhältnis steht. Du warst immer verständnisvoll und verfügbar für fachliche, sowie überfachliche Diskussionen.

Another huge thank you belongs to the whole AK Meier group for the perfect working environment in- and outside the laboratory over all these years.

Des Weiteren möchte ich mich bei meinen Firmenpartnern, BASF SE und puren gmbh für die gute Zusammenarbeit und Finanzierung bedanken. Ein Dankeschön gebührt auch dem Karlsruhe House of Young Scientists (KHYS) für die Förderung meines dreimonatigen Auslandsaufenthaltes an der KTH in Stockholm.

I would like to thank you, Mats, for giving me the opportunity to spent three month in your working group. Thanks for all the scientific discussions and suggestions as well as the general information you shared about Stockholm and Sweden. Additionally, I would like to thank the whole FPT department for welcoming me so warmly. Thanks Arne, Dan and Jamie for the nice after-work hours in the kitchen.

A big thank you belongs to a very amazing person: Luli. Thanks for your help before, during and after my stay at KTH. A great friendship arose from the very first days and I am looking forward to visiting you soon in Stockholm.

Vielen Dank an Anja, Clara, Frank, Jonas, Luis, Pete und Roman für das Korrekturlesen. Weiterhin möchte ich mich bei Rebecca Seim, Benjamin Felker, Anika Göcke und Cindy Konstandin für die Unterstützung im Labor bedanken.

Ein besonderer Dank gebührt dir, Niggisch. Wir kennen uns seit den ersten Semestern und haben uns - auf mir unerklärliche Weise - für einige Jahre aus den Augen verloren, bis wir letztlich beide zeitgleich zur Masterarbeit im Arbeitskreis gelandet sind. Über die letzten Jahre hat sich unsere Freundschaft durch unzählige Laborstunden, Fußballsessions sowie „Feierabend-Mopeten“ zusammengeschweißt und für mich zu etwas wirklich Besonderem

gemacht. Maxi, ein riesiges Dankeschön geht natürlich auch an dich. Du hast mich während meiner Masterarbeit direkt in die Laborfamilie aufgenommen, wodurch sich eine riesige Freundschaft entwickelt hat. Ich danke euch beiden auch für die zahlreichen „The Crew“-Abende. Weiterhin möchte ich mich bei dir, Hauser, für die gemeinsame Studien- und WG-Zeit bedanken, welche durch etliche „Criminal Minds“-Folgen geprägt war. Es bedeutet mir sehr viel Freunde wie euch zu haben, auf die man sich immer verlassen kann!

Mein größter Dank gebührt meiner Familie. Papa, Mama danke, dass ihr den Grundbaustein dafür gelegt habt, wo ich heute stehen darf. Danke für eure bedingungslose Liebe und Unterstützung, dass ihr immer an mich geglaubt habt und immer für mich da seid! Vielen Dank auch an die vielen überfachlichen Diskussionen am Küchentisch durch dein unbegrenztes medizinisches, biologisches und agrarwissenschaftliches Fachwissen, Mama. Verena dir möchte ich für die ganzen pharmazeutischen Fachbegriffe danken, die du mir bei sehr fragwürdigen Debatten beigebracht hast. Ich bin unfassbar froh einen großen Bruder wie dich, Frank, haben zu dürfen. Danke vor allem für die vielen gemeinsamen Sporteinheiten, Mittags- und Kaffeepausen. Line, ich danke dir von ganzem Herzen für deine Liebe und Unterstützung, dass du stets Verständnis für mich zeigst und mir insbesondere in den letzten Wochen immer wieder aufs Neue den Rücken gestärkt hast.

II. Abstract

In recent decades, the synthesis of monomers and polymers from renewable resources as well as the development of sustainable chemical processes has become of great interest as a result of a generally increasing environmental awareness and the depletion of fossil resources. Especially, the synthesis of aliphatic polyether polyols, which have versatile applications depending on their structure and molecular weight, is typically limited to the ring-opening polymerization of petroleum based oxiranes, oxetanes and tetrahydrofuran. Polyols are most often used for the synthesis of polyurethanes representing an important class of polymers due to their wide range of thermal and mechanical properties. The properties of the polyurethane depend on the structure, functionality and molecular weight of the polyol. Therefore, the development of new synthesis strategies towards renewable polyols is mandatory for “maintaining the needs of the present generation without compromising the ability of future generations to meet their own needs”.

In this work, the synthesis of a broad spectrum of different aliphatic polyether polyol structures was enabled by the gallium(III) bromide catalyzed reduction of aliphatic polyesters with silanes. Since many polyesters can be obtained by polycondensation of biobased dicarboxylic acids and diols, this reaction system leads to renewable polyether polyols. The influence of four polyester structures and two reducing agents, namely 1,1,3,3-tetramethyldisiloxane and triethylsilane, on the reaction system were studied. Subsequently, the reaction conditions were optimized and scaled-up to 60 g polyester. The investigated reduction of aliphatic polyesters was further transferred to cellulose acetate, enabling a novel synthesis route towards the widely applied ethyl cellulose.

Moreover, fully biobased aromatic polyester polyols obtained from the sugar based 2,5-furandicarboxylic acid were synthesized. The reaction conditions were optimized and scaled-up to 100 g dicarboxylic acid. Consecutively, the aromatic polyester polyols were applied in polyurethane rigid foams. The thermal and mechanical properties of these foams were compared to those synthesized by a commercially used aromatic polyester polyols based on the petroleum based phthalic acid.

Furthermore, renewable aliphatic polyester polyols were synthesized from different biobased dicarboxylic acids and the end groups were modified into amine groups. Half of the obtained polyesters were reduced to the corresponding polyether diamines *via* the gallium bromide catalyzed reaction. Finally, these diamine prepolymers were reacted with two different epoxides, based on linseed oil and lignin, into fully biobased thermosets. Thereby, the

influence of the different polymeric backbones on the thermal and mechanical properties were analyzed.

III. Zusammenfassung

In den letzten Jahrzehnten gewann die Herstellung von Monomeren und Polymeren aus nachwachsenden Rohstoffen sowie die Entwicklung nachhaltiger chemischer Prozesse großes Interesse. Gründe hierfür sind das allgemein zunehmende Umweltbewusstsein und die Erschöpfung fossiler Ressourcen. Insbesondere die Synthese von aliphatischen Polyether-Polyolen, die abhängig von ihrer Struktur und Molekulargewicht vielseitig einsetzbar sind, beschränkt sich typischerweise auf die ringöffnende Polymerisation von erdölbasierten Oxiranen, Oxetanen und Tetrahydrofuran. Meistens werden Polyole für die Synthese von Polyurethanen verwendet. Polyurethane stellen eine wichtige Klasse von Polymeren dar, da sie ein breites Spektrum an thermischen und mechanischen Eigenschaften aufweisen, welche wiederum von der Struktur, Funktionalität und dem Molekulargewicht des Polyols abhängen. Daher ist die Entwicklung neuer Synthesestrategien für erneuerbare Polyole notwendig, um den Bedarf der heutigen, aber auch der zukünftigen Generationen zu decken.

In dieser Arbeit wurden verschiedene aliphatische Polyether-Polyole durch die katalytische Reduktion von Polyestern hergestellt. Hierfür wurde als Katalysator Gallium(III)-bromid und als Reduktionsmittel verschiedene Silane verwendet. Viele Polyester-Polyole sind durch Polykondensation von biobasierten Dicarbonsäuren und Diolen zugänglich, weshalb dieses Reaktionssystem zu erneuerbaren Polyether-Polyolen führt. Daher wurde der Einfluss von vier Polyesterstrukturen und den zwei Reduktionsmitteln, 1,1,3,3-Tetramethyldisiloxan und Triethylsilan, auf das Reaktionssystem untersucht. Die Reaktionsbedingungen wurden optimiert und die Synthese konnte im Labormaßstab auf 60 g Polyester skaliert werden. Die untersuchte Reduktion von aliphatischen Polyestern wurde auf Celluloseacetat übertragen, was einen neuen Syntheseweg zur weit verbreiteten Ethylcellulose ermöglicht.

Weiterhin wurden vollständig biobasierte aromatische Polyester-Polyole aus der zuckerbasierten 2,5-Furandicarbonsäure synthetisiert. Die nachfolgende Optimierung der Reaktionsbedingungen ermöglichte ein Scale-up auf bis zu 100 g Dicarbonsäure. Anschließend wurden die aromatischen Polyester-Polyole in der Herstellung von Polyurethane Hartschäume eingesetzt. Die thermischen und mechanischen Eigenschaften dieser Schaumstoffe wurden mit denen eines handelsüblichen Schaumstoffes auf der Basis von erdölbasiertem aromatischem Polyester-Polyol verglichen.

Außerdem wurden erneuerbare aliphatische Polyester-Polyole aus verschiedenen biobasierten Dicarbonsäuren synthetisiert und die Endgruppen zu Aminogruppen modifiziert. Die Hälfte der erhaltenen Polyester wurde durch die mit Gallium(III)-bromid katalysierte Reaktion zu den entsprechenden Polyether-Diaminen reduziert. Schließlich wurden diese

Zusammenfassung

Polyester- und Polyether-Diamine mit zwei verschiedenen Epoxiden auf der Basis von Leinöl und Lignin zu vollständig biobasierten Duroplasten umgesetzt. Dabei wurde der Einfluss der verschiedenen polymeren Grundgerüsten auf die thermischen und mechanischen Eigenschaften analysiert.

Table of Content

I. Danksagung I

II. Abstract III

III. Zusammenfassung V

1 Introduction 1

2 Theoretical Background 3

2.1 Green Chemistry 4

2.2 Renewable Resources 8

2.2.1 Cellulose 9

2.2.2 Lignin 12

2.3 Polyurethanes 14

2.3.1 Synthesis 15

2.3.2 Application 18

2.3.3 Recycling 23

2.4 Polyols 25

2.4.1 Aliphatic Polyether Polyols 26

2.4.2 Biobased Polyols 32

2.4.3 Poly(ethylene furanoate) PEF 36

2.5 Reduction of Esters to Ethers 40

3 Aim of this work 45

4 Results und Discussion 47

4.1 Catalytic Reduction of Esters 48

4.1.1 Synthesis of Aliphatic Polyether Polyols *via* $GaBr_3$ catalyzed reduction of Polyesters 49

4.1.2 Catalytic Reduction of Cellulose Acetate 64

4.2 Synthesis and Application of Fully Biobased Aromatic Polyester Polyols 71

4.2.1 Synthesis of 2,5-Furandicarboxylic Acid Based Aromatic Polyester Polyols 72

4.2.2 Application of 2,5-Furandicarboxylic Acid Based Aromatic Polyester Polyols for Polyisocyanurate Rigid Foams 90

4.3 Synthesis and Modification of Aliphatic Polyether and Polyester Polyols for Application in Thermosets 94

4.3.1 Synthesis and Characterization of Biobased Aliphatic Polyether and Polyester Diamines 95

4.3.2 Application of Biobased Aliphatic Polyether and Polyester Diamines in Thermosets 111

5 Conclusion and Outlook 125

6 Experimental Section 129

6.1 Materials 129

6.2 Characterization Methods 130

6.3 Experimental Procedure 134

6.3.1 Experimental Procedures and Supporting Information of Chapter 4.1 134

6.3.2 Experimental Procedures and Supporting Information of Chapter 4.2 146

6.3.3 Experimental Procedures and Supporting Information of Chapter 4.3 152

7 Appendix 167

7.1 Abbreviations 167

7.2 List of Figures 172

7.3 List of Schemes 175

7.4 List of Tables 178

7.5 List of Equations 180

7.6 List of Publications 181

8 Bibliography 183

1 Introduction

Nowadays, in times of depleting fossil resources and a generally increasing environmental awareness, the development of sustainable chemical processes as well as the synthesis of monomers and polymers from renewable materials have become of great interest. Since the beginning of the industrial revolution in the 19th century and the introduction of steam power, generated from coal, several new fabrication technologies and chemical production pathways have been developed. The continuous advancement of science and technology led to an increase of the world population from 2.5 billion people in 1950 to the present 7.9 billion, besides a steadily improved standard of living.[1] As a result, the exploitation of fossil resources continues to increase annually and these resources will be depleted in the next decades without a significant change of their exploitation.[2] Furthermore, the oil price has risen disturbingly in the last twenty years and will lead to supply bottlenecks in the future.[3] The main problem is the dependence on fossil resources, since 80% of the worlds global energy mix is fossil based and they are the basis of important platform chemicals used for daily life commodities such as polymeric materials.[4-5] The worldwide plastic production is steadily increasing and has climbed from 348 million tons (2017) to 359 (2018) accompanied by drastic environmental pollution.[6] Especially, the micro plastic pollution of natural ecosystems and the oceans destroys habitats of many living beings. In combination with the climate change caused by high emissions of greenhouse gases, the use of fossil resources is a serious problem forcing mankind to find solutions in terms of a more reasonable use of these raw materials in combination with sustainable alternatives. Currently, less than 1% of the produced plastics are so-called bioplastics.[7] According to the latest market data compiled by European Bioplastics, the production will further increase from 2.11 million tons to approximately 2.97 million tons in 2025.[7] Compared to the rising general demand of plastics, it is crucial to accelerate this growth by the investigation of more sustainable alternatives.

Sustainability was first introduced and defined in the “Brundtland Report” by the United Nations World Commission on Environment and Development (WCED) in 1987 as “development that meets the needs of the present without compromising the ability of future generations to meet their own needs”.[8] Therefore, a major challenge to ensure the availability of fossil resources and to minimize the production of greenhouse gases,

is the sustainable use of biomass as declared by the UN World Summit on Sustainable Development in 2002.[9] In a world without fossil fuels, biomass plays a unique role as the only renewable carbon source for the production of all carbon products, such as hydrocarbon fuels, organic bulk and fine chemicals.[10-11] In this scenario, biomass and other renewable energy sources such as wind, water or solar power, can also provide a significant amount of energy for the modern society. For instance, in Germany already 17% of the total primary energy consumption was covered by bio-energy in 2020.[12] Moreover, renewable resources can partly substitute fossil based fuels, since already 6.5% of the used fuels in Germany 2020 were biofuels, besides a generally increasing amount of electrical means of transport.[13] However, it also has to be mentioned that the industrial use of biomass may compete with the food supply.[14] Therefore, novel processes in the agricultural und forestry section showed that biomass can be obtained in large amounts as a byproduct within this sector.[15],[16] Moreover, currently only 3% of the estimated global production of biomass (10^{11} tons *p.a.*), which is divided into 60% terrestrial and 40% aquatic biomass, are cultivated.[17]

A closer look into the chemical and pharmaceutical industry shows that the production of organic chemicals in Germany still strongly depends on fossil resources. In 2019, the most used resource with 13.3 million tons (69%) was still crude oil, whereas only 2.6 million tons (13%) of the applied raw materials were renewable.[18] These data reveal possible ways to substitute fossil with renewable materials, but people all over the world have the obligation to contribute to a more sustainable development.

2 Theoretical Background

This chapter summarizes recent investigations in academia and industry and gives an overview of the state of the art as well as fundamental insights into different topics relevant for this work. Chapter 2.1 summarizes the history and basics of sustainability and Green Chemistry, including guidelines and tools for assessing the sustainability of different chemical procedures. In Chapter 2.2, the use of renewable resources in the German chemical industry is briefly discussed. Moreover, two important renewables, namely cellulose and lignin, are described in more detail. Subsequently, chapter 2.3 covers a large and versatile class of polymers: polyurethanes. Herein, the synthesis strategies, applications and recycling of polyurethanes are discussed in detail. Chapter 2.4 deals with polyols: first, different synthesis methods of industrially relevant aliphatic polyether polyols are described, followed by the state of the art of biobased polyols and the possible substitution of their fossil based counterparts. Finally, poly(ethylene furanoate) is highlighted as an important polyol, showing a high potential in the near future. In chapter 2.5, a short summary of relevant reduction methods for (poly)esters to (poly)ethers is given.

2.1 Green Chemistry

The concept of Green Chemistry emerged in the 1990s and is defined as the “design of chemical products and processes to reduce or eliminate the use and generation of hazardous substrates”.[19] Since the definition of sustainability in the Brundtland Report in 1987,[8] many improvements in the chemical industry and our modern society were based on this concept of sustainability. Green Chemistry explains how chemistry and chemical engineering developments should be realized to protect and benefit the economy, people, and the planet. The main goal of Green Chemistry is to address substitutions of hazardous substances and those associated with global issues such as climate change, energy and food production, availability of a safe an adequate water supply and the presence of toxic sub stances in the environment.[20] Moreover, Green Chemistry includes life cycle considerations, such as the use of more sustainable or renewable feedstocks and a designation for end of life or the final disposition of the product. A general guideline for the design of sustainable chemical processes, the so-called Twelve Principles of Green Chemistry, was introduced in 1998 by Anastas and Warner (**Table 1**).[21]

Table 1 The Twelve Principles of Green Chemistry.[21]

Entry	Principle	Description
1	Prevention	It is better to prevent waste than to treat or clean up waste after it is formed.
2	Atom Economy	Synthetic methods should be designed to maximize the incorporation of all materials used in the process into the final product.
3	Less Hazardous Chemical Syntheses	Whenever practicable, synthetic methodologies should be designed to use and generate substances that pose little or no toxicity to human health and the environment.
4	Designing Safer Chemicals	Chemical products should be designed to preserve efficacy of the function while reducing toxicity.

5	Safer Solvents and Auxiliaries	The use of auxiliary substances (*e.g.* solvents, separation agents, etc.) should be made unnecessary whenever possible and, when used, innocuous.
6	Design for Energy Efficiency	Energy requirements of chemical processes should be recognized for their environmental and economic impacts and should be minimized. If possible, synthetic methods should be conducted at ambient temperature and pressure.
7	Use of Renewable Feedstocks	A raw material or feedstock should be renewable rather than depleting whenever technically and economically practicable.
8	Reduce Derivatives	Unnecessary derivatization (use of blocking groups, protection/ deprotection, temporary modification of physical/chemical processes) should be minimized or avoided if possible, because such steps require additional reagents and can generate waste.
9	Catalysis	Catalytic reagents (as selective as possible) are superior to stoichiometric reagents.
10	Design of Degradation	Chemical products should be designed so that at the end of their function they break down into innocuous degradation products and do not persist in the environment.
11	Real-Time Analysis for Pollution Prevention	Analytical methodologies need to be further developed to allow for real-time, in-process monitoring and control prior to the formation of hazardous substances.
12	Inherently Safer Chemistry for Accident Prevention	Substances and the form of a substance used in a chemical process should be chosen to minimize the potential for chemical accidents, including release, explosions, and fires.

These principles enable a fundamental understanding of the foundation of the field as well as the variety of strategies available to advance Green Chemistry goals. There are many ways to reduce or eliminate hazardous substances, to minimize their impact on living beings as well as on the environment, and to maximize the energy efficiency. Especially, the first principle of preventing waste is important for chemical processes, not only on an industrial scale. Recent research, reported in numerous scientific journals, focused on novel catalysts[22] and biocatalysts,[23] exploitation of renewable feedstock from biomass[24] as well as the application of sustainable solvents.[25] After 20 years, the Twelve Principles were reviewed and reevaluated by Anastas *et. al*.[26] A broad spectrum of research and review articles not only from academia, but also of improved industrial processes, were reported by the authors. Moreover, they outlined that the Twelve Principles are an interconnected system, since these principles enable a design synergy and should not be seen as twelve independent factors.

Green Chemistry is generally based on the comparison of different processes. Therefore, an evaluation tool is necessary that quantifies processes in terms of sustainability and environmental compatibility. The first method is the atom economy, which was introduced in 1991 by Trost and can be determined according to **Equation 1**.[27]

Equation 1 Definition of the atom economy according to Trost.[27]

$$\text{Atom economy } [\%] = \frac{\text{Molecular weight of the desired product}}{\sum \text{Melocular weight of all reactants}} * 100\%$$

This concept is useful for a quick comparison and evaluation of different synthesis possibilities, bearing some downsides. First, the atom economy assumes a theoretical yield of 100% besides a stoichiometric use of all reactants and only considers the molecular weight. Moreover, no auxiliary reagents and solvents are included in this calculation.

Another evaluation method introduced by Sheldon, the E-Factor (environmental factor), can overcome these disadvantages as shown in **Equation 2**.[28-29] This definition considers the masses of the involved compounds instead of their molecular weights and is further taking the waste and side products into account. Herein, waste is defined as everything besides the desired products excluding water, since otherwise a meaningful comparison of the processes becomes difficult.

Equation 2 Definition of the E-Factor according to Sheldon.[29]

$$\text{E} - \text{Factor} = \frac{\text{mass of waste}}{\text{mass of desired prodcuts}}$$

The E-Factor offers a simple tool for measuring the efficiency of chemical reactions and processes, but strongly depends on the boundary conditions, *e.g.* if the synthesis of starting materials or auxiliars are also included in the calculation. Some typical E-Factors for different industry segments are displayed in **Table 2**.

Table 2 Typical E-Factors for different industry segments.[28]

Industry segment	**Production [tons per year]**	**E-Factor [kg waste/ kg product)**
Oil refining	10^6-10^8	< 0.1
Bulk chemicals	10^4-10^6	< 1-5
Fine chemicals	10^2-10^4	5-50
Pharmaceuticals	10-10^3	25-100

2.2 Renewable Resources

The finiteness and increasing depletion of fossil resources will eventually force the chemical industry to resort to renewable resources for our daily life commodities. However, 87% of all resources used by the chemical industry in Germany 2019 were still fossil-based, showing the strong dependence on theses raw materials (**Figure 1**). In recent years, numerous reports were based on the development of new technologies and synthesis routes in academia, but the transfer towards industry remains slow. Only 2.6 million of the total 19.4 million tons of used raw materials in chemical industry (Germany 2019) were based on renewable resources, as depicted in **Figure 1**.[18]

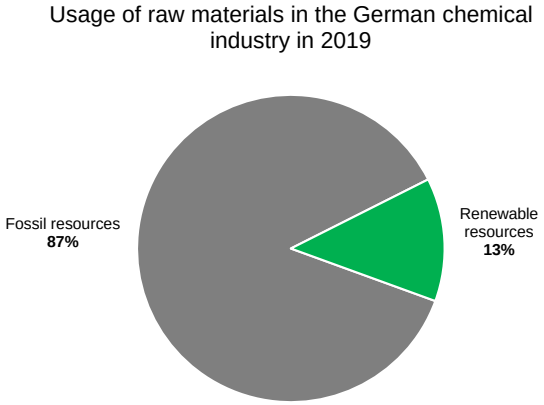

Figure 1 Usage of raw materials in the German chemical industry in 2019.[18]

The main part of biobased resources consisted of fats and oils, followed by dissolving pulp and starch (**Figure 2**). The use of dissolving pulp is challenging due to the processing and separation of cellulose, hemicellulose, and lignin. Nonetheless, two renewable resources, cellulose and lignin, which offer a great potential for the chemical industry, are briefly introduced in the following subchapter.[30]

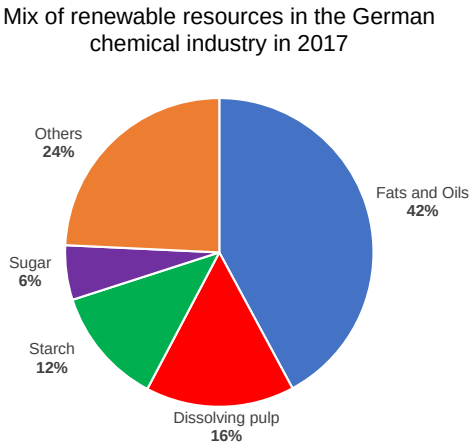

Figure 2 Share of different renewable resources used in the German chemical industry in 2017.[18]

2.2.1 Cellulose

Cellulose is the most abundant biopolymer on earth, with interesting characteristics such as biocompatibility, biodegradability, low cost, as well as high thermal and mechanical stability.[31] It was first isolated by Payen in 1837, who was able to determine the molecular formular of $C_6H_{10}O_5$ *via* elemental analysis.[32] Cellulose is a linear homopolymer of β-1,4 linked D-glucopyranose units, also known as anhydroglucose units (AGU). Cellobiose, the repeating unit of cellulose, is comprised of two AGU, which are connected through a glycosidic bond (**Scheme 1**). The AGU consists of one primary hydroxyl group at the C6 position and two secondary hydroxyl groups at C2 and C3 (**Scheme 1**).[33] An important characteristic in cellulose chemistry is the so-called degree of substitution (DS), which describes the average number of modified hydroxyl groups per AGU. Hence, the DS can range from zero to three. The degree of polymerization (DP) can vary from 150 to 10000 and depends on the source and treatment methods of cellulose.[31]

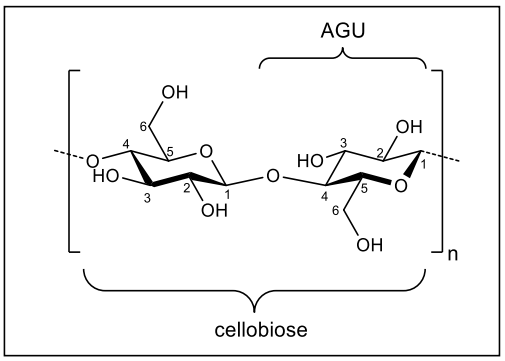

Scheme 1 General cellulose structure with cellobiose as repeating unit.

For instance, ethyl cellulose (EC) is an important cellulose derivative, bearing ethoxy groups instead of hydroxy groups, with applications ranging from organic soluble thermoplastic products to water soluble food additives.[34-35] EC is used in the pharmaceutical industry as a thickening agent in creams, lotions, and gels or for microencapsulation of drugs due to its versatile properties.[36-41] For instance, it is applied as a binder in tablets or as a tablet coating material for taste masking and controlled release, whereby no additional release modifier is required.[42-45] Furthermore, EC can be processed by hot-melt extrusion into dosage forms for model drugs, such as diclofenac sodium, diltiazem, ibuprofen or guaifenesin.[46-49] Another application is as a polymeric gelator for oleogels enabling the reduction of undesired saturated and trans fatty acids, while maintaining the fat crystal network for many examples.[50-55] A summary of all oil-structuring systems with EC was reviewed in 2016 by Davidovich-Pinhas, Barbut and Marangoni.[56] The thermal and mechanical properties of the EC oleogel and the

influence of different parameters were widely studied.[57-58] EC is tasteless, odorless, non-caloric, biocompatible and inert to alkalis and diluted acids.[59] With a DS above 2.5, EC becomes much less thermoplastic and is not useful as a material in plastics. The flexibility is retained even when unplasticized until -40 °C and 15 wt% plasticizer are sufficient for most applications.[60-61] The solubility depends on the DS, whereby EC is water soluble for a DS of 1.0-1.5 and becomes soluble in organic solvents for a DS of 2.2-2.6.[60-61] The viscosities are influenced by the solvent, the DS and the molecular weight.[36, 62] EC is further applied in heat-sealing adhesives, coatings (paper, cloth, leather), cheap casting plastics, and electrical insulators.[60]

EC is typically synthesized from alkali cellulose, obtained from wood or cotton linters in concentrations of 50 wt% NaOH or higher, and ethyl chloride under high pressure (820-965 kPa) and elevated temperatures (90-150 °C) in solvents such as benzene or toluene (**Scheme 2**).[34, 60-61] Subsequent, the product is spin dried to 50-60% water content and homogenized in a screw extender. Different viscosity grades are obtained, depending on the molecular weight of the cellulose backbone.[36, 62] Several other synthesis strategies of cellulose ethers were investigated, however none of these were suitable for EC.[63-65]

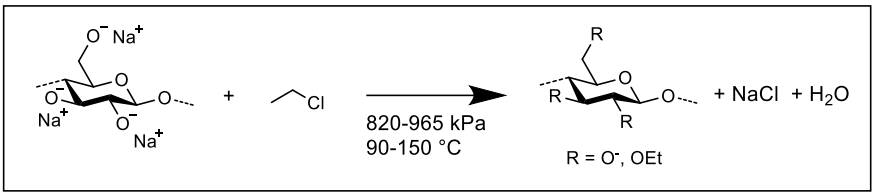

Scheme 2 Typical synthesis of EC from alkali cellulose and ethyl chloride.

In this work, a new synthesis route towards ethyl cellulose was investigated through the catalytic reduction of cellulose acetate (CA) as discussed in chapter 4.1.1. CA is industrially synthesized in a heterogeneous mixture of cellulose using an excess of acetic anhydride in acetic acid with sulfuric acid as a catalyst. This leads to cellulose triacetate with a DS of 2.8-3.0.[66-67] CA with lower DS is obtained *via* partial hydrolysis of cellulose triacetate.[68] Many new synthesis strategies based on a homogenous functionalization using ionic liquids were investigated, showing better control of the DS compared to the heterogeneous acetylation, but never overcoming the lab-scale due to their high cost and poor recyclability.[69-70] Another synthesis approach from Meier *et al.* focused on a homogenous, switchable solvent system of CO_2 and an organic superbase, 1,8-diazabicyclo[5.4.0]undec-7-ene (DBU), in DMSO (**Scheme 3**).[71] Thereby, cellulose was converted into cellulose carbonate, which was either modified *in situ* with vinyl acetate into CA or regenerated to cellulose by releasing the CO_2 pressure. This enabled

a more sustainable synthesis of CA since all reagents and solvents were recycled and reused, while vinyl acetate is less toxic than acetic anhydride.

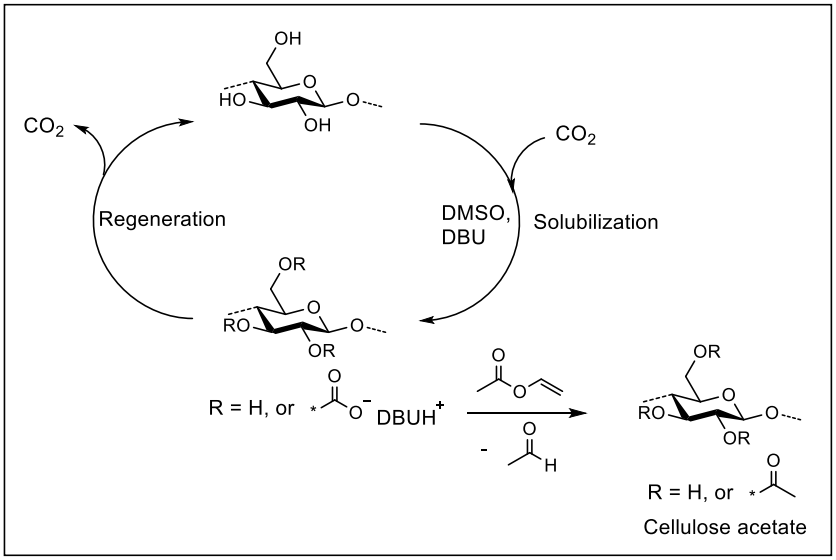

Scheme 3 Synthesis of CA using a CO_2 switchable solvent system of DMSO and DBU.

CA is used for many applications such as coatings, membranous filters, textiles, high absorbency products, thermoplastics, sheets for food packaging, cosmetics, pharmaceuticals, cigarette filters, or hypoallergenic surgical products.[66, 68, 72-75]

Other industrially used cellulose derivates, which are not relevant for this work, include for instance methyl cellulose (MC) and carboxymethyl cellulose (CMC). The application of MC depends on the degree of methylation and ranges from thickener in food industry, to admixture of concrete in civil constructions to pharmaceutical industry.[76-77] CMC is an anionic, water-soluble polysaccharide which is prepared by the reaction of monochloroacetic acid and alkali cellulose and applied in detergent, pharmaceutical, paint, paper and textile industry.[78] Nevertheless, also other cellulose ether and ester derivates are widely used, especially in the food and pharmaceutical industry.[79]

2.2.2 Lignin

Lignin is a highly abundant biopolymer, which is incorporated in the cell walls of plants and wood, and is the only renewable resource with an aromatic structure available on a large scale.[80] Together with cellulose and hemicellulose, lignin is one of the major components of lignocellulosic biomass. In plant cell walls, lignin acts as a binder of the lignocellulosic matrix between hemicellulose and cellulose.[81] Lignin consists of three main building blocks: coumaryl alcohol, coniferyl alcohol and sinapyl alcohol (**Scheme 4**). The phenylpropanes are typically connected *via* β-O-4, β-5 and β-β' bonds.[82]

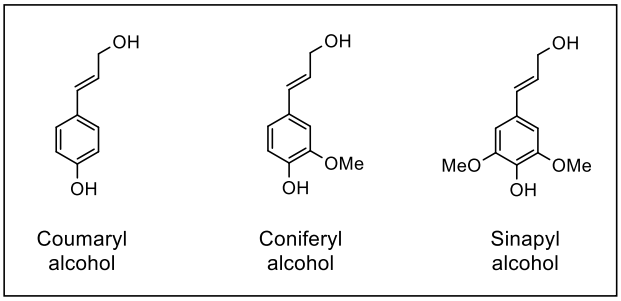

Scheme 4 Phenylpropane building blocks of lignin.

The lignin content and the ratio of its building blocks varies for different wood types as summarized in **Table 3**.[83] Softwood has the highest lignin content of 27-33 wt% and mainly consists of coniferyl alcohol, while hardwood contains the same amount of sinapyl and coniferyl alcohol within lignin and 18-25 wt% lignin in the plant. In both wood types, no coumaryl alcohol is present. Grasses have small amounts of coumaryl alcohol while showing similar lignin contents to hardwood besides a higher ratio of coniferyl to sinapyl alcohol.

Table 3 Overview of different wood types, their lignin content, and the ratio of building blocks.[83]

Wood type	Lignin/ wt%	Coumaryl alcohol [%]	Coniferyl alcohol [%]	Sinapyl alcohol [%]
Softwood	27-33	0	90-95	5-10
Hardwood	18-25	0	50	50
Grasses	17-24	5	70-75	20-25

Lignin is mainly obtained as a byproduct of the pulp and paper industry. In 2010, only 2% of the annually produced 50 million tons of technical lignin was fabricated into products while 98% was burned as low-value fuel.[84] In general, four different pulping processes are applied on an industrial scale as reviewed by Sels and coworkers.[85] The

most prominent process with 90% usage is the so-called kraft pulping.[86] In this process, lignocellulosic biomass is reacted with white liquor, an aqueous solution of sodium hydroxide and sodium sulfide, at 170°C, whereby depolymerization of the lignin structure occurs through cleavage of the ether linkages.[87] Subsequently, cellulose is removed followed by incineration of the remaining pulp mixture, also known as black liquor, to generate energy for the pulp mill. Kraft lignin can be separated from the black liquor by precipitation through acidification and it bears thiol groups due to the incorporated sulfur, which can be easily oxidized under these conditions.[83, 88] The second most applied process is called sulfite pulping.[88-89] Herein, lignocellulosic biomass is treated with sulfites to generate oligomerized lignin which has a higher sulfur content than kraft lignin.[83, 89] Depending on the counter ion of the sulfite, which is mostly sodium, ammonium, magnesium or calcium, either alkaline, neutral or acidic condition are required.[83, 90-91] Lignin can finally be separated *via* ultrafiltration, extraction or precipitation.[88] Another process is the soda pulping, which is similar to the kraft pulping, but without sodium sulfite.[83, 91-92] This process is less efficient and competing side reactions occur to a larger extent, however the main advantage is access to sulfur-free lignin. Moreover, this process is historically used for non-woody biomass such as straw, miscanthus, sugar cane, and more.[83, 88, 91] At latest, organosolv pulping is a common method, whereby biomass is treated with organic solvents in combination with mineral acids and/or water instead of pure aqueous media.[93-94] Hereby, lignin is extracted more effectively and can be separated from hemicellulose by precipitation from pulping liquor yielding organosolv lignin.[95-96] Different solvents for the extraction such as alcohols,[97] polyols,[98] cyclic ethers,[99] organic acids,[96] and ketones[100] were investigated. The organosolv process is a comparatively eco-friendly alternative to the kraft process.[15] Many other pulping processes have been developed resulting in lignin with different structures and properties.[85]

Lignin is mostly used for the production of polymeric materials. For instance, it can be directly used for polyurethane-, polyester-, phenolic-, or epoxy resins due to the hydroxyl groups.[101] However, a selective and controlled reaction is challenging because of the different reactivities of the present hydroxyl groups. Hence, the selection of the wood type and the pulping process plays a key role for the application of lignin in polymeric materials.

2.3 Polyurethanes

Polyurethanes (PUs) represent an important class of polymers, covering 7.9% of the plastics demand for Europe in 2018, due to their versatile thermal and mechanical properties.[6] Industrial PUs is synthesized by the polyaddition of polyisocyanates and polyols as first introduced by Otto Bayer *et al.* (**Scheme 5**).[102]

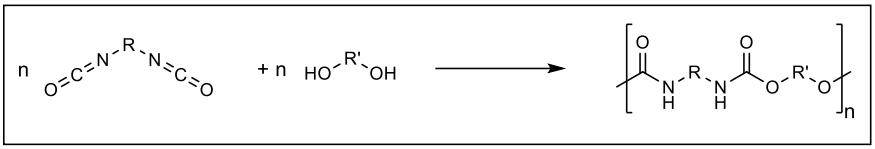

Scheme 5 Synthesis of polyurethanes *via* polyaddition of polyisocyanate and polyol.

The chemical structure and morphology are tuned by the functionality of polyol and polyisocyanate with variation possibilities from showing thermoplastic or elastomeric to thermoset behavior. Instead of polyols, also other polynucleophiles can be used in the polyaddition reaction with polyisocyanates, which are all included in the class of PU.[103-105] This enables a wide range of applications in construction, automotive, textiles, biomedicine and many other industry sectors.[106-107] The synthesis and application of different polyurethanes was reviewed by Akindoyo *et al.*[108] and Engels *et al*.[109] In the following subchapters, the synthesis (chapter 2.3.1), application (chapter 2.3.2) and recycling methods (chapter 2.3.3) of PUs are described in detail.

2.3.1 Synthesis

Nowadays, polyurethanes can be synthesized in several ways.[110] However, all industrial PUs are produced *via* polyaddition of polyisocyanates with macro-polyols as already described above (**Scheme 5**). Thereby, a wide range of additives including flame retardants, pigments, crosslinkers, fillers, blowing agents and surfactants can be used for the synthesis, while the reaction is catalyzed by a broad spectrum of suitable organo- and metal catalysts, controlling selectivity and reactivity.[111] Thus, tailored product properties can be adjusted by the structure and functionality of polyol and polyisocyanate, the catalyst and additives. In general, the reaction between isocyanate and polyol is slow at room temperature due to the phase incompatibility. Here, the less dense polyol phase is often polar, whereas the denser polyisocyanate phase is typically non-polar. Hence, the mixing equipment plays and important role for the synthesis of PUs.[112]

The most common polyisocyanates for industrial synthesis are summarized in **Scheme 6** and can be divided into aromatic and aliphatic isocyanates. The two most important aromatic polyisocyanates are methylene diphenyl diisocyanate (MDI) and toluene diisocyanate (TDI), which are used as isomeric mixtures on industrial scale. The main representatives of aliphatic and cycloaliphatic polyisocyanates are hexamethylene diisocyanate (HDI), isophorone diisocyanate (IPDI), and hydrogenated methylene diphenyl diisocyanate (H_{12}MDI).[113] In general, aromatic isocyanates are more reactive than their aliphatic counterparts.[114-115]

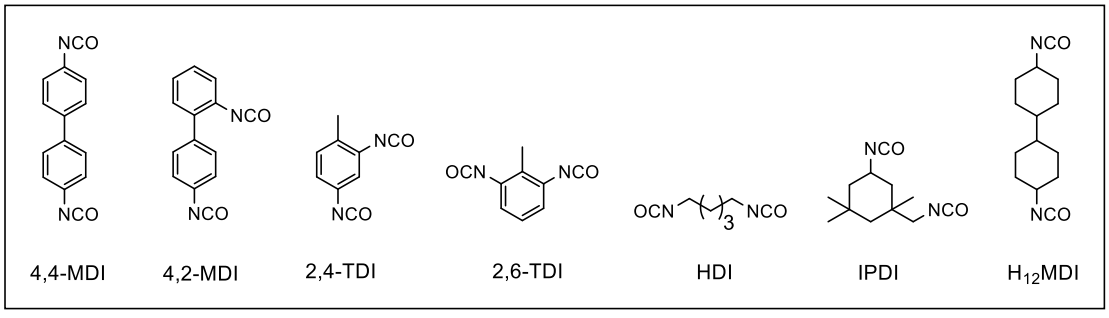

Scheme 6 Most common polyisocyanates for industrial applications.

Besides different polyisocyanates, various polyols are applied for PU synthesis, which is discussed in chapter 2.4.1. Most industrially used polyols are polyethers based on the ring-opening polymerization (ROP) of propylene oxide (PO) or ethylene oxide (PO). The properties of the resulting PU are adjusted by the functionality, molecular weight, and chemical structure of the polyol. For instance, polyether polyols with a functionality of two to six and a molecular weight up to 18 kg/mol are used for flexible PUs, while

polyester polyols with two to three functional groups and molecular weights below 2 kg/mol are mainly applied in rigid PU foams (**Scheme 7**).[116-117]

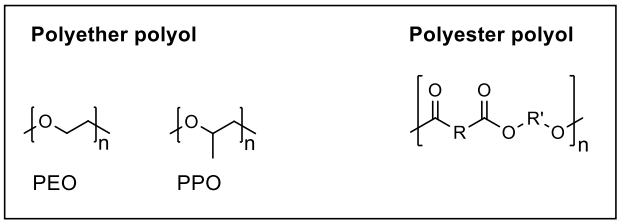

Scheme 7 Structure of most common polyether polyols poly(ethylene oxide) PEO and poly(propylene oxide) PPO as well as the general structure of a polyester polyol.

To obtain branching within the polyurethane structure, a higher functionality than two is required, which can be achieved either by polyols obtained from higher functional alcohols or by polyisocyanate (**Scheme 8**). For instance, commercially MDI is obtained as a mixture of higher oligomers. Without a purification step, this mixture is used to obtain branched polyurethanes (**Scheme 8a**).[118-119] Moreover, TDI is reacted with trimethylolpropane leading to an isomeric mixture with a high ratio of trifunctional isocyanate under certain conditions (**Scheme 8b**).[120] Another approach is the trimerization of isocyanates into so-called isocyanurates, controlled by specific catalysts and reaction conditions (**Scheme 8c**).[121-123] Multifunctional isocyanates are produced through a secondary reaction of diisocyanate with the urea group of a PU prepolymer, synthesized with an excess of diisocyanate compared to polyol (**Scheme 8d**).

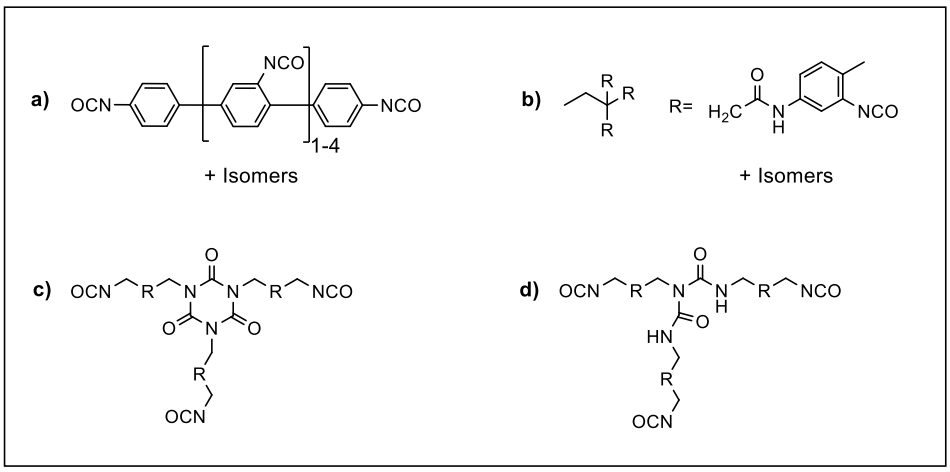

Scheme 8 Different ways to obtain polyfunctional isocyanates.

Nowadays, new synthesis strategies in terms of sustainability are of great interest, since industrial PUs are still obtained from petroleum-based polyols and isocyanates synthesized from highly toxic phosgene and the corresponding amines. Various biobased alternatives for the polyol component were already investigated and are discussed in chapter 2.4.2. A promising synthesis route is based on the synthesis of

non-isocyanate polyurethanes (NIPU) *via* either transurethanization of biobased carbamates and diols or the polyaddition of *bis*-cyclic carbonates with diamines (**Scheme 9**). The sustainable carbamate synthesis was reviewed by Meier[124] and Rokicki *et al.*,[125] while Cramail and coworkers reported a detailed overview of different sustainable synthesis routes towards *bis*-cyclic carbonates.[126]

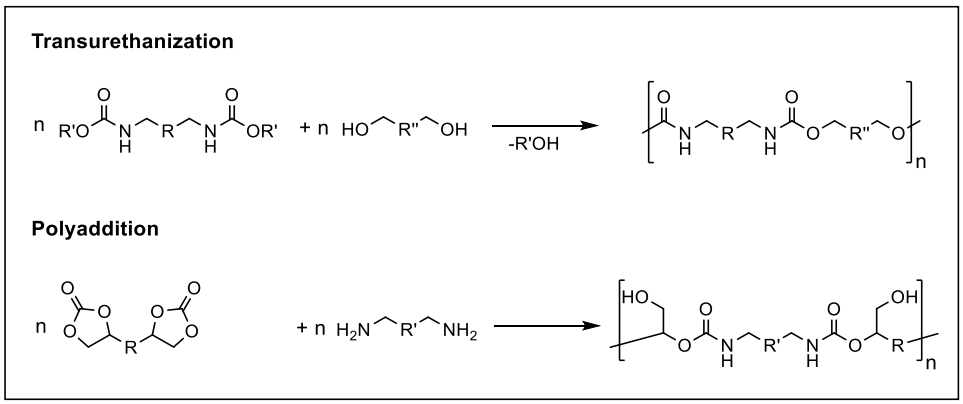

Scheme 9 Different synthesis routes of non-isocyanate polyurethane (NIPU).

2.3.2 Application

PUs can either be classified by their morphological, chemical, and physical properties into thermoplastic, elastomers, and thermosets, or by their application. In this work, the latter classification is chosen, since the physical and chemical properties of PU for certain applications often overlap with the material scientific definition of thermoplastics, elastomers, and thermosets due to their versatile tuned properties (**Figure 3**). Consecutively, the main applications are briefly summarized.

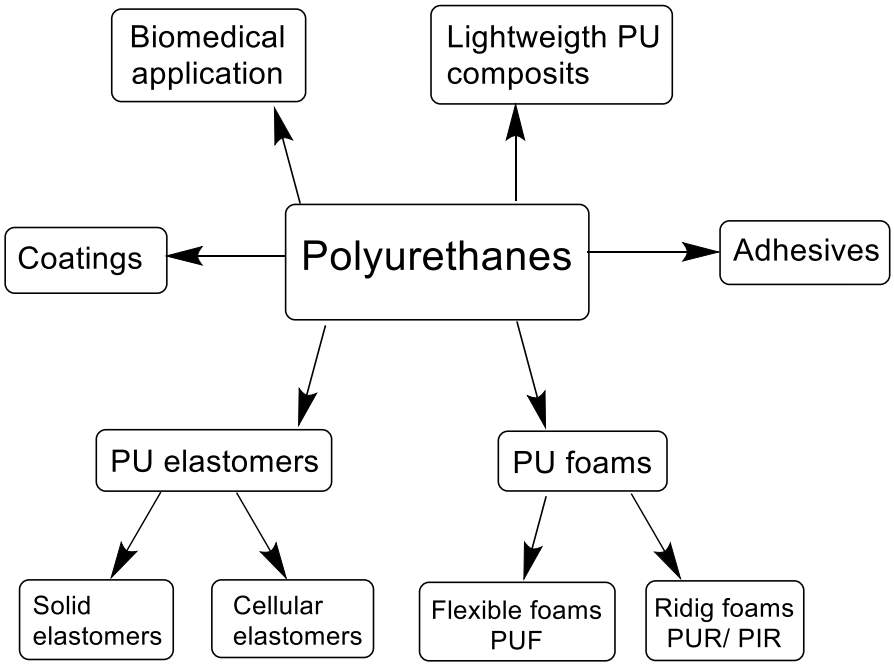

Figure 3 Classification of polyurethanes by their applications.

Polyurethane foams

PU foams represent, with 66% of all PUs, the by far largest application field. The foams can be divided into flexible polyurethane foams (PUF), used for furniture cushions, mattresses, molded foam seats in cars and liquid metal filters, and rigid foams (PUR), applied in construction, refrigeration and the piping/tubing industry.[127] The foaming of PU is typically based on the exothermic reaction of water and isocyanate forming CO_2 as blowing agent and an amine, subsequently reacting into an urea (**Scheme 10**). This reaction is crucial for obtaining the foam structure while it is also increasing the reaction speed due to the released reaction heat.

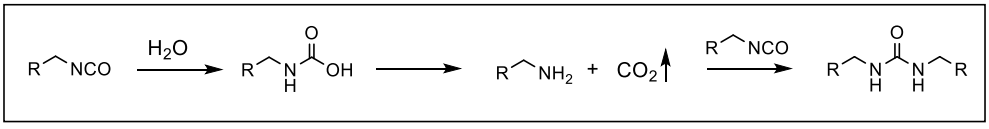

Scheme 10 Formation of CO_2 as blowing agent through the reaction of isocyanate and H_2O.

Flexible PU foams (PUF) consists of hard and soft segments, leading to the desired flexibility. The synthesis is based on two main steps: blowing and gelling. First, the blowing step is performed as described in **Scheme 10** through the reaction of isocyanate and water. Subsequently, gelling occurs as a result of the crosslinking reaction of polyol and polyisocyanate.[128] For flexible PU foams, chain extender can be added to increase the flexibility, however, the tensile and tear properties of the PUF are decreased.[129] This class of PU is widely used because of the variety of foam types, long term use characteristics, breathability, and efficient manufacturing methods. Thus, no other material can compete with the wide property range of flexible foams. PUF are further divided into conventional flexible foams (55% of all PUF), highly resilient (HR) flexible foams, covering 35% of all PUF, and others.[130-131] In conventional flexible foams, the functionality of polyols is typically three, while having a low molecular weight and a high poly (propylene oxide) PPO content, which results in mainly secondary OH-groups. The polyol is mostly crosslinked by TDI as isocyanate component. The physical properties of the conventional PUF can be optimized by the addition of copolyols. In contrast, high resilient flexible foams exhibit higher crosslinking, while the polyol chain length is higher than in conventional PUF since polyols with higher molecular weights (up to 12 kg/mol) are used. Typical polyether polyols have a functionality between three and six and are based on PPO, modified with PEO end groups, which leads to primary OH-groups showing a higher reactivity. TDI and MDI are mostly used for this subclass of PUF.[109]

Polyurethane rigid foams (PUR) are strongly crosslinked closed-pore materials typically produced by MDI and mostly polyester polyols with low molecular weights.[132] The mechanical and thermal properties of the rigid foam are adjusted by the number of adhesives, whereby the density is controlled by the addition of an organic blowing agent, mostly a mixture of pentane, and the water content. Moreover, the properties of the rigid foams are adjusted by the stoichiometric ratio of polyisocyanate and polyol as well as the type of catalyst, leading to different contents of polyisocyanurate (PIR) structures in the final foam. Thus, PIR foams are a subclass of rigid foams, whereby during the PUR synthesis polyol and polyisocyanate is added in equivalent amounts. In general, PIR shows better fire retardation behavior than PUR and thus, less flame retardants are required.[133] The thermal conductivity of PU foams is determined by the density and hence, by the blowing agent and the resulting pore size, since pentane is incorporated in the pores having a lower thermal conductivity than air.[134] PU rigid foams play a key role for a variety of applications in construction, refrigeration, and the piping/tubing industry, because they offer a unique combination of material and processing characteristics. In the construction industry, mostly PIR rigid foams are applied due to the above mentioned better thermal and mechanical properties. Besides PIR, also PU

sandwich-structure composites, a stiff metal skin filled with rigid PU foams connected through strong self-adhesive properties, are used within this sector.[135] Technical insulation represents another large field of application, where mainly PUR is used for thermal insulation in 95% of all refrigerators. The sufficient stiffness in conjunction with minimum weight and lower thermal conductivity reduces the energy consumption significantly.[136] Another industrial application of PU rigid foams is in insulating pipes, such as oil and gas pipelines or in chemical plants covering hot and cold media. Insulating from -196 °C to 150 °C poses high demands on the material properties and therefore, most properties are adjusted to individual needs.[137]

PU Elastomers

Another large application field of PUs are elastomeric materials, used in applications depending on good dynamics and low wear. Such elastomers, have a good long-term dynamic performance, high rebound resilience, low dynamic stiffening, high abrasion and tear propagation resistance, and excellent resistance to fats and oils.[138] For elastomeric PU mostly poly(tetrahydrofuran) is used as polyol compound, while the polyisocyanates are manufactured as prepolymers to reduce the formed heat during processing.[139] These prepolymers are obtained by the polyaddition of polyol using an excess of polyisocyanate and a subsequent distillation of unreacted isocyanate (**Scheme 11**). Moreover, often chain extenders are added for increased flexibility of the final PU elastomer.

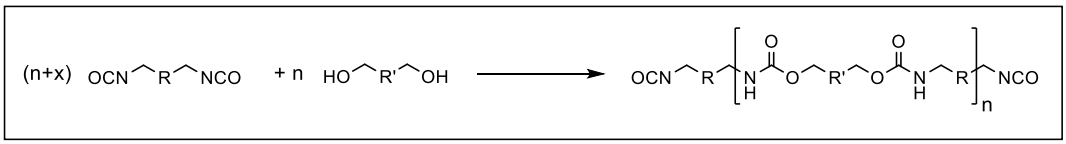

Scheme 11 Synthesis of polyisocyanate prepolymers.

PU elastomers can be separated into two groups, cellular (40%) and solid PU elastomers (60%). Cellular elastomers have a higher raw density (300-700 kg/m^3) than typical PU foams and are mostly applied in footwear (shoe soles), integral foam as well as vibration and noise damping. Solid elastomers typically have densities of 1200 kg/m^3 and are used in synthetic leather, elastomeric fibers, spray elastomers and thermoplastic PU (TPU). TPU are manufactured using numerous processing methods such as extrusion, blow, compression and injection molding.[140] TPU have several applications in automotive, footwear and construction.[141-142] Another notable field is their off-shore and underwater application due to their stability against hydrolysis, mostly based on extensively branched polyether polyol systems and MDI.[143]

Lightweight construction with fiber composites based on PU

The use of fiber composite materials has grown steadily in recent years due to industrial sectors such as aviation, wind power, construction, and transportation. They are based on a plastic matrix, mostly unsaturated polyester, vinyl ester or epoxy thermosets, combined with glass fibers. The matrix material determines the functional properties (e.g. thermal resistance) and processing conditions of the composite. Therefore, composites based on a PU matrix offer a broad spectrum of possible applications due to their versatile properties such as high chemical resistance and flexibility. For instance, these composites are applied in vehicle and sanitary products.[109, 144]

Biomedical application

Another application field of PU is in bio- and blood compatible materials such as catheters or artificial hearts, because of their extensive structure and property diversity.[145] In such PU materials, no solvent, monomers, chain extender or other additive, which may cause toxic effects in the body, should remain.[146] Mostly polyether polyols are used within this application field, since they offer a higher hydrolytical stability than polyester polyols. For instance, TPUs show biomedical application possibilities, such as drug release in vaginal rings due to water-insolubility and non-ionic properties.[147] Moreover, the hemocompatibility of the material can be tuned by surface modification *via* hydrophilic/ hydrophobic balance or by the addition of ionic groups in the polymer backbone leading to so-called polyurethane ionomers (PUI).[148] The ionic groups are introduced by either using an ionic diol or ionic groups containing diisocyanate.[148-149]

Coatings[150-152]

PUs are often used in high-quality coatings for automotive fibers, metal, wood, plastic, and textile coatings because of their diverse formulation options, fast drying and variable properties.[153] In general, for every coating material, the properties are adjusted by the structure of the polyol and the polyisocyanate. Automotive finishes exist of four layers.[154] The first layer is the electrodeposition coat, which protects the metal from corrosion and is mostly made of epoxy resins, followed by the primer surfacer to smoothen the surface and protecting the underlying layer against stone chipping. Here, PU are applied because of their high impact resistance, particularly at low temperatures. The next layer is called base coat, which is mainly used for color and pigments for special effects followed by the high-quality clear coat, covered by PU for high brilliance and resistance in general. PUs are also used in metal coatings in combination with epoxy primer, offering better corrosion protection, higher surface quality and weather resistance. These

coatings are used in vehicles, railways, airplanes as well as in construction and agricultural machinery. Moreover, PUs are used for wood coatings in parkette flooring, windows, doors, and other constructions, since they offer high surface quality and a great variability. For this application, PUs are mostly combined with acrylates to combine air drying with UV-curing, also known as dual-cure system.[155] Another notable application of PU coatings is for plastics, because in many cases the plastic itself is not resistant against weather, scratching, cleaning agents and solvents. Here, the unique combination of flexibility and surface tension of the PU coating is the ideal solution for these top coatings. Finally, also textile coatings such as clothing, technical textile and synthetic leather are covered by PU to tune the physical and haptic properties besides an increasing wearing comfort and target functions of the product.

Adhesives

PU adhesives are used in a range of demanding applications, since they show a high performance. Polyisocyanate, polyol and manufacturing technology are adjusted to the needed properties, processing requirements and cost considerations. PU adhesives enable a broad field of application because they can be supplied in numerous ways, such as in solvents or as waterborne dispersion.[156-157] Some application examples are as footwear adhesives for bonding of soles, where PU adhesives show a high bond strength besides the ability to bond to a variety of different substrates.[158] Other applications are as flexible packaging adhesive, in construction and furniture applications acting as barrier membrane and in transportation enabling the use of lightweight metals, plastics and composites.[159]

2.3.3 Recycling

The steadily increasing demand of PUs in our daily life requires a significant amount of resources for their synthesis. Therefore, recovery and recycling processes are necessary, to "enable needs of the present generation without compromising the ability of future generations to meet their own needs". Common recycling methods for PUs can be categorized into four main classes: mechanical recycling, chemical recycling, thermochemical recycling, and energy recovery (**Figure 4**).

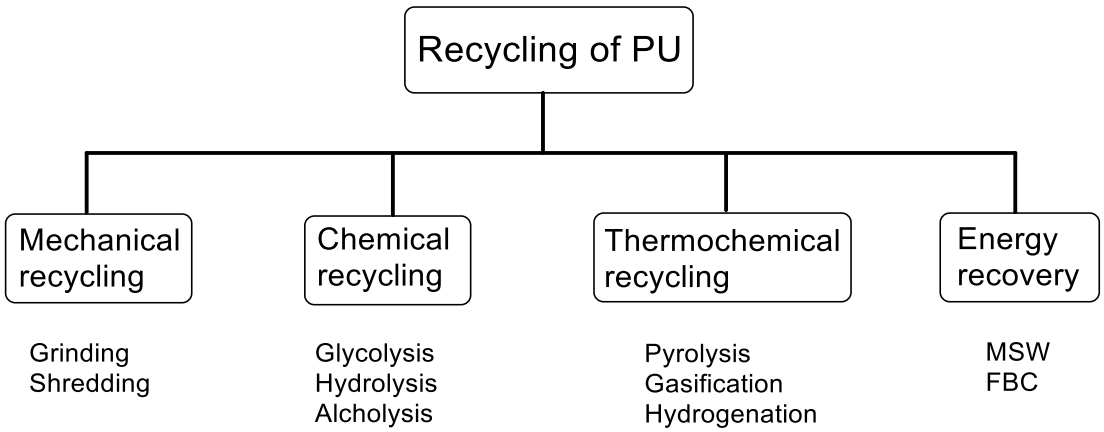

Figure 4 Overview of different recycling methods for PU.

Mechanical recycling are physical treatments such as grinding or shredding of PU into powder. The obtained PU powder can either be used directly as filling for pillows, toys, etc. (primary mechanical recycling) or can subsequently be processed in different ways.[160] For instance, new polyol may be added to obtain new PU, used in automotive seating.[161] Moreover, PU powder can be mixed with either binders and pressed or adhesives and cured under heat and pressure.[162] Another possibility is the compression molding at 180 °C and 350 bar, which leads to new PU for automotive applications.[163] However, this method is not suitable for colored polymers. Further processing methods of the PU powder, for instance injection molding, are feasible and allow the recycling of crosslinked PU leading to thermo shaped products.[163]

Chemical recycling can be performed in many ways. By far the most widely used method for PU recycling is glycolysis, whereby grinded PU, mainly flexible and rigid PU foams, are mixed with an excess of high boiling glycol and catalyst at temperatures between 180 and 220 °C (**Scheme 12a**). Usually, diethylene glycol (DEG) is used with diethanol amine (DEA) as coreagent. The temperature must be adjusted, since too low temperatures result in low catalytic activity, while high temperatures lead to high undesired side reactions. The obtained polyols can be used for new PU materials.[164-166] Another method is based on the hydrolysis of PU into polyols and amines under

superheated steam and oxygen-free conditions (**Scheme 12b**). The obtained polyols can either be used as effective fuels or for polyurethane synthesis, if the reaction conditions are adjusted.[167-169] However, this method suffers from unfavorable economics and lack of markets for the recycled products.[170] A further chemical recycling method is the alcoholysis, whereby alcohols are mixed with PU at elevated temperatures to produce the original polyol and urethane products, which must be separated afterwards (**Scheme 12c**).[163, 171]

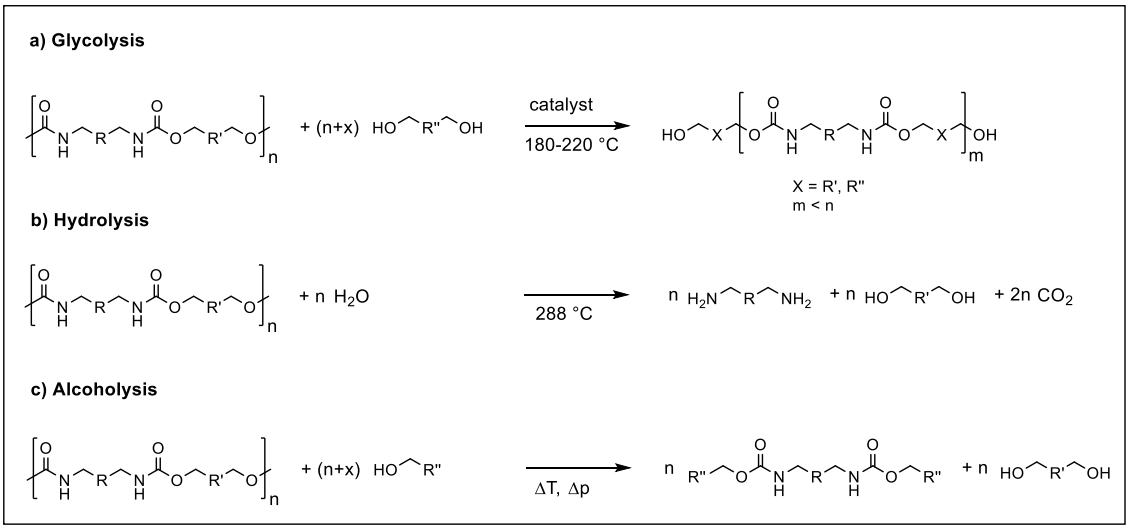

Scheme 12 Chemical recycling methods for PU.

Thermochemical recycling can be performed by pyrolysis, gasification, or hydrogenation. In the pyrolysis method, PU is heated under oxygen-free conditions leading to gas, oil, and char.[172-173] Several conditions and a broad range of PU materials were tested followed by a processes optimization to obtain a high oil content, for further fuel applications.[174-175] In gasification, the waste derived fuels from heated plastics are treated with air and oxygen at 1200-1500 °C and 20-80 bar leading to the formation of hydrogen and carbon monoxide (syngas), used for the synthesis of methanol or alcohols *via* hydroformylation.[176-177] Another thermochemical recycling method is the hydrogenation, which is basically a pyrolysis under hydrogen atmosphere forming gaseous and liquid products. However, for this method a high purity of gases and oils from the pyrolysis is required, leading to high costs.[178]

The energy recovery process is mostly applied, if no other recycling methods are suitable because of either lack of application of the obtained products or processing issues. Hereby, PU is fully burned to generate the maximum amount of electricity by different combustion strategies, such as municipal solid waste (MSW) or fluidized bed combustion (FBC).[179] Different combustion methods were investigated in various studies.[171]

2.4 Polyols

As already described in chapter 2.3, the properties of PUs strongly depend on the functionality, structure, and molecular weight of the polyols. Polyols can be classified according to the chemical structure of their polymeric backbone into four main groups: aliphatic polyether polyols, aliphatic polyester polyols, aromatic polyether polyols and aromatic polyester polyols. The largest group of polyols are the aliphatic polyether polyols which are mainly applied in elastomeric and thermoplastic PU and is described in subchapter 2.4.1. However, most polyols used in the chemical industry are still petroleum based. With regard to sustainability, besides the broad application spectrum of PU, various synthesis routes using renewable starting materials were investigated and already applied on an industrial scale. An overview of different biobased polyols is given in subchapter 2.4.2. In subchapter 2.4.3, the potential of a promising aromatic polyester polyol, poly(ethylene furanoate) PEF, is highlighted.

2.4.1 Aliphatic Polyether Polyols

Aliphatic polyether polyols represent an important class of polymers that are commercially used for a broad variety of applications such as polyurethane synthesis,[180] surfactants,[181] pharmacy,[182] biomedicine[183] and more. The physical properties of polyether polyols vary from liquids with low viscosity to soft waxes to thermoplastic materials depending on the chemical building blocks, functionalities, and molecular weights.[184] The main representatives are generated by ring-opening polymerization (ROP) of epoxide monomers ethylene oxide (EO), propylene oxide (PO) and less often butylene oxide (BO). These epoxides are readily available in industry from different oxidation methods of the respective alkenes.[185] Nevertheless, also four- and five-membered cyclic ethers, such as tetramethylene oxide (TMO), can be polymerized in ROP (**Scheme 13**).

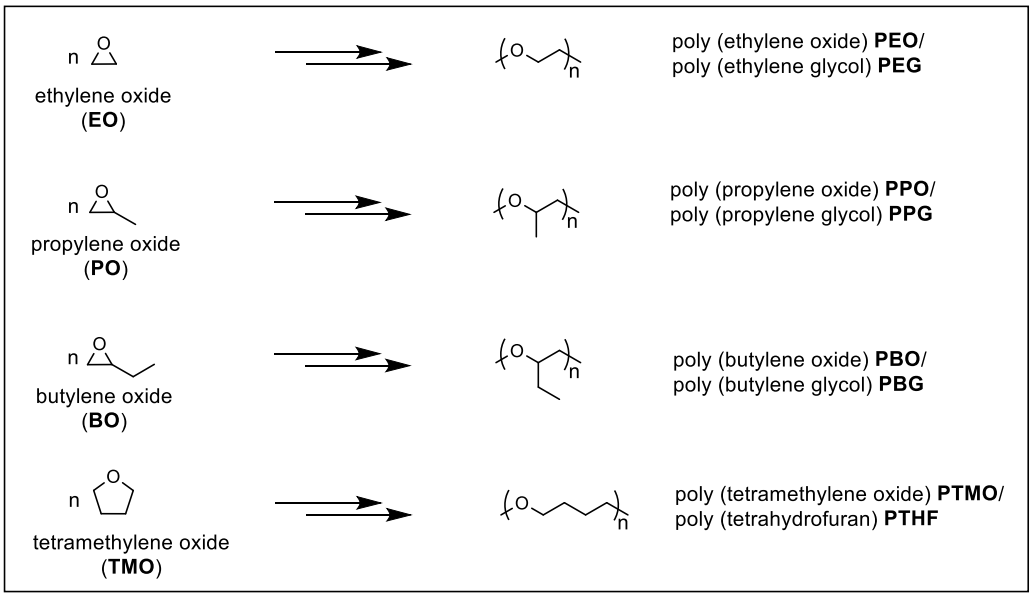

Scheme 13 Overview of the main aliphatic polyether polyol representatives.

As a result of the high ring strain of epoxides, they can be polymerized by anionic, cationic, or coordinative insertion ROP. The polymerization of EO with alkali metal hydroxides or zinc chloride was first reported in 1863 by Wurtz[186] and further studied by Staudinger and Lohmann in 1929,[187] establishing a variety of alkali and alkaline earth metal compounds as catalysts. The mechanism of base initiated or anionic polymerization of EO was established by Flory ten years later, predicting a Poisson-type distribution for a living chain-growth polymerization.[188]

In the anionic ROP, water or an alcohol as well as alkaline catalysts, mostly alkali metal compounds with high nucleophilicity, are required for the initiation step (**Scheme 14**). The initiation step is followed by the propagation through further nucleophilic attack of

the anionic chain end until either termination or a transfer reaction occurs (**Scheme 14**). For instance, highly basic initiator systems can abstract a proton from the methyl group, leading to an extensive chain transfer to the PO monomer and thus an allyl alkoxide is formed through elimination. This undesired reaction leads to a chain stop and therefore, lower molecular weights besides increased dispersities.[189-191] For POE with high molecular weights, alkali metal hydrides, alkyls, aryls, hydroxides, alkoxides or amides are required. Moreover, polar and aprotic solvents such as THF, dioxane or DMSO are preferred.[192] Ring-opening polymerization in bulk is also possible, however only low molecular weights besides high dispersities are obtained.[193] In general, the addition of crown ethers strongly increases the reaction rate through complexation of the cation counterion.[194-195] Moreover, since primary hydroxyl groups exhibit higher reactivity than secondary alkoxides, the polymerization rate of EO is faster than that of PO. The kinetics of the anionic polymerization of EO was reviewed by Penczek *et al*.[196] Furthermore, the active alkoxide chain end is rather stable with respect to termination during the living polymerization. Thus, facile and quantitative end-functionalization is possible.[197-199]

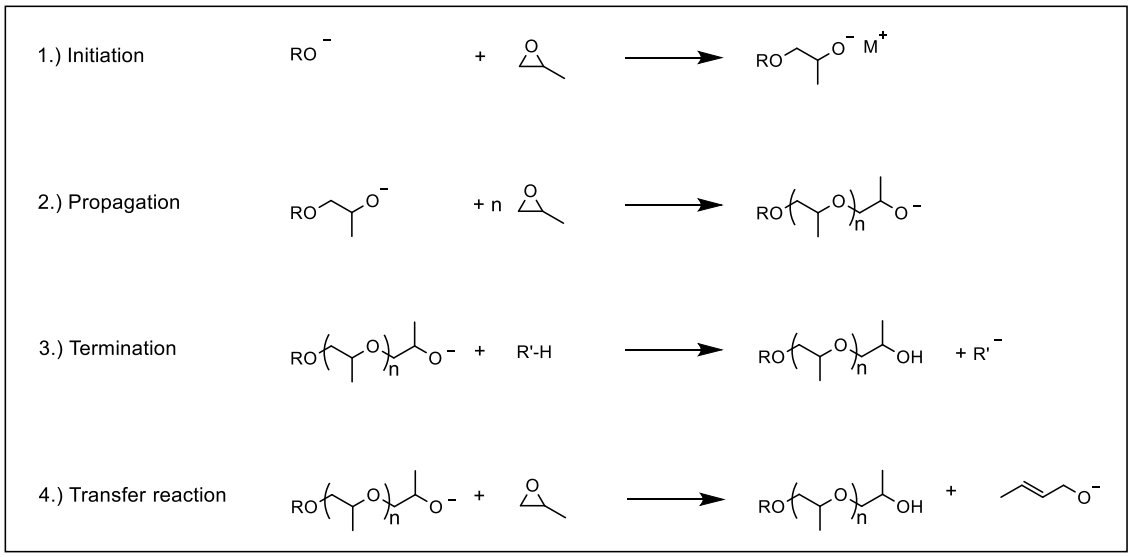

Scheme 14 Mechanism of anionic ROP, exemplarily shown for PO.

In order to address the problem of chain transfer, the activated monomer approach, a new technique based on the anionic ROP was introduced by Deffieux *et al.* (**Scheme 15**).[200] Hereby, the activation of the monomer results from an interaction between Lewis acids and the epoxide ring, whereby the initiation occurs through the formation of an “ate complex” between the Lewis acid and a weak nucleophile. In this method, the transfer reaction of to the anionic ROP can be completely suppressed for optimized initiator systems leading to high molecular weight polyether polyols with low dispersities.[200-205] Especially for PO and higher alkylidene oxides, this method enables selective and fast polymerization, further the regioselectivity is controlled by only head-

to-tail chain growth.[200-201] For this reaction system, non-complexing and aprotic solvents such as 2-methyltetrahydrofuran are required.[206]

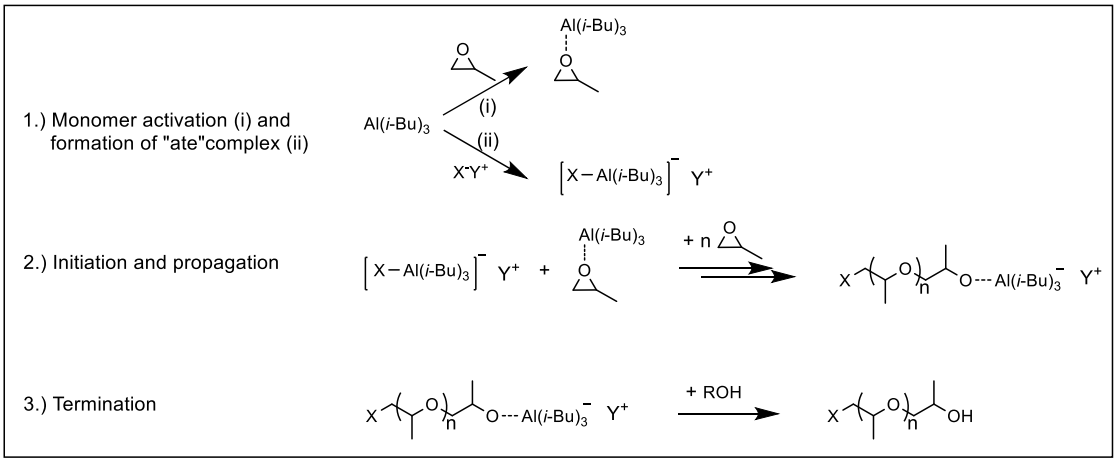

Scheme 15 Activated monomer mechanism of the anionic ROP, exemplarily shown for PO.

Similar to the activated monomer mechanism of the anionic ROP, the monomer is activated by the coordination of a metal complex to the oxygen in the coordination polymerization (**Scheme 16**). Hereby, the activation is followed by a nucleophilic attack of the ligand as initiation step. Through this technique, very high molecular weights above 100.000 g/mol were achieved.[207] Numerous initiators were investigated with respect to kinetics and molecular weight.[208-211]

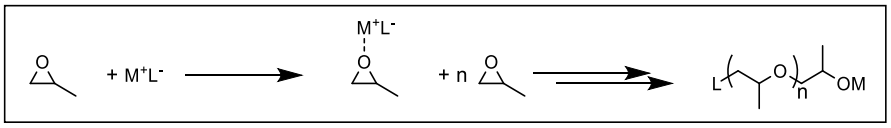

Scheme 16 Coordinative insertion ROP mechanism, exemplarily shown for PO.

Another possible ring-opening polymerization is the cationic or acid catalyzed polymerization, which follows two different mechanism as shown in **Scheme 17**. The activated chain-end mechanism (ACE) and the activated monomer mechanism (AM). In the ACE mechanism, the activated center is the tertiary oxonium ion on the chain end. A nucleophilic attack of the oxygen atom in the cyclic monomer leads to propagation. However, for PEO and PPO the intermolecular nucleophilic attack of an oxygen atom resulting in propagation competes with the intramolecular attack of an oxygen atom within the growing chain, so-called backbiting, leading to the formation of 1,4-dioxane or crown ether structures as side products (**Scheme 17**).[212-214] In the AM approach, an active hydrogen compound, such as an alcohol or glycol, is added for the initiation step, which ring-opens the oxonium ion formed through protonation of the catalyst. Subsequently, the propagation of all monomers occurs until a termination by proton or ion transfer arises. Herein, the active center is located on the monomer due to rapid

proton transfer and thus, a better control over molecular weights is obtained (**Scheme 17**).[215-218] However, both mechanism compete and are influenced by the monomer concentration. For instance, in order to achieve a predominant AM mechanism, a low monomer concentration is required and can be conducted through slow monomer addition. Especially, for four- and five- membered cyclic ethers, such as tetrahydrofuran, cationic ROP plays an important role, since these monomers are not suitable for anionic ROP.[219]

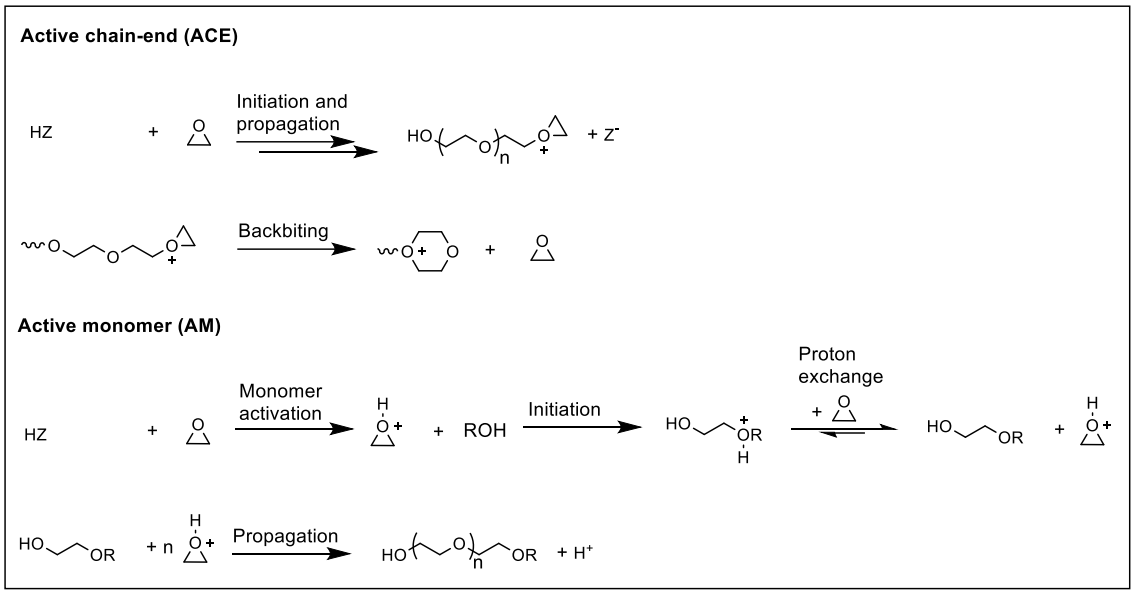

Scheme 17 Active chain-end (ACE) mechanism (top) and active monomer (AM) mechanism (bottom) of cationic ROP, exemplarily shown for EO.

Poly(ethylene oxide) PEO is often called poly(ethylene glycol) PEG, especially for low molecular weights below 30.000 g/mol and biomedical applications. PEG shows unique behavior in terms of solubility since it is, in contrast to other polyethers, highly water-soluble in almost every concentration while exhibiting a low immunogenicity, antigenicity, and toxicity.[220-222] The high water solubility is caused by a compatibility of the distance of the oxygen atoms in the polymer structure and the distance of the hydrogen atoms in water molecules.[220] Thus, PEG is a highly biocompatible polymer for pharmaceutical, cosmetic, and medical applications and is used for an wide range of products within these sectors.[223-224] Various review articles on PEG were published in recent years.[207, 225-227]

In poly(propylene oxide) PPO, also known as poly(propylene glycol) PPG, mostly a racemic PO monomer is used for the ROP leading to isotactic and hence, non-crystalline, flexible PPG. The water solubility differs from PEG because the methyl group in each repeating unit sterically shields the polymer backbone. Hence, only low molecular weighted PPO is water soluble under specific conditions.[228] As a result of the flexibility

and non-crystallinity, PPG is often used for the synthesis of flexible polyurethane foams (PUF). Moreover, the properties of PPG can be tuned by multifunctional initiators in the anionic ROP such as glycerol, pentaerythritol or sorbitol.[106] The occurrence of a chain transfer reaction shown in **Scheme 14** can be influenced by the counterion and the addition of crown ethers.

Through living polymerization, many copolymers of ethylene oxide and propylene oxide were synthesized to adjust their properties for certain applications.[229-233] For instance, PPG suffers from poor reactivity of the secondary hydroxyl group for PU synthesis and thus, EG is often added in the final stage of the polymerization. However, the humidity resistance decreases by the addition of a PEG block.

The properties of poly(butylene oxide) PBO are similar to those of PPO, while PBO is more hydrophobic resulting in a disadvantage for many applications. Hence, BO is often used as comonomer to modify the properties of other polyethers.[234]

Next to epoxides, aliphatic polyether polyols are also synthesized from oxetanes. Poly(oxetane)s are less prevalent, and the properties can vary from fully amorphous liquids to highly crystalline solids and are strongly dependent on the symmetry, steric demand and polarity of the side-chains of the oxetane monomer. Oxetanes are less reactive than oxiranes due to their lower ring strain.[235] The polymers are only soluble in concentrated sulfuric acid or pyridine, while resisting common organic solvents.[236] The solubility can be adjusted through copolymerization with different oxiranes or functionalized oxetanes enabling new applications.[237-239]

Poly(tetramethylene oxide) PTMO, also known as poly(tetrahydrofuran) PTHF, can be obtained by cationic ROP of THF and is commercially available in low molecular weights, since they are mainly used for PU and polyester synthesis due to their excellent elastomeric properties. PTHF is obtained with viscosities ranging from sticky, viscous oil up to solid material, depending on the molecular weight and is soluble in many polar and nonpolar organic solvents.[219]

Apart from ROP of cyclic ethers, polyethers can also be synthesized by a variety of different ways. In 1850, Williamson introduced the first synthesis of an ether *via* nucleophilic substitution of alkali alkoxide and alkylating reagent such as a haloakane.[240] Polyethers can be synthesized *via* acid catalyzed polycondensation of glycols, which is reversible under strong acidic conditions.[241] High molar mass poly(oxyalkylene)s with four to twelve methylene units were obtained by polyetherification at relatively low temperatures (130°C) in Brønsted acid ionic liquids.[242] In 2019, Sardon *et. al* reported the self-condensation of diols in bulk, catalyzed by non-eutectic acid-base

organocatalysts, such as methanesulfonic acid and 1,5,7-triazabicyclo[4.4.0]dec-5-ene (TBD).[243]

Furthermore, polyethers were synthesized *via* acyclic diene metathesis (ADMET)[244-246] of α,ω-diene ether, or thiol-ene polymerization.[247-248] However, no polyols were obtained by these synthesis pathways, since the polyethers and poly(thio)ethers did not bear hydroxyl end groups (**Scheme 18**).

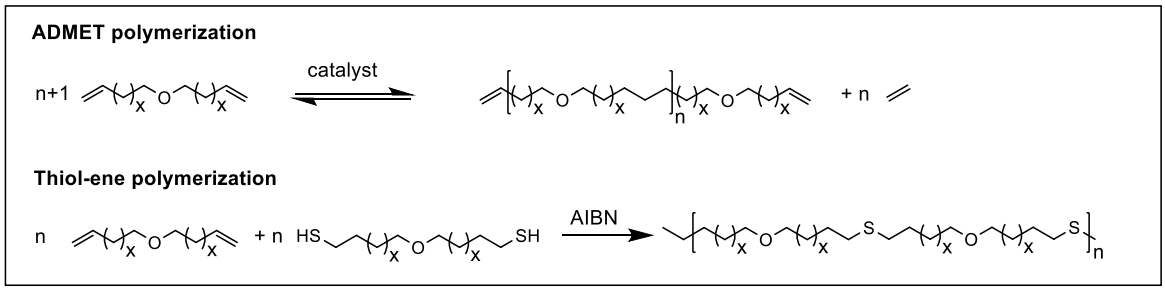

Scheme 18 ADMET polymerization (top) and thiol-ene polymerization (bottom) of α,ω-diene ether.

In 2018, Meier and Biermann *et al.* reported the catalytic reduction of aliphatic polyesters to medium and long chain aliphatic polyethers enabling a broad spectrum of different polyether repeating units (**Scheme 19**).[249] This approach is discussed in detail in chapter 2.5.

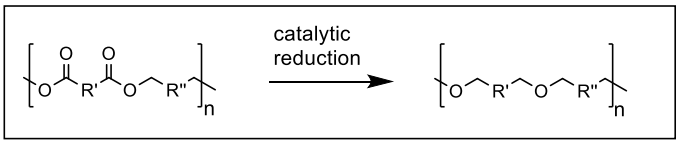

Scheme 19 Catalytic reduction of polyester to polyether.

2.4.2 Biobased Polyols

Polyols are mostly used in the synthesis of polyurethanes (PU). Regarding the rising interest in sustainable materials, the investigation of biobased polyol structures in academia and industry increased significantly over the last decades. Especially for polyurethanes (PU), covering 7.9% of the European plastic demand,[7] many approaches were investigated based on the synthesis of biobased polyols, as reviewed by Avérous *et. al*.[250] Another overview on the large research field of biobased polyols for polyurethane application was published by Sardon and Jehanno *et al.* in 2021.[251] The latter also summarized the current strategies of biobased polyols for industry. The structure and properties of polyurethanes strongly depend on the chemical structure, functionality, and molecular weight of the used polyol. Particularly, the versatility of the polyol structure enabled a broad source of biobased raw materials for different applications. Since the largest applications of PU are flexible (PUF) and rigid foams (PUR), as already described in chapter 2.3.2 suitable biobased polyols for these applications are introduced in the following.

For instance, biobased short chained glycols, such as glycerol or ethylene glycol, can be directly used for PU synthesis, but the resulting properties are not suitable for PU foams. Therefore, these glycols can be added to other biobased polyols to tune the foam properties. Glycerol, which is highly available, cheap and non-toxic, can be mixed with vegetable oils such as tung oil[252] or castor oil,[253-254] thus increasing the OH values of the polyol blend in order to obtain PUR. Crude glycerol is obtained as byproduct of biodiesel production and consists of a mixture of glycerol, methanol, water, soap, fatty acid methyl esters, fatty acids, monoglycerides and diglycerides decreases the foam rigidity compared to glycerol.[254] However, crude glycerol can be used for polyols, whereby glycerol would lead to non-processable polyols.[255-256] Besides glycerol, 1,3-propane diol,[257] ethylene glycol, or diethylene glycol[258] are used for PU foams. Saccharides, such as sorbitol or pentaerythritol, enable a highly branched polyol if combined with palm oil[259-261] or modified palm kernel oil,[261] improving the properties of the obtained PUR.

Aliphatic polyether polyols are obtained from ring-opening polymerization of biobased ethylene oxide, propylene oxide or butylene oxide as already described in chapter 2.4.1.[262-264] These polyols are mostly used for the synthesis of PUFs, since they provide better mechanical properties.[123] The functionality can be increased by the addition of saccharides as initiators for the ROP, thus enabling the synthesis of hard foams from the respective polyols.[265-266]

Aliphatic polyester polyols are obtained by polycondensation or ring-opening polymerization (**Scheme 20**).[267-268] In general, polyester polyols are often used in PIR synthesis, since they offer a higher rigidity than polyether polyols.[269] Polyester polyols used for PU foams are often based on adipic acid or phthalic anhydride and glycols such as trimethylolpropane.[123, 270] Moreover, several studies showed a catalyst-free synthesis based on 1,2-propane diol, 1,5-pentane diol or sorbitol.[271-272] Furthermore, renewable polyester polyols can be synthesized *via* ring-opening polymerization of lactones or lactides (**Scheme 20**).[273-274]

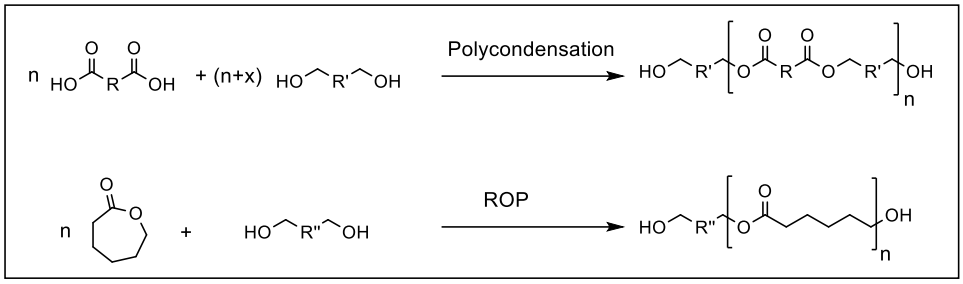

Scheme 20 Synthesis of biobased polyester polyols *via* polycondensation of biobased dicarboxylic acids and diols (top) and ROP of ε-caprolactone (bottom).

Many researchers worked on the synthesis of polyols from vegetable oils offering a versatile source of different structures, but often further functionalization of the triglycerides was necessary. Mostly, epoxidation followed by ring opening, transamidation, transesterification, hydroformylation, metathesis or ozonolysis was conducted.[275-279] Polyols based on soybean oil often decrease the mechanical properties of PUF[280] and only a few methods were investigated for the application in PUR.[281] Castor oil can be used directly as polyol, but is shows poor reactivity.[282] Thus, further modification is necessary to obtain higher OH-values and/or more reactive primary OH groups for PUR application.[283-288] Polyols based on palm oil mostly lead to flexible PU foams.[289-293] Microalgae, an interesting source of triglyceride since it does not compete with food or land surface for growth, can be converted into polyols through epoxidation followed by ring-opening reaction and applied in PUR.[294-297] Similar modifications are reported on many other vegetable oils, enabling a broad spectrum of different biobased polyols with different properties.[252, 256, 298-301] Another possible renewable resource for biobased polyols are terpenes. For instance, thiol-ene coupling enables the synthesis of polyols based on limonene or α-phellandrene (**Scheme 21**).[302-303]

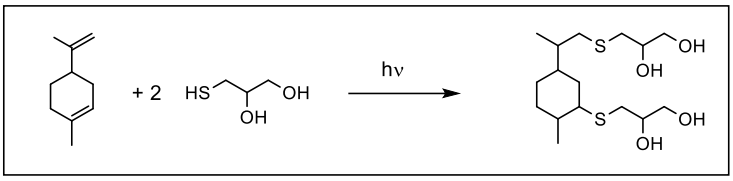

Scheme 21 Thiol-ene reaction of limonene and 1-thioglycerol.

The availability of aromatic structures in renewable resources in large amounts is limited to mostly lignocellulosic biomass. Thus, aromatic polyether polyols are only obtained as a mixture of aliphatic polyether polyols by the solvolysis liquefaction of lignocellulosic biomass from wood.[304-305] Various protocols were published using different biomass sources and solvents for the solvolysis to obtain varying blends of polyols.[306-314] Solvents take a key role in this process to overcome the high biomass viscosity, influencing the properties of the final PU foam.[306-308] Moreover, tannins can be extracted from lignocellulosic biomass for the use of PU and can be partly added to different polyols increasing the aromatic content.[315-316] Another possible pathway to obtain lignin and tannin alkoxylated polyether polyols is the alkoxylation of lignocellulosic biomass.[317-321] However, for the application as rigid PU foams, only a partial substitution of commercial and conventional polyols by the aromatic polyether polyol is possible.[322-323]

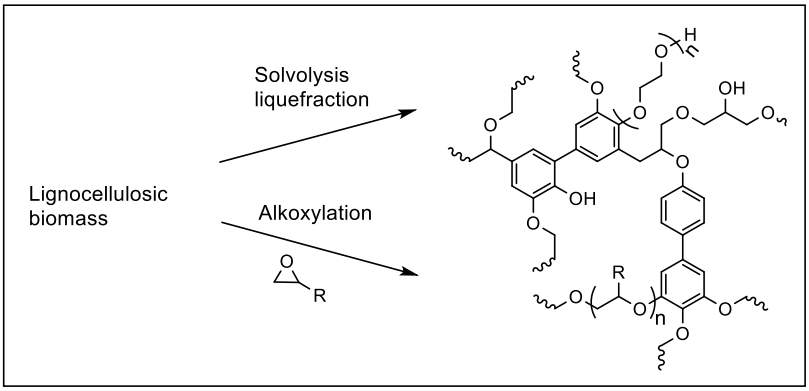

Scheme 22 Synthesis of biobased aromatic polyether polyols derived from lignocellulosic biomass.

Aromatic polyester polyols are obtained by glycolysis of poly(ethylene terephthalate) (PET) and PUs.[324-326] The obtained aromatic polyester polyol is not directly processable and thus, esterification with biobased aliphatic dicarboxylic acids, such as adipic acid or sebacic acid, and other polyols is necessary, losing aromatic content (**Scheme 23**).[325, 327] Through this synthesis pathway, the properties of the final PU foam can be tuned by the use of different monomers in the esterification procedure.

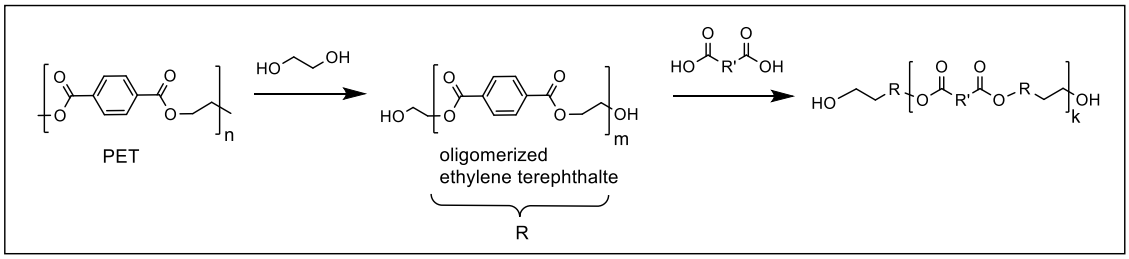

Scheme 23 Synthesis of renewable aromatic polyester polyols *via* glycolysis followed by esterification with biobased aliphatic dicarboxylic acids.

2.4.3 Poly(ethylene furanoate) PEF

In the last decades, the interests in poly(ethylene furanote) PEF emerged, since it represents a promising fully biobased alternative to the fossil based poly(ethylene terephthalate) PET, used in fibers and bottles (**Scheme 24**), which is one of the largest volume industrial polymers with a global production of almost 24 million tons *p.a.* (2018).[328] Due to the general increasing environmental awareness and the depletion of fossil resources, PET becomes an obvious target for manufacturing from renewable resources. PET is synthesized *via* polycondensation of ethylene glycol and terephthalic acid (TPA), which is obtained from *p*-xylene. Recently, *Coca Cola* produced up to 30 wt% biobased PET by existing technologies using biobased-ethylene glycol obtained from bioethanol and is currently working on establishing the production of fully biobased PET.[329] In order to gain fully biobased PET, a synthesis route for *p*-xylene from biomass is required and many examples in academia, reviewed by Collias *et al.*,[330] and industry already found solutions to overcome this challenge.[331] Another approach to produce bottles based on 100% renewable resources is the replacement of PET by PEF. Life-cycle assessment of bio-derived PEF compared to the petroleum based PET showed a reduction of greenhouse gases of up to 55%.[332] Moreover, PEF bottles revealed improved barrier properties, especially with respect to oxygen permeability, than their petroleum based alternatives.[17]

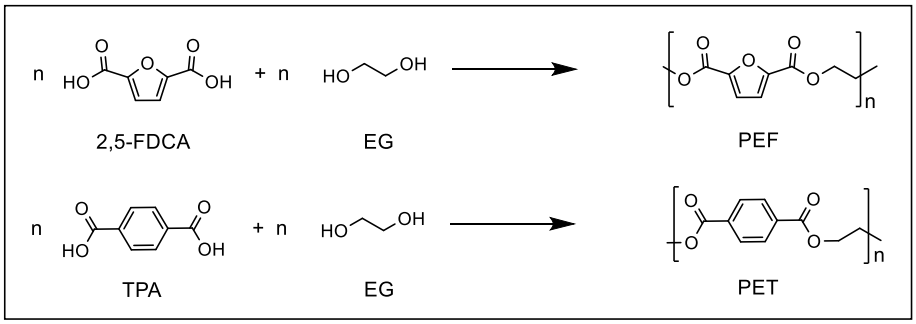

Scheme 24 Synthesis of PEF (top) and PET (bottom).

PEF is derived from 2,5-furandicarboxylic acid (FDCA) and ethylene glycol (EG). Resulting from the promising properties of PEF bottles, a high number of reports were published in recent years covering different synthesis pathways for FDCA, besides polymerization strategies to obtain high molecular weighted PEF. Moreover, FDCA was identified as one of the top twelve sugar derived platform chemical by the U.S. Department of Energy in the year 2004.[333] The most applied synthesis route towards FDCA is based on the oxidation of hydroxymethylfurfural (HMF) derived from corn based fructose as shown in **Scheme 25a**. Afonso and coworkers summarized different synthesis strategies of HMF in 2011.[334] The main challenge of the dehydration of

fructose to HMF is the selectivity towards the desired product, since HMF is unstable resulting in side products such as levulinic acid.[335] However, HMF can be synthesized in a high yields of 80% with 90% conversion of fructose through a bi-phasic reactor, in which the acid catalyzed dehydration occurs in aqueous solution. DMSO is added to suppress the side reaction, while HMF is continuously extracted into an organic phase of methyl isobutyl ketone.[336] *Avantium* showed that this side reaction can be suppressed by the *in situ* synthesis of HMF ethers if an alcohol is used as solvent. The obtained ethers are subsequently oxidized to FDCA.[337] Currently, *Avantium* is building a flagship plant for the synthesis of biobased FDCA and PEF until 2024, demonstrating that this method is feasible on an industrial scale.[338] For the oxidation of HMF to FDCA, different catalysts were investigated, such as metal bromides in acetic acid,[339] rare metallic nano-particles based on Pt,[340-341] Ru,[342] or Au,[343] bimetallic catalysts,[344] and enzyms[345-346]. Another synthesis route towards FDCA is based on the oxidation of furfural, obtained from lignocellulose into 2-furoic acid and consecutive reaction with CO_2 *via* carbonate promoted C-H carboxylation, catalyzed by $CsCO_3$ at 200-260°C (**Scheme 25b**). Another follow-up reaction of 2-furoic acid is the Henkel reaction into a mixture of 2,4-, 2,5- and 3,4-FDCA at 300-500°C and high pressure (**Scheme 25c**).[347-348] As an alternative to these harsh conditions, the synthesis of 2,5-diacetyl furane (DAF) through a two-step Friedel crafts reaction under mild conditions is promising. A subsequent iodoform reaction leads to 2,5-FDCA in high purities (> 99%), while the used acetic acid and iodoform are recycled (**Scheme 25d**).[349] Biobased ethylene glycol (EG) can be accessed by either chemocatalytic conversion of cellulosic or lignocellulosic biomass or dehydration of biobased ethanol.[350-351]

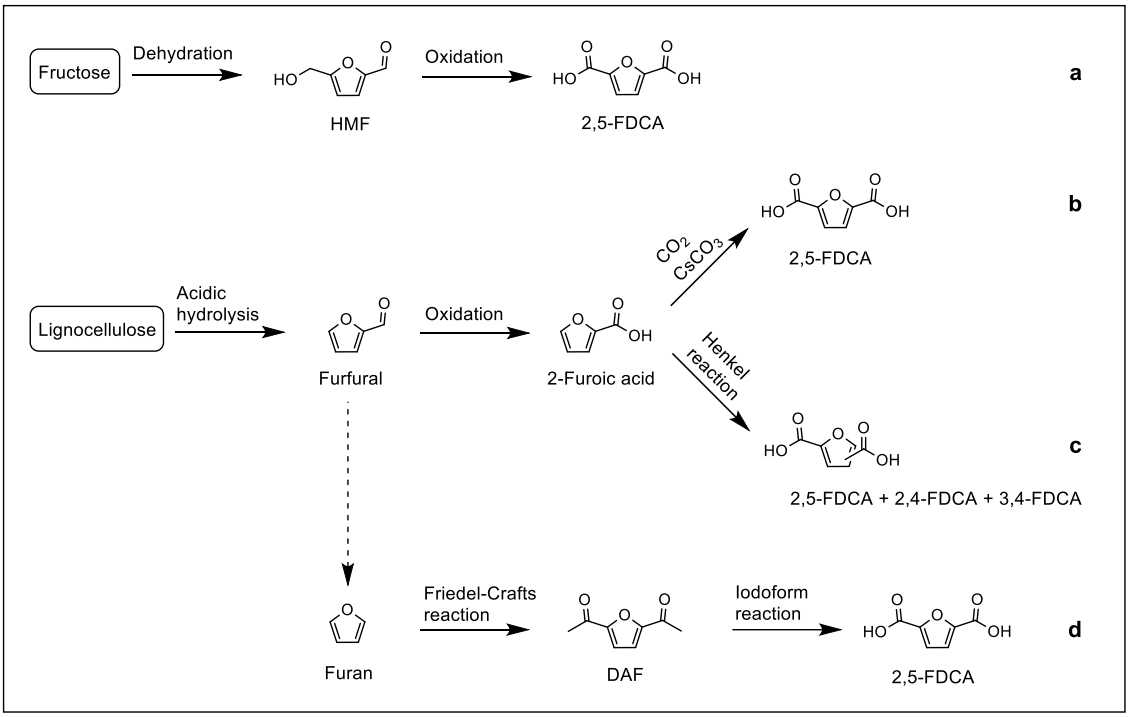

Scheme 25 Overview of different FDCA synthesis routes: **a** Oxidation of HMF obtained *via* dehydration of fructose, **b** carbonate-promoted C-H carboxylation of 2-furoic acid, **c** Henkel reaction of 2-furoic acid, **d** Iodoform reaction of DAF.

PEF is typically synthesized *via* melt polycondensation of 2,5-FDCA or dimethyl 2,5-furandicarboxylate (DMFD) and EG under high temperatures (**Scheme 26**). The first catalyst for this system was lead oxide, as introduced by Moore *et al*.[352] The problem during the polycondensation is a discoloration and degradation of the product. PEF melts at around 220°C, while the degradation temperature is around 330°C.[353] The discoloration can be caused by sugar based impurities in the monomer, occurring side reactions such as decarboxylation or the presence of various additives.[354] It was further determined that the discoloration of PEF correlates with the amount of FDCA, the used catalyst and the reaction time.[355-356] However, a colorless precipitation was obtained after dissolving PEF in a mixture of chloroform and trifluoroacetic acid and precipitation in methanol.[357] In recent years, the influence of different catalysts and reaction conditions on molecular weight, discoloration and reactivity were studied. [355, 357-363] High molecular weights of up to 83 kg/mol can be industrially obtained by melt polymerization and subsequent solid state post condensation.[361] Especially for the application in PEF bottles, high molecular weights are required while a discoloration is undesired. However, to obtain high M_n, harsh conditions and long reaction times are necessary, which correlate with an enhanced discoloration. Morbidelli *et al.* investigated a novel synthesis strategy in 2018 in order to overcome this problem (**Scheme 26**).[353] Their approach is based on a rapid ring-opening polymerization of cyclic PEF oligomers within minutes. First, dimethyl 2,5-furandicarboxylate and EG were prepolymerized under relatively mild

conditions and short reaction times to obtain linear oligomerized ethylene furanoate (OEF) with molecular weights below 5 kg/mol. Consecutive depolymerization leads to the formation of ethylene furonate cycles with different ring sizes ranging from two up to four monomer units. Finally, PEF is obtained through a subsequent ring-opening polymerization of the ethylene furanote cycles. However, the ROP requires a high boiling, removable liquid plasticizer, since the cycles have melting points above the degradation temperature of PEF. As soon as the ROP starts, the obtained PEF melts under these conditions and thus a self-plasticizing effect occurs. Through this synthesis route, colorless PEF with molecular weights above 30 kg/mol can be produced.

Thermal, mechanical and barrier properties, as well as the dynamics of crystallization and structural characterization such as chain conformation of PEF were studied and compared to PET for different molecular weights and copolyesters.[335, 361, 364-365]

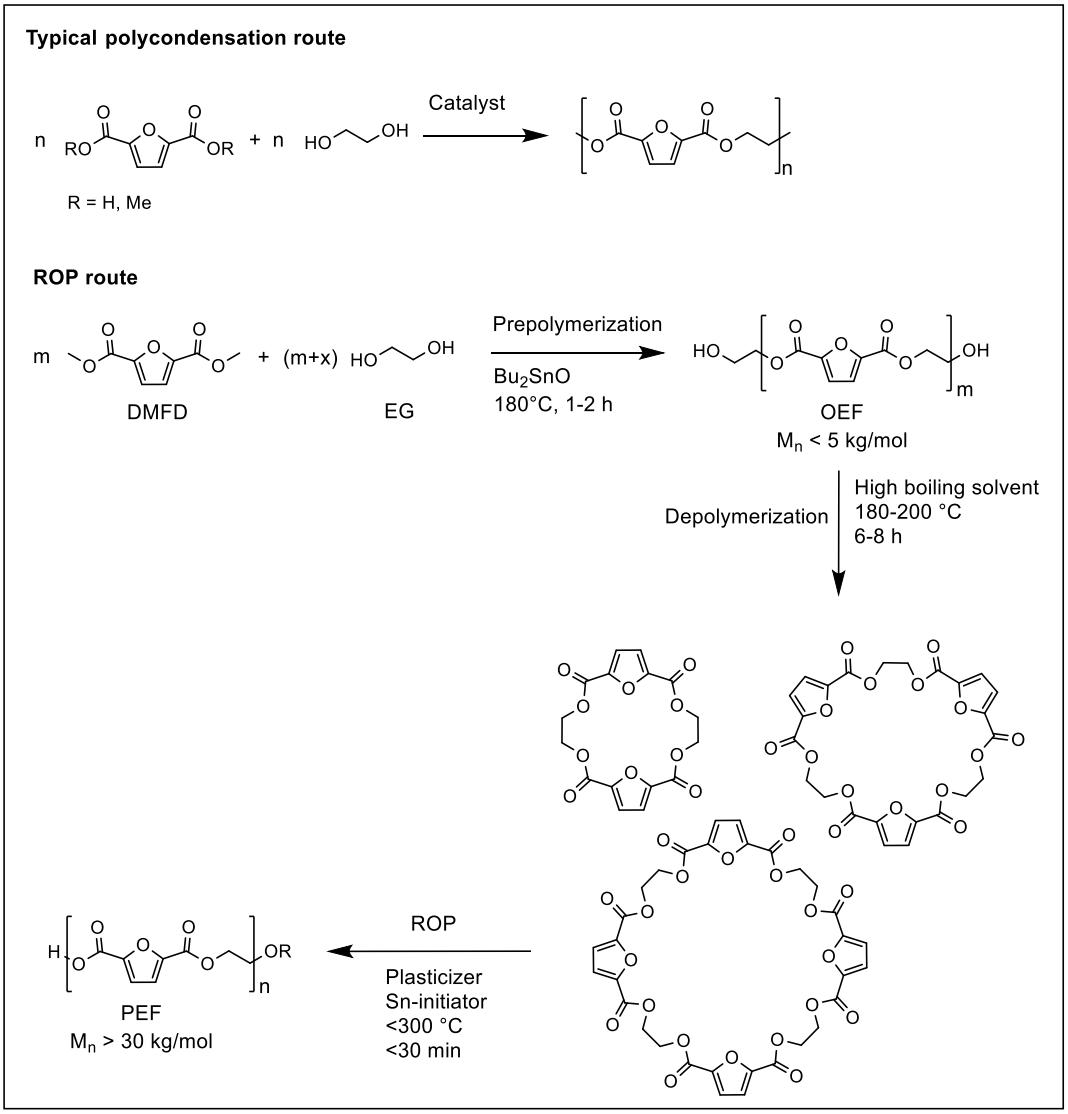

Scheme 26 Typical polycondensation synthesis route of PEF (top) and the ROP route introduced by Morbidelli and coworkers (bottom).[353]

2.5 Reduction of Esters to Ethers

The reduction of esters was first reported in 1960 by Pettit *et al.* on steroids using a large excess of boron trifluoride diethyl etherate and hydrides such as $LiAlH_4$ or $NaBH_4$.[366-369] One example is shown in **Scheme 27**.

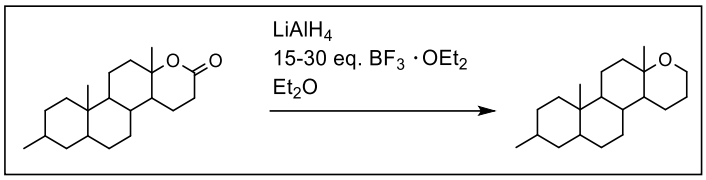

Scheme 27 Exemplary reduction of an ester to the corresponding ether on steroids using $LiAlH_4$, introduced by Petitt and coworkers.[367]

The first reduction using silanes as reducing agents instead of hydrides was introduced in 1969 by Tsurugi *et al*.[370-372] Herein, ethers were obtained from the corresponding esters *via* reduction with trichlorosilane and γ-irradiation for several structures such as aliphatic esters or lactones in quantitative yields (**Scheme 28**).

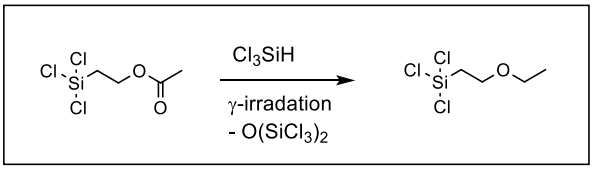

Scheme 28 First reduction of an ester to an ether using silanes as reducing agents under γ-irradiation, reported by Tsurugi and coworkers.[371]

Several years later, Baldwin and coworkers reported a similar reaction system also using trichlorosilane under UV-irradiation postulating deoxygenation as a side reaction leading to alkanes in their systems.[373] First metal-catalyzed reductions with silane reducing agents were reported in 1995. Reduction of aliphatic, aromatic, linear, branched, and cyclic esters were performed in the presence of a manganese catalyst and $PhSiH_3$.[374] Subsequently, several reports based on different metal catalyst, silanes and substrates were published.[375-380] A promising approach is the combination of a trivalent indium salt and hydrosilane, enabling an efficient reaction applicable to a broad spectrum of functional groups. It is feasible for e.g. the dehalogenation of organic halides,[381] reduction of alcohols,[382] aryl ketones[383] and enones,[384] the reductive aldol reaction[385] and the deacetoxylation of propargylic acetates.[386] The reduction of amides to amines was reviewed in detail by Nagashima *et al*.[387]

In 2007, Sakai and coworkers reported a detailed investigation of the influence of different indium salts, hydrosilanes and solvents on the catalytic reduction of esters to their corresponding ethers (**Scheme 29**).[388] For the studied esters, chloroform seemed

to be the best solvent, while Et_3SiH showed the highest efficiency of the investigated reducing agents. Moreover, the best results were obtained with $InBr_3$, whereas other indium salts such as $InCl_3$, $In(OTf)_3$ or $In(OAc)_3$ gave no conversion at all.

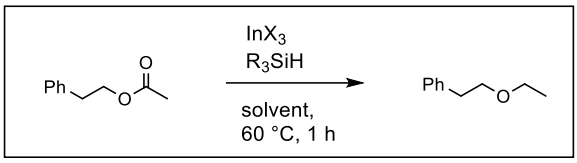

Scheme 29 Indium-catalyzed reduction of esters to ethers using different hydrosilanes and solvents.[388]

Furthermore, a plausible mechanism was proposed by Sakai *et al.*, but no conclusive evidence has been provided yet (**Scheme 30**).[388] The active species of the catalyst is formed *via* transmetalation between $InBr_3$ and Et_3SiH followed by the formation of a radical $InBr_2$ species. Subsequently, the reaction with the carboxyl groups and hydrogen abstraction through the silane forms a radical ether species, which leads to the final ether by the hydrogen abstraction from $InBr_2H$, while the $InBr_2$-radical species is regenerated. As a byproduct, hexaethylene disiloxane is formed.

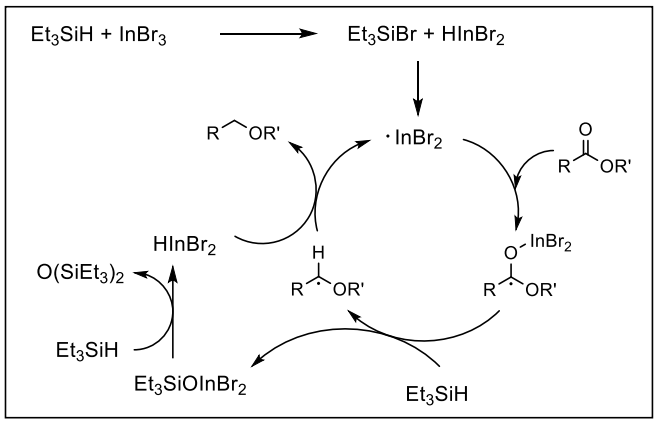

Scheme 30 Proposed mechanism of the indium catalyzed reduction of esters.[388]

Biermann *et al.* applied the catalytic reduction of Sakai on long chain aliphatic unsaturated fatty acid esters such as methyl oleate (**Scheme 31**).[389] Consecutively, the results were successfully transferred to high oleic sunflower oil.[390] The authors reported a better selectivity of the desired ethers if $GaBr_3$ was used instead of $InBr_3$, because of the possible reduction of the ether to an alcohol. No detectable side reactions of the triglyceride were observed, while all ester groups were converted. Moreover, the catalyst loading was reduced to 0.5 - 1 mol% per ester group and 1,1,3,3-tetramethyldisolxane (TMDS) was used as reducing agent. Due to the use of TMDS instead of triethylsilane, polydimethylsiloxane (PDMS) was obtained as byproduct, enabling an easy work-up of the product through distillation. TMDS is produced as byproduct by the silicon industry

and is thus an inexpensive, commercially available reductant.[391] Furthermore, Biermann and coworkers expanded the system to lactones.[389]

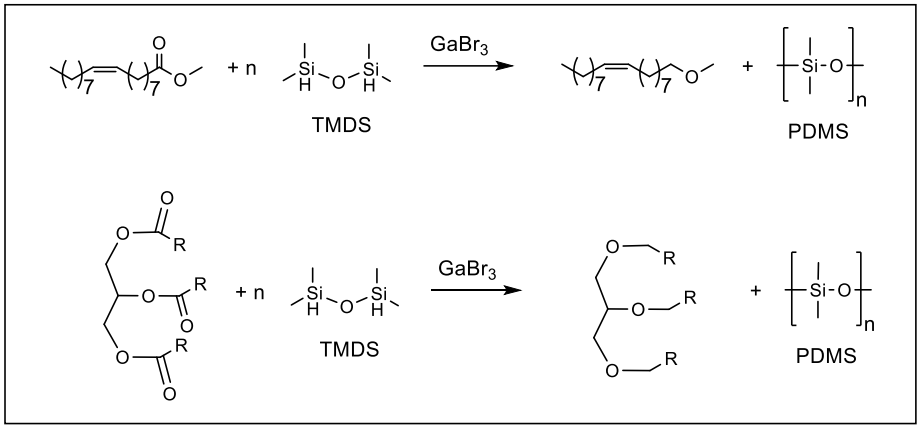

Scheme 31 $GaBr_3$ catalyzed reduction of methyl oleate and a triglyceride with TMDS.

Meier and Biermann *et al.* synthesized fatty acid derived aliphatic long chain polyethers *via* the combination of the catalytic ester reduction and ADMET or thiol-ene polymerization (**Scheme 32**).[248] First α,ω-diene esters were synthesized through esterification of fatty acids and diols or dimethyl dicarboxylates and ω-unsaturated alcohols. Subsequently, the corresponding α,ω-diene ethers were obtained through the catalytic reduction with TMDS and $GaBr_3$, followed by either ADMET or thiol-ene polymerization.

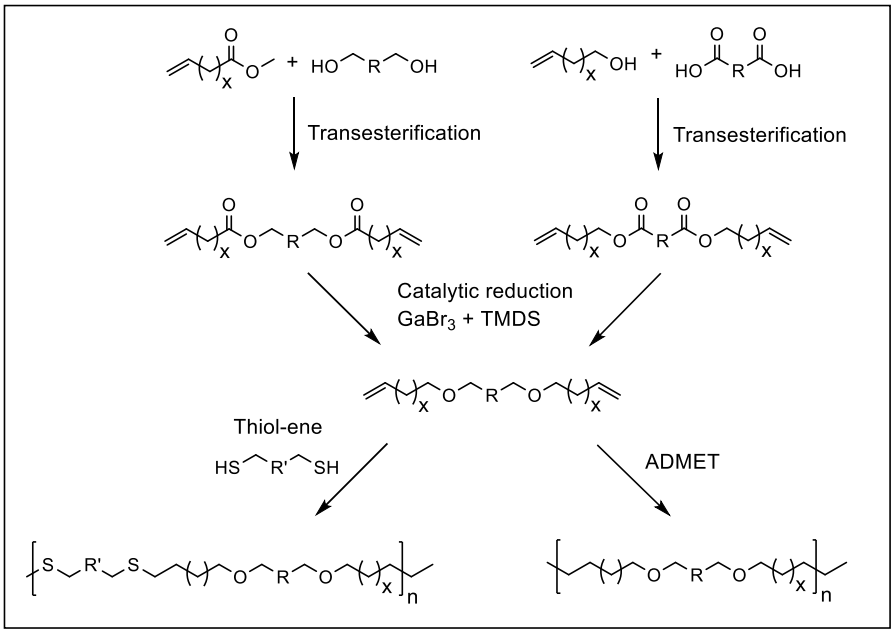

Scheme 32 Synthesis of renewable polyethers enabled by the $GaBr_3$ catalyzed reduction of aliphatic esters.

The authors also transferred the catalytic reduction to renewable polyesters, produced *via* polycondensation of biobased monomers or ROP of lactones, to obtain renewable

medium and long chain aliphatic polyethers (**Scheme 33**).[249] However, the side reaction of the ethers to the corresponding alcohols leads to cleavage of the polyether backbone, which depends on the structure of the investigated polyesters, as described.

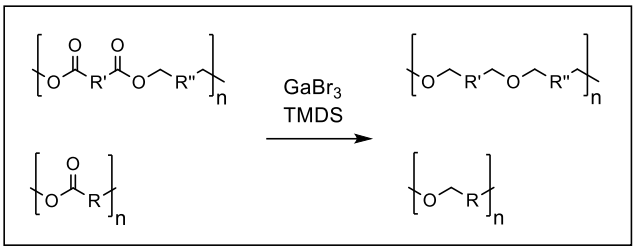

Scheme 33 $GaBr_3$ catalyzed reduction of renewable polyester.

3 Aim of this work

The aim of this work is the synthesis and modification of novel polyol structures and their applications in polyurethane rigid foams and fully biobased epoxy thermosets.

First, the focus is set on the synthesis of different aliphatic polyether polyols *via* gallium bromide catalyzed reduction of the corresponding polyester polyols. Thereby, the influence of the polyester structure and different reducing agents on this reaction system as well as suitable reaction conditions for possible scale-up reactions are investigated. The results are transferred to the reduction of cellulose acetate enabling a novel synthesis route towards the widely applied ethyl cellulose.

In the second part of this work the synthesis of fully biobased aromatic polyester polyols and the possible substitution of their petroleum based counterparts in polyurethane rigid foam applications are of interest. Therefore, 2,5-furandicarboxylic acid is polymerized with biobased ethylene glycol or diethylene glycol in a polycondensation reaction aiming for low molecular weights to obtain a processable polyol. Afterwards, the fully biobased aromatic polyester polyols are reacted with polyisocyanurate to polyurethane rigid foams and their thermal and mechanical properties are analyzed and compared to the foams synthesized from a typical petroleum based polyol.

Finally, the synthesis of biobased aliphatic polyester and polyether polyols as well as their end group modification to diamines are studied. These diamine prepolymers are intended to be cured with biobased polyepoxides into epoxy thermosets. The fully biobased thermosets are compared regarding their thermal and mechanical properties, evaluating the influence of the different epoxide and diamine structures.

4 Results und Discussion

The following chapter summarizes and discusses the results obtained from this PhD work. Chapter 4.1 describes the catalytic reduction of different ester moieties with gallium bromide and silanes as reducing agents, investigating the influence of different ester structures on this reaction system. In chapter 4.2, the synthesis of fully biobased aromatic polyester polyols based on 2,5-furandicarboxylic acid and different glycols as well as their applications in polyurethane rigid foams are discussed. Chapter 4.3 combines the results of the preceding chapters for the synthesis of fully biobased aliphatic polyester and polyether polyols and their further end group modifications to amine groups. Finally, the obtained diamine prepolymers are cured with epoxides based on linseed oil and lignin into fully biobased thermosets and their mechanical and thermal properties are studied.

4.1 Catalytic Reduction of Esters

In this chapter, the $GaBr_3$ catalyzed reduction of various ester structures is investigated, using different silanes as reducing agents. In chapter 4.1.1, the influence of four different aliphatic polyester structures and two reducing agents, 1,1,3,3-tetramethyldisiloxane and triethylsilane, is studied. Subsequently, the reaction conditions are optimized for possible scale-up reactions. In chapter 4.1.2, the reduction is transferred to cellulose acetate enabling a new synthesis route towards ethyl cellulose. As a result of the homogenous synthesis of cellulose acetate in a CO_2-switchable solvent system, good control of the DS is accessible, leading to the synthesis of EC with different DS.

4.1.1 Synthesis of Aliphatic Polyether Polyols *via* $GaBr_3$ catalyzed reduction of Polyesters

In the following chapter, the $GaBr_3$ catalyzed reduction of polyesters into polyethers using silanes as reducing agents, as first introduced by Sakai and coworkers[386] and later applied to triglycerides and polyesters by Meier and Biermann *et al.*[249] (chapter 2.5), is further studied. Herein, four different polyesters, obtained from short-chain dicarboxylic acids and diols, were investigated (**Scheme 34**). The influence of the polyester structure and two different reducing agents, 1,1,3,3-tetramethyldisiloxane (TMDS) and triethylsilane (TES), on the described reaction system was examined (**Scheme 34**). Finally, the reaction conditions were adjusted for possible scale-up reactions.

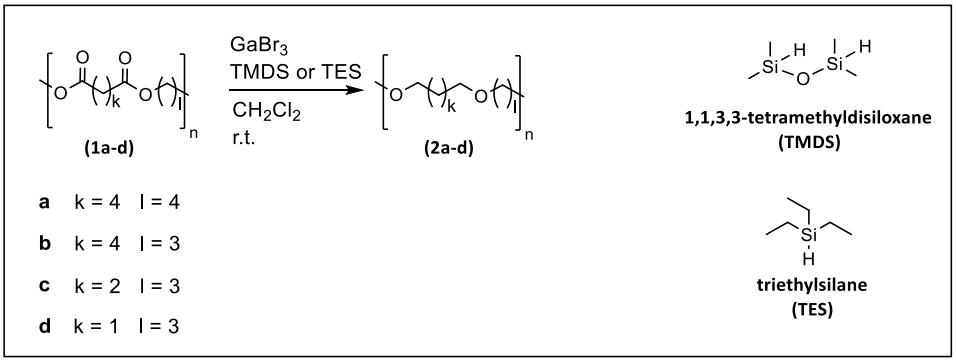

Scheme 34 Overview of the $GaBr_3$ catalyzed reduction of four different polyesters **1a-d** and the studied reducing agents.

The introduced polyesters were synthesized on a large scale *via* polycondensation of adipic (AA), succinic (SA) or malonic acid (MA) and 1,4-butanediol (BD) or 1,3-propanediol (PD) by our industrial partner BASF SE as shown in **Table 4**. Upon receiving, the obtained polyesters were fully analyzed *via* SEC-, IR-, NMR (^1H, ^{13}C) analysis and the OH and acid values were determined through titration (**Table 4**).[1] Since an application of the desired polyether polyols in PU synthesis was aimed for, generally low molecular weights, typical for polyols, were determined for all polyesters. Moreover, the degree of polymerization (X_n) for polyester **1a**, **1b** and **1d**, calculated trough the OH values, coincide with the ones determined *via* proton NMR spectroscopy, assuming only hydroxyl end groups. This assumption is in accordance with the low acid values of the polyesters (**Table 4**).

[1] The titrations of the OH and acid values were performed by BASF SE.

Table 4 Overview of the four different polyesters **1a-d**, their molecular weights as well as OH and acid values.

Poly-ester	Dicarb-oxylic acid	Diol	Acid value [mg KOH/ g]	OH value [mg KOH/ g]	X_n (OH value)	X_n[1] (NMR)	M_n[1] (NMR) [g/mol]
1a	AA	BD	0.36	110	5.0	5.1	1100
1b	AA	PD	<0.1	56.4	10.8	10.5	1950
1c	SA	PD	/[2]	/[2]	/[2]	13.3	2200
1d	MA	PD	<0.1	56.6	13.7	13.3	1950

[1]For the assumption of only OH end groups.

[2]No information provided from the manufacture.

The proton NMR spectra of polyester **1a**, **1b** and **1d** showed a strong water signal with a chemical shift of 3.33 ppm in DMSO-d_6.[2] Since gallium bromide is sensitive towards moisture, the remaining water within the polyester was removed through reprecipitation of polyesters **1a** and **1b**, while **1c** was used without further purification due to its low water content. Polyester **1d** was dried under reduced pressure, since it was a high viscous oil. For the reprecipitation, polyester **1a** and **1b** were dissolved in dichloromethane, slowly added into cold methanol, and filtered. Hereby, the precipitated polyesters were obtained in yields of 38% and 50%, respectively (**Table 5**, Fraction I). Due to the low yields, the filtrated was stored for one day at -20 °C, which led to an additional precipitation of 23% and 30% of the initially used polyester **1a** and **1b**, respectively (**Table 5**, Fraction II). Finally, the mother liquor was concentrated under reduced pressure (**Table 5**, Fraction III). In this experiment, a fundamental understanding of the fractionated precipitation was aimed for and thus, the overall yield was neglected. The alcohol end groups as well as the molecular weight have a strong impact on the solubility of the polyesters and thus, a fractionation, as also determined by SEC measurements, was observed (**Figure 5**). When *n*-hexane was used as antisolvent instead of methanol, almost quantitative precipitation and little fractionation of the molecular weight were obtained (**Figure 5**). For both solvents, the proton NMR spectra after precipitation indicated an efficient removal of the water. Therefore, *n*-hexane was used as antisolvent for further precipitations.

[2] Because DMSO-d_6 always contains some water residue, the amount of remaining water in the polyesters were not quantified.

Table 5 Precipitation fractions of polyesters **1a** and **1b** in methanol and *n*-hexane.

Antisolvent	Fraction	Description	Yield 1a [%]	Yield 1b [%]
MeOH	I	Precipitation at r.t.	38	50
	II	Precipitation at -20 °C after 24 h	23	30
	III	Concentrated mother liquor	22	10
n-hexane	-	Precipitation at r.t.	85	94

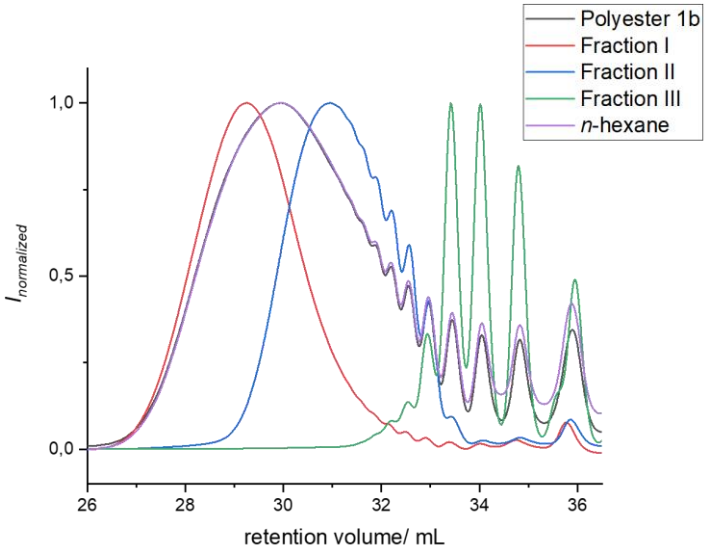

Figure 5 SEC traces of polyester **1b** and the precipitation fractions according to **Table 5**, measured in THF.

First test reactions for the reduction of the polyesters were successfully conducted using 5 mol% $GaBr_3$ and 1.10 eq. TMDS per ester group under inert conditions in DCM at room temperature. The reaction process was followed *via* IR spectroscopy and the obtained polyethers were fully analyzed (IR, ^{1}H-, ^{13}C-NMR, SEC-ESI). Following, the analysis is exemplarily shown for polyether **2b**. The successful reduction of the ester groups was indicated in the proton NMR spectrum by the shift of the signal assigned to the CH_2 group adjacent to the carboxylic group with a chemical shift of 2.35 to 1.55 ppm (**Figure 6**, signal 1 and 1'). Moreover, the chemical shift of the signal assigned to the CH_2 group adjacent to the ester oxygen (signal 3) was shifted from 4.15 to 3.45 ppm, while a new signal appeared at 3.35 ppm as a result of the reduction of the carboxylic group into a CH_2 group (signal 8'). The successful reduction was further evidenced by the vanishing C=O-vibration with a wavenumber of 1720 cm^{-1} besides an increasing C-O-C-vibration at 1107 cm^{-1} for the ether groups in the corresponding IR spectrum (**Figure 6**). Furthermore, representative masses of the desired polyether oligomers were found in

the mass spectrum of the ESI coupled SEC, whereas the difference of *m/z* for the different oligomers corresponded the mass of the repeating unit of **2b** (**Figure 7**). Two different mass distributions were observed for polyether **1b**, having either two C4 end groups, or one C4 and one C6 end group. Finally, the high-resolution mass analysis of an exemplarily chosen **2b** octamer underlined the formation of the desired polyether, since the measured exact mass as well as the isotopic pattern were identical with the calculated ones (**Figure 7**). Polyethers **2b-d** were analyzed in the same way as shown in the experimental section (chapter 6.3.1).

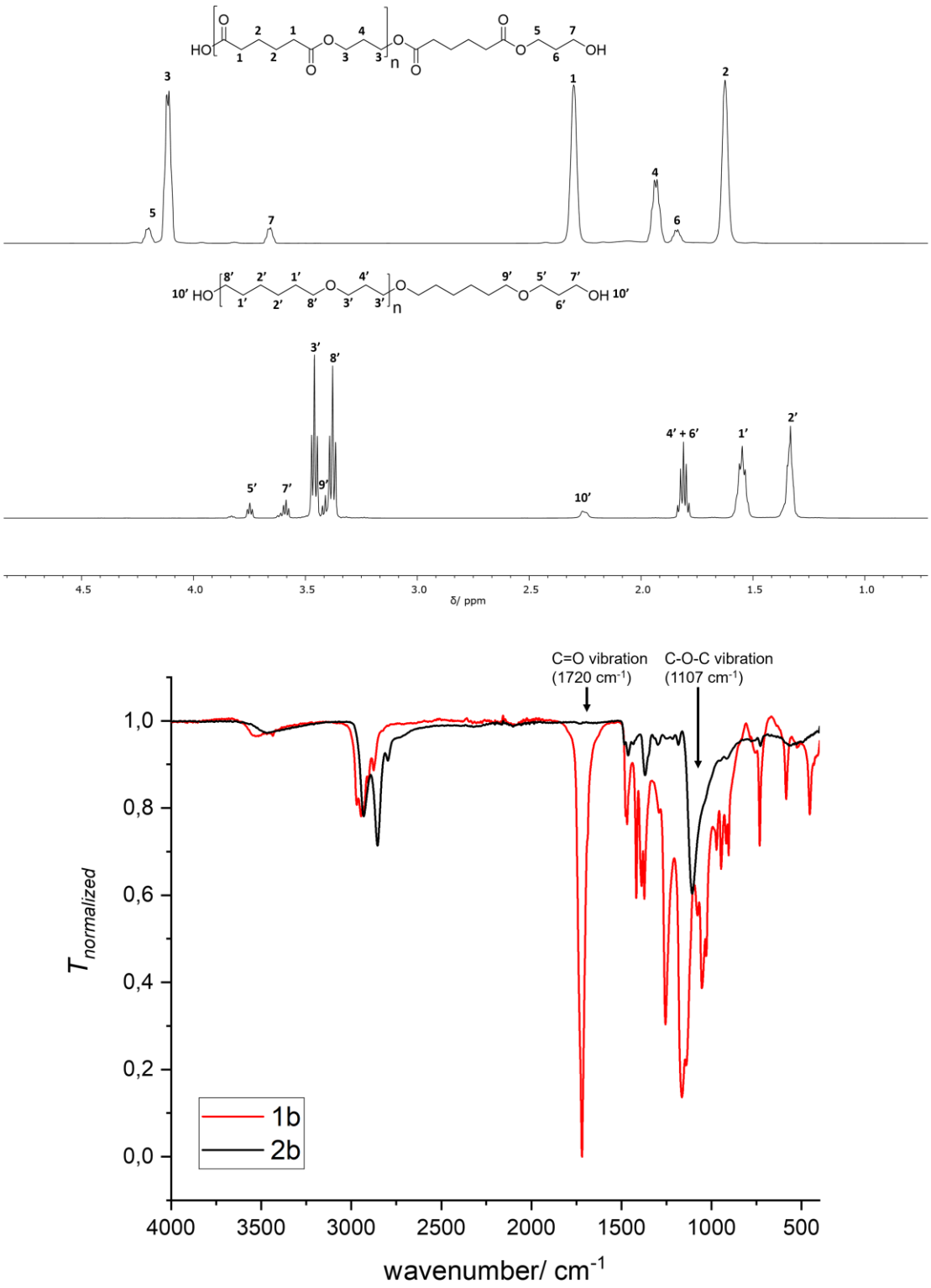

Figure 6 Top: ^{1}H-NMR analysis of polyester **1b** (top) and polyether **2b** (bottom) measured in $CDCl_3$. Bottom: normalized ATR-IR spectra of polyester **1b** (red) and polyether **2b**, referenced on the CH_2 vibration of **1b** at 2935 cm^{-1} (black).

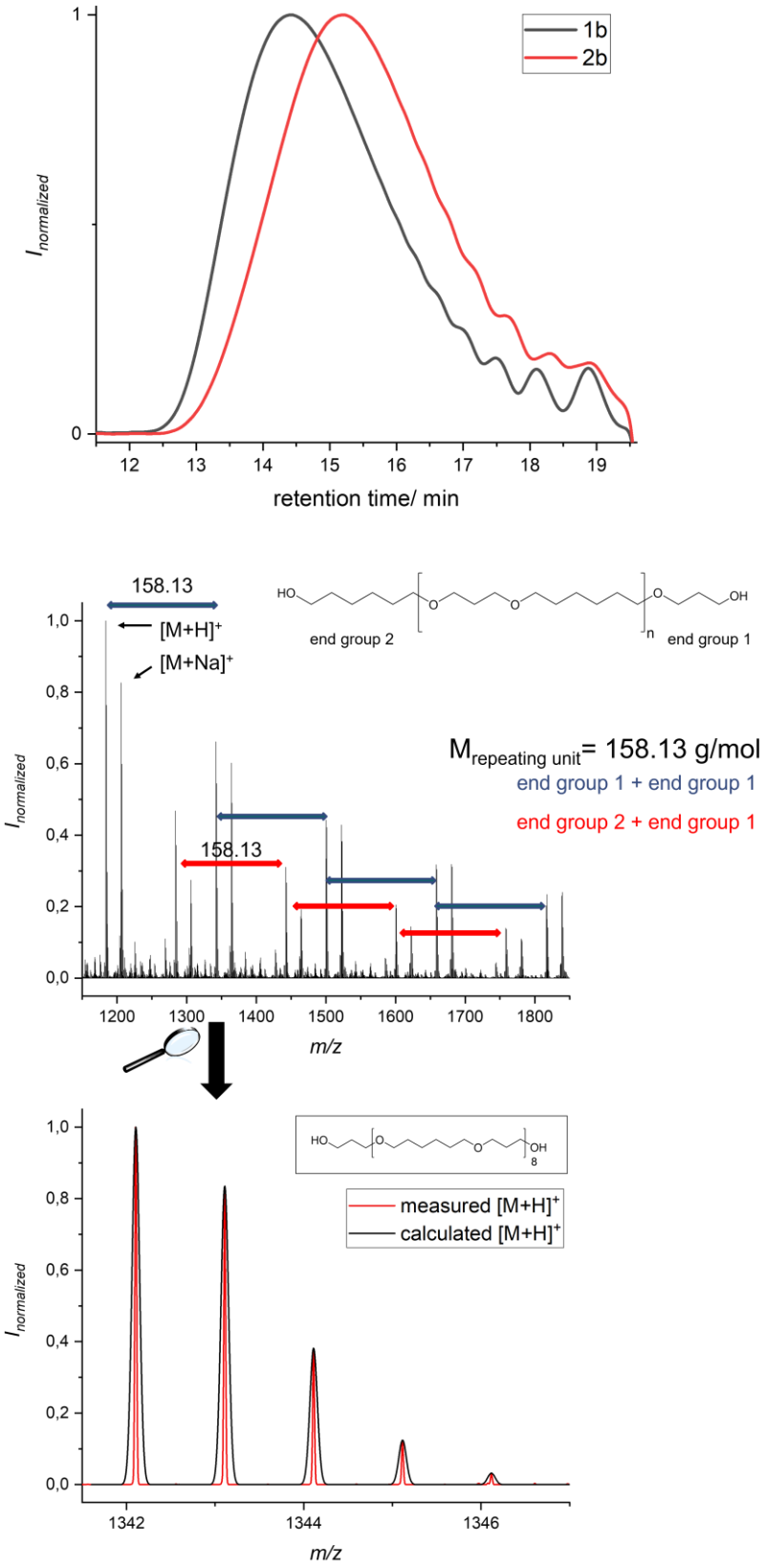

Figure 7 SEC-ESI measurement of polyester **1b** (black) and polyether **2b** (red) with corresponding ESI spectra of polyether **2b** and high resolution for an exemplarily chosen oligomer.

Subsequently, the influence of the polyester composition was investigated using 2.20 eq. of TMDS and 5 mol% $GaBr_3$ per repeating unit. Polyester **1a**, obtained from AA and BD, was less reactive than polyester **1b**, which was synthesized from AA and PD, since quantitative conversion of **1b** was observed after 24 h, while only 70% of **1a** was converted after 48 h. The conversion was determined *via* proton NMR spectroscopy by comparing signals 1 and 1' as shown in **Figure 6**. Therefore, the reaction rate was higher for the propanediol unit compared to the butanediol analogue. A possible explanation is the closer distance between the two ester groups in the polymeric backbone, which might favor the coordination of the catalyst. However, for polyether **2a**, a triplet with a typical chemical shift of a methyl group of 0.9 ppm was observed in the proton NMR spectrum (**Figure 8**). This indicates a possible overreduction of the ether to the corresponding alcohol and an alkyl end group, which is a known side reaction of this system.[249] A similar signal was not obtained for polyether **2b**, implying no overreduction of polyether **2b** under these conditions.

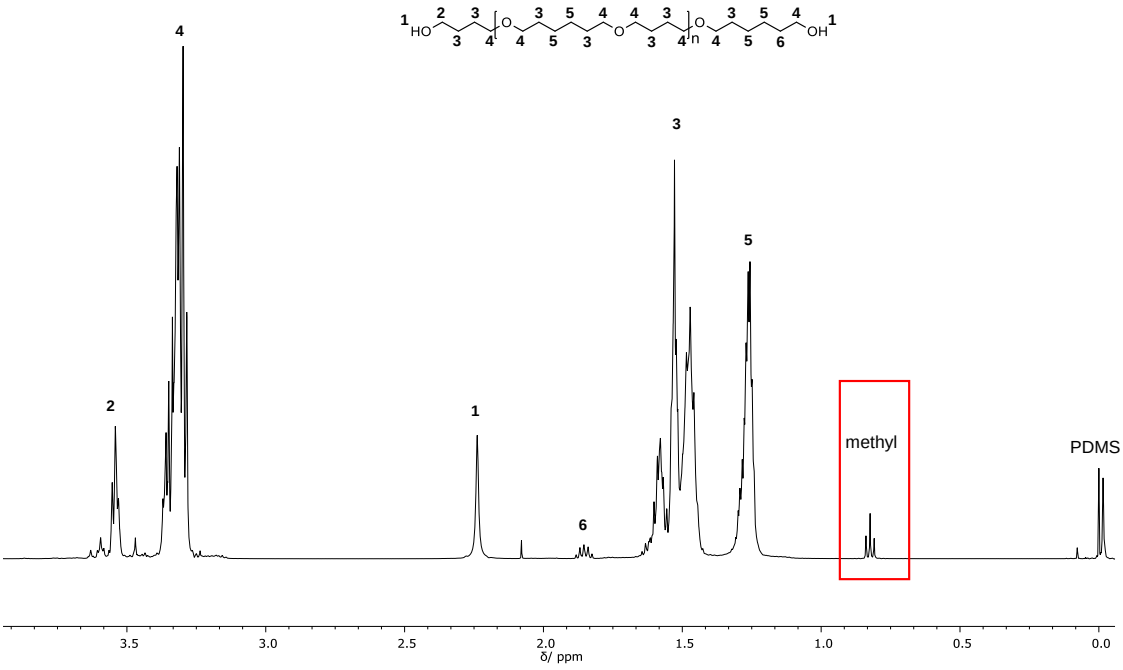

Figure 8 Exemplary ^{1}H-NMR spectrum of polyether **2a**, measured in $CDCl_3$.

Polyester **1c** showed a similar reactivity compared to **1b** and also a slight overreduction was observed due to the presence of the signal in the proton NMR spectrum with a chemical shift of 0.9 ppm. Thus, the difference between the C4 and C6 dicarboxylic acids had no significant influence on the reaction rate, while a dependency on the side reaction was indicated. The highest reactivity was observed for polyester **1d**, whereby almost quantitative conversion was obtained after four hours, as determined by IR spectroscopy.

However, a high degradation was indicated by the signal at 0.9 ppm in the ^{1}H-NMR spectrum. Thus, the difference between C3 and C4 dicarboxylic acid is strongly influencing the reaction rate of the reduction, which is in accordance with the previous observations of the C4 and C3 diol in polyester **1a** and **1b**. Summarizing, the structure of the polyester influences the reaction rate of the reduction, because an increase of the reaction speed was observed for the propanediol unit compared to the butanediol unit. Moreover, the reaction rate was the highest for malonic acid, while no difference was observed for succinic and adipic acid. Thus, the closer the polyester groups are in the polymeric backbone, the faster the reduction seems to be for similar reaction conditions. The influence on the side reactions of the four investigated polyesters is discussed later in more detail. Following, the reaction conditions using TMDS as reducing agent were varied for polyesters **1a-d** in order to establish more suitable conditions for a possible scale-up reaction. First, the concentration was increased from 20 mg polyester/mL in DCM to 50 mg/mL using 5 mol% $GaBr_3$. After 2 h, almost full conversion on a 500 mg scale for polyester **1b** was determined *via* IR spectroscopy, while 24 h were necessary in 20 mg/mL for the same results (**Table 6**, Entries 1+2). Thus, the reaction rate of the reduction was increased for a higher polyester concentration. When the catalyst loading was decreased to 1 mol%, even after five days of reaction time, only 85% of polyester **1b** was converted, as determined *via* proton NMR spectroscopy (**Table 6**, Entry 3). Hence, a higher catalyst loading seemed to be necessary, whereby almost quantitative conversion of **1b** was obtained for 2 mol% after 6 hours (**Table 6**, Entry 4). A possible reason for this strong difference in reactivity is the hydrolysis of the gallium bromide. Already traces of water lead to a high relative amount of hydrolyzed catalyst when only 1 mol% catalyst was used and as a result, the ratio of active catalyst species was probably even lower. This relative amount of hydrolyzed catalyst is decreasing the more catalyst is used.

Table 6 Optimization of the reaction conditions for possible scale-up reactions with TMDS.

Entry	Concentration [mg/mL]	*t*	mol% $GaBr_3$	Conversion [%]
1	20	24 h	5	>99[1]
2	50	2 h	5	>99[1]
3	50	5 d	1	85[2]
4	50	6 h	2	>99[1]

Conditions: 500 mg polyester **1b**, 2.20 eq. TMDS/ repeating unit, r.t., DCM.

[1]determined *via* IR spectroscopy

[2]determined *via* ^{1}H-NMR spectroscopy

The reaction conditions of 2.20 eq. and 2 mol% $GaBr_3$ per repeating unit as well as 50 mg polyester/mL DCM were applied on a 10 g scale, where longer reaction times were necessary, especially for polyester **1a**, to ensure > 99% conversion because the mixing was more difficult compared to the smaller scale. However, the reduction was successful on the larger scale and therefore, a further scale-up to 40 g polyester **1a-d** was conducted as summarized in **Table 7**. For polyester **1a**, after 64 hours neither full conversion nor any further increase of the conversion was observed and hence, 0.1 mol% additional catalyst was added. The reaction was stopped after seven and nine days, respectively, showing > 99% conversion of the ester groups (**Table 7**, Entries 1+2). Nonetheless, for polyester **1b**, quantitative conversion was obtained after 18 hours, while only 96% polyester **1c** was converted after this reaction time (**Table 7**, Entries 3+4). Therefore, the reaction was stirred over the weekend to achieve full conversion (**Table 7**, Entry 5). In general, quantitative conversion was aimed for and thus, these high reaction times were necessary, since the reaction rate was strongly decelerated for > 90% conversion. For polyesters **1a** and **1c**, a slight overreduction was indicated analogous to the previous observations on smaller scales by a methyl group in the proton NMR. The scale-up reaction of polyester **1d** showed full conversion after 18 hours, besides strong degradation of the polymeric backbone due to the mentioned side reaction (**Table 7**, Entry 6).

Table 7 Scale-up reactions of polyester **1a-d** with TMDS.

Entry	Polyester	Conversion (NMR) [%]	*t*	X_n (NMR)[1]	Yield [%]
1	**1a**	>99	9 d	2.5	22
2	**1a**	>98	7 d	3.3	42
3	**1b**	>99	18 h	10.0	72
4	**1b**	>99	18 h	10.0	54
5	**1c**	>99	4 d	6.3	97
6	**1d**	>99	18 h	1.6	51

Conditions: 40.0 g polyester, 2 mol% $GaBr_3$, 2.20 eq. TMDS, 50 mg/mL.
[1]After work-up

The major challenge of this reaction system was the separation of the polyethers from the byproduct, poly(dimethylsiloxane) PDMS, since the obtained polyethers were highly viscous liquids due to their low molecular weights and hence, precipitation was not possible. Therefore, the polyethers were dissolved in a mixture of methanol and water to then extract PDMS with petroleum ether. However, **Table 7** clearly shows, that this work-up procedure suffers from reproducibility besides overall bad yields for polyester **1a**. A reason for this is the rather good solubility of the polyether **2a** in petroleum ether and the resulting poor phase separation. In general, moderate yields were obtained for polyethers **2b** and **2d** by this procedure. This synthesis protocol was also suitable for polyester **1c** showing almost quantitative yields. However, for all polyesters except of **1b**, a degradation of the polymeric backbone through the overreduction side reaction was indicated by the X_n after work-up determined *via* proton NMR spectroscopy. Within this context, it has to be mentioned, that the analysis after the work-up procedure has to be treated with caution, since high amounts of the polyether were removed, except of polyether **2c** (**Table 7**). Also, the accuracy of the X_n determined *via* ^{1}H-NMR spectroscopy is marginally fluctuating through a slight overlap of the corresponding signals. Thus, SEC measurements were performed to strengthen these observations. The SEC traces of all polyesters **1a-d** and polyethers **2a-d** are shown in **Figure 9**, underlining the degradation observed by the decreased X_n in the proton NMR spectra of polyether **2a**, **2c** and **2d**. For polyether **2b**, no degradation was determined in the proton NMR spectrum by the missing signal of 0.9 ppm besides similar X_n for polyether and polyester. As a result of the reduction of an ester into an ether group, the molecular weight of the repeating unit is decreasing and thus, the M_n of the polyether is in general lower for the same X_n, as indicated in the SEC traces of polyester **1b** and polyether **2b**

(**Figure 9**). The influence on the side reaction is addressed later in this chapter. However, the above mentioned reaction conditions were not suitable for polyester **1d**, since the degradation of the polymeric backbone through the overreduction was too high, leading to unreactive alkyl end groups, acting as chain stoppers in further PU applications (**Figure 9**).

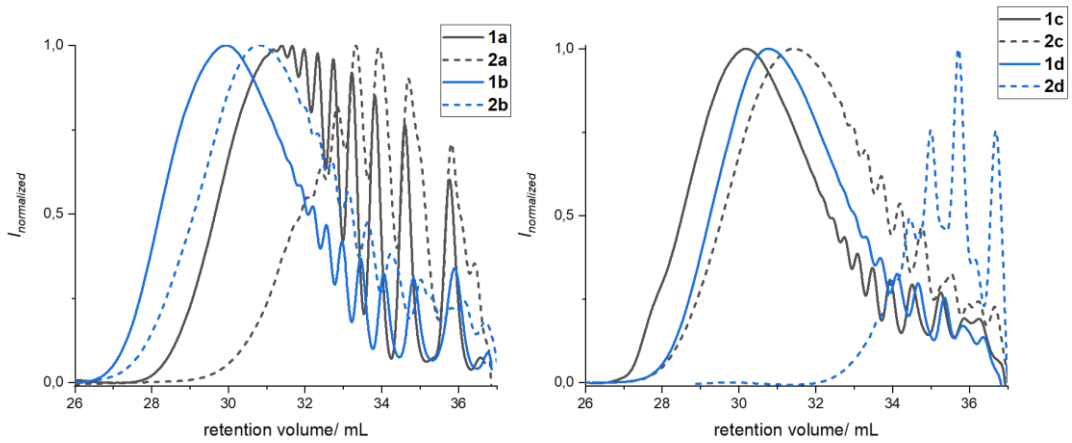

Figure 9 SEC traces of polyester **1a-d** and polyether **2a-d** according to **Table 7** after work-up, measured in THF.

Thus, a different reducing agent, triethylsilane (TES), was investigated addressing the problems during the work-up procedure, since TES is only dimerizing to hexaethyldisiloxane (HEDS) instead of polymerizing to PDMS. Therefore, the byproduct could be removed through distillation at 130 °C under reduced pressure leading to higher yields and better reproducibility. Nevertheless, under these harsh conditions, also polyethers with lower molecular weights were distilled. Another drawback is the evaporation surface issues of the distillation on a lab-scale, whereby for scale-up reactions always siloxane remained in the final polyethers. On a 500 mg approach, hexaethyldisiloxane and unreacted TES were quantitively removed.

Consecutively, the influence of TES instead of TMDS on the gallium bromide catalyzed reduction of polyester **1a-d** was studied. For all polyester **1a-d**, the reaction rate for TES was lower compared to TMDS. For instance, after 4 hours full conversion was obtained for polyester **1a** with TMDS, while only 90% of **1a** was converted for TES under the same reaction conditions. The degradation for polyester **1a-c** could not be detected due to overlapping signals of the methyl group with the TES signals in the proton NMR spectrum at 0.9 ppm and hence, only the X_n was determined. Moreover, the crude SEC traces of **1a** with TES as reducing agent showed similar retention volumes compared to the starting material, indicating a low degradation rate (**Figure 10**). The crude SEC of the reduction with TMDS showed species with way higher M_n due to the formed PDMS as a

side product (**Figure 10**). Therefore, no information was achieved through the SEC crude measurements with TMDS.

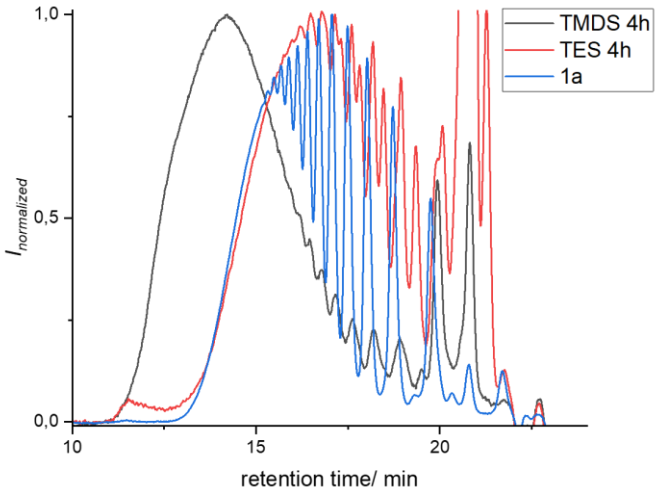

Figure 10 SEC trace of polyester **1a** compared to the crude SEC traces of the reduction of polyester **1a** with TES and TMDS after 4 hours, measured in THF.

Polyester **1b** showed full conversion already after one hour on a 500 mg scale under these reaction conditions, as determined by proton NMR spectroscopy. For the TES approach, 97% of polyester **1b** was converted after 24 hours for the same reaction conditions. Polyester **1c** showed the same trend in reactivity, while similar X_n for both reducing agents were determined *via* ^{1}H-NMR spectroscopy. This observation was further underlined through similar SEC traces after work-up. For polyester **1d**, a lower concentration and catalyst loading was applied due to the high reaction rate. Hereby, **1d** was fully converted after 4 hours with TMDS, while almost full conversion was observed for TES after 66 hours for the same reaction conditions. However, still strong degradation of polyether **2d** was detected in the proton NMR spectrum and thus, polyether **1d** was not suitable for this reaction system either.

Since for polyester **1c** no significant decrease in the side reaction for TES was observed and quantitative yields were obtained by the scale-up with TMDS besides generally higher reaction rates, TES was not further investigated as reducing agent for polyester **1c**. Additionally, for polyester **1b** no degradation besides moderate yields for the scale-up with TMDS were observed, while the reaction rate was significantly higher compared to TES. Therefore, the reaction conditions for TES were further optimized in terms of possible scale-up reactions only for polyester **1a**. The concentration was increased from 50 mg/mL up to 125 mg/mL, showing a steady increase of the reaction rate, while full conversion was obtained after 4.5 hours instead of 19 hours. Moreover, the obtained

SEC traces after work-up were both similar, indicating no difference in degradation. This observation was strengthened through similar X_n observed by ^{1}H-NMR spectroscopy. The catalyst loading was decreased to 0.5 mol% showing only 50% conversion of polyester **1a** after 96 hours. Thus, again 2 mol% were necessary, whereby almost full conversion was observed after 96 hours, determined *via* proton NMR spectroscopy. Subsequently, scale-up reactions of 50 g and 60 g polyester **1a** were successfully conducted showing full conversion of the ester groups after four and five days, respectively, determined *via* proton NMR spectroscopy (**Table 8**). However, as already mentioned before, the removal of the byproduct was more difficult due to the lower surface/ volume ratio on a lab-scale (**Table 8**). This problem can be solved by several distillations on smaller scales and combination afterwards. The X_n indicated still a small amount of side reactions leading to degradation in the polymeric backbone, while the SEC traces showed a slight shift towards higher retention times, implying a higher observed molecular weight (**Figure 11**). Since the molar mass of the repeating unit decreases during this reaction, a possible explanation is the increase of the hydrodynamic radius of the polyether compared to the polyester precursor in THF. This assumption is in accordance with the results obtained from Meier and Biermann *et al.*[249] This indicated a lower degradation compared to the scale-up reactions with TMDS (**Figure 9**). However, the SEC traces of the scale-up with TMDS and TES cannot be compared directly, since the instrument was changed during this project.

Table 8 Scale-up reactions of polyester **1a** with TES.

Entry	Scale [g]	*t* [d]	Conversion (NMR) [%]	X_n (NMR)	mol%[1] HEDS (NMR)
1	50	4	>99	3.8	14
2	60	5	>99	3.5	19

Conditions: 2 mol% $GaBr_3$, 125 mg/mL, 4.40 eq. TES

[1]per polyether repeating unit

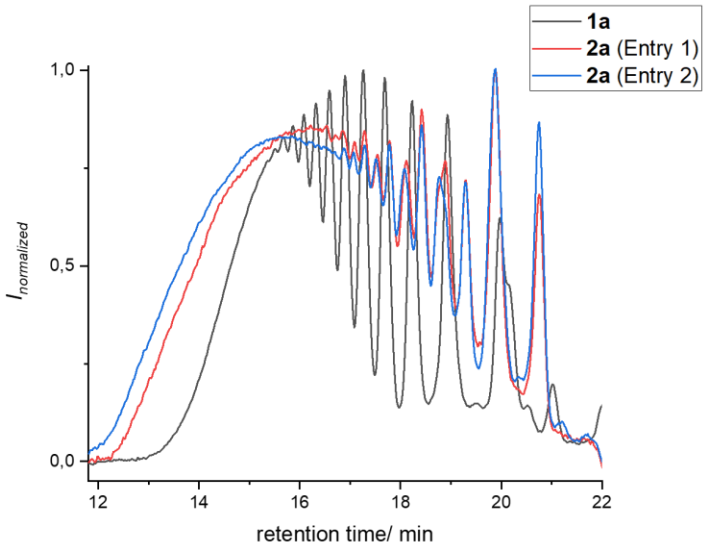

Figure 11 SEC traces of the scale-up reactions of polyester **1a** with TES according to **Table 8**, measured in THF.

The influence of different parameters such as polyester structure, reducing agent and reaction conditions on the side reaction were addressed in this paragraph. First, a high degradation was obtained for polyester **1d**, which shows the smallest distance between the ester groups in the polymeric backbone. The degradation is also accompanied by higher reaction rates and thus, the reactions were not stopped immediately after full conversion. As a result of the catalytic activity of $GaBr_3$, even for higher reaction times, and the addition of reducing agent in a small excess, this can influence the reduction of the polyether to the undesired alcohol and alkyl end group. Hence, further investigations with lower reaction rates are necessary to clarify this assumption. For polyester **1a**, a slight degradation was obtained for TMDS, while the scale-up approaches with TES indicated almost no degradation even after several days as determined *via* NMR and SEC analysis (**Figure 9** vs **Figure 11**). The signal with a chemical shift of 0.9 ppm in the proton NMR spectrum, which indicates the overreduction, was already observed when most of the polyester was converted with TMDS. Thus, for polyester **1a** no relation between overreduction and reaction time was observed for TES. However, a correlation cannot be excluded for the use of TMDS, since the overreduction is hard to quantify by crude analysis and a possible work-up may falsify the results as described before. Moreover, the concentration did not increase the degradation for TES, when the reaction was stopped immediately after full conversion, as discussed in the aforementioned paragraph. The catalyst loading showed no influence on the overreduction with TES, determined *via* SEC measurements after work-up. Nevertheless, no overreduction was indicated for polyester **1b** in the TMDS approach besides higher reaction rates compared to TES. This observation suggests that the overreduction is independent from the

reaction rate, while the polyester structure strongly influences this side reaction. For polyester **1c**, the same trend in reactivity besides similar X_n after work-up were observed for both reducing agents as determined by proton NMR and SEC analysis. Summarizing, the main influence of the overreduction is the polyester structure in combination with the reducing agent, whereby no clear trend was observed. Polyester **1a** mainly shows this side reaction when TMDS is used, while for **1b** the overreduction was not observed for this reducing agent. For **1c** and **1d** both reducing agents showed a decrease in X_n. Moreover, the side reaction was difficult to quantify through crude analysis and an effect of the reaction time cannot be excluded. In general, no influence of concentration and catalyst loading was obtained for one example. Thus, more detailed investigations on the kinetic parameters of the polyester reduction and side reaction are necessary to clarify possible trends.

In conclusion, all polyesters **1a-d** were successfully reduced to their corresponding polyether **2a-d** using two different reducing agents, TES and TMDS, catalyzed by $GaBr_3$. A scale-up reaction of up to 60 g polyester was conducted and all polyethers were fully analyzed *via* NMR-, IR-, and SEC-ESI analysis. In general, TES showed a lower reactivity compared to TMDS, while no clear trend of the influence on the side reaction was observed for both reagents. Moreover, the reduction of the ether to an alcohol, accompanied by a cleavage of the polymer backbone, was dependent on the polymer structure. Hereby, no clear tendency for the different polyester monomers were observed, but the limits of this reduction seem to be achieved for polyester **1d**, which was synthesized from malonic acid and 1,3-propanediol. Besides the reactivity, the main difference between both reducing agents was the work-up procedure. Especially for polyethers with low molecular weights, for which a precipitation was not feasible, TES was a promising reducing agent due to the possible removal by distillation, leading to almost quantitative yields. However, the removal of the side product by this work-up was limited to high surface/ volume ratios. In contrast, the liquid polyethers were dissolved in a mixture of methanol and water due to their low X_n, while PDMS was extracted with petroleum ether. However, the rather good solubility of the polyethers in petroleum ether resulted in poor phase separation depending on the polyether structure and hence, lower yields. Furthermore, for all polyethers and reducing agents, silylated end groups were obtained, lowering the reactivity of the polyols for further PU applications. To overcome this problem, an oxidation of the silyl ether end groups would be plausible. Moreover, the side reaction leading to alkyl end groups, limits the applications of the polyethers in certain fields. Nonetheless, a fundamental understanding of this reaction system was herein investigated, showing the advantages of different polyester structures, and reducing agents as well as the boundaries of this reduction protocol.

4.1.2 Catalytic Reduction of Cellulose Acetate

In this subchapter, the reduction of cellulose acetate with $GaBr_3$ and TMDS as reducing agent is described. This reaction system allows a synthesis strategy for ethyl cellulose in a more sustainable fashion than the commercial route, using alkali cellulose and ethylene chloride at high temperature under pressure (chapter 2.2.1). Since CA can be obtained with different DS through a homogeneous acetylation in a switchable solvent system (SSS) of DBU, DMSO and CO_2, this reaction enables the synthesis of EC with different DS. Herein, various reaction conditions and solvents are investigated using $GaBr_3$ as catalyst besides TMDS as reducing agent (**Scheme 35**).

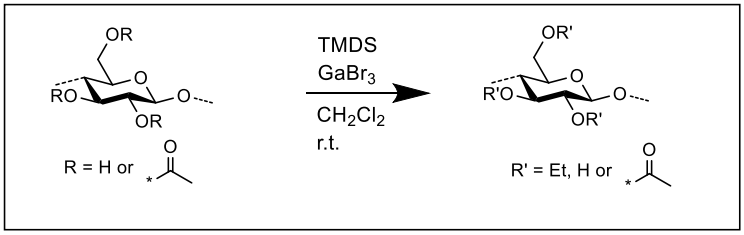

Scheme 35 Synthesis of ethyl cellulose through reduction of cellulose acetate with TMDS catalyzed by $GaBr_3$.

In a first test reaction of 20 mg CA/mL DCM (DS_{CA} = 2.8-2.9[3]), 5 mol% $GaBr_3$ and 3.30 eq. TMDS (1.10 eq. per ester group) under inter conditions, the viscous reaction mixture turned into an insoluble gel, after more than 50% TMDS was added *via* a syringe pump (**Figure 12**). IR measurement of the obtained gel showed a conversion of CA as the C=O vibration with a wavenumber of 1740 cm^{-1} decreased, accompanied by an increased C-O-C vibration at 1050 cm^{-1} (**Figure 13**). In general, the crude IR spectra cannot be normalized to a specific vibration for a better comparison, since the only constant vibration, the C-O-C vibration of the pyranose ring of the cellulose backbone, overlaps with the PMDS and ethoxy vibrations. Two further signals at a wavenumber of 790 cm^{-1} and 1260 cm^{-1} were assigned to the polysiloxane. Nonetheless, a qualitative information was obtained by the crude IR measurements.

[3] Information provided by the supplier.

Figure 12 Pictures of the reduction of cellulose acetate with TMDS catalyzed by $GaBr_3$ in DCM.

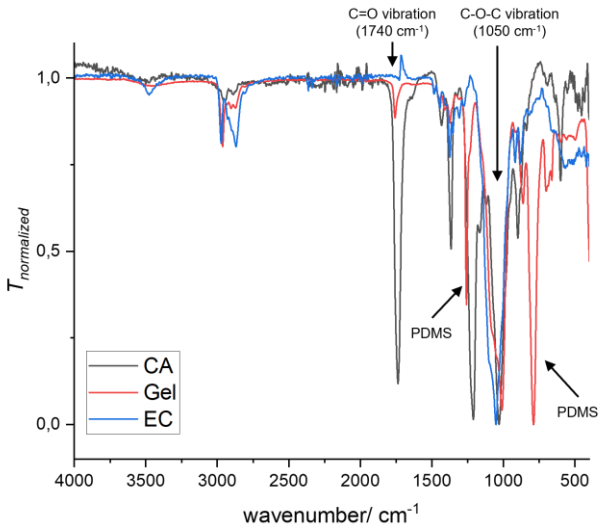

Figure 13 IR spectra of cellulose acetate (CA), the obtained gel, and commercially available ethyl cellulose (EC) as reference substance.

Next, the influence of different reaction parameters on the gel formation were studied. When the concentration was lowered from 20 mg/mL to 3.33 mg/mL, a gelation occurred showing no influence of the concentration on this phenomenon. However, for 3.33 mg/mL the gel content was smaller compared to the 20 mg/mL approach, whereby the complete reaction mixture turned into a gel. The rate of TMDS addition did not affect the gel formation, because an addition over 24 hours also yielded a gel. Furthermore, no relation between the catalyst loading and gel formation was shown, because even for 1 mol% $GaBr_3$ and a concentration of 3.33 mg/mL a gelation took place. Interestingly, already before the reducing agent was added into the reaction mixture, a slight transparent gel formation was observed, which increased with the amount of catalyst.

The size and cloudiness of the gel increased, after TMDS was added. Thus, the catalyst coordination of the cellulose acetate leads to a possible crosslinking of the cellulose backbone through strong intermolecular interactions. This assumption is discussed later in this chapter. Within this series of experiments, full conversion of the cellulose acetate was obtained for a high catalyst loading of 20 mol% $GaBr_3$, determined *via* IR spectroscopy (**Figure 14**). Moreover, the gel was filtered off after the reaction and the filtrate was concentrated under reduced pressure. The IR spectra of gel and concentrated filtrate were compared for many experiments showing no tendency of a higher conversion in any cases. Exemplary IR spectra of the concentrated filtrate and the gel for 5 mol% and 20 mol% $GaBr_3$ are depicted in **Figure 14**. Since the gelation was independent from the conversion of the CA, this arises the assumption of a fractionation of the molecular weight caused by the solubility.

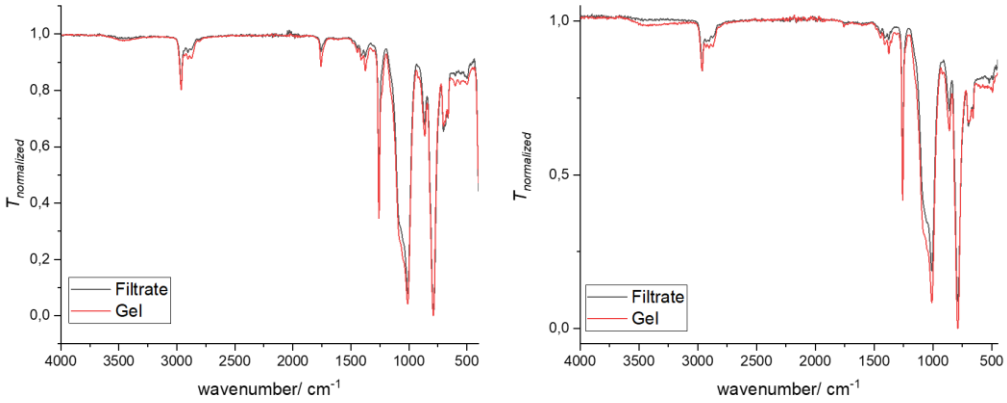

Figure 14 IR spectra of gel and concentrated filtrate for 5 mol% (left) and 20 mol% $GaBr_3$ (right).

In the following paragraph, the molecular weight and DS of the cellulose acetate, as well as the solubility, were further studied. First, the DS of three different cellulose acetates, provided from Sigma Aldrich (SA), Acros Organics (AO) and synthesized *via* the switchable solvent system (SSS) by Jonas Wolfs[4] were compared (**Table 9**). CA supplied by Sigma Aldrich showed the lowest DS of 2.6, while the CA from Acros Organics and SSS had in average 2.8-2.9 and 2.97 acetyl groups per AGU (**Table 9**).[5] Afterwards, the different CA were analyzed *via* HFIP SEC measurements (**Figure 15**). The CA from AO had the highest M_w, followed by the homogeneous synthesized CA and the one provided from SA, determined *via* PMMA standards. Subsequently, the reduction protocol was applied on CA obtained from AO and the SSS, leading in both cases to a gel, while the CA from SA was not completely soluble in DCM. Hence, the molecular

[4] Jonas Wolfs is currently a PhD student in our working group.
[5] The information of the DS from the commercial CA was provided from the supplier, while the DS of the synthesized CA was determined *via* ^{31}P-NMR spectroscopy.

weight and the slightly different DS did not influence the gel formation for the two investigated CA. Nonetheless, when the DS decreased, the solubility of the cellulose derivate in DCM also decreased, showing a lower limit of possible DS in this solvent.

Table 9 Overview of DS and molecular weight of three different CA.

Entry	CA	DS	M_n (HFIP)[1] [g/ mol]	M_w (HFIP)[1] [g/ mol]
1	AO	2.8-2.9[2]	9.3×10^{-4}	3.0×10^{-5}
2	SA	2.6[2]	4.5×10^{-4}	9.5×10^{-4}
3	SSS	2.97[3]	4.3×10^{-4}	1.6×10^{-5}

[1]Determined by PMMA standards.

[2]Information provided by supplier.

[3]Determined *via* ^{31}P-NMR spectroscopy.

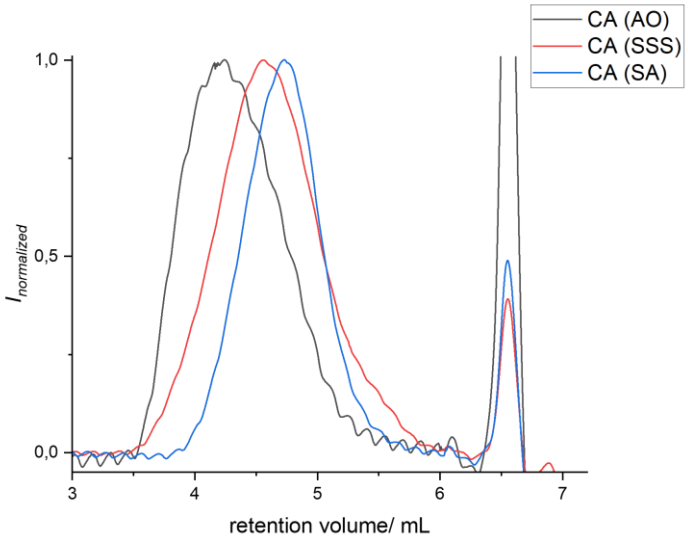

Figure 15 HFIP SEC traces of three different CA obtained from Acros Organics (AO), Sigma Aldrich (SA) and the switchable solvent system (SSS), measured in HFIP.

Following, a fundamental solubility study for the three different CA, the obtained gel and a commercially available ethyl cellulose as reference was performed. Therefore, all cellulose derivates were tried to dissolve at a concentration of 10 mg/mL in common organic solvents at room temperature for 24 hours as summarized in **Table 10**. However, for the EC no information of the DS was provided by the manufacturer, while the molecular weight was determined to $M_w = 1.6 \times 10^{-5}$ g/mol *via* HFIP SEC analysis.

Table 10 Solubility study for three different CA, EC, and the obtained gel.

Solvent	CA (SA)	CA (AO)	CA (SSS)	EC	Gel
Chloroform	X	Almost	✓	✓	X
Dichloromethane	X	✓	✓	✓	X
Diethyl ether	X	X	/[1]	X	X
Dimethyl acetamide	✓	✓	/[1]	✓	X
Dimethyl sulfoxide	✓	✓	✓	Partly	X
Hexafluoro isopropanol	✓	✓	✓	✓	X
Methanol	X	X	/[1]	✓	X
Pyridine	✓	Almost	/[1]	✓	X
Tetrahydrofuran	✓	X	X	✓	X
Toluene	Partly	Partly	/[1]	✓	X

[1]was not determined

The solubility study revealed that the DS had a strong influence on the solubility of CA, as shown by the different solubility behaviors for the CA supplied from SA compared to one form AO. For instance, for a DS higher than 2.6, CA was no longer soluble in THF, while the solubility in $CHCl_3$ and DCM increased (**Table 10**). Moreover, ethyl cellulose was soluble in many different solvents. In contrast, the obtained gel was insoluble in all investigated solvents (**Table 10**). However, no information of the DS for the reference EC was provided, which also influenced the solubility. In addition to that, the molecular weight was similar to the M_w of CA synthesized from the switchable solvent system, indicating that the insolubility was not caused by the molecular weight of the CA. However, since already a slight decrease in DS influenced the solubility of the CA in DCM a precipitation could occur as a result of an overreduction of the CA. The overreduction would lead to hydroxyl groups, but in the corresponding IR spectra of the gel no OH-vibration (2.800-3650 cm^{-1}) were observed. Moreover, this would not explain the gelation. According to the literature, EC is water soluble in the DS range of 1.0-1.5, while the solubility in organic solvents is achieved in the range of 2.4-2.5.[60] Thus, the reduction of cellulose acetate with a DS > 2.5 without overreduction should lead to EC insoluble in DCM. In contrast, the IR spectra of the concentrated filtrate indicated full conversion without visible OH-vibration, while it was still soluble in DCM (**Figure 14**). The SEC traces of the concentrated filtrate, compared to the commercial EC and CA (SSS) showed a strong decrease in the molecular weight (**Figure 16**). Concluding, a possible

explanation of the gel formation is the insolubility of EC with high molecular weights besides a DS > 2.5 in DCM.

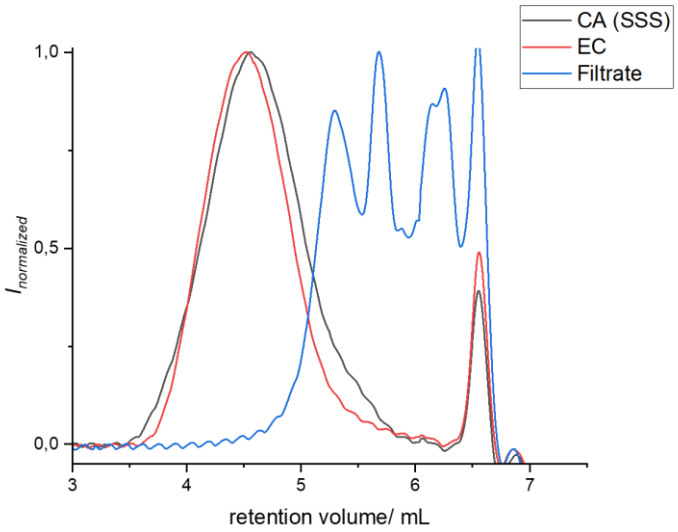

Figure 16 HFIP SEC traces of CA (SSS), commercially EC and the concentrated filtrate.

Nonetheless, the gelation of CA when only $GaBr_3$ was added without reducing agent was not explained by this assumption. As already mentioned before, this effect can be caused by strong intermolecular interactions of the cellulose backbone as a result of the close distance forced by the coordination of the catalyst. Therefore, the gel was tried to be dissolved in different strong coordinating ligands/ solvents such as acetyl acetone, potassium triflate in methanol and *N,N,N',N'',N''*-pentamethyldiethylenetriamine without any success. A possible explanation can be a diffusion problem of the ligands to the metal center, which is incorporated in the gel, and thus, this experiment do not disprove this assumption. For a better result, the ligand should be mixed with the catalyst before being added to the dissolved CA, but due to the sensitivity towards moisture of the gallium catalyst, dry solvents were necessary. As a result, different solvents were investigated, which also enable the use of the CA supplied from Sigma Aldrich with a lower DS. This may influence the solubility behavior of the EC according to the literature (**Table 11**). Even when not completely dissolved CA in DCM was applied, a gelation occurred, while the conversion was determined *via* crude IR spectroscopy (**Table 11**, Entry 1). Interestingly, when dry tetrahydrofuran (THF) or dimethyl acetamide (DMAc) were used as solvents, no gelation and reduction took place, since the catalyst was probably deactivated through the coordination of the solvents (**Table 11**, Entries 2-3). This observation strengthens the assumption of the coordination effect of the catalyst on the gelation. When toluene was used as solvent, the temperature was increased to 80 °C to fully dissolve the CA, showing no gelation besides very low conversion in the IR spectrum after several days (**Table 11**, Entry 4). A reason for this observation can be the

higher agility of the polymer chains through the increased temperatures leading to weaker intermolecular interactions.

Table 11 Investigation of different solvents for the reduction of CA supplied from Sigma Aldrich.

Entry	Solvent	*T* [°C]	CA dissolved?	Gelation?	Conversion? (IR)
1	DCM	r.t.	X	✓	✓
2	DMAc	r.t.	✓	X	X
3	THF	r.t.	✓	X	X
4	Toluene	80	✓	X	✓

Conditions: 500 mg CA (SA), 5 mol% $GaBr_3$, 10 mg/mL, 3.30 eq. TMDS

Concluding this chapter, the reduction of cellulose acetate worked for different cellulose acetates, but a gelation occurred, which limited further work-up procedures and analysis of the product. The gel formation was already observed before the reducing agent was added and showed no influence on various reaction parameters. This indicated that this phenomenon is caused strong intermolecular interactions of the cellulose backbone through the close distance of the polymer chains due to the coordination of the catalyst. This assumption is strengthened by the observations of different solvents and temperatures, where no reaction and gelation occurred in THF or DMAc, probably due to the coordination of the solvent. Moreover, an increase of the temperature to 80 °C in toluene led to a homogeneous solution as a result of the higher agility of the polymeric chains. This theory can be further investigated by adding bidentate ligands, such as acetyl acetone, in sub-stochiometric amounts to the catalyst before added to the CA solution. Another plausible assumption of the gelation is the limited solubility of the product, which also depends on the DS. According to the literature, EC should be insoluble for a DS > 2.5 in common organic solvents. However, the concentrated filtrate showed no OH-vibration in the crude IR spectrum besides full conversion of the ester vibration. This indication can be further examined through a DS determination *via* ^{31}P-NMR, requiring a possible work-up procedure such as precipitation in *n*-hexane, to remove the PDMS byproduct. Additionally, the use of TES instead of TMDS can facilitate the possible work-up procedure, since no polysiloxanes are obtained as byproducts by this reducing agent. Furthermore, the molecular weight of the soluble EC was way lower than the ones of the starting material. In addition, the IR spectra of the gel and concentrated filtrate were identical, indicating a fractionation of the molecular weight due to different solubility behavior or intramolecular interactions. In general, EC was obtained by the catalytic reducing of CA with $GaBr_3$, but further experiments and work-up procedures are necessary to understand the cause of the gelation even better.

4.2 Synthesis and Application of Fully Biobased Aromatic Polyester Polyols[6]

In this chapter, the synthesis and characterization of fully biobased aromatic polyester polyols from sugar based 2,5-furandicarboxylic acid as well as their application in polyisocyanurate foams are described. In chapter 4.3.1, different reaction conditions and glycols are investigated to obtain a processable polyol. Subsequently, scale-up reactions with the optimized reaction conditions are studied. In chapter 4.3.2., the obtained polyester polyols are applied in the synthesis of polyisocyanurate rigid foams, and their mechanical and thermal properties are described.

[6] Parts of this chapter were submitted as a manuscript to the journal ACS Applied Polymer Materials titled “A fully biobased aromatic polyester polyol for polyisocyanurate rigid foams: poly(diethylene furanoate)”.

4.2.1 Synthesis of 2,5-Furandicarboxylic Acid Based Aromatic Polyester Polyols

In this chapter, the synthesis of aromatic polyester polyols based on 2,5-furandicarboxylic acid (FDCA) with low molecular weight for subsequent application in PIR rigid foams is described. Therefore, the use of different glycols and the influence of surfactants are investigated, the reaction conditions are optimized and scaled-up on a laboratory scale.

First, FDCA was converted with biobased ethylene glycol to a fully biobased PEF (**Scheme 36**). As discussed in chapter 2.4.3, latest research aimed for high molecular weight PEF as a PET alternative. Most approaches reported in the literature were based on dimethyl furan-2,5-dicarboxylate instead of FDCA to avoid hydrolysis of the applied catalyst during the polycondensation. In this work, a very low molecular weight besides a direct use of FDCA was desired to obtain processable polyols for PU applications.

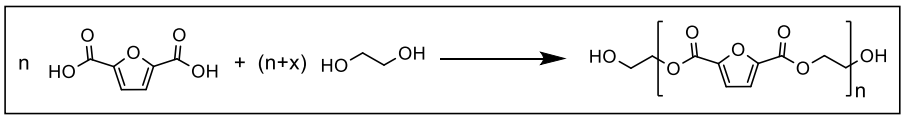

Scheme 36 Synthesis of poly(ethylene furanoate) (PEF).

Different literature protocols for the esterification and polycondensation were investigated. In a first approach, FDCA was esterified with 4.00 equivalents of EG for 2 hours under a gentle argon flow at 175 °C in the absence of a catalyst. This reaction step was followed by a polycondensation of the obtained diester under high vacuum ($1*10^{-1}$ mbar) and 175 °C for 7 hours, catalyzed by Sb_2O_3 (**Scheme 37**).[362]

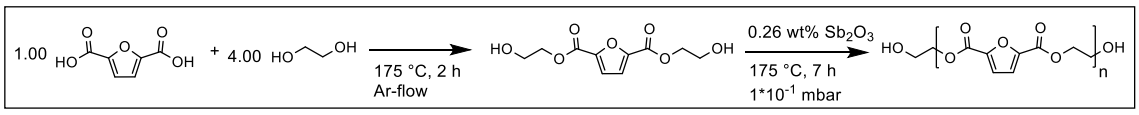

Scheme 37 Esterification of FDCA with 4.00 eq. EG and subsequent antimony(III) oxide catalyzed polycondensation.[362]

The progress of the esterification reaction was analyzed *via* ^{1}H-NMR spectroscopy. The successful reaction was confirmed by the vanishing signal of the carboxylic acid proton with a chemical shift of 13.5 ppm combined with a shift of the signal assigned to the aromatic protons of the furane ring from 7.28 ppm towards a higher chemical shift, as depicted in **Figure 17**. Furthermore, two new signals at 4.30 ppm and 3.66 ppm were observed and can be assigned to the CH_2 groups of the esterified EG unit (**Figure 17**). The aromatic region of the proton NMR spectrum showed several furan species, which can be assigned to unreacted FDCA, mono- and diesterified FDCA as well as

oligomerized ethylene furanoate as depicted in **Figure 18**. Oligomerization was also indicated by the signal with a chemical shift of 4.70 ppm from the CH_2 group of the ethylene glycol unit in the oligomeric backbone, which was shifted compared to the CH_2 groups of the end group represented by the signals at 4.30 ppm and 3.66 ppm (**Figure 18**). These observations were underlined by mass spectrometry, where masses for $[M+H]^+$ were detected for the FDCA diester (main peak), besides the monoester and the dimerized ethylene furanoate bearing two EG end groups.

The conversion of FDCA was determined *via* proton NMR spectroscopy according to **Equation 3**. For the esterification protocol depicted in **Scheme 37**, 78% of FDCA was converted, while little oligomerization occurred. Subsequently, polycondensation of the reaction mixture led to an insoluble solid and hence, neither size-exclusion chromatography (SEC) nor NMR analysis was feasible for the product. Concluding this approach, a successful esterification reaction was conducted without catalyst as was desired, but the polycondensation led to an insoluble product, indicating the formation of PEF with high molecular weights. However, for this work a processable polyol with low molecular weight was aimed for, showing that these conditions were not suitable.

Equation 3 Calculation of FDCA conversion *via* ^{1}H-NMR spectroscopy.

$$\text{conversion}\,[\%] = \left(1 - \frac{\int \mathrm{H}_{7.27\ \mathrm{ppm}}}{\int \mathrm{H}_{7.30-7.46\ \mathrm{ppm}} + \int \mathrm{H}_{7.27\ \mathrm{ppm}}}\right) * 100\%$$

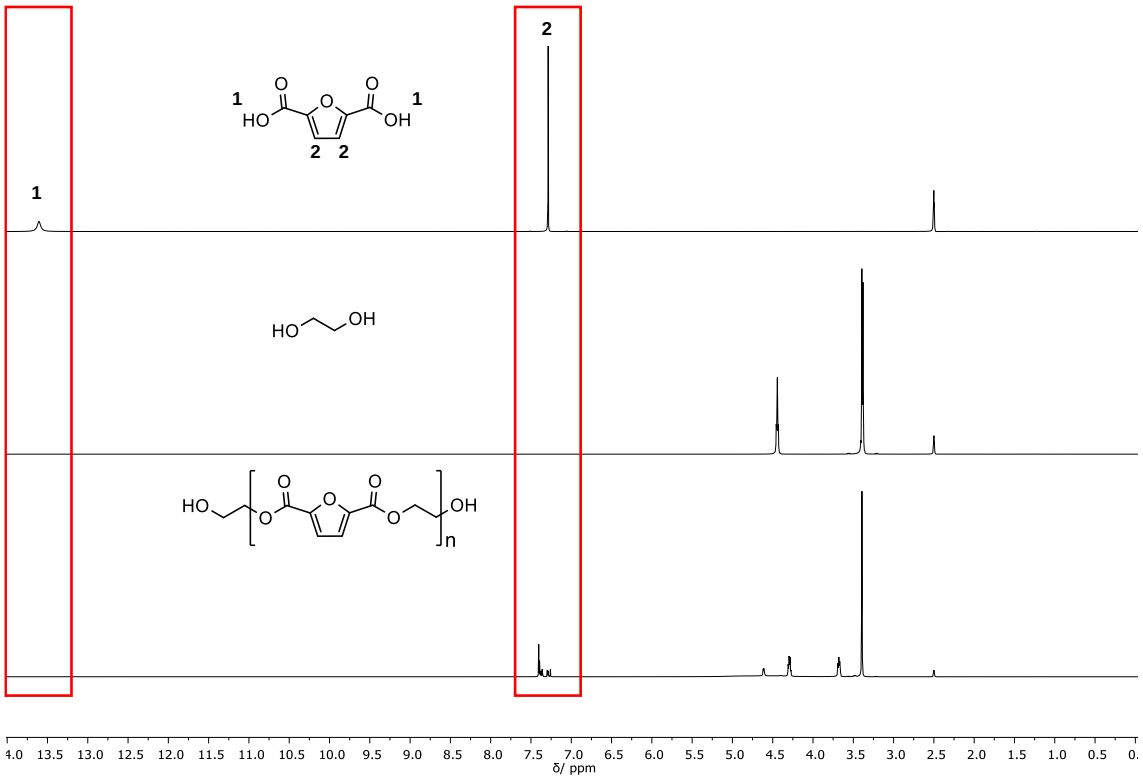

Figure 17 ^{1}H-NMR spectra of FDCA (top), EG (center) and the reaction mixture according to **Scheme 37** (bottom), measured in DMSO-d_6.

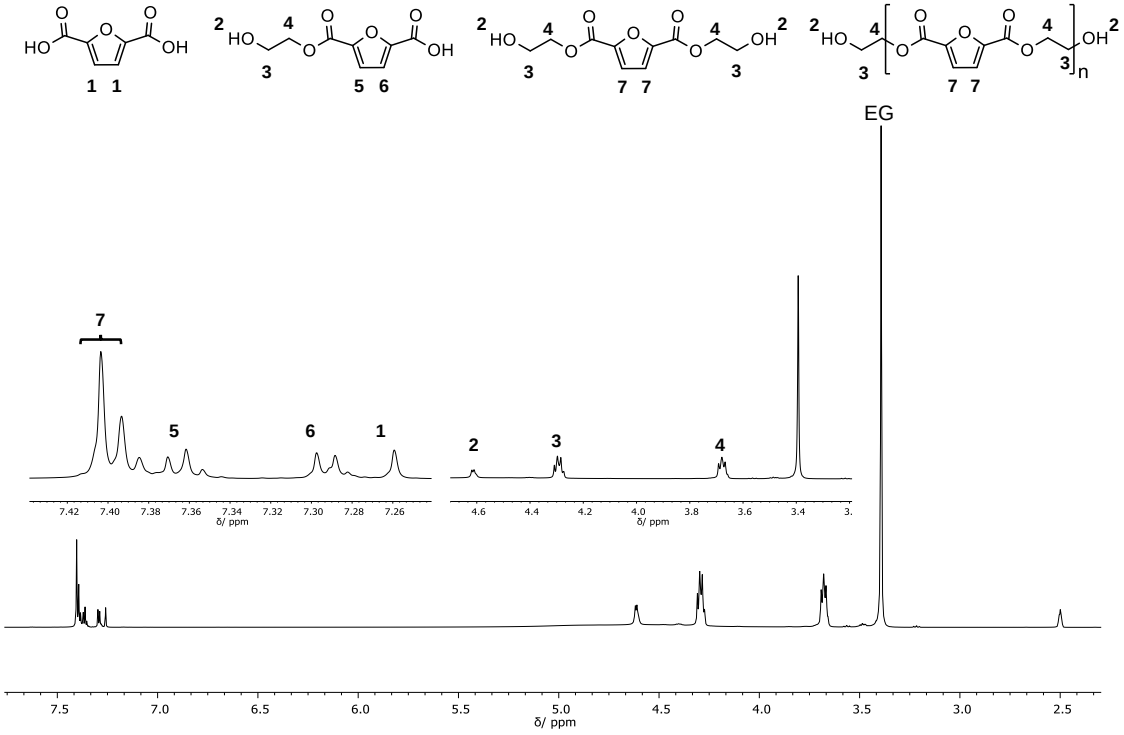

Figure 18 ^{1}H-NMR spectrum of the PEF crude mixture after the esterification step, assigning all furane species, measured in DMSO-d_6.

As an alternative approach, different conditions were investigated using 2.20 eq. EG and $Ti(O^iPr)_4$ as catalyst, while a temperature ramp of 160-190 °C was applied for 4 hours under a gentle argon flow. The consecutive polycondensation was performed at 210 °C under high vacuum ($1*10^{-1}$ mbar) for 2-2.5 hours (**Scheme 38**).[357]

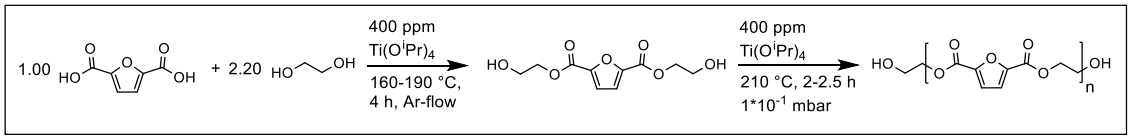

Scheme 38 Titanium(IV) isopropoxide catalyzed esterification of FDCA with 2.20 eq. EG and subsequent polycondensation.[357]

The esterification reaction was again followed *via* proton NMR spectroscopy, showing 60% conversion of FDCA besides little oligomerization, while the subsequent polycondensation reaction led once more to an insoluble product.

In a third approach, FDCA was esterified with a 100-fold excess of EG at 75 °C for 6 hours catalyzed by hydrochloric acid (**Scheme 39**).[392] Here, only 66% of FDCA was converted yielding a high ratio of mono-esterified FDCA and almost no oligomerization, determined *via* proton NMR spectroscopy.

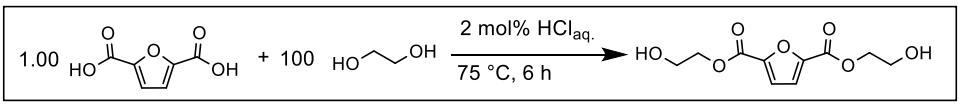

Scheme 39 Hydrochloric acid catalyzed esterification of FDCA with 100 eq. EG.[392]

Summarizing, all approaches investigated so far showed a successful esterification of FDCA with EG. When temperatures above 160 °C were applied, already oligomerization without a catalyst occurred. The conversion of FDCA was higher in the non-catalyzed approach using 4.00 eq. EG compared to the second protocol using a titanium catalyst and 2.20 eq. EG due to the linear dependency of the concentration on the reaction rate.[7] Furthermore, in both approaches, the applied argon flow suggested a removal of EG leading to a changed stoichiometric ratio during the reaction. The consecutive polycondensation led in both cases to an insoluble solid, which was not processable. The third protocol using a 100-fold excess of EG at lower temperatures is also not expedient since a high ratio of monofunctionalized FDCA and no oligomerization was obtained. Thus, this approach was not further studied.

[7] Here, it has to be mentioned that both approaches cannot be compared directly, since different reaction conditions (catalyst, temperature) were applied. Thus, the reaction constant (*k*) varied for both approaches. Moreover, a second-order reaction was assumed for the polycondensation.

$$\frac{\mathrm{d[FDCA]}}{\mathrm{dt}} = -k[\mathrm{FDCA}][\mathrm{EG}]$$

As evaporation of EG seemed to be a problem, the necessity of the applied argon flow was investigated. The reactions according to **Scheme 37** and **Scheme 38** were repeated under the same conditions except for the argon flow. For the uncatalyzed esterification at 175 °C and 4.00 eq. EG, 87% of FDCA was converted after 2 hours besides a high monoester ratio, determined *via* proton NMR spectroscopy (Entry 1, **Table 12**). For longer reaction times, the conversion of FDCA was increased to 99% while the ratio of monoester to diester and oligomer progressively decreased (Entries 2+3, **Table 12**). When the esterification reactions were performed with 2.20 eq. EG, a temperature ramp of 160-190 °C and catalyzed by either $Ti(O^iPr)_4$ or $Sn(Oct)_2$ without a continuous argon flow, only 52% and 54% of FDCA was converted for both catalysts after 4 hours (Entries 4+5, **Table 12**). Hence, the same results compared to the aforementioned esterification with a continuous argon flow were obtained, showing that an argon flow was not necessary for the herein investigated polycondensation. On the contrary, the reproducibility was increased since the stochiometric ratio was not influenced by the argon flow. However, the conversion of FDCA was lower for 2.20 eq. and catalyst compared to 4.00 eq. without catalyst for the same reaction times, while the ratio of monoester to diester and oligomer was similar for the catalyzed and non-catalyzed reactions (Entries 2+4+5, **Table 12**).

To achieve a better understanding of the influence of the catalyst on the studied reaction system, $Ti(O^iPr)_4$ and $Sn(Oct)_2$ were used under the same reaction conditions as the uncatalyzed approach (4.00 eq. EG and 175 °C). Here, full conversion of FDCA was already obtained after 6 hours accompanied by a lower monoester to diester and oligomer ratio compared to the non-catalyzed reaction, where 99% FDCA was converted after 8 hours (Entries 2+6+7, **Table 12**). Hence, the reaction rate of the esterification of FDCA and EG was probably increased if a catalyst was added, while both catalysts show a similar activity.

Table 12 Esterification of FDCA and EG for different reaction conditions without argon flow.

Entry	eq. EG	Catalyst	*T* [°C]	*t* [h]	Conversion of FDCA (NMR) [%]	Yield monoester (NMR) [%]	Yield diester + oligomer (NMR) [%]
1	4.00	/	175	2	87	39	48
2	4.00	/	175	4	87	29	58
3	4.00	/	175	8	99	16	83
4	2.20	$Ti(OiPr)_4$	160-190	4	52	17	35
5	2.20	$Sn(Oct)_2$	160-190	4	54	18	36
6	4.00	$Ti(OiPr)_4$	175	6	99	8	91
7	4.00	$Sn(Oct)_2$	175	6	99	7	92

Conditions: 1.00 eq. FDCA, 400 ppm catalyst (according to FDCA), without argon flow.

To summarize, a continuous argon flow was not necessary for the studied reaction, it even lowered the reproducibility due to removal of EG. Moreover, two industrially relevant catalysts were investigated showing a good catalytic activity.

After the first fundamental investigations on the reaction system, the molecular weight of the desired polyol was adjusted to obtain PEF with low molecular weights as a processable polyol. As described in the beginning of this chapter, a polycondensation reaction under high vacuum led to insoluble products, while oligomerization was already observed at atmospheric pressure. Therefore, the degree of polymerization (X_n) was adjusted through the molar ratio of FDCA and EG according to the Carothers equation (**Equation 4**). Hereby, a molecular weight between 400 and 1000 g/mol was aimed for.

Equation 4 Carothers equation for A-A/B-B systems with *p* = conversion and *r* = stochiometric ratio of reactants.

$$X_n = \frac{1 + r}{1 + r - 2pr}$$

$$r = \frac{N_A}{N_B} < 1$$

The influence of different stochiometric ratios, catalyst concentrations, temperatures, and reaction times on the molecular weight were studied and monitored *via* ^{1}H-NMR

spectroscopy. Consecutively, the degree of polymerization (X_n) was calculated by the ratio of the signals for the CH_2 groups assigned to the EG unit of the end group, with a chemical shift of 4.30 and 3.66 ppm, and of the polymer backbone at 4.62 ppm, respectively (**Figure 19**).[8] Then, the molecular weight was calculated using the determined degree of polymerization (**Equation 5**). The conversion of FDCA was calculated according to **Equation 3** and the mono-/ diester ratio was determined analogously by the ratio of the furan protons as assigned above (**Figure 18**).

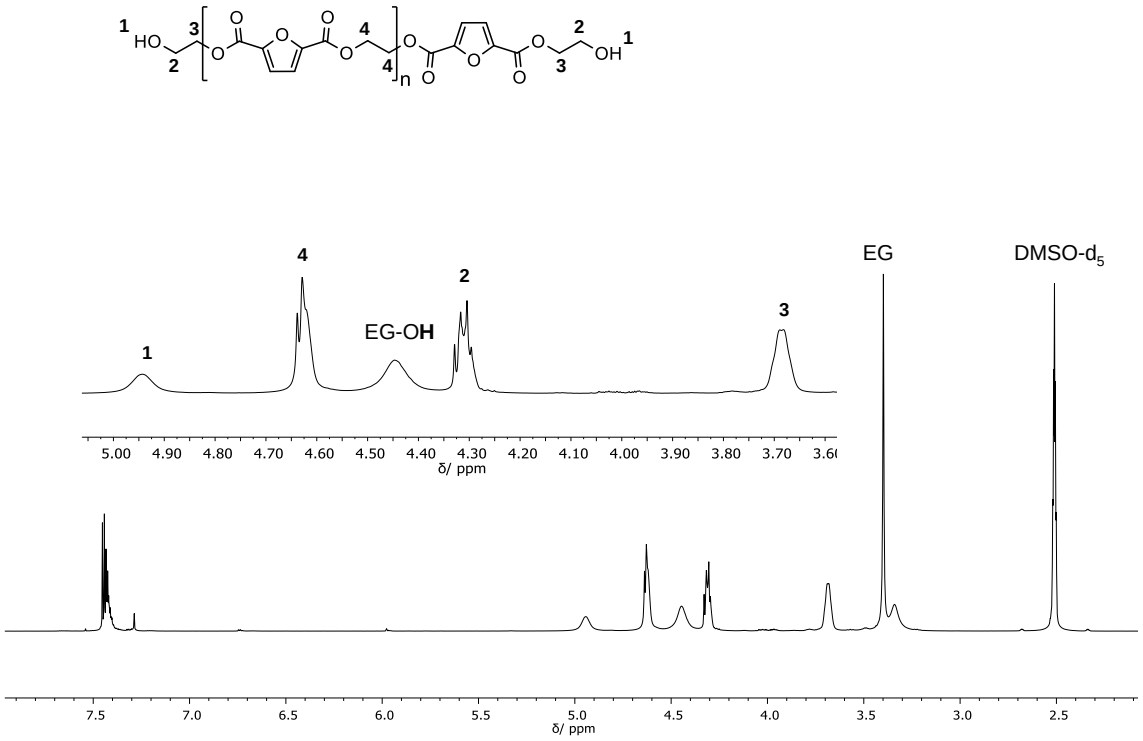

Figure 19 Exemplary ^{1}H-NMR spectrum of PEF measured in DMSO-d_6, used to determine the X_n.

Equation 5 Calculation of M_n (NMR) with X_n determined *via* ^{1}H-NMR spectroscopy, normalized on the four protons of the EG end group ($\delta_{3.66\ ppm}$), measured in DMSO-d_6.

$$M_n = M_{diester} + X_n * M_{repeating\ unit}$$

$$X_n = \frac{\int \mathrm{H}_{4.62\ \mathrm{ppm}}}{4}$$

[8] The proton NMR spectrum was normalized to four protons for the two identical signals for the C**H$_2$**OH end groups, since only EG end groups were assumed.

First screening reactions of different equivalents of EG without a catalyst and with either titanium(IV) isopropoxide or antimony(III) oxide at 175 °C for 6 hours are summarized in **Table 13**. In general, the assumption of an increasing reaction rate for the catalyzed esterification reaction was underlined by these results, where for instance only 85% FDCA was converted without catalyst for 2.00 eq. EG, while under the same conditions already 96% and 97% of FDCA were converted when a catalyst was used (Entries 2+5+8, **Table 13**). The same trend was observed for 1.50 eq. EG (Entries 3+6+9, **Table 13**).[9] In all cases, a steam formation was observed directly after titanium(IV) isopropoxide was added into the reaction mixture. This indicates that isopropanol was formed and evaporated due to a ligand exchange with EG or hydrolysis of the catalyst caused by remaining water in the EG. However, a catalytic activity was still observed. Furthermore, small differences between both applied catalysts were shown by the results in **Table 13**, because antimony(III) oxide led to a higher ratio of monoester for the same conversions of FDCA compared to titanium(IV) isopropoxide (Entries 3-9, **Table 13**).

The assumption of only EG end groups made in **Equation 5** led to falsified values for the molecular weight for less than 2.00 eq. EG and a high ratio of monoester. This is indicated by the M_n and the corresponding conversions of FDCA for Sb_2O_3 compared to the reactions without catalyst (Entries 1-3+7-9, **Table 13**). However, an increasing molecular weight was observed if the amount of EG was lowered, which is in accordance with the Carothers equation (**Equation 4**). In general, the molecular weights were low.

[9] It has to be mentioned that oligomerization was required to obtain full conversion of FDCA.

Table 13 Screening of different eq. of EG and catalysts for the polycondensation of FDCA and EG at 175 °C for 6 hours.

Entry	Eq. EG	Catalyst	Conversion of FDCA (NMR) [%]	Yield monoester (NMR) [%]	Yield diester + oligomer (NMR) [%]	M_n (NMR) [g/mol]
1	3.00	/	93	6	87	340
2	2.00	/	85	9	76	400
3	1.50	/	47	7	40	410
4	3.00	$Ti(O^iPr)_4$	98	4	94	290
5	2.00	$Ti(O^iPr)_4$	96	3	93	470
6	1.50	$Ti(O^iPr)_4$	78	7	70	430
7	3.00	Sb_2O_3[1]	98	10	88	300
8	2.00	Sb_2O_3[1]	97	20	77	320
9	1.50	Sb_2O_3[1]	79	16	63	350

Conditions: 1.00 eq. FDCA, 1 mol% catalyst, 175 °C, 6 h.

[1]Small amount of catalyst led to high weighing error.

In the following, the influence of temperature and reaction time was investigated for the approach without catalyst.[10] For longer reaction times, the conversion of monoester was increased up to 95% for 3.00 eq. EG at 175 °C accompanied by a slight increase of the molecular weight compared to 6 hours (Entries 1-2, **Table 14**). The yield of diester and oligomers was increased further when higher temperatures were applied as shown in Entry 3 of **Table 14**, while the molecular weight was similar. When the equivalents of EG were decreased to 1.50 eq., the same trend was observed, while the influence of the temperature was higher (Entries 4-6, **Table 14**). Here, also full conversions of FDCA and monoester were determined *via* proton NMR spectroscopy, implying a higher degree of oligomerization underlined by the higher molecular weight of 740 g/mol compared to 460 g/mol (Entries 5-6, **Table 14**). During this series of experiments, the color of the obtained PEF polyols changed from bright brown at 175 °C to dark brown at 200 °C, which is in accordance with the literature.[354-355] Unfortunately, all obtained products were solids despite the low molecular weights and were thus not processable as polyols for PU foams.

[10] Due to the higher conversions for the catalyzed approach, the influence of temperature and reaction time was easier to determine in the non-catalyzed reaction.

Table 14 Screening of different temperatures and reaction times without the use of a catalyst.

Entry	eq. EG	*T* [°C]	*t* [h]	Conversion of FDCA (NMR) [%]	Yield monoester (NMR) [%]	Yield diester + oligomer (NMR) [%]	M_n (NMR) [g/mol]
1	3.00	175	6	98	18	79	290
2	3.00	175	24	98	5	93	330
3	3.00	175-200[1]	24	99	0	99	310
4	1.50	175	6	47	7	40	410
5	1.50	175	24	60	9	54	460
6	1.50	175-200[1]	24	>99	0	>99	740

Conditions: 1.00 eq. FDCA, without catalyst.

[1]T was increased to 200 °C after 6 hours.

In summary, a fundamental understanding of the esterification of FDCA with EG was obtained through these investigations. The conversion increased by increasing the excess of EG, the temperature, the reaction time or by the addition of a catalyst. The molecular weight decreased when EG was added in excess according to the Carothers equation (**Equation 4**). However, the obtained PEF showed not to be a suitable aromatic polyester polyol for PU application since already low molecular weight oligomer mixtures were isolated as solids. Hence, diethylene glycol (DEG) instead of EG was subsequently investigated to obtain the desired fully biobased aromatic polyester polyol poly(diethylene furanoate) (PDEF, **Scheme 40**).

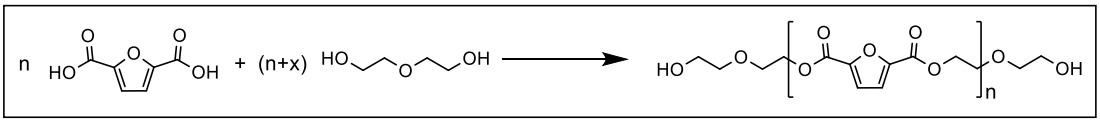

Scheme 40 Synthesis of poly(diethylene furanoate) (PDEF) from FDCA and diethylene glycol (DEG).

In a first test reaction, FDCA was reacted with 1.50 eq. DEG without catalyst at 175°C for 3 days, yielding an insoluble solid as product (**Scheme 41**).

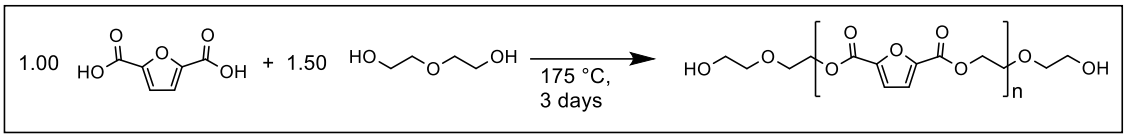

Scheme 41 Non-catalyzed synthesis of PDEF with 1.50 eq. DEG at 175 °C for 3 days.

To achieve lower molecular weights, the temperature was lowered to 100 °C, while the amount of DEG was increased to 4.00 eq. In this case, no conversion of FDCA was observed after three days. Thus, the temperature was increased to 160°C for one day yielding > 99% conversion of FDCA, determined *via* proton NMR spectroscopy. The product was again a dark brown solid but was still soluble in hot DMSO. For further investigations and optimization, a commercial aromatic polyester polyol used for PU rigid foams, based on phthalic acid and DEG (PDEP, polyol **1**), was chosen as a reference substrate. First proton NMR analysis of this commercial polyol showed 0.50 eq.[11] unreacted DEG besides several small signals in the high field indicating the use of additional surfactants or plasticizer to tune the viscosity of the final polyol (**Figure 20**).

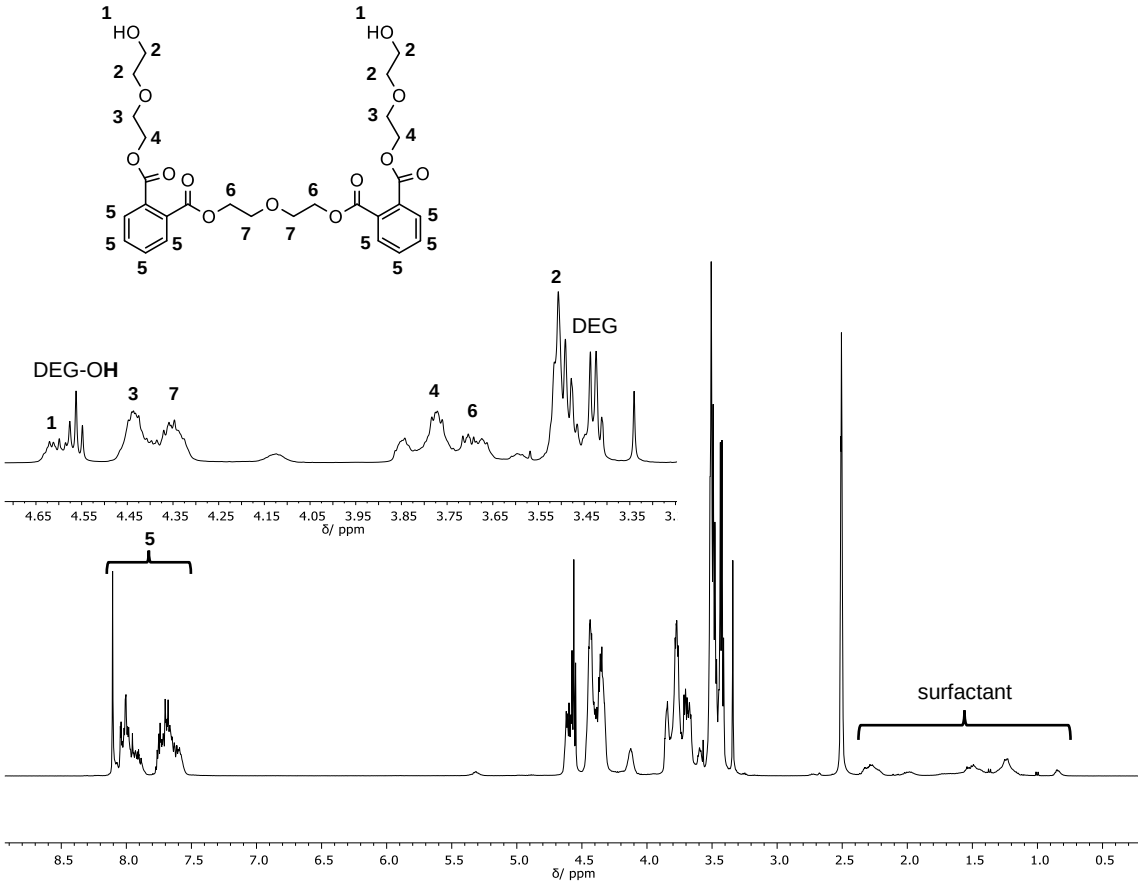

Figure 20 ^{1}H-NMR spectrum of commercial phthalic acid based polyester polyol (polyol **1**, bottom) and the zoom-in (top), measured in DMSO-d_6.

[11] Normalized on 1.00 eq. phthalic acid

Following, the major challenge was the optimization of the reaction conditions to obtain the desired PDEF (**Scheme 40**) as a processable oil. Typical OH values of commercial polyester polyols for PU rigid foams are 240 mg KOH/g, including the amount of unreacted glycol. Thus, a desirable molecular weight of the PDEF polyol was calculated to be around M_n= 470 g/mol (**Equation 6**). This M_n will underestimate the M_n of the polyester polyol since the excess of glycol was not considered in this calculation. Furthermore, the degree of polymerization X_n for the desired PDEF was calculated to X_n = 1.6 (**Equation 7**). According to the Carothers equation for A-A/B-B systems, the stoichiometric ratio of DEG and FDCA was calculated to r = 0.24 for p = 1 (**Equation 4**). However, for all practical purpose, the assumption made in **Equation 4** was not appropriate, since full conversion (p = 1) was not ensured and already small differences in conversion showed a significant impact on the observed molecular weight. Furthermore, the condensate was constantly removed to reach high conversions, whereby DEG was also partly evaporated with the formed water. Hence, the initial molar ratio will change during the reaction, influencing the molecular weight. Thus, the above calculated values provide a valuable starting point for the investigated polymerization, but the reaction conditions must be optimized by varying the amount of DEG to obtain a low excess of glycol, the desired molecular weight and a still processable viscosity.

Equation 6 Calculation of *Mn*. z = functionality of polyol.

$$M_n = \frac{z * 56.106 \frac{\mathrm{g}}{\mathrm{mol}}}{\mathrm{OH\ value}\ \left[\frac{\mathrm{mg\ KOH}}{\mathrm{g}}\right]}$$

Equation 7 Calculation of X_n.

$$X_n = \frac{M_n - M_{end\ group}}{M_{repeating\ unit}}$$

Reaction control was conducted *via* ^{1}H-NMR spectroscopy, as depicted **Figure 21**. The conversion of FDCA can be determined analogously to the PEF approaches (**Equation 3**). The degree of polymerization was calculated using the signal 5 and signal 2 from the assigned CH_2-group of the diethylene glycol unit in the polymer backbone and end group at 3.80 ppm and 3.70 ppm, respectively (**Equation 8**). The excess of unreacted DEG was determined by the isolated signal of the O(C***H*****$_2$**$CH_2OH)_2$ protons with a chemical shift of 3.40 ppm (**Equation 9**).

Equation 8 Determination of X_n *via* ^{1}H-NMR with X_n = 1 for n = 0. ^{1}H-NMR was normalized to the aromatic protons of the furan repeating unit.

$$X_n = 1 + \frac{\int \mathrm{H}_{3.80\ \mathrm{ppm\ (repeating\ unit)}}}{\int \mathrm{H}_{3.70\ \mathrm{ppm\ (end\ group)}}}$$

Equation 9 Calculation of excess DEG in wt% *via* ^{1}H-NMR. ^{1}H-NMR was normalized to the aromatic protons of the furan repeating unit.

$$wt\%\ (\mathrm{excess\ DEG}) = \frac{\left(\int \mathrm{H_{DEG}}/_4 * (n_{FDCA} + n_{comonomer}) * M_{DEG}\right)}{\sum m_{reactants}} * 100\%$$

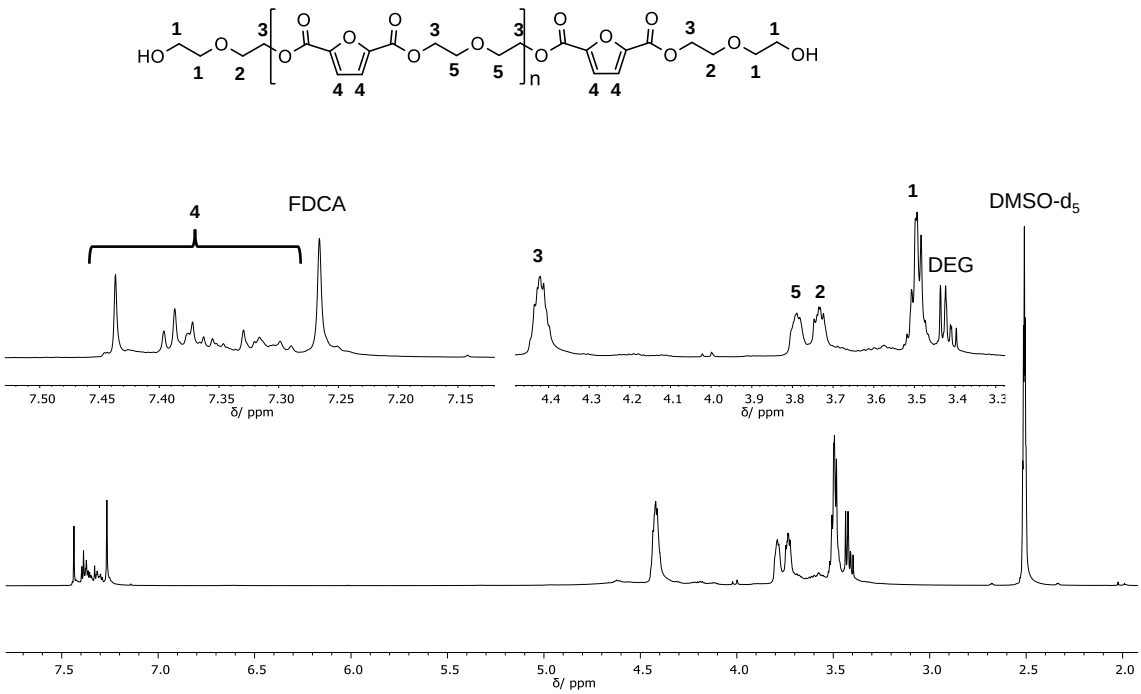

Figure 21 Exemplary ^{1}H-NMR spectrum of PDEF, used to determine the conversion of FDCA, excess of DEG and X_n, measured in DMSO-d_6.

First, the influence of titanium(IV) isopropoxide on the polymerization shown in **Scheme 40** was investigated to transfer the observed results from PEF, described above in this chapter, to PDEF. Titanium(IV) isopropoxide is a typical catalyst for the industrial synthesis of several esterification and transesterification products. The catalyst showed a good catalytic activity, enabling almost full conversion of FDCA (> 99%) after 24 hours. A reference reaction without a catalyst gave only 70% conversion of FDCA after

24 hours, clearly showing that a catalyst is beneficial. Thus, this catalyst was used for further studies.

As described above, the molar ratio of DEG and FDCA had to be adjusted experimentally to find the best agreement between full conversion, desired X_n and low excess of DEG. During this series of experiments, the reaction was stopped as soon as the heterogeneous solution of FDCA and DEG turned into a homogeneous melt. At this point, a high conversion of FDCA to the corresponding esters, bearing melting points below 160°C, was observed. After one hour, already 95% FDCA was converted using 3.00 eq. DEG, determined by ^{1}H-NMR spectroscopy through the ratio of signals with a chemical shift of 7.27 ppm and 7.30-7.46 ppm, respectively, as depicted in **Figure 21** (Entry 1, **Table 15**). Moreover, the degree of polymerization (X_n = 1.5) was close to the desired calculated one, but under these conditions 1.75 eq. unreacted DEG remained in the polyol (Entry 1, **Table 15**). X_n and excess of DEG were calculated as described above *via* the signals with a chemical shift of 3.70 ppm, 3.80 ppm and 3.40 ppm of the corresponding proton NMR (**Figure 21**, signal 2, 5 and 1). When only 2.50 eq. of DEG were used, the similar values for conversion and X_n were observed, while the excess of DEG was decreased to 1.25 eq (Entry 2,**Table 15**). Entry 3 **Table 15** showed that also Brij® L4 (**Scheme 42**) can be added as surfactant, with the aim to decrease viscosity, without a negative impact on the reaction system. The slightly lower X_n can be explained by the surfactant bearing one OH group, thus acting as chain stopper in the polycondensation. Also, the overall amount of reactive OH groups is slightly higher compared to Entry 2. The most suitable results were obtained using 2.00 eq. DEG as depicted in Entry 4 of **Table 15**, whereby the excess of DEG was lowered to 1.00 eq. Since a homogeneous solution was already observed after 35 minutes, only 85% of the dicarboxylic acid was converted and hence, the amount of unreacted DEG was further decreased for higher conversions. When longer reaction times were applied, the conversion of FDCA was increased to up to 99%, accompanied by an increased X_n of 1.7, while the excess of DEG was lowered to 0.75 eq. after 2.5 hours. All polyols that were obtained in this series of experiments were high viscous oils enabling the application for PU rigid foams.

Table 15 Optimization of reactions conditions for the synthesis of PDEF using different eq. of DEG.

Entry	Glycol	*t*	Conversion FDCA (NMR) [%]	X_n (NMR)	Excess of DEG (NMR) [wt%]	Excess of DEG (NMR) [eq.]
1	3.00 eq. DEG	1 h	95	1.5	38	1.75
2	2.50 eq. DEG	1 h	94	1.5	30	1.25
3	2.50 eq. DEG 0.10 eq. Brij® L4	1 h	95	1.4	28	1.25
4	2.00 eq. DEG	35 min	85	1.5	28	1.00

Conditions: 1.00 eq. FDCA (1.00 g), 5 mol% $Ti(O^iPr)_4$, 160 °C.

The viscosity of the polyester polyol was further decreased by copolymerization of biobased aliphatic dicarboxylic acids such as succinic acid (SA, **Scheme 42**) or adipic acid (AA, **Scheme 42**), while maintaining the fully biobased character of the polyol. Entries 1 and 2 of **Table 16** showed almost full conversion of FDCA and SA or AA, while the degree of polymerization was as desired. For the approach using succinic acid, the excess of DEG was slightly higher, related to not fully converted FDCA. In general, longer reaction times were necessary compared to the results described in **Table 15**, due to a scale-up to almost 5.00 g dicarboxylic acid, which made the mixing with a magnetic stirrer more difficult. Another approach was the copolymerization of phthalic acid (PA, **Scheme 42**) to maintain the fully aromatic character of the dicarboxylic acid. In that case, the polyol was no longer fully biobased due to the petroleum based phthalic acid. Entry 3 of **Table 16** showed full conversion of FDCA and PA besides 0.55 eq. excess of DEG. However, the degree of polymerization cannot be determined due to overlapping signals in the proton NMR spectrum. For this study, a fully biobased character was aimed for and thus, copolymerization of a petroleum based aromatic carboxylic acid was not further studied.

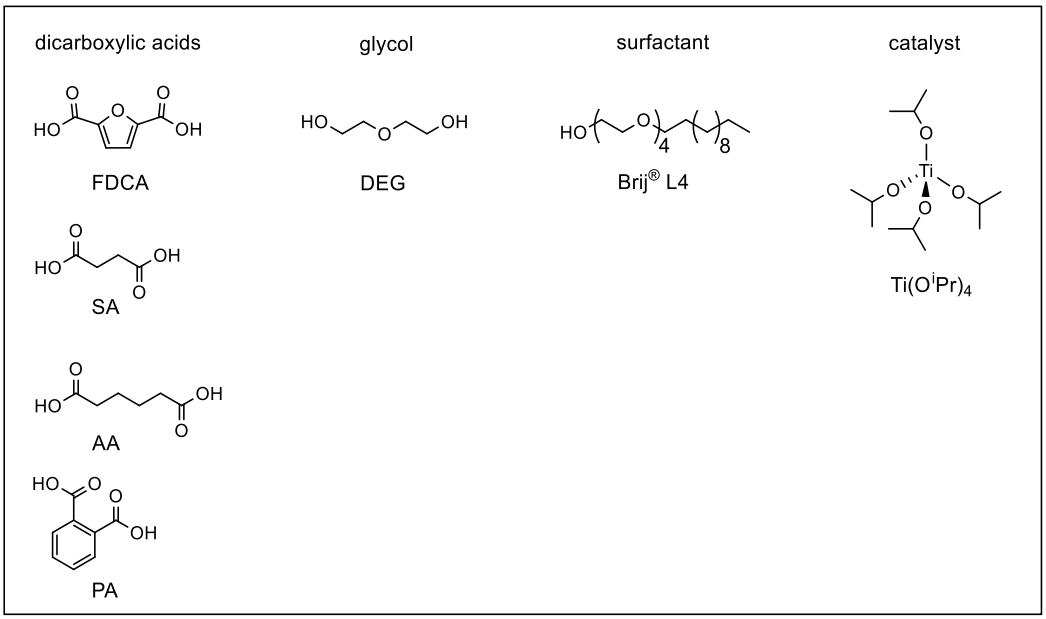

Scheme 42 Structural overview of used chemicals for the oligomerization of FDCA.

Table 16 Copolymerization of different dicarboxylic acids with FDCA.

Entry	Comonomer	Conversion FDCA/ Comonomer (NMR) [%]	X_n (NMR)	Excess of DEG (NMR) [wt%]	Excess of DEG (NMR) [eq.]
1	0.20 eq. AA	>99/>99	1.6	21	0.75 eq.
2	0.20 eq. SA	95/>99	1.6	25	0.90 eq.
3	0.20 eq. PA	>99/>99	/[1]	15	0.55 eq

Conditions: 0.80 eq. FDCA (4.00 g), 2.00 eq. DEG, 5 mol% $Ti(O^iPr)_4$, 160 °C, 44-66 h.

[1]could not be determined due to overlapping signals.

For a subsequent PU synthesis, the next step was a scale-up of selected reactions up to 100 g dicarboxylic acid, which was successfully conducted applying the optimized conditions for a homopolymer of FDCA (polyol **2**) and copolymers containing 10 mol% of either SA (polyol **3**) or AA (polyol **4**, **Table 17**). The polycondensation was stirred for two to six days to ensure full conversion of the carboxylic acid groups since the presence of a carboxylic acid group would deactivate the amine catalyst for the PU foaming, as also observed herein. The mixing on a lab scale for these scale-up reactions was less efficient than on a smaller scale. However, even after the long reaction times that were applied, the X_n remained in the range of the desired value, showing a good control of the molecular weight under the optimized reaction conditions. This observation was

confirmed by the SEC traces of polyols **2-4** (**Figure 22**). Furthermore, the amount of unreacted DEG was similar to the commercial polyol **1** (**Table 17**). As already mentioned in the beginning of this chapter, the desired degree of polymerization was slightly underestimated, since measured OH values also considered the excess of DEG remaining in the polyol. This was shown by the comparison of the SEC traces of the commercial polyol **1** (black) and the fully biobased polyester polyols **2-4** (**Figure 22**). A comparison of the determined OH values *via* proton NMR spectroscopy without DEG and the measured ones including the unreacted DEG is shown in **Table 17**. As expected, the measured values of 300-350 mg KOH/g were higher than of the commercial polyol **1** (**Table 17**), but especially for this system higher OH values are necessary as higher X_n led to highly viscous and therefore not processable PDEF. Moreover, the OH values determined *via* ^{1}H-NMR spectroscopy can be correlated to the measured ones proving that this method is suitable.

Table 17 Scale-up reactions of polyol synthesis using FDCA as well as FDCA with 10 mol% of SA or AA.

Polyol	Dicarboxylic acids	X_n (NMR)	Excess of DEG (NMR) [wt%]	Excess of DEG (NMR) [eq.]	OH (NMR) excluding excess of DEG [mg KOH/g]	OH (measured) including excess of DEG [mg KOH/g]
1	PA[2]	/[3]	16	0.5	/[3]	240
2[1]	1.00 eq. FDCA	1.8	19	0.7	210	364
3[1]	0.90 eq. FDCA 0.10 eq. SA	2.0	17	0.6	220	330
4[1]	0.90 eq. FDCA 0.10 eq AA	1.7	20	0.7	230	350

[1]**Conditions:** 1.00 eq. FDCA (100 g), 2.00 eq. DEG, 5 mol% $Ti(O^iPr)_4$, 160 °C, 2-6 days.

[2]no further information provided by the manufacturer.

[3]not determined due to overlapping signals in the proton NMR.

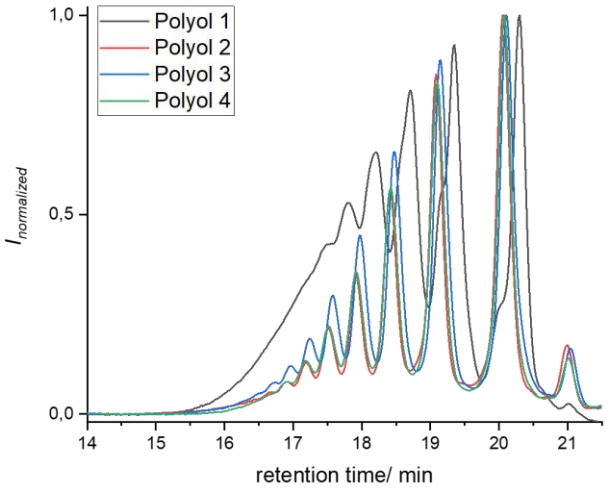

Figure 22 SEC traces of the commercial polyester polyol PDEP (polyol **1**) and the final biobased polyester polyols **2-4**, measured in THF.

In conclusion, a new one-pot synthesis route towards biobased aromatic polyester polyols with low molecular weights based on FDCA and two glycols, EG and DEG, was investigated. The use of EG led to insoluble, not processable polyols. The reaction conditions of the polycondensation of FDCA and DEG were optimized in terms of degree of polymerization and excess of remaining DEG to ensure a still processable, viscous polyol. The surfactant Brij® L4 could be added to the reaction mixture without negative impact on the reaction system, decreasing the viscosity even further. The reduced viscosity was also achieved by either copolymerizing 10-20 mol% of a biobased aliphatic dicarboxylic acid (SA/ AA), maintaining the fully biobased character of the polyol, or copolymerizing phthalic acid instead. The polyol synthesis was scaled-up to 100 g of dicarboxylic acid, still showing a good control of the molecular weight. The measured OH values were slightly higher compared to the commercial reference polyol PDEP, but higher X_n would have led to not processable PDEF polyols.

4.2.2 Application of 2,5-Furandicarboxylic Acid Based Aromatic Polyester Polyols for Polyisocyanurate Rigid Foams

The fully biobased polyols **2-4** are processed with methylene diphenyl diisocyanate (MDI) to PIR rigid foams. The synthesis and analysis of the PIR foams were performed by our industrial partner puren gmbh. For the synthesis, two different, well established, procedures using either a stoichiometric ratio of isocyanate to polyol of 3:1 or 2:1, were applied. Different thermal and mechanical properties are obtained through a higher isocyanate excess due to more isocyanurate structures in the final PU foam. For the 2:1 approach, the mixing and processing is better, besides an increased biobased content compared to the procedure using 3.00 eq. isocyanate per polyol. To increase the mixability of polyol, isocyanate, and pentane, 15 mol% of a commercial trifunctional polyether polyol (polyol **5**) is added to the mixture using a threefold excess of isocyanate.

All three biobased polyols showed a suitable reactivity for both procedures, since a good and very fast foaming took place, also in comparison to the commercial polyol **1**. The reaction between polyol **2** and MDI started 20 seconds after mixing both components, as shown on the left-hand side of **Figure 23**. The fast foaming can be observed in the center of **Figure 23**, while after 50 seconds, the foaming was completed (right-hand side, **Figure 23**). Polyols **3** and **4** showed similar reactivity. In all foams, the through-hardening was very fast.

Figure 23 Foaming of polyol **2** with MDI. Left: 25 seconds after addition of MDI, center 30 seconds after addition of MDI, right: final foam 50 seconds after addition of MDI

Finally, important properties of the obtained PIR rigid foams were investigated. It has to be mentioned that the amount of FDCA based polyester polyols enabled only one experiment for each procedure. Thus, absolute values must be caught with caution but a good relative comparison between the herein investigated fully biobased and the commercial petroleum based polyols was observed. Moreover, the exact procedure must

be optimized and adjusted for every polyol and application in terms of water content, amount of flame retardant and catalyst.

The PIR foam synthesized from the 2:1 procedure of the fully biobased PDEF polyol (polyol **2**) showed similar thermal conductivity at 23 °C ($\lambda_{23°C}$) and flame behavior compared to the petroleum based polyol **1** (Entries 1+2, **Table 18**). The pentane miscibility or the reaction rate and therefore the reaction heat of both reaction mixtures was marginally different due to a slightly increased density of the FDCA based polyol **2** compared to polyol **1** (Entries 1+2, **Table 18**). The compressive strength in rising direction (σ_m) was lower for polyol **2** (203 kPa), compared to the commercial polyol **1** (255 kPa) due to the higher OH value and viscosity of polyol **2**. The PIR foam obtained from the AA copolymerized polyol (polyol **4**) showed a similar density, thermal conductivity and flame behavior compared to polyol **2** (Entries 2+4, **Table 18**). The compressive strength for polyol 4 (261 kPa) was higher than for the FDCA homopolymer (203 kPa), which goes along with decreased viscosity, as already discussed before (Entries 2+4, **Table 18**). However, the density, thermal conductivity, and mechanical properties of the PIR foams obtained by the copolymerized polyols **3** and **4** were slightly different (Entries 3-4, **Table 18**). Since only 10 mol% of aliphatic dicarboxylic acid were added during the polyol synthesis, it was very unlikely that these observations were caused by the different structures of the succinic acid in polyol **3** compared to the adipic acid in polyol **4**. A better mixing during the PIR foaming was more likely and thus, the foaming must be repeated for a better validity. However, an overall comparison of all mechanical and thermal properties of the PIR foams obtained by the biobased polyols **2-4** and the commercial polyol **1** showed similar results (Entries 1-4, **Table 18**).

In the following, the mechanical and thermal properties of the PIR foams obtained by the procedure using a threefold excess of isocyanate were analyzed (Entries 5-8, **Table 18**). The PIR foam of polyol **2** showed a similar thermal conductivity (23.1 mW/m*K) and compressive strength (296 kPa) compared to the commercial polyol **1** (23.4 mW/m*K and 283 kPa), besides an identical density of 33.4 kg/m^3 (Entries 5-6, **Table 18**). The flame behavior was slightly better for the commercial polyol **1**, which can be explained by a higher oxygen content of polyol **2** due to the furan ring in the polyester backbone (Entries 5-6, **Table 18**). At the same time, the influence of 10 mol% biobased aliphatic carboxylic acid in the PIR foam from polyol **3** and **4**, compared to polyol **2**, was only marginal. The density was slightly lower, although the thermal conductivity and σ_m was marginally increased, while showing the same flame behavior (Entries 6-8, **Table 18**).

Table 18 Thermal and mechanical properties of the PIR rigid foams for polyols **1-4**.

Entry	Polyol	Ratio of isocyanate/ polyol	Density [kg/m^3]	$\lambda_{23°C}$[1] [mW/ m*K]	Highest flame within 20 sec [cm]	σ_m[2] [kPa]
1	polyol **1**	2	31.2	23.4	14	255
2	polyol **2**	2	33.5	23.3	15	203
3	polyol **3**	2	36.1	22.8	14	238
4	polyol **4**	2	33.3	23.3	15	261
5	0.85 eq. polyol **1** 0.15 eq. polyol **5**[3]	3	33.4	23.4	10	283
6	0.85 eq. polyol **2** 0.15 eq. polyol **5**[3]	3	33.4	23.1	13	296
7	0.85 eq. polyol **3** 0.15 eq. polyol **5**[3]	3	32.4	23.5	13	300
8	0.85 eq. polyol **4** 0.15 eq. polyol **5**[3]	3	32.3	23.9	13	309

[1]thermal conductivity at 23°C

[2]compressive strength in rising direction

[3]commercial trifunctional polyether polyol

Summarizing, the herein introduced fully biobased polyester polyols showed high reactivity with MDI and the through-hardening was fast. Application tests of the PIR foams obtained from the fully biobased polyols **2-4** synthesized by the procedure using a threefold excess of isocyanate besides 15 mol% of a commercial trifunctional polyether polyol showed similar density, thermal conductivity, and mechanical properties compared the PIR foam from the commercial polyol **1**. The flame behavior was slightly better for the phthalic acid based polyol due to a higher oxygen content of the furan unit in the polymer backbone for polyols **2-4**. Thus, the commercial petroleum based polyol can be substituted by the FDCA based polyol and the processibility was increased through succinic or adipic acid copolymerized polyols due to slightly lower viscosities. However, in this approach the biobased content of the final PIR foam was rather low. This was increased by a different procedure using a twofold excess of isocyanate per polyol, whereby no additional polyether polyol was necessary. The mechanical and thermal properties were similar for the different polyols but fluctuated and thus, these

observation must be strengthened through reproduction. Nonetheless, these results showed a possible substitution of the petroleum based polyol through the fully biobased aromatic polyester polyols PDEF for certain industrial applications.

4.3 Synthesis and Modification of Aliphatic Polyether and Polyester Polyols for Application in Thermosets

The synthesis and analysis of fully biobased polyester and polyether diamines from different renewable dicarboxylic acids, 1,4-butanediol and 10-undecylenic acid is described in chapter 4.3.1. The optimized reaction conditions for the polycondensation reaction from chapter 4.2.1 as well as for the $GaBr_3$ catalyzed reduction of polyesters from chapter 4.1.1 are applied in this synthesis route. In chapter 4.3.2, the diamine prepolymers are cured with epoxidized linseed oil and epoxidized lignin, yielding fully biobased aliphatic and aromatic thermosets. Hereby, the influence of the different epoxide structures and reactivities as well as the influence of the different polymeric backbones of the diamine prepolymers on the thermal and mechanical properties of the cured material are investigated.

4.3.1 Synthesis and Characterization of Biobased Aliphatic Polyether and Polyester Diamines

In this chapter, a new synthesis route towards fully biobased aliphatic polyether and polyester diamines for subsequent application in thermosets is described. This strategy is based on a polycondensation of different dicarboxylic acids and 1,4-butanediol, whereby 10-undecylenic acid was added as monofunctional monomer, i.e. “chain stopper”, to obtain double bond end groups. Following, the end group modified polyesters were divided into two fractions, whereof one was reduced to the corresponding polyethers *via* the $GaBr_3$ catalyzed reaction system, as extensively studied in chapter 4.1.1. Finally, the end groups of all polyethers and polyesters were converted into amine groups through a thiol-ene reaction with cysteamine hydrochloride. An overview of the synthesis route is given in **Scheme 43**. Since 10-undecylenic acid is a pyrolysis product of ricinoleic acid and cysteamine can be synthesized through the decarboxylation of cysteine, the obtained polymeric diamines are fully biobased.

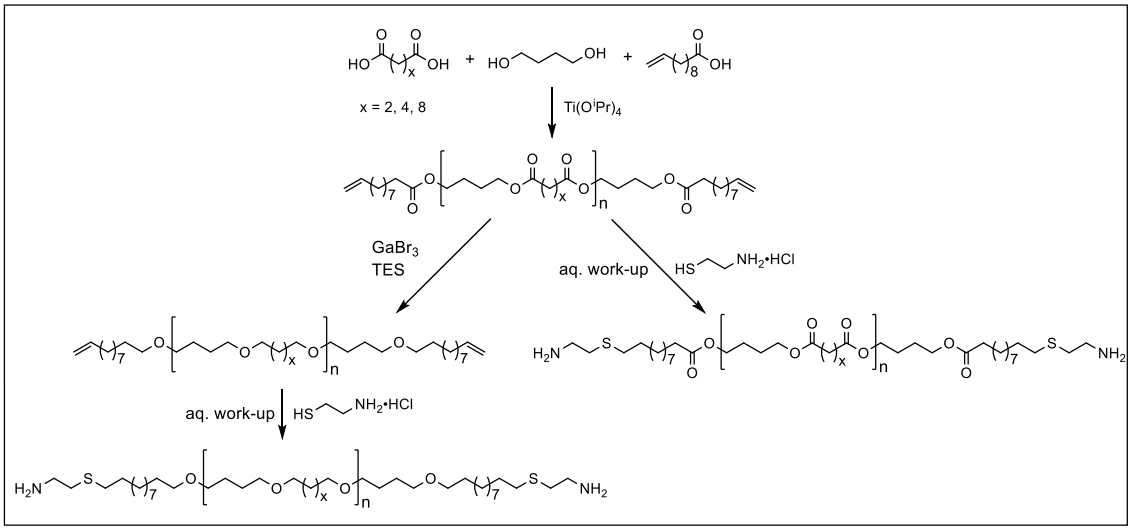

Scheme 43 Synthesis route towards fully biobased polyether and polyester diamines starting from different dicarboxylic acids and 1,4-butanediol.

First, the polycondensation reactions of different dicarboxylic acids with 1,4-butanediol (BD) and 10-undecylenic acid (UC) were conducted yielding polyesters with double bond end groups. Therefore, a one-pot polymerization was investigated, and the molecular weight was adjusted by the stoichiometry of dicarboxylic acid, BD, and UC as calculated *via* the Carothers Equation (**Equation 4**, chapter 4.2.1). First test reactions were performed with succinic acid (SA), using the optimized reaction conditions from chapter 4.2.1, targeting two different M_n values of 3900 and 1900 g/mol (**Scheme 44**, **Table 19**). In general, low molecular weights were aimed to ensure solubility for subsequent modification and cross-linking reactions.

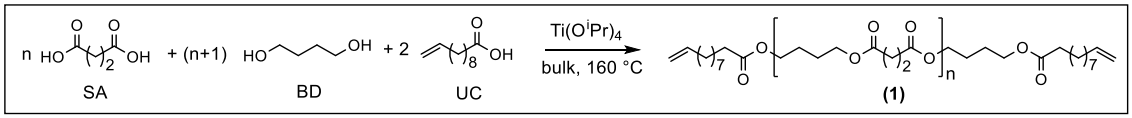

Scheme 44 One-pot polymerization of succinic acid (SA), 1,4-butanediol (BD) and 10-undecylenic acid (UC).

The reaction process was monitored *via* proton NMR spectroscopy, as exemplarily shown in **Figure 24**. The CH_2 groups of the succinic acid (**Figure 24**, signal 1+1') and the CH_2 group adjacent to the carbonyl of UC (**Figure 24**, signal 3+3') were slightly shifted towards the high field after esterification. The chemical shift of the CH_2 group of BD next to the hydroxyl group was changed from 3.7 to 4.1 ppm after esterification (**Figure 24**, signal 2+2'). After 6 days, BD and UC were fully converted, according to the NMR monitoring, while still a small amount of non-esterified SA was detected, indicating either undesired carboxylic end groups or unreacted SA. The latter is less likely due to the step-growth mechanism of the polycondensation. Similar observations were obtained for a different stochiometric ratio of the reactants (**Table 19**, Entry 2). Furthermore, already lower molecular weight oligomers showed solubility issues in DMSO and THF leading to a falsified determination of the M_n determined by THF SEC measurement (**Table 19**). The solubility limit depending on the molecular weight of the oligomers is indicated in the corresponding SEC trace. The unsymmetric distribution and the "cut off" around 15.0 to 15.5 min is clearly visible compared to the expected normal distribution of a step-growth polymerization (**Figure 25**). Moreover, the X_n could not be determined due to overlapping signals of the esterified SA and the SA end group in the corresponding proton NMR spectrum. In theory, full conversion of the carboxylic acid should be obtained as no BD had remained and equimolar ratios of carboxylic acids (from SA and UC) and diol functions were applied. Thus, only UC end groups were assumed, if BD was fully converted. A reasonable explanation for the observation of carboxylic acid groups was a change in the equimolar ratio of the reagents during the reaction due to the evaporation of BD at 160 °C,[12] ultimately leading to an excess of carboxylic acid functions. Hence, the stoichiometry had to be adjusted empirically. This is in accordance with the observations for the synthesis of PEF and PDEF described in chapter 4.2.1.

[12] The boiling point of BD is with 230 °C (according to the supplier) considerably higher than the applied temperature (160 °C). However, as the reaction was performed in an open flask to remove the forming water of the esterification for six days, it can be assumed that a small amount of BD also evaporated.

Table 19 First test reactions of the one-pot polymerization of succinic acid (SA), 1,4-butanediol (BD), and 10-undecylenic acid (UC) after six days.

Entry	eq. SA	eq. BD	eq. UC	M_n (calc.) [g/mol]	M_n (SEC)[1] [g/mol]
1	0.9	1.0	0.2	3700	2600
2	0.8	1.0	0.4	1900	1900

Conditions: 5.00 SA, 160 °C, 5 mol% $Ti(O^iPr)_4$

[1]Oligomer was only partly soluble in the eluent (THF), however a sample was prepared and measured.

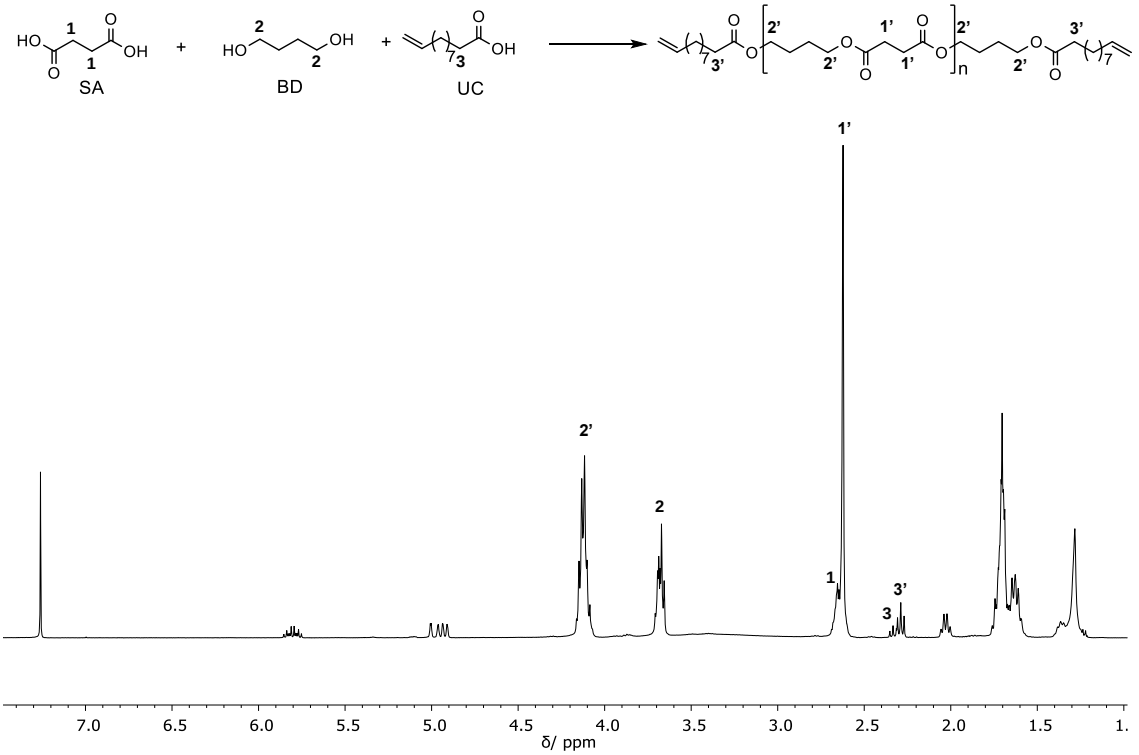

Figure 24 Exemplary ^{1}H-NMR spectrum of the one-pot polymerization of succinic acid (SA), 1,4-butandiol (BD) and 10-undecylenic acid (UC) after 2 hours, measured in $CDCl_3$. Conversions of the starting materials are highlighted by the shift of the CH_2 groups of SA, the α-carbonyl CH_2 group of UC and BD.

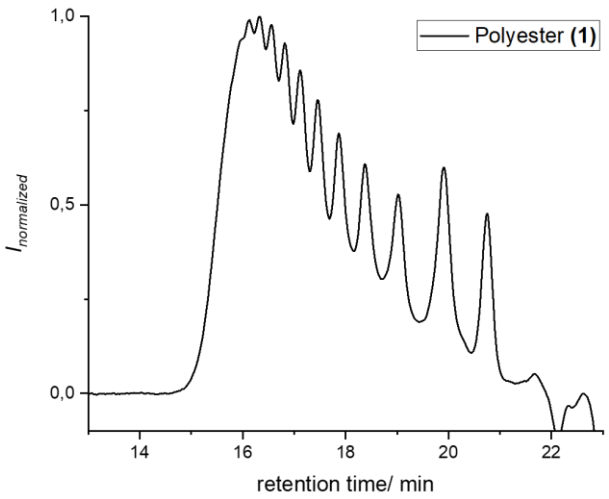

Figure 25 SEC trace of polyester **(1)** in THF, showing a “cut off” at lower retention times between 15.0 and 15.5 min as they were not soluble.

Since the adjustment of the stochiometric ratio of three components to ensure a certain molecular weight, while maintaining solely UC end groups was anticipated to be quite complex, another synthesis route was established. The second strategy was based on a polycondensation of dicarboxylic acid and an excess of BD, followed by an end group modification with an excess of UC in a pseudo one-pot polymerization (**Scheme 45**). Moreover, to address the solubility issues, adipic acid (AA) and sebacic acid (SeA) were chosen as biobased dicarboxylic acids instead of succinic acid (SA). The advantage of this synthesis route is the easier adjustment of the molecular weight and end groups through post-polymerization modification. Nonetheless, some downsides, such as the use of an excess of BD and UC in terms of sustainability, which also requires a work-up[13] after this synthesis step, are accompanied by this strategy.

[13] In comparison, the one-pot approach led to readily available oligomers without further purification.

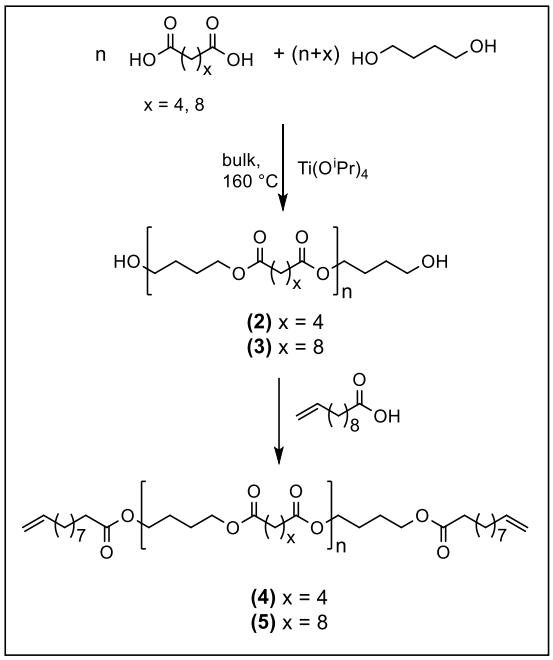

Scheme 45 Pseudo one-pot polymerization of adipic acid (AA) or sebacic acid (SeA) with 1,4-butanediol (BD) and 10-undecylic acid (UC).

In a first test reaction of 5.00 g AA with 1.20 eq. BD and 5 mol% Ti(O^{i}Pr)$_4$, full conversion of AA was obtained after 24 h and the M_n was determined to 2100 g/mol by THF SEC using PMMA standards. Subsequently, an excess of UC was added to the reaction mixture and stirred for further 17 h at the same temperature showing full conversion of the OH end groups *via* proton NMR spectroscopy. Hence, a scale-up using 30.0 g AA was performed under the same reaction conditions, whereby a similar molecular weight of M_n = 2250 g/mol was obtained after 12 hours, determined *via* SEC (**Table 20**, Entry 1a). The higher reactivity compared to the 5.00 g approach was probably a result of the better mixing through a mechanical stirrer. For the following end group modification at large scale, still a slight amount of OH end groups (< 10%) were detected in the proton NMR spectrum after 28 hours, while the conversion of OH groups stagnated (**Table 20**, Entry 1b). Nonetheless, the reaction was stopped since also the hydroxyl end groups are reactive in ring-opening reaction of epoxides forming thermosets, which is discussed in the next subchapter (chapter 4.3.2). For the precipitation, the polyester was dissolved in DCM, but only a cloudy solution was obtained. A small amount of this solution was filtered through a syringe filter showing identical SEC traces and proton NMR spectra before and after filtration, indicating a side product, which was insoluble in THF, DCM and $CDCl_3$. The side reaction is further indicated by a small shoulder at higher retention times after purification in the SEC traces (**Figure 26**). However, this side reaction was not further studied, because the polyester was obtained in a yield of 72% after filtration of the cloudy solution and precipitation in cold *n*-hexane. The precipitated polyester showed a good solubility in DCM. The yield loss is explained first by the filtration of the

hypothesized side product and second by the fact that lower oligomers were soluble in *n*-hexane as indicated in the SEC traces before and after work-up (**Figure 26**). Hence, the SEC molecular weight of polyester **(4)** is significant higher compared to the hydroxyl group terminated polyesters **(2)** (**Table 20**, Entries 1a+1b). In accordance with that, the M_n determined by ^{1}H-NMR spectroscopy also increased after the end group modification. (**Table 20**, Entries 1a+1b). The reaction system was successfully transferred to sebacic acid showing full conversion of SeA after 15 hours besides a M_n of 2450 and 1350 g/mol, determined *via* SEC and ^{1}H-NMR, respectively (**Table 20**, Entry 2a). The end group modification also showed a residual amount of remaining hydroxyl end groups (< 10%), since the conversion stagnated after 34 hours (**Table 20**, Entry 2b). Moreover, the polyester **(5)** was not completely soluble in DCM as a result of a possible side reaction, while the filtration was more difficult compared to the polyester based on AA. Several filtration procedures were investigated without success and the final separation was performed *via* centrifugation and decanting. Subsequently, the precipitation of the polymer solution in *n*-hexane led to a soluble polyester **(5)** in DCM with a yield of 54%. The SEC traces are displayed in **Figure 26**, showing, analogously to the AA based polyester **(4)**, a loss of lower oligomers besides a small shoulder towards lower retention times. Furthermore, small amounts of UC[14] were detected by proton NMR after precipitation for both polyesters **(4)** and **(5)**. Interestingly, the M_n determined by ^{1}H-NMR spectroscopy increased significantly for polyester **(5)** compared to polyester **(4)**, after the end group modification. A possible explanation is a higher amount of unreacted UC for polyester **(4)**, since the M_n values were determined by the double bond signals in the proton NMR spectra. Additionally, a larger shoulder was observed in the SEC of polyester **(5)**, indicating a higher concentration of side product compared to polyester **(4)**, which leads to higher molecular weights. Moreover, during the end group modification further polymerization occurs due to remaining OH end groups and thus, the higher reaction times for polyester **(5)** compared to polyester **(4)** also influenced the M_n.

[14] The exact amount of unreacted UC was not determined due to overlapping signals with the UC modified end groups.

Table 20 Scale-up reaction of the polycondensation with adipic acid (AA) and sebacic acid (SeA) as well as subsequent end group modification with 10-undecylenic acid (UC).

Entry	Polyester	Reaction step	*t* [h]	Conversion (NMR) [%]	M_n (SEC) [g/mol]	M_n (NMR) [g/mol]
1a	**(2)**	Polycondensation	12	>99	2250	1300[1]
1b	**(4)**	End group modification	28	>90	3400	1900[2]
2a	**(3)**	Polycondensation	15	>99	2450	1350[1]
2b	**(5)**	End group modification	34	>90	3650	3100[2]

Conditions: 30.0 g dicarboxylic acid, 1.20 eq. BD, 160 °C, 5 mol% $Ti(O^iPr)_4$ for both reaction steps.

[1]Assuming only OH end groups, including unreacted BD.

[2]Assuming only double bond end groups.

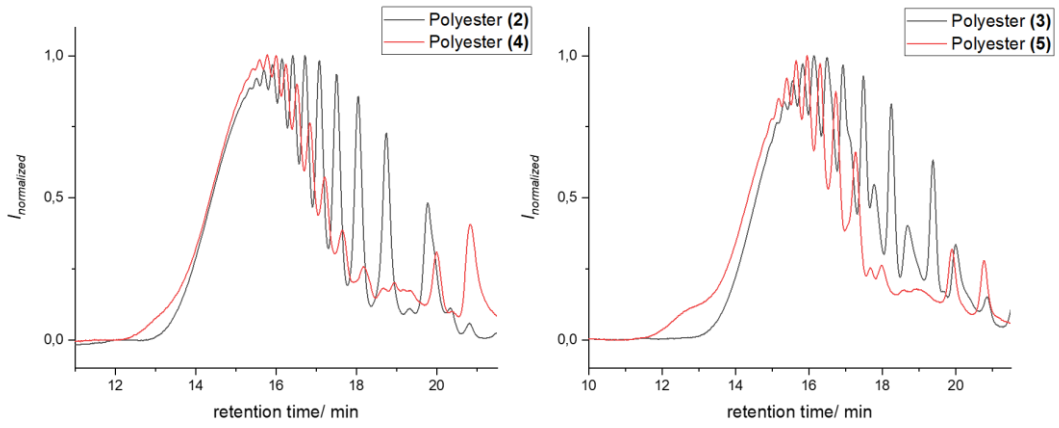

Figure 26 SEC traces of adipic acid (AA) based polyester **(2)** and **(4)** (left) and the sebacic acid (SeA) based polyester **(3)** and **(5)** (right), before (black) and after (red) end group modification with 10-undecylenic acid (UC) and precipitation in *n*-hexane.

Subsequently, the polyesters were divided into two different batches, whereof one was modified with the $GaBr_3$ catalyzed reduction to obtain the corresponding polyethers. For the adipic acid based polyester **(4)**, this reaction system was already optimized as described in chapter 4.1.1. Hence, the reduction was performed under inert conditions on a 10.0 g scale in 125 mg polyester/mL DCM, using 2.20 eq. TES per ester group and 2 mol% $GaBr_3$ (**Scheme 46**).

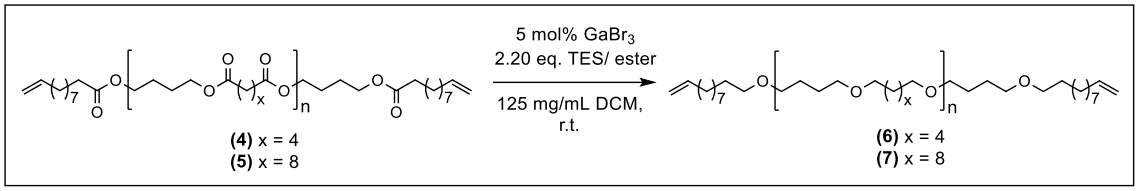

Scheme 46 $GaBr_3$ catalyzed reduction of the end group modified polyester based on adipic acid (AA) and sebacic acid (SeA) with TES.

For the polyester **(4)** based on AA, full conversion of the ester groups was observed after three days, determined *via* proton NMR spectroscopy through the change of the chemical shift of the CH_2 group adjacent to the carboxylic acid from 2.30 ppm to 1.55 ppm (**Figure 27**, signal 1+1'). Polyether **(6)** was obtained in a yield of 9.10 g (87%) and a molecular weight of M_n = 2400 g/mol, determined *via* SEC measurements (**Table 21**, Entry 1). In addition, 13 mol% silyl species remained in the polyether after distillation. For the determination of the molecular weight, also the solvent peak was integrated due to the overlapping signals. Moreover, the SEC traces showed compounds with a higher retention time caused by the different hydrodynamic radius of the polyether in THF as discussed in detail in chapter 4.1.1 (**Figure 28**). Furthermore, the M_n determined by proton NMR spectroscopy was similar to the M_n of polyester **(4)** (**Table 20**, Entry 1b vs. **Table 21**, Entry 1). The reduction was transferred to the sebacic acid based polyester **(5)**, leading to full conversion after three days as determined *via* proton NMR spectroscopy. Polyether **(7)** was obtained in a yield of 9.21 g (89%) including 13 mol% silyl species per repeating unit besides a molecular weight of M_n = 3650 g/mol (**Table 21**, Entry 2). However, the SEC trace showed an unexpected, unsymmetric distribution at higher retention times (**Figure 28**). During the sample preparation a high resistance was observed for the filtration with a syringe filter, which indicates a poor solubility of the SeA based polyether in THF. A molecular weight of M_n = 2900 g/mol was determined *via* ^{1}H-NMR spectroscopy, which is in accordance with the M_n of polyester **(5)** (**Table 20**, Entry 2b vs **Table 21**, Entry 2). Thus, the polyether was used as obtained for further modification reactions.

Table 21 $GaBr_3$ catalyzed reduction of adipic acid (AA) and sebacic acid (SeA) based polyester **(6)** and **(7)** after three days showing 13 mol% silyl species per repeating unit, determined *via* ^{1}H-NMR spectroscopy.

Entry	Polyether	Conversion (NMR) [%]	M_n (SEC)[1] [g/mol]	M_n (NMR)[2] [g/mol]	Yield [%]
1	**(6)**	>99	2400	1750	87
2	**(7)**	>99	3650	2900	89

Conditions: 10.0 g Polyester, 2.20 eq. TES per repeating unit, 2 mol% GaBr3, 125 mg/mL DCM.

[1]Solvent peak overlayed with respective signals but was still integrated.

[2]Assuming only double bond end groups.

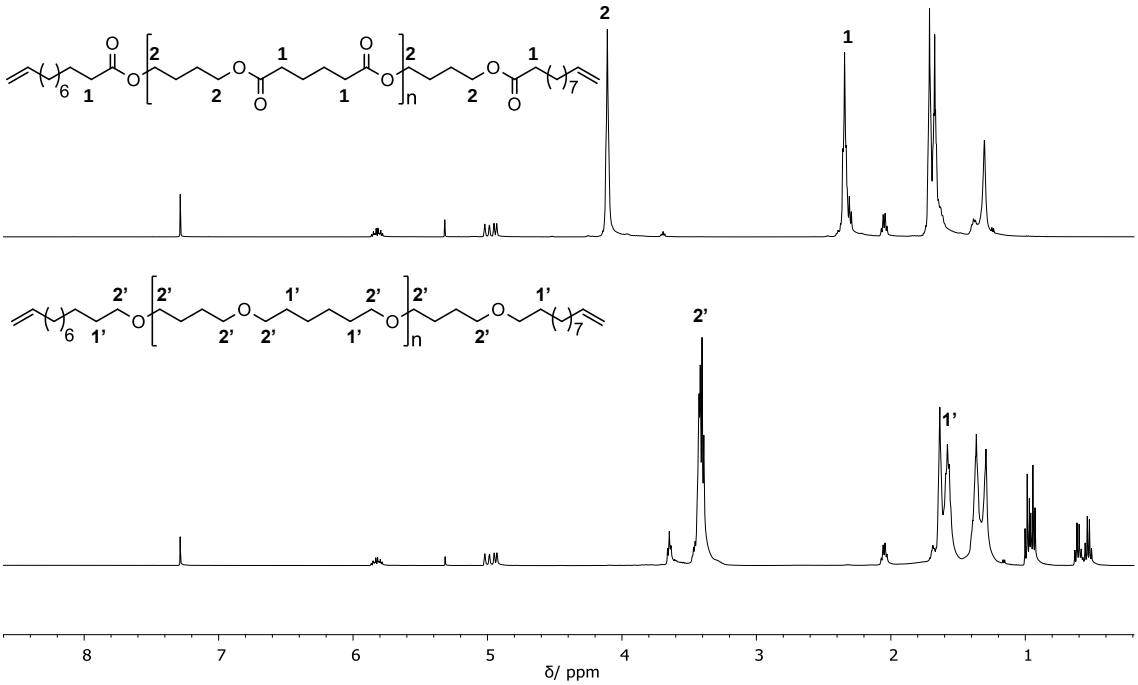

Figure 27 Exemplary ^{1}H-NMR spectra of the $GaBr_3$ catalyzed reduction with TES of the adipic acid based polyester **(4)** (top) to the polyether **(6)** (bottom), measured in $CDCl_3$.

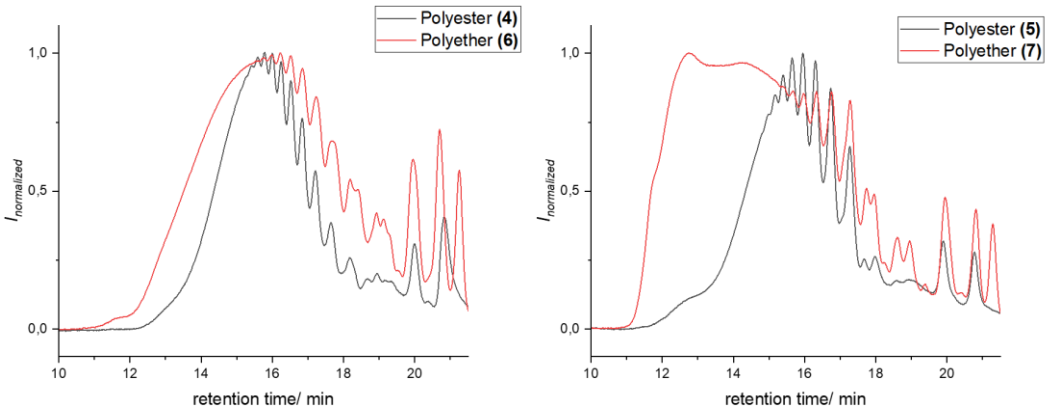

Figure 28 SEC traces of the adipic acid based polyester **(4)** and polyether **(6)** (left) and the sebacic acid based polyester **(5)** and polyether **(7)** (right), measured in THF.

Finally, the double bond end groups of polyester **(4)** and **(5)** as well as of polyether **(6)** and **(7)** were converted into amine groups *via* thiol-ene reaction with cysteamine (**Scheme 47**). Test reactions were performed for polyester **(4)** in DCM using 10 mol% 2,2-dimethoxy-2-phenylacetophenone (DMPA) under UV light irradiation with a wavelength of 365 nm at room temperature. Since cysteamine was not soluble in DCM, DMSO was added as co-solvent, resulting in a homogenous solution (DCM:DMSO ratio 5:1). However, no conversion of the double bonds was determined *via* proton NMR spectroscopy after five days. Therefore, cysteamine hydrochloride was used instead in a mixture of DCM and methanol (ratio 3:1). Full conversion of the double bonds was shown by the vanishing signals with a chemical shift of 5.8 and 4.9 ppm, after 26 hours (**Figure 29**, signals 1+2). Following, the reaction conditions were successfully transferred on a 200 mg scale to the polyether **(6)**, for which all double bonds were converted after 26 hours.

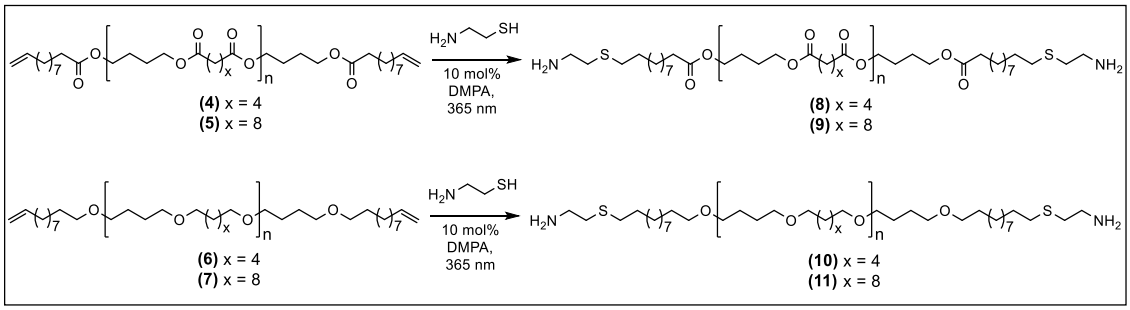

Scheme 47 Thiol-ene reaction of the adipic acid (AA) and sebacic acid (SeA) based end group modified polyester **(4)** and **(5)** as well as of the corresponding polyether **(6)** and **(7)**.

The scale-up reaction of 10.0 g the AA based polyester **(4)** showed full conversion after 15 hours. After purification, 1-2 mol% disulfide side product per repeating unit were observed *via* ^{1}H-NMR spectroscopy. The work-up was performed through several

washing steps with saturated, aqueous sodium carbonate solution and water to deprotonate the ammonium salt yielding the free amine. The phase separation was insufficient due to similar densities of DCM and saturated sodium carbonate solution and in addition, the polymer acted as surfactant. The scale-up of polyester **(4)** was divided into two 10.0 g batches to ensure a sufficient irradiation (**Table 22**, Entries 1a+b). Since both polyesters **(8a)** and **(8b)** showed similar amounts of disulfide and molecular weights after work-up, both batches were combined. Furthermore, polyester **(8b)** was stirred considerably longer than **(8a)**, proving that the reaction was finished after 15 hours. Polyester **(5)** as well as polyethers **(6)** and **(7)** were converted in the same way into the respective diamines and the results are summarized in **Table 22**. Comparing all SEC traces of the diamines with their respective analogues with double bond end groups a very similar distribution is shown after the thiol-ene reaction, as expected (**Figure 30**). For polyether **(10)** a slightly lower molecular weight was obtained according to SEC. However, even having a small set of data, it seemed unreasonable why polyether **(7)** exhibited a considerably different distribution compared to the corresponding obtained diamine **(11)**. Furthermore, polyether diamine **(11)** depicts similar distributions than the other polyether and esters (**Figure 30**). In Addition, the M_n of polyester **(9)** as well as of polyethers **(10)** and **(11)**, determined by proton NMR spectroscopy, were similar to the respective polymers with double bond end groups, while the M_n of polyesters **(8)** were slightly increased (**Table 22**). Nevertheless, a generally good correlation between the molecular weights determined *via* SEC and NMR measurements was observed for the herein synthesized polyesters and polyethers.

Table 22 Summary of thiol-ene reactions of polyester **(4)** and **(5)** as well as of polyether **(6)** and **(7)**.

Entry	Diamine	Polyester/ Polyether	*t*	M_n (SEC)[1] [g/mol]	M_n (NMR)[2] [g/mol]	Mol% disulfide (NMR)	Yield [%]
1a	**(8a)**	**(4)**	15 h	2400	2700	1-2	93
1b	**(8b)**	**(4)**	72 d	2400	2700	1-2	86
2	**(9)**	**(5)**	14 h	2600	3100	1-2	91
3	**(10)**	**(6)**	4 d	2000	1600	1-2	86
4	**(11)**	**(7)**	3 d	2300	3000	<1	84

Conditions: 2.00 eq. cysteamine hydrochloride per double bond, 10 mol% DMPA, 365 nm, r.t.

[1]Solvent peak integrated

[2]Assuming only diamine end groups.

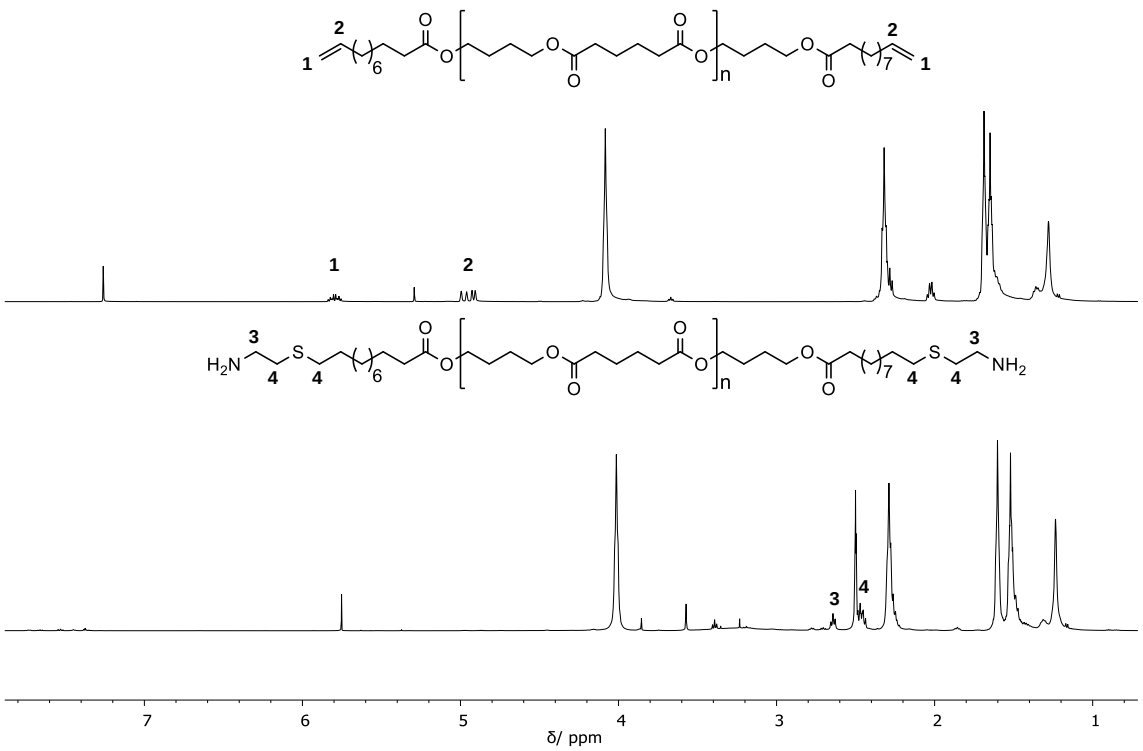

Figure 29 Exemplary ^{1}H-NMR spectra of adipic acid based polyester **(4)** with double bond end groups, measured in $CDCl_3$ (top) and of the diamine polyester **(8)**, measured in DMSO-d_6 (bottom), showing the complete conversion of the double bonds by the applied thiol-ene reaction.

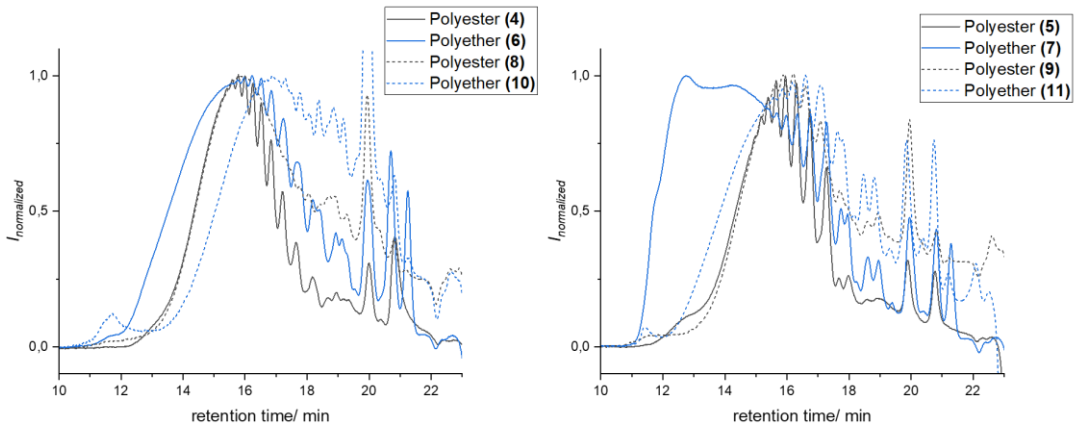

Figure 30 SEC traces of adipic acid based polyester **(4)** and polyether **(6)** before and after thiol-ene reaction (left) yielding the corresponding diamines **(8)** and **(10)** and the sebacic acid base polyester **(5)** and polyether **(7)** before and after thiol-ene reaction (right) yielding the corresponding diamines **(9)** and **(11)**, measured in THF.

In the proton NMR spectra of all polyester and polyether diamines, no amine protons were detected neither in $CDCl_3$ nor DMSO-d_6, which arises the question whether the amine or the ammonium salt is predominant. The comparison of the proton NMR spectra before and after work-up indicated the successful deprotonation due to shift of the signals assigned to the adjacent CH_2 group of the amine end group before and after the work-up

procedure (**Figure 31**, signals 1-3). Moreover, in the IR spectra the characteristic δ-NH_2 (scissor) vibration for primary amines with a wavenumber of 1565 cm^{-1} was observed for both polyesters (**Figure 32**). Interestingly, this vibration was not detected in the IR of the polyethers. Thus, a commercially available PEG and PPG based diamine, named Jeffamine®, was measured as reference, whereby also no δ-NH_2 (scissor) vibration was observed. Hence, this observation is probably caused by the polyether structure itself but was not further studied. Nonetheless, further analytic methods, such as a proton NMR spectroscopy at lower temperatures are necessary to clearly verify the deprotonation of the ammonia salt. Moreover, a modification reaction could be applied, which are known to proceed only with the amine but not its salt.

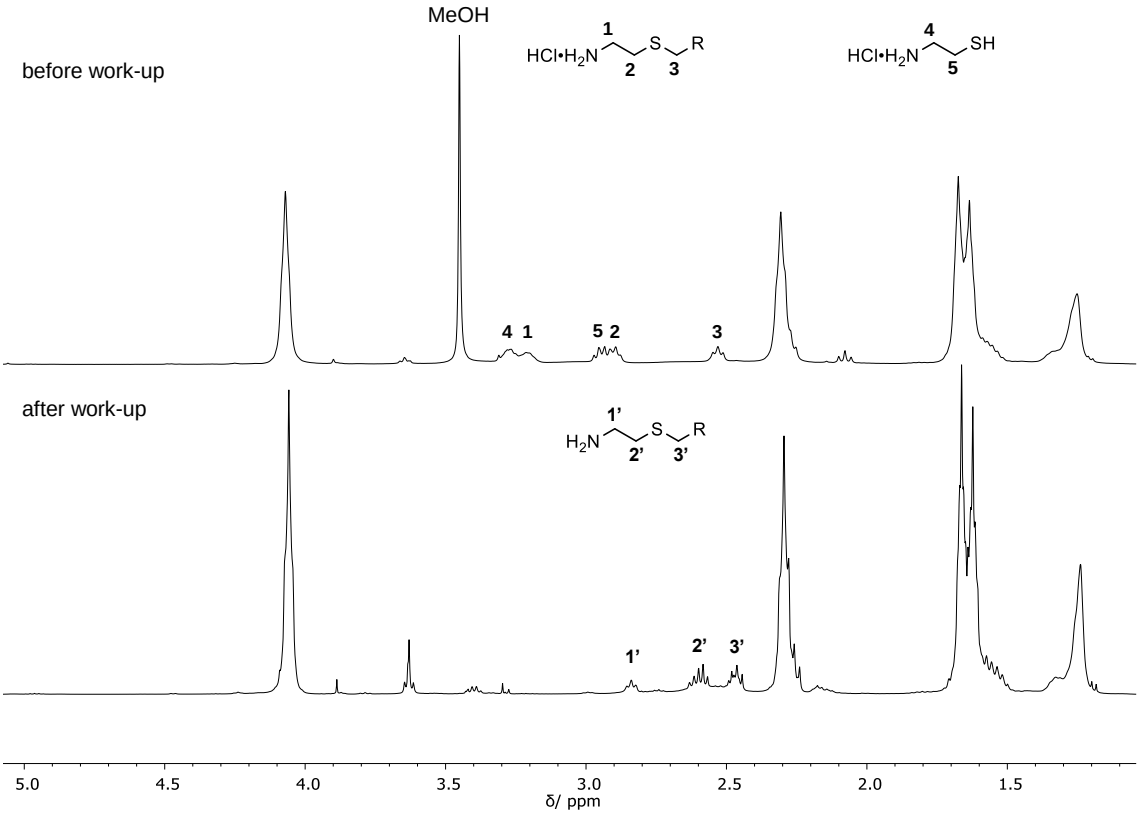

Figure 31 ^{1}H-NMR of polyester **(8)** before (top) and after work-up (bottom), measured in $CDCl_3$.

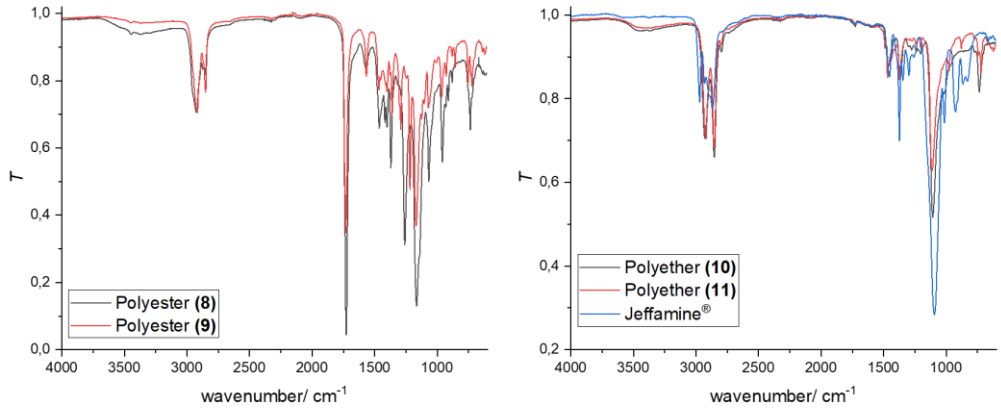

Figure 32 IR spectra of polyester diamines **(8)** and **(9)** (left) as well as of polyether diamines **(10)**, **(11)** and Jeffamine® (right).

Finally, thermal analysis was performed for all diamines **(8)**-**(11)** *via* DSC and TGA (**Figure 33**). For all polyester and polyether diamines, no glass transition temperatures were detected, while melting points between 26°C and 53 °C were determined, as summarized in **Table 23**. The SeA based polyester and polyether diamines **(9)** and **(11)** showed higher melting points than their adipic acid based analogues **(8)** and **(10)**, probably because their longer aliphatic chains in the polymeric backbone allowed stronger interactions. Moreover, T_m was higher for the polyesters compared to the corresponding polyethers, presumably due to stronger dipole-dipole interactions of the carbonyl functions (**Table 23**). These observations are in accordance with a previous study on the thermal properties of different polyester and polyether structures reported by Meier and Biermann *et al*.[249] The degradation of the adipic acid based polyester diamine **(8)** started at $T_{d5\%}$ = 245 °C, while the degradation temperature at the turning point was determined to T_d = 300 °C (**Table 23**, Entry 1). For the sebacic acid based polyester diamine **(9)**, the degradation started at $T_{d5\%}$ = 275 °C and the degradation temperature was determined to T_d = 400 °C (**Table 23**, Entry 2). Both polyether diamines **(10)** and **(11)** showed a T_d of 400°C, while $T_{d5\%}$ was 230 °C for polyether **(10)** and 250 °C for polyether **(11)** (**Table 23**, Entries 3+4). In general, a higher thermal stability was observed for the sebacic acid based diamines, compared to the adipic acid analogues and the polyesters show slightly higher $T_{d5\%}$ than the corresponding polyethers. For the SeA based polyester **(9)** and polyether **(11)** the same char yield of 13% was obtained, determined at 600 °C *via* TGA (**Table 23**, Entries 2+4). The thermal degradation analysis yielded 14% char for the AA based polyester **(8)**, besides 5% for the corresponding polyether **(10)** (**Table 23**, Entries 1+3).

Table 23 Summary of M_n and thermal analysis data for all diamines.

Entry	Diamine	M_n (SEC)[1] [g/mol]	M_n (NMR) [g/mol]	T_m (DSC) [°C]	$T_{d5\%}$ [°C]	T_d[2] [°C]	Char yield [%]
1	**(8)**	2400	2700	42	245	300	14
2	**(9)**	2600	3100	53	275	400	13
3	**(10)**	2000	1600	26	230	400	5
4	**(11)**	2300	3000	45	250	400	13

[1]Determined *via* PMMA standard in THF. Solvent peaks were integrated.

[2]Determined *via* turning point.

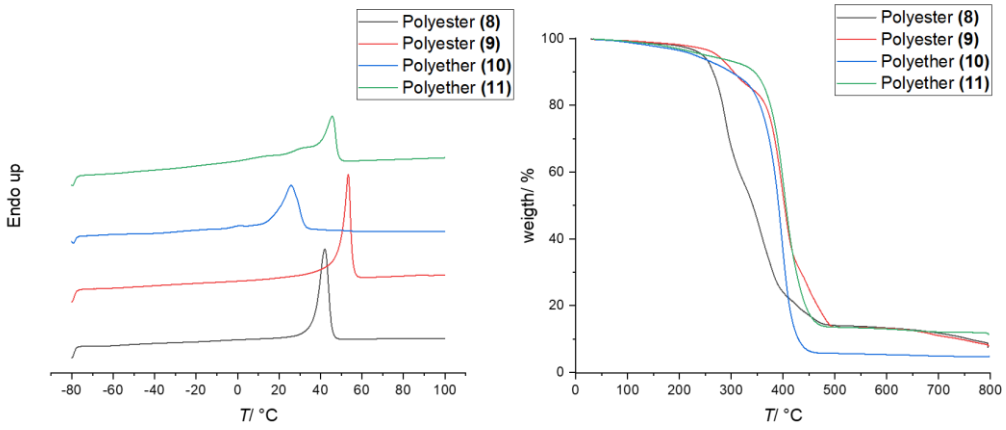

Figure 33 Second heating cycle of the DSC measurement (left) and TGA measurement (right) of the polyester and polyether diamines **(8)**-**(11)**.

In conclusion, fully biobased polyesters were synthesized *via* polycondensation of AA or SeA and BD followed by an end group modification with UC acid in a pseudo one-pot polymerization, leading to double bonds as the majority of the end groups. A direct one-pot polymerization of all three compounds was investigated as well and was assumed to be more complicated due to evaporation of BD under the applied reaction conditions. As a results, undesired carboxylic acid end groups were obtained by the changed stoichiometry. Subsequently, one half of the polyesters were successfully converted into the corresponding polyethers *via* the $GaBr_3$ catalyzed reduction with TES as investigated in chapter 4.1.1. Finally, the end groups of both polyesters and polyethers were modified into amine groups *via* thiol-ene reaction with cysteamine hydrochloride. All reactions were optimized to allow synthesis in multigram scale. The deprotonation of the obtained ammonia salt was indicated by a change of the chemical shift of the end group assigned signals in the proton NMR spectra before and after work-up. Moreover, the characteristic δ-NH_2 (scissor) vibration was detected in the IR

spectra of the polyesters. This vibration was not observed for the herein synthesized polyethers, but also not for a commercially available PEG/ PPG based diamine (Jeffamine®). Thermal analysis showed melting points from 26 °C to 53 °C, besides degradation starting from 230 to 275 °C. In general, the degradation temperature at the turning point was higher for the SeA based polyester diamine **(9)** (400 °C) than for the adipic acid based analogues (300 °C), while the polyether showed similar T_d of 400 °C. Furthermore, the adipic acid based polyether showed a higher thermal stability compared to the corresponding polyesters.

4.3.2 Application of Biobased Aliphatic Polyether and Polyester Diamines in Thermosets

The fully biobased polyester and polyether diamines are converted with epoxidized lignin (EL) and epoxidized linseed oil (ELO), which mainly consists of the trifunctional α-linoleic acid (47%), bifunctional linolic acid (24%) and monounsaturated oleic acid (19%), into thermosets. Moreover, the influence of the chemical structure of the diamines and the epoxides on the thermal and mechanical properties of the obtained thermoset as well as the different reactivities of the terminal epoxides in the EL compared to the internal epoxides in the ELO are investigated. Therefore, the curing parameters are optimized for both epoxides followed *via* DSC analysis and IR spectroscopy. Subsequently, all diamines are cured with both epoxides in poly(tetrafluoroethylene) (PTFE) molds forming films for the determination of the mechanical properties *via* dynamic mechanical thermal analysis (DMTA). A schematic overview of the thermoset synthesis is given in **Scheme 48**.

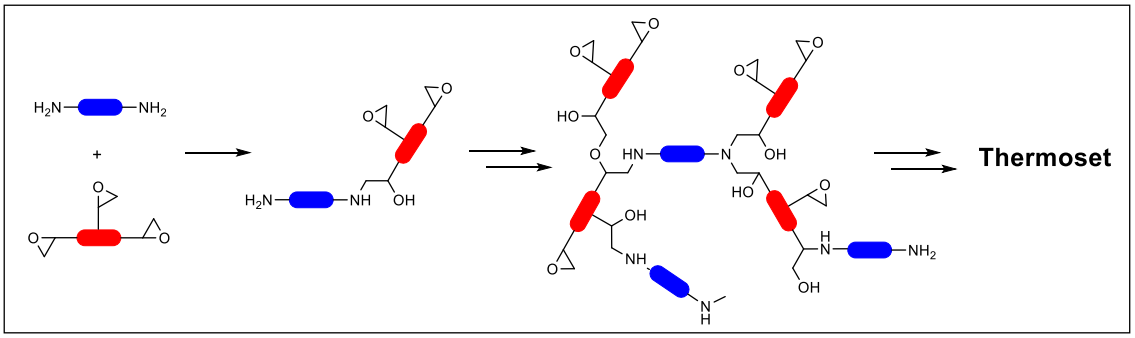

Scheme 48 Schematic overview of the thermoset synthesis from different diamines (blue) with epoxidized linseed oil or epoxidized lignin (red).

First of all, IR spectra of the adipic acid based polyester **(8)** and polyether **(10)** were overlayed with those of linseed oil (LO) and epoxidized linseed oil (ELO) to assign the characteristic vibrations for monitoring the conversion. **Figure 34** illustrates the isolated epoxy vibration with a wavenumber of 800 and 820 cm^{-1}, respectively, besides the isolated δ-NH_2 (scissor) vibration of the polyester diamine at 1565 cm^{-1} and the N-H wagging vibration at 880 cm^{-1}.

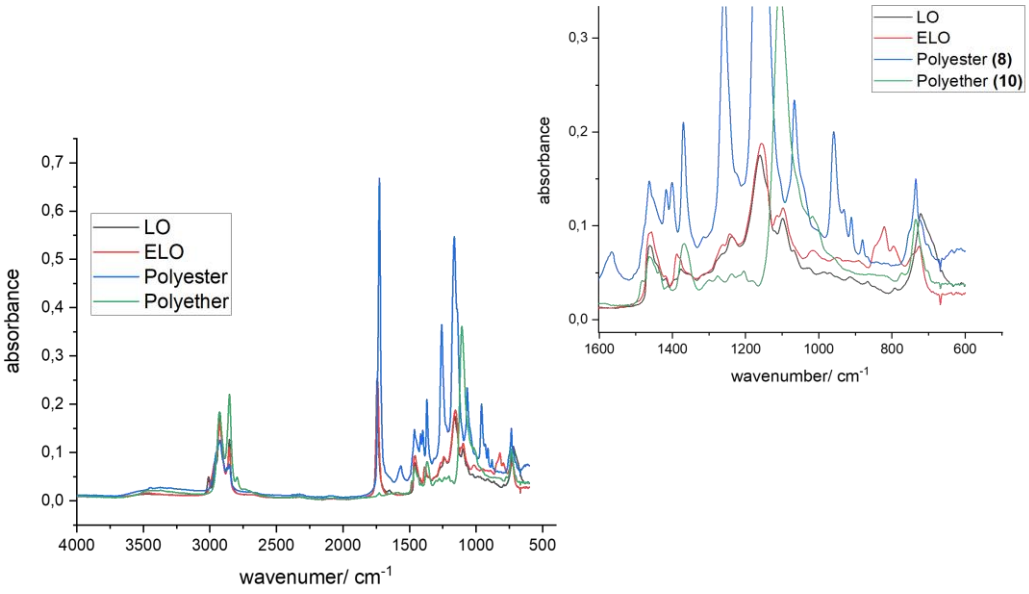

Figure 34 IR spectra of polyester **(8)**, polyether **(10)**, linseed oil (LO) and epoxidized linseed oil (ELO, left) and the zoom-in (right).

First curing tests at 120 °C with a molar ratio of diamine to epoxide of R = 0.5 (0.50 eq. diamine per epoxy group[15]) showed no conversion in the IR spectrum after 17 hours, while a melting point was observed in the second heating cycle of DSC analysis, indicating unreacted diamine.[16] The stochiometric ratio of diamine to epoxide was set to R = 0.5, since each amine group can react with two epoxides *via* nucleophilic ring opening. Thus, the curing temperature was increased to 180°C leading to a decrease of the primary N-H bending at 1565 cm^{-1}, the N-H wagging at 880 cm^{-1} and the epoxy vibration at 820 cm^{-1} in the corresponding IR spectra after 17 hours (**Figure 35**). This was accompanied by an increase of a vibration with a wavenumber of 620-650 cm^{-1}, assigned to the OH out-of-plane deformation vibration of secondary alcohols (**Figure 35**). Additionally, this observation were strengthened by a detected T_g at -43 °C, besides a strong decrease in the intensity of a melting point, determined *via* DSC analysis (**Figure 35**). Hence, the diamine was converted almost quantitatively into secondary or tertiary amines shown by the decrease of T_m in the DSC and the N-H bending vibration in the IR spectrum. Moreover, the IR spectra of the cured sample indicated a literature known amidation side reaction[393] through the increasing C=O amide vibration at 1650 cm^{-1} next to the C=O ester vibration. A successful curing test of the sebacic acid based polyester **(9)** was obtained, while the conversion of the diamine,

[15] The epoxy content of ELO was determined *via* ^{1}H-NMR spectroscopy.
[16] For thermosets no melting points are expected due to the high cross-linking. The observed melting point in the second heating cycle of the DSC analysis coincides with the melting point of the respective diamine according to chapter 4.3.1.

determined *via* DSC, was lower compared to polyester **(8)** under the same reaction conditions.

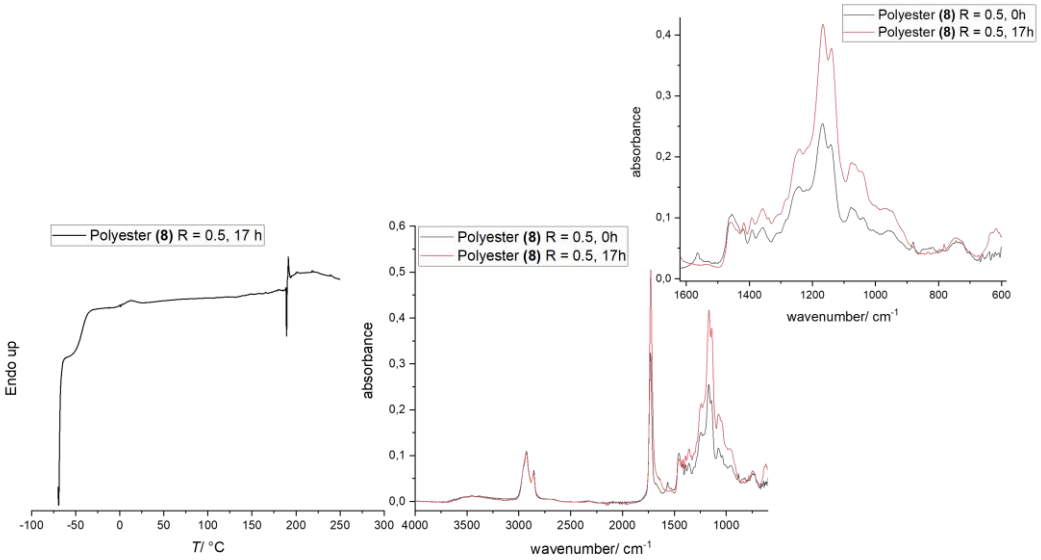

Figure 35 Second heating cycle of the DSC measurement (left) and IR spectra (center) before and after curing of polyester **(8)** with R = 0.5 at 180 °C for 17 hours as well as the zoom-in (right).

Next, the stochiometric ratio (R value) of diamine and epoxide, the curing temperature as well as the reaction time was varied for polyester **(8)**, monitored *via* IR and DSC measurements. The curing temperature had a strong influence on the reaction rate, because unreacted diamine, assigned by the melting point in the DSC traces, was obtained for temperatures below 180°C and 72 hours (**Figure 36**).[17] The IR spectra for the cured sample at 125 °C showed the N-H bending vibration (1565 cm^{-1}) besides the N-H wagging (880 cm^{-1}) of the diamine (**Figure 36**). For the samples cured at 140 °C for 72 hours, a high conversion of the primary amine is shown by the vanishing N-H bending vibration, however secondary amines were indicated by the still present N-H wagging vibration and thus, the sample was not fully cured. In addition, a shift of the T_g in the second heating cycle towards higher temperatures was observed, the higher the conversion of diamine was. The exothermic peak in the DSC before the melting point is caused by a high cooling rate, leading to incompleted crystallization during the cooling cycle (**Figure 36**). Below the T_g of the polymer, probably no crystallization took place and thus, the crystallization occurred again above a certain temperature during the following heating cycle. This assumption was strengthened by the same measurements with a

[17] Since for all DSC measurements the second heating cycle was analyzed, the sample further cures during the first heating cycle if the diamine is not fully converted which may falsify the obtained conversions. Nonetheless, only qualitative information was used.

lower cooling rate, whereby the exothermic peak was not observed during the second heating (chapter 6.3.3,**Figure S 22**).

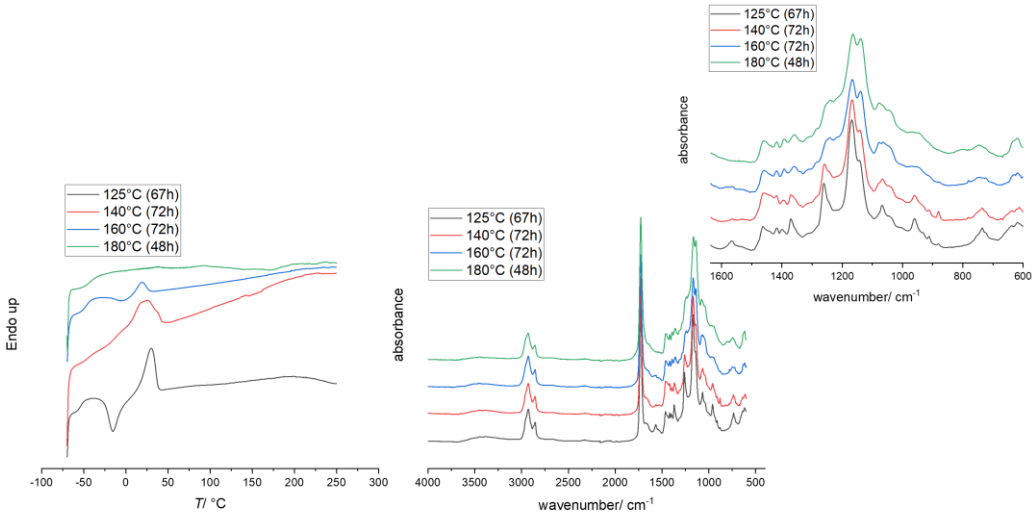

Figure 36 Second heating cycle of the DSC measurement (left) and IR spectra (center) of the curing of polyester **(8)** with ELO (R = 0.5) under different temperatures as well as the zoom-in (right).

Subsequent the R value of polyester **(8)** was varied using values of 0.5, 1.0 and 2.0 for 180 °C. The DSC traces showed a small melting point for an R value of 2 after 48 hours at 180 °C, indicating still unreacted diamine, while full conversion of the diamine was observed for R < 1 (**Figure 37**). In the corresponding IR spectra, the N-H bending (1565 cm^{-1}), N-H wagging (880 cm^{-1}) and epoxy vibration (820 cm^{-1}) disappeared while the vibration of the secondary alcohol (620-650 cm^{-1}) increased for all R values (**Figure 37**). Concluding, a higher R value than 0.5 was not necessary.

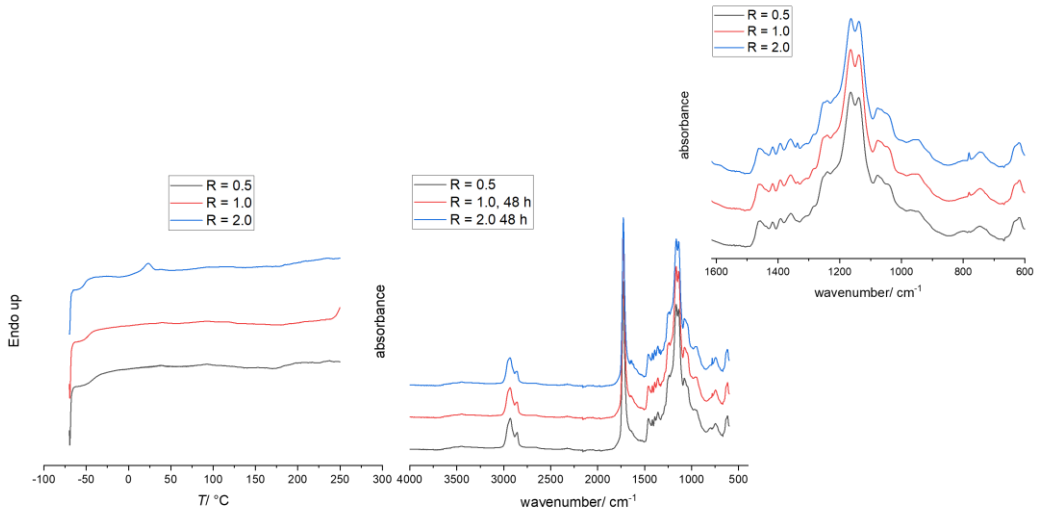

Figure 37 Second heating cycle of the DSC measurement (left) and IR spectra (center) for different R values of polyester **(8)** and ELO cured at 180 °C for 48 hours as well as the zoom-in (right).

Furthermore, the R value was decreased to 0.25 while the temperature was lowered to 160 °C combining two screening approaches due to the long reaction times. For a meaningful comparison, a reference sample with an R value of 0.5 was cured under these conditions. The DSC traces showed in both cases no full conversion after 72 hours, which is in accordance with the already described influence of the curing temperature (**Figure 38**). The corresponding IR spectra indicated almost full conversion for both approaches (**Figure 38**).

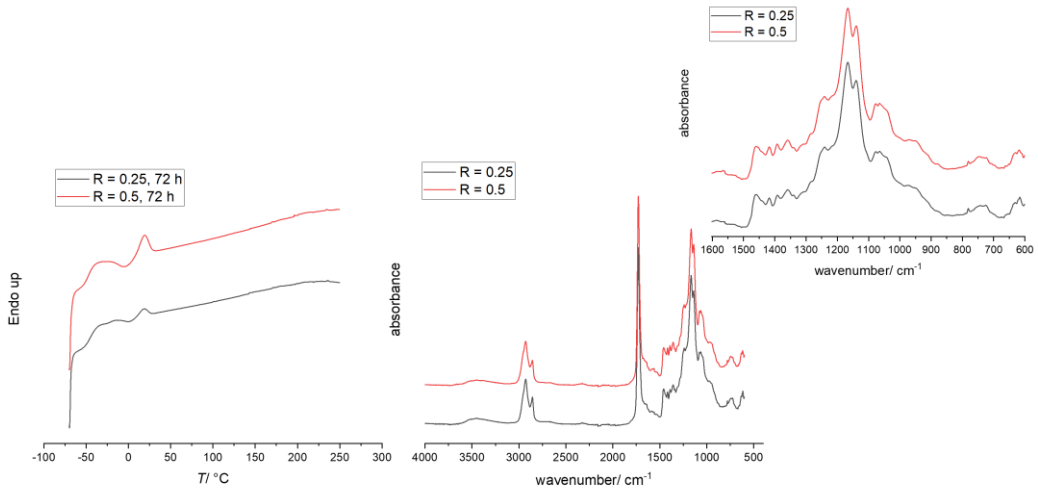

Figure 38 Second heating cycle of the DSC measurement (left) and IR spectra (center) for different R values of polyester **(8)** and ELO cured at 160 °C for 72 hours as well as the zoom-in (right).

Summarizing, the best results for the curing of polyester **(8)** with ELO were obtained at 180 °C for 48-72 hours, and an R value of either 0.5 or 0.25. It has to be mentioned, that the R value was based on the M_n calculated *via* proton NMR spectroscopy for both starting materials and having in mind that a certain error margin has to be expected by these calculations no exact stochiometric amount was probably to adjusted. For further mechanical analysis, films of all polyester and polyethers with ELO were cured in a PTFE mold with an R value of 0.5 and 0.25 on a 400 mg scale. The DSC traces after 72 hours at 180 °C showed in both cases no melting point for polyester **(8)**, while polyester **(9)** was only fully converted for R = 0.25. DSC analysis of the corresponding polyether showed still unreacted starting material for both stochiometric ratios for polyethers **(10)** and **(11)** (**Figure 39**). These observations could indicate a possible overestimation of the molecular weight of the diamines **(9)**, **(10)** and **(11)**.[18] Additionally, a T_g was clearly visible for the films cured with polyesters **(8)**, **(9)** and polyether **(11)**, while no T_g was determined *via* DSC analysis for the polyether **(10)** cured films with ELO (**Figure 39**). All measurements including glass transition and decomposition temperatures are summarized in **Table 24**. The following trend towards was indicated: For a lower ratio of diamine a higher T_g was observed in all samples. The SeA based polyester **(9)** and polyether **(11)** showed similar T_g in the cured film, however some of them showed still unreacted diamine. Concluding, the T_g of SeA based polyester **(9)** and -ether **(11)** was negligibly affected by the different polymeric backbones. In contrast, a strong discrepancy of the T_g for the AA based polyester **(8)** compared to SeA based polyester **(9)** was shown, while no T_g was observed for the AA based polyether **(10)**. The T_d of the polyether cured samples were slightly higher than the ones of the corresponding polyesters (**Table 24**). The R value influenced the degradation temperature only marginally for the polyester **(9)** and polyether **(10)** cured samples, while no difference at all was detected for polyester **(8)** (**Table 24**). The TGA traces of all cured films indicated a one-step degradation mechanism, as exemplarily shown for R = 0.5 (**Figure 40**). The char yield was not influenced by the stoichiometric ratio and showed similar values for the adipic acid based polyester **(8)** and polyether **(10)** cured films (**Table 24**).

[18] Since higher molecular weights would result into a lower amount of amine groups and thus, altered stoichiometry leading to unreacted amin groups.

Table 24 Overview of the thermal analysis of the polyester and polyether diamines cured films with ELO.

Entry	Diamine	R value	T_g [°C]	$T_{d5\%}$ [°C]	T_d [°C]	Char yield [%]
1	(8)	0.5	-36	305	370	23
2	(8)	0.25	-28	310	370	23
3	(9)	0.5	-44	310	370	18
4	(9)	0.25	-36	320	390	18
5	(10)	0.5	/	320	390	24
6	(10)	0.25	/	305	400	24
7	(11)	0.5	-43	320	385	26
8	(11)	0.25	-40	/	/	/

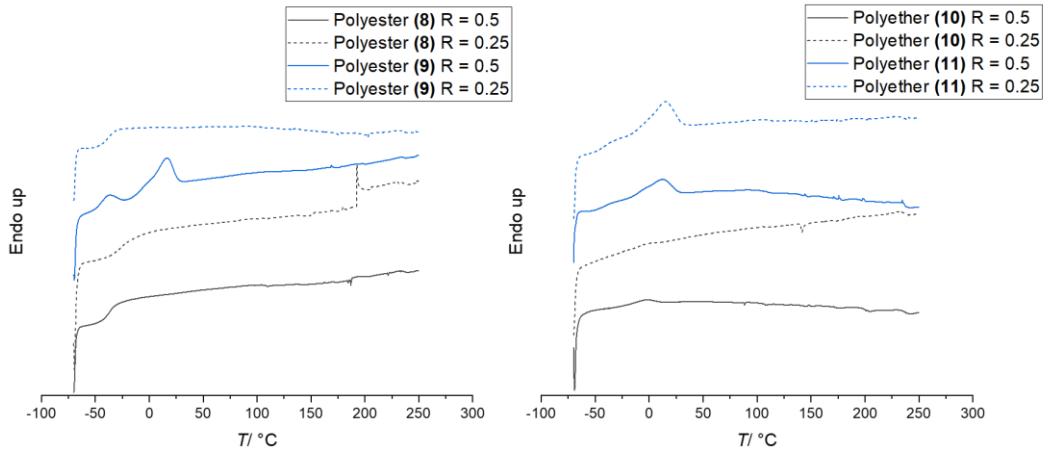

Figure 39 Second heating cycle of the DSC measurements of the polyester (left) and polyether diamines (right) cured films with ELO at 180 °C for 72 hours.

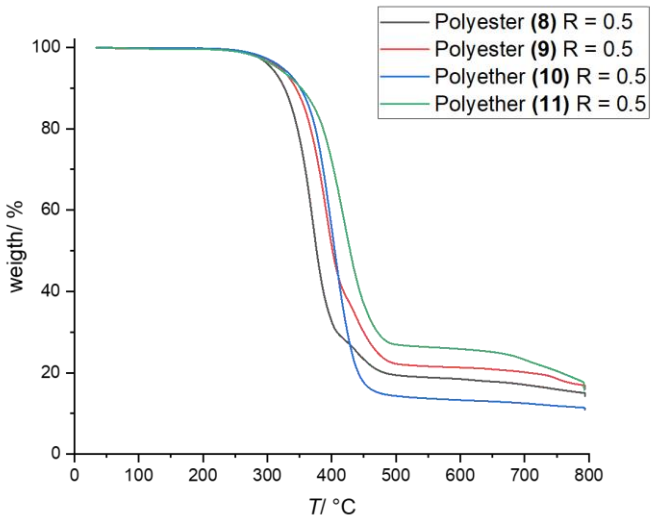

Figure 40 TGA measurements of the polyester and polyether diamines **(8)**-**(11)** cured films with ELO for R = 0.5.

For the cured films, IR spectra were recorded twice, once from the top side of the film and once from to bottom side (**Figure 41**). Interestingly, the IR spectra of the bottom side showed in all films, except for polyether **(10)**, an intensive N-H bending vibration at 1565 cm^{-1}, which was independent from the R value, indicating unreacted primary amine. In contrast, the top sides of the same films, exhibited no N-H bending assuming full conversion of the diamines. This observation indicates a mixing issues or phase separation between diamine and ELO, which was not observed on a smaller scale. This assumption is especially plausible for polyether **(11)**, for which almost no C=O ester vibration of the triglyceride was detected on the bottom side of the sample besides a very intensive N-H wagging vibration. Moreover, the C=O amide vibration was more intensive in the IR spectra recorded on the top side of the films.

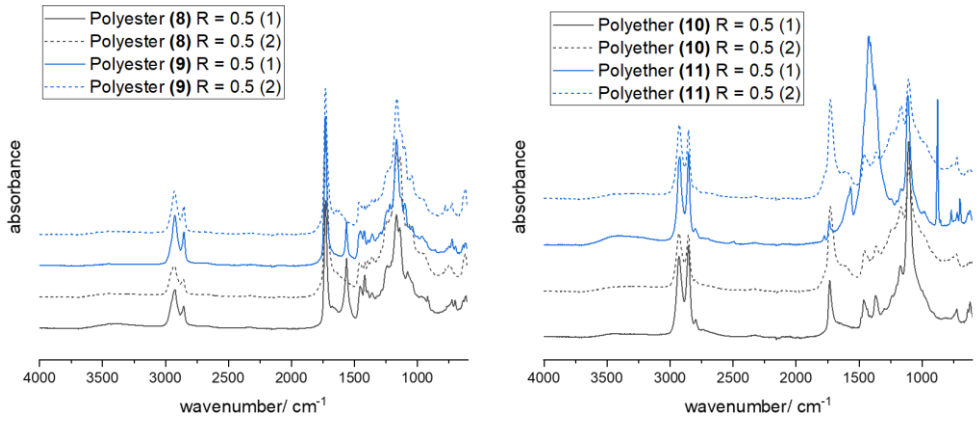

Figure 41 IR spectra of the diamine films cured with ELO and R = 0.5, measured from the bottom side (1) and the top side (2).

This inhomogeneity was further highlighted, especially for the polyethers, by the broad distribution of the tan *δ* values measured by DMTA (**Figure 40**). The tangent of the phase angel *δ* describes the ratio between the loss modulus *E"* and the storage modulus *E'*.[19;[394]] For a homogenous sample, a narrow peak for tan *δ* is expected, showing a sharp phase transition from the glassy to the rubbery state by a fast decrease in storage and loss modulus. In **Figure 40**, the storage modulus and tan *δ* for the amine cured films with ELO and an R value of 0.5 are exemplarily shown, while the corresponding measurements of R = 0.25 showed similar traces and are depicted in the experimental section as well as the loss modulus *E"* (chapter 6.3.3). Due to the high inhomogeneity, the mechanical and thermal properties of the polyether were not reliable and thus, only those of the polyesters were discussed. In general, the obtained storage modulus ranges from 2850 MPa to 3670 MPa for the glassy state, determined at -100 °C, which are similar to values of amine cured ELO thermosets reported in the literature (**Table 25**).[393, 395] The cross-linking density of a thermoset is proportional to the storage modulus in the rubbery state.[396] The higher *E'* in the rubbery state for the films cured with R = 0.5 compared to R = 0.25 indicates a higher cross-linking density (*E'* was determined at 150 °C). This assumption is in accordance with the theory, since an excess of ELO for R = 0.25 leads to unreacted epoxide groups and thus, a lower cross-linking density. Therefore, the amount of networking points per triglyceride is ideally doubled when a stochiometric ratio of R = 0.5 is used compared to 0.25 eq. diamine per epoxy group. This is further strengthened by the higher *E'* in the glassy state for R = 0.5 (**Table 25**). Furthermore, the AA based polyester **(8)** cured samples exhibited a higher elastic behavior compared to the once obtained from the SeA based polyester **(9)** (**Table 25**). Additionally, the transition temperature, T_α, determined by the maxima in tan *δ*, confirmed the trends observed from the T_g obtained by DSC measurements (**Table 25**). However, this trend was not consistent with the observed increased cross-linking density for an R value of 0.5, since also higher T_α and T_g had to be expected for a higher cross-linked material. Hence, strong intermolecular interactions between the polymer chains through secondary forces such as hydrogen bonding or dipole-dipole interactions are indicated, since these interactions are neglectable for the cross-linking density determined *via E'* at 150 °C.

[19] The storage modulus *E'* is measuring the stored energy of a viscoelastic material and is thus representing the elastic portion, while the loss modulus *E"* is measuring the energy dissipated as heat, representing the viscous portion. The phase angle *δ* describes the response in the resulting displacement (strain) after an oscillatory force was applied (stress). In a purely elastic material, that shift is zero and the stress and strain occur in phase, meaning a direct response of the applied force. In a purely viscous material, the phase difference is 90 degree. Thus, tan *δ* is measuring the damping of a material.

Table 25 DMTA analysis of the polyester cured films with ELO.

Entry	Diamine	R value	$E'_{-100\ °C}$ (MPa)	$E'_{150\ °C}$ (MPa)	T_α [°C]	T_g [°C] (DSC)
1	**(8)**	0.5	3670	30	-14	-36
2	**(8)**	0.25	3030	19	-6	-28
3	**(9)**	0.5	3340	39	-31	-44
4	**(9)**	0.25	2850	19	-22	-36

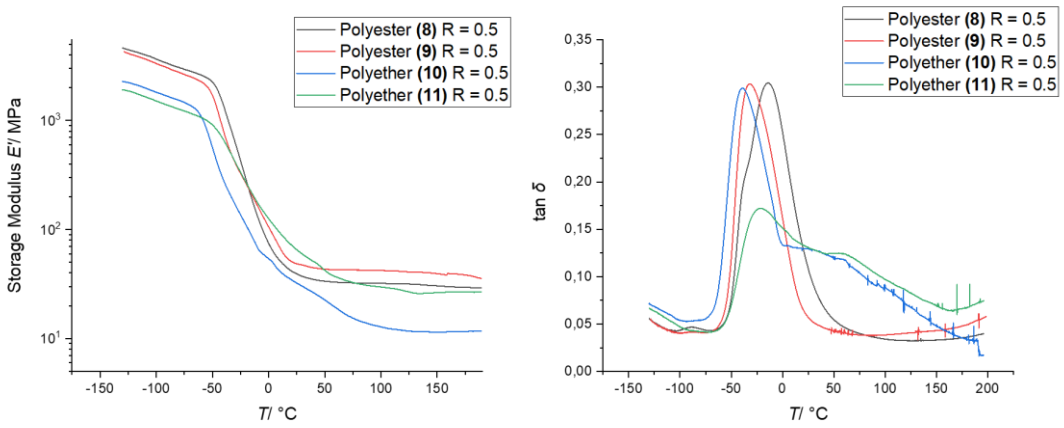

Figure 42 Storage modulus *E'* (left) and tan *δ* (right), determined *via* DMTA measurements of the diamine films cured with ELO with R = 0.5.

Summarizing, all polyester and polyether diamines were sucessfully cured with ELO under optimized conditions at 180 °C for 72 hours and were fully analyzed *via* IR-, DSC-, TGA- and DMTA analysis. However, for all samples an inhomogenity was observed as a result of an incompatibility or bad miscibility of the diamines and ELO. Especially, the polyether cured films showed pronounced broad transitions, as determined by DMTA, and thus, the mechanical properties were not meaningful. Nonetheless, the mechanical and thermal properties of the polyester cured materials indicated some trends for the chemical structures of the polymeric backbones and the stochiometric ratios. For instance, lower T_g and T_α were observed for the sebacic acid based polyester compared to the adipic acid based analogues. In addition, the storage modulus, representing the elastic behavior of the material, was higher for the adipic acid based polyester and decreased, when the stochiometric ratio was lowered from equimolar (R = 0.5), to R = 0.25. This was in accordance with a higher cross-linking density determined by the storage modulus in rubbery state.

Following, the adipic acid and sebacic acid based polyester and polyether diamines were cured with epoxidized lignin (EL) yielding a fully biobased thermoset with aromatic

structures. A first curing test of equimolar amounts of polyester **(8)** and (EL)[20] (R = 0.5) at 180 °C for 5 hours showed full conversion of the primary amine, indicated by the absence of a melting point *via* DSC. Additionally, the IR spectrum showed a decrease in the epoxy vibration at 909 cm^{-1}. However, the N-H bending vibration at 1565 cm^{-1} was overlapping with a not assigned vibration of the lignin structure (**Figure 43**).

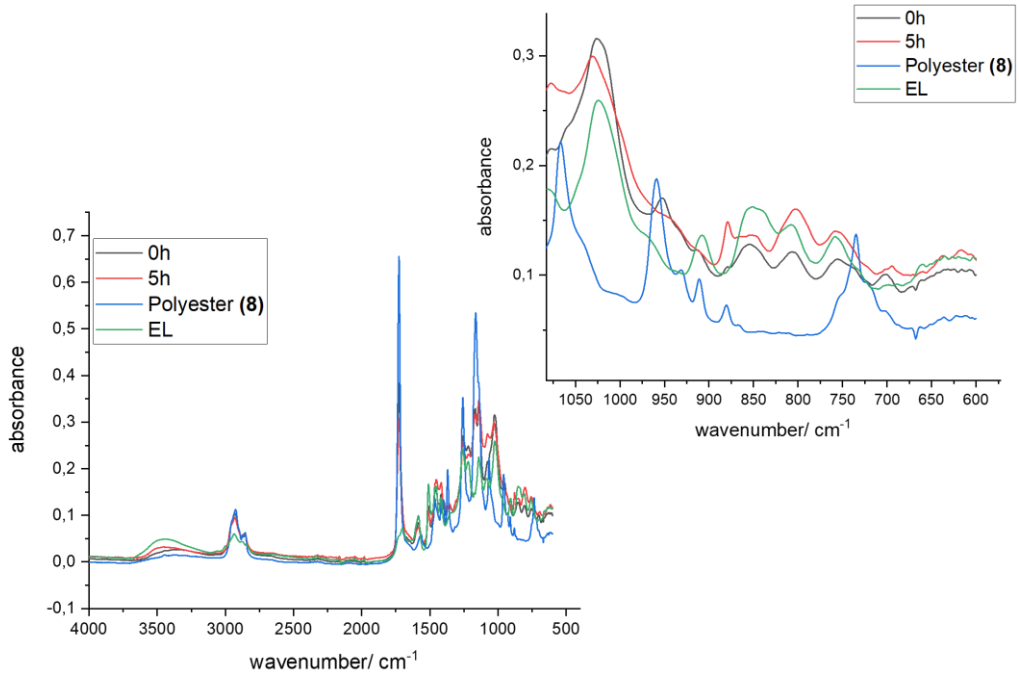

Figure 43 IR spectrum of polyester **(8)** cured epoxidized lignin (EL) with R = 0.5 for 5 hours at 180 °C, compared to the IR spectra of polyester **(8)**, EL and before curing (0 h, left) as well as the zoom-in (right).

Subsequently, the curing parameters were optimized for polyester **(8)** and EL. First of all, the stochiometric ratio of amine to epoxide was altered applying R values of 0.5, 1.0 and, 2.0 and cured at 180 °C for 7 hours. Hereby, unreacted diamine was observed when an excess of polyester **(8)** was added, determined by the melting point in the DSC and the N-H wagging vibration at 880 cm^{-1} (**Figure 44**). Hence, a higher stoichiometric ratio than R = 0.5 was not appropriate.

[20]The herein used EL was synthesized by Iuliana Ribca (KTH, Stockholm). The epoxy content of 2.3 mmol/g was determined by an external standard, namely 4-nitrobenzaldehyde, *via* proton NMR spectroscopy.

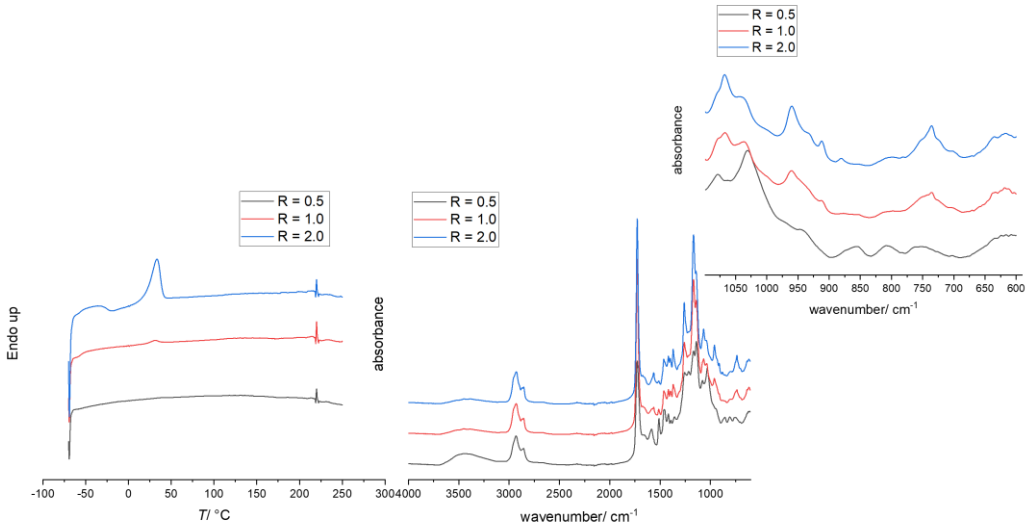

Figure 44 Second heating cycle of the DSC measurements (left) and IR spectra (right) of polyester **(8)** cured with EL for different R values at 180 °C after 7 hours.

As a next step, the curing temperature was lowered for an equimolar ratio (R = 0.5) to 100 °C for 2 hours, followed by a post-curing at 125 °C for further 2 hours. Hereby, the DSC traces of the second heating cycle showed no melting point of the starting material, complemented by the absence of the N-H wagging vibration corresponding IR spectrum. Finally, the R values were lowered to 0.4 and 0.3, respectively. No remaining primary diamine groups were visible in the second heating cycle of the DSC measurements, while still unreacted epoxide groups were indicated by the epoxy vibration at 909 cm^{-1} in the corresponding IR spectra (**Figure 45**).

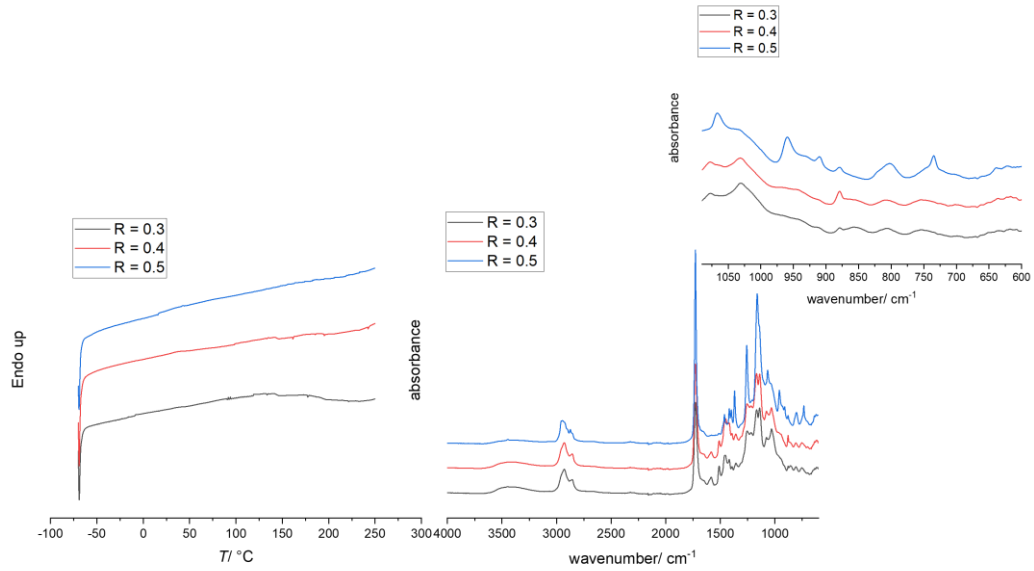

Figure 45 Second heating cycle of the DSC measurements (left) and IR spectra (center) of polyester **(8)** cured EL for different R values at 100 °C (125 °C) after 2 h (2 h) as well as the zoom-in (right).

Consequently, films for further mechanical analysis of all polyester and polyethers with EL were cured in a poly(tetrafluoroethylene) (PTFE) mold with an R value of 0.5 on a 400 mg scale for 2 hours at 100 °C and 3 hours at 125 °C. Thereby, only polyester **(8)** yielded a film, while all other diamines were incompatible with the epoxidized lignin due to miscibility issues. However, the obtained film was extremely inhomogeneous, as shown by the corresponding DMTA measurement, while unreacted starting material was still present in the DSC measurement (**Figure 46**). Thus, no meaningful information about the thermal and mechanical properties were obtained.

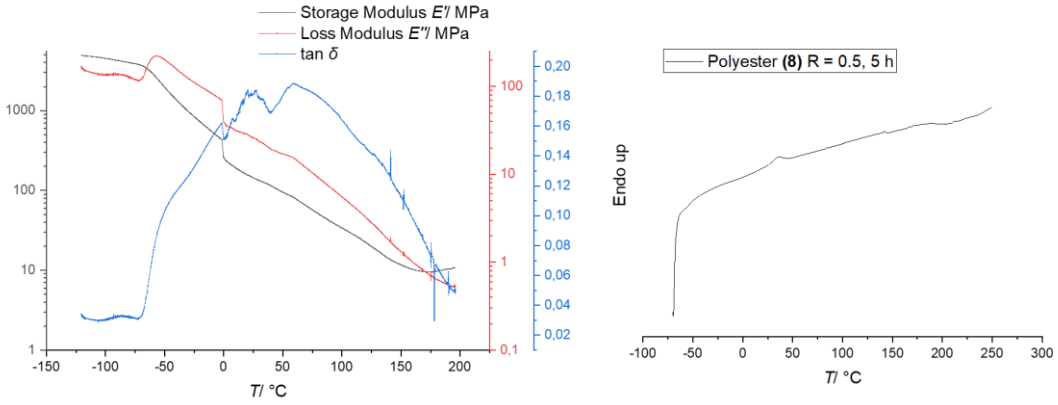

Figure 46 DMTA measurement (left) and DSC trace of the second heating cycle (right) of the polyester **(8)** cured film with EL and R = 0.5 at 100 °C for 2 h and subsequently at 125 °C for 3 h.

In conclusion, the terminal epoxides of the epoxidized lignin showed a higher reactivity with the polyester and polyether diamines, than the internal epoxy groups of ELO, whereby already full conversion of the diamine was observed for 2 hours at 100 °C and 3 hours post-curing at 125 °C compared to 180 °C and 72 hours for ELO. However, for all samples inhomogenity was observed as a result of an incompatibility or miscibility issues of the diamines and EL. Hence, no films were obtained for the sebacic acid based polyester **(9)** and both polyether diamines, while the adipic acid based polyester **(8)** cured with EL yielded a film which was an extremly inhomogenous material. This was shown by a very broad transition in the DMTA measurements. These results indicated that the starting materials were not suitable for each other. For further investiagtion on this approach of fully renewable thermosets using EL and polyester or -ether diamines the incompatibility of the compounds has to be examined in more detail. One opportunity is the addition of a second aromatic epoxide compound, such as bisphenol-A-digylcidylether, to increase the compatibility of the heterogeneous lignin with the diamine prepolymers.

In conclusion of this chapter, the fully biobased polyester and polyether diamines showed a good reactivity with the terminal epoxides of the epoxidizied lignin and moderate

reactivites with the internal oxiranes of the epoxidized linseed oil, while suffering from incompatibility or mixing issues. Epecially, the inhomogenity of the aromatic lignin structure impeded good materials obtained by the diamine prepolymers. The polyether diamines cured ELO thermosets showed very broad transitions in DMTA measurements as a result of the high inhomogenity of the sample, as further underlined by the corresponding IR spectra. Nontheless, good results were observed for the adipic acid and the sebacic acid based polyester **(8)** and **(9)**, showing expected trends considering the different chemical structures of the polymeric backbones. For instance, the T_g and T_α was lower for the longer aliphatic chain length of the sebacic acid in the polyester repeating unit, compared to the adipic acid, while the mechanical properties were slightly lower too. In addition, a higher cross-linking density was indicated for a equimolar ratio of diamine and epoxides by the higher *E'* in the rubbery state compared to the samples cured with an excess of epoxide. All polyester based thermosets showed an one-step degradation, while the T_d remained similar. Therefore, fully biobased thermosets with good thermal and mechanical properties were obtained from the polyester diamines.

5 Conclusion and Outlook

This work investigated the synthesis of novel polyol structures and their applications in polyurethanes and epoxy thermosets. It is divided into three parts. In the first subchapter the gallium bromide catalyzed reduction of aliphatic polyester polyols is investigated. The second part covers the synthesis of fully biobased aromatic polyester polyols based on 2,5-furandicarboxylic acid and their application in polyisocyanurate foams. In the third subchapter, renewable polyester and polyether polyols were synthesized and their end groups modified to amine groups. Subsequently, all diamine prepolymers were cured with two different renewable epoxides into fully biobased thermosets and their thermal and mechanical properties were analyzed.

In the first subchapter of this work, a gallium(III) bromide catalyzed reduction of aliphatic polyesters with silanes, which enables a broad spectrum of different aliphatic polyether polyol structures, was investigated. Therefore, the influence on the reaction rate of four polyester structures and two reducing agents, namely 1,1,3,3-tetramethyldisiloxane (TMDS) and triethylsilane (TES), were studied. The reaction rates for the reduction using TMDS as reducing agent, followed a clear trend. The closer the distance between the carbonyl groups in the polyester backbone, the higher the observed reaction rate. For instance, the polyester obtained from malonic acid and 1,3-propanediol showed a higher reaction rate compared to the polyester synthesized from adipic acid and 1,3-propanediol. The same trend was observed for the latter polyester, showing lower reaction times compared to the adipic acid and 1,4-butanediol based polyester. In general, the reduction with TMDS showed higher reaction rates compared to TES. The work-up procedure was challenging as a result of the low molecular weights of the polyether polyols obtained as viscous liquids. Hence, the polyether polyols were dissolved in a mixture of methanol and water, while the byproduct of the reduction using TMDS, polydimethylsiloxane (PDMS), was removed from the polyethers through several washing steps with petroleum ether. Because of similar densities between polyethers and petroleum ether, this work-up procedure suffers from reproducibility and low yields depending on the polyether structure. Thus, with the use of TES instead of TMDS, a distillation was possible and ensured high yields. However, on a larger scale, unreacted TES and byproduct hexaethyl disiloxane remained in the polyether polyols after distillation. Furthermore, for all polyethers and reducing agents, silylated end groups were obtained, limiting the reactivity of the polyol for further PU applications. To overcome this problem, an oxidation of the silyl ether end groups would be plausible. In

general, the reduction of the ester groups was accompanied by an overreduction of the desired ethers into the corresponding alcohols as side reaction. This led to a degradation of the polymeric backbone as well as alkyl end groups, which are not reactive for further polyurethane application. The polyester structure in combination with the reducing agent affected this side reaction, however no clear trend was observed. The limits of this reaction system were indicated for polyesters synthesized from malonic acid and 1,3-propanediol, where the degradation due to overreduction was too high. Further investigations should focus on the mechanism and kinetics of this side reaction, to obtain a better insight into the limiting parameter of this useful reduction method. Finally, the reaction was successfully scaled-up to 60 g polyester. The gallium bromide catalyzed reduction was transferred to cellulose acetate (CA), enabling a novel synthesis route towards the widely applied ethyl cellulose (EC) with good control over the degree of substitution (DS). The reduction showed full conversion as determined *via* IR spectroscopy besides a gelation of the reaction mixture. Three CA with different molecular weights and DS were studied. However, the gelation was not affected by the different cellulose acetates and already occurred in the absence of the reducing agent, when the catalyst was added to the CA solution. Thus, the gelation is presumably caused by intermolecular interactions of the cellulose backbone as a result of the close distance of the polymeric chains through the catalyst coordination. To further examine this assumption, bidental ligands such as acetyl acetone should be mixed in sub-stochiometric amounts with the catalyst before added to the CA solution. In addition to that, the solubility of the EC in most organic solvents depends on the ethoxy content. Therefore, a determination of the DS would be necessary to further investigate this hypothesis. However, a precise analysis of the DS requires a possible work-up procedure to remove the siloxane byproducts. This can be facilitated through the use of TES instead of TMDS, since only hexaethyl disiloxane and no polysiloxanes are obtained as byproduct by this reducing agent.

In the second subchapter, fully biobased aromatic polyester polyols with low molecular weights were synthesized from the sugar based 2,5-furandicarboxylic acid (FDCA). Thereby, the one-pot polymerization of FDCA and two glycols, ethylene glycol (EG) and diethylene glycol (DEG), were investigated. However, the use of EG led to insoluble, non-processable polyols. The reaction conditions of the polycondensation of FDCA and DEG yielding poly(diethylene furanoate) (PDEF), were optimized in terms of degree of polymerization (X_n) and excess of remaining DEG to ensure a still processable, not too viscous polyol. Moreover, the surfactant Brij® L4 was added to the reaction mixture without negative impact on the reaction system, further decreasing the viscosity. The reduction of viscosity was also achieved by either copolymerizing 10-20 mol% of a

biobased aliphatic dicarboxylic acid (succinic or adipic acid), maintaining the fully biobased character of the polyol, or copolymerizing phthalic acid instead. The polyol synthesis was scaled-up to 100 g of dicarboxylic acid, still showing good control over the molecular weight. The measured OH values of the obtained biobased polyols were slightly higher compared to a commercial, petroleum based reference polyol, but a higher X_n would have led to non-processable PDEF. Subsequently, the fully biobased aromatic polyester polyols were applied in polyisocyanurate (PIR) foams and the thermal und mechanical properties were compared to those synthesized by the commercially used, petroleum based reference polyol. Thereby, all PIR foams obtained from the FDCA based polyols showed similar densities, thermal conductivities, and mechanical properties, compared to the reference PIR foam. The flame behavior was slightly better for the phthalic acid based polyol compared to the biobased polyols due to a higher oxygen content of the furan unit in the polymer backbone. Thus, these results showed a possible substitution of the petroleum based polyol through the fully biobased aromatic polyester polyols based on PDEF for certain industrial applications.

In the third subchapter, the fully biobased polyesters were synthesized *via* polycondensation of adipic acid or sebacic acid and 1,4-butanediol followed by an end group modification with 10-undecylenic acid in a pseudo one-pot polymerization leading to double bond end groups. A direct one-pot polymerization of all three compounds was more complicated due to evaporating butanediol under the applied reaction conditions resulting in undesired carboxylic acid end groups, as a result of the changed stoichiometry. Subsequently, half of the polyesters were successfully converted into the corresponding polyethers *via* the $GaBr_3$ catalyzed reduction. Finally, the end groups of both, polyesters and polyethers, were modified into amine groups *via* thiol-ene reaction with cysteamine hydrochloride. Thermal analysis of the obtained diamine prepolymers showed melting points from 26 °C to 53 °C, besides degradation starting from 230 to 275 °C. In general, the degradation temperature at the turning point (T_d) was higher for the sebacic acid based polyester diamine **(9)** (400 °C) than for the adipic acid based analogues (300 °C), while the polyether showed similar T_d of 400 °C. Furthermore, the adipic acid based polyether showed a higher thermal stability compared to the corresponding polyesters. Finally, the different diamine prepolymers were cured into fully biobased thermosets with two different epoxides, based on linseed oil and lignin. Thereby, all diamines showed a good reactivity with the terminal epoxides of the epoxidized lignin (EL) besides moderate reactivities with the internal oxiranes of the epoxidized linseed oil (ELO). All biobased thermosets suffered from inhomogeneities caused by incompatibility or miscibility issues of the diamine prepolymers and the epoxides. Especially, the inhomogeneity of the aromatic lignin structure was too high for

obtaining good materials. Moreover, the polyether diamines cured ELO thermosets showed broad transitions in DMTA measurements. Nevertheless, good results were observed for the adipic acid and the sebacic acid based polyester diamines, showing trends of the different chemical structures of the polymeric backbones. The glass transition temperature T_g and T_α, determined by the maximum of tan δ in the DMTA measurements, of the cured thermosets were lower for the longer chain length of the sebacic acid in the polyester repeating unit, compared to the adipic acid. The mechanical properties were slightly lower for the thermosets obtained from the sebacic acid based polyester. In addition, a higher cross-linking density was indicated for a equimolar ratio of diamine and epoxide by the higher storage modulus in the rubbery state compared to the same samples cured with an excess of epoxide. All polyester based thermosets showed an one-step degradation, while T_d was similar. Therefore, fully biobased thermosets with good thermal and mechanical properties were obtained from the polyester diamines.

Overall, novel polyol structures were synthesized through the gallium bromide catalyzed reduction of polyesters or the polycondensation reaction of biobased platform chemicals. Furthermore, the obtained polyols were applied in polyisocyanurate rigid foams as well as in epoxy thermosets and their thermal and mechanical properties were determined.

6 Experimental Section

6.1 Materials

Unless otherwise noted, all solvents and reagents were used as received without further purification.

1,1,3,3-tetramethyldisiloxane (97%, Sigma Aldrich), 1,4-butanediol (99%, Alfa Aesar), 10-undecylenic acid (98%, Sigma Aldrich), 2,2-dimethoxy-2-acetophenone (99%, Sigma Aldrich), 2,5-furandicarboxylic acid (98%, BLDpharm), 4-nitrobenzaldehyde (98%, Sigma Aldrich), acetyl acetone (> 99%, Sigma Aldrich), adipic acid (99%, Acros Organics), antimony trioxide (99%, Sigma Aldrich), Brij L4® (Sigma Aldrich), CATALYST LB (Huntsman), cellulose acetate (Acros Organics; 97%, Sigma Aldrich), chloroform (99.8%, Fisher Chemicals), chloroform-d (99.8 atom% D, Eurisotop), cysteamine (95%, Sigma Aldrich), cysteamine hydrochloride (98%, Acros Organics), DABCO® TMR13 (Evonik), Desmodur® 44V70L (Covestro), Desmophen® V657 (Covestro), dichloromethane (HPLC grade, VWR), dichloromethane anhydrous (> 99.8%, Sigma Aldrich), diethylene glycol (99%, chemPUR), dimethyl acetamide (> 99.9%, Sigma Aldrich), dimethyl sulfoxide (> 99.9% Fisher Chemicals), dimethyl sulfoxide-d_6 (99.9 atom% D, Sigma Aldrich), epoxidized linseed oil (Nordic United Coatings AB (Sweden)), ethyl cellulose (Sigma Aldrich), ethylene glycol (99%, chemPUR), gallium(III) bromide (99.999%, Sigma Aldrich), hexafluoro isopropanol (99%, fluorochem), hydrochloric acid (37%, VWR), Jeffamine-D400 (Huntsman), linseed oil (Linotech AB (Sweden)), methanol (> 99.8%, VWR), *N,N,N′,N′,N″*-pentamethyldiethylenetriamine (> 98%, Acros Organics), *n*-hexane (97%, VWR), pentane (60% cyclohexane, 40% isopentane, Julius Hoesch), petroleum ether (> 90% Sigma Aldrich), phthalic acid (> 99.5%, Sigma Aldrich), POLYCAT® 36 (Evonik), potassium trifluoromethanesulfonate (98%, Sigma Aldrich), pyridine (> 99.5% Fisher Chemicals), sebacic acid (99%, Sigma Aldrich), STRUKSILON KOCT 15 (Schill+Seilacher), succinic acid (99%, Acros Organics), TEGOSTAB® B84510 (Evonik), tetrahydrofuran (> 99.8%, VWR), tetrahydrofuran anhydrous (> 99.9%, Sigma Aldrich), tin(II) 2-ethylhexanote (95%, Alfa Aesar), titanium(IV) isopropoxide (97%, Sigma Aldrich), toluene (> 99.8% Fisher Chemicals), triethylphosphate (PROCHEMA), triethylsilane (99%, Sigma Aldrich), tris(chlorisopropyl) phosphate (PROCHEMA).

6.2 Characterization Methods

Nuclear magnetic resonance spectroscopy (NMR)

^{1}H-NMR and ^{13}C-NMR spectra were recorded on Bruker Advance DRX (500 MHz for ^{1}H- and 126 MHz for ^{13}C-NMR) or Bruker Ascend™ 400 (400 MHz for ^{1}H- and 101 MHz for ^{13}C-NMR) spectrometer at ambient temperature. The chemical shifts for ^{1}H-NMR and ^{13}C-NMR spectra were reported in ppm relative to the solvent signal DMSO-d_5 (^{1}H-NMR: 2.50 ppm; ^{13}C-NMR: 39.52 ppm) or $CHCl_3$ (^{1}H-NMR: 7.26 ppm; ^{13}C-NMR: 77.16 ppm) Data for ^{1}H-NMR were reported as follows: multiplicity (s = singlet, d = doublet, t = triplet, q = quartet, quint = quintet, sext = sextet, m = multiplet, b = broad) and assignment. Furthermore, correlated spectroscopy (COSY), heteronuclear single quantum coherence (HSQC) and heteronuclear multiple bond correlation (HMBC) were carried out to determine the structures.

Size exclusion chromatography (SEC)

For SEC, three different systems were used:

A PSS SECcurity^2 GPC system based on Agilent infinity 1260 II hardware. The system is equipped with a refractive index detector SECcurity² RI, a column oven "(Bio)SECcurity² column compartment TCC6500", a "standard SECcurity²" autosampler, isocratic pump "SECcurity² isocratic pump". THF (flow rate 1 mL/min) at 30 °C was used as mobile phase. The analysis was performed using the following column system: Two columns PSS SDV analytical (3 µm, 300 × 8.0 mm^2, 1000 Å) with a PSS SDV analytical precolumn (3 µm, 50 × 8.0 mm^2). For the calibration, narrow linear poly(methyl methacrylate) standards (Polymer Standards Service, PPS, Germany) ranging from 102 to 62200 Da were used.

Size exclusion chromatography (SEC) was performed on an Agilent 1200 system, comprising an auto-sampler, a Plgel 5 µm bead-size guard column (50 × 7.5 mm^2), one Plgel 5 µm Mixed E column (300 × 7.5 mm^2), three Plgel 5 µm Mixed C columns (300 × 7.5 mm^2) and a differential refractive index detector as well as an UV detector using THF as eluent at 35 °C with a flow rate of 1 mL/min. The SEC system was calibrated using linear poly(styrene) standards ranging from 370 to 6 × 10^6 g/mol or poly(methyl methacrylate) standards ranging from 800 to 2.2 × 10^6 g/mol. All SEC calculations were carried out relative to poly(methyl methacrylate) calibration.

SEC in hexafluoro isopropanol was performed on a Tosoh EcoSEC HLC-8320 SEC system. HFIP (flow rate 0.40 mL/min) at 35 °C was used as mobile phase. The analysis was performed on a three-column system: PSS PFG Micro pre-column (3.0 × 0.46 cm^2,

10000 Å), PSS PFG Micro (25.0 × 0.46 cm^2, 1000 Å) and PSS PFG Micro (25.0 × 0.46 cm^2, 100 Å). The system was calibrated with linear poly(methyl methacrylate) standards (PSS, M_p:102-981 kg/mol).

Infrared spectroscopy (IR)

For IR analysis, two different systems were used:

A PerkinElmer Spectrum 100 instrument was used. FT-IR spectra were acquired in attenuated total reflection (ATR) mode with an MKII Golden Gate accessory (Specac Ltd.) equipped with a diamond crystal. Each measurement was averaged over 16 scans between 4000 and 600 cm^{-1} at room temperature.

Infrared spectra were recorded using a Bruker Alpha-p instrument with ATR technology in a range of v = 400–4000 cm^{-1} with 12 scans per measurement at room temperature.

Orbitrap electrospray-ionization mass spectrometry (ESI-MS)

Mass spectra were recorded on a Q Exactive (Orbitrap) mass spectrometer (Thermo Fisher Scientific, San Jose, CA, USA) equipped with an atmospheric pressure ionization source operating in the nebulizer assisted electrospray mode. The instrument was calibrated in the m/z range 150-2000 using a standard containing caffeine, Met-Arg-Phe-Ala acetate (MRFA) and a mixture of fluorinated phosphazenes (Ultramark 1621, all from Sigma-Aldrich). A constant spray voltage of 3.5 kV, a dimensionless sheath gas of 6, and a sweep gas flow rate of 2 were applied. The capillary voltage and the S-lens RF level were set to 68.0 V and 320 °C, respectively. For the interpretation of the spectra, molecular peaks $[M]^+$, peaks of pseudo molecules $[M+H]^+$ and $[M+Na]^+$ characteristic fragment peaks are indicated with their mass to charge ratio (m/z) and their intensity in percent, relative to the most intense peak (100%).

Size exclusion chromatography-electrospray ionization mass spectrometry (SEC-ESI)

Size exclusion chromatography-electrospray ionization mass spectrometry (SEC-ESI MS) spectra were recorded on a LTQ Orbitrap XL Q Exactive mass spectrometer (Thermo Fisher Scientific, San Jose, CA, USA) equipped with a HESI II probe. The instrument was calibrated in the m/z range 74-1822 using premixed calibration solutions (Thermo Scientific). A constant spray voltage of 4.6 kV, a dimensionless sheath gas of 8, and a dimensionless auxiliary gas flow rate of 2 were applied. The capillary temperature and the S-lens RF level were set to 320 °C and 62.0 V, respectively. The Q Exactive was coupled to an UltiMate 3000 UHPLC System (Dionex, Sunnyvale, CA, USA) consisting of a pump (LPG 3400SD), autosampler (WPS 3000TSL), and a thermostated column department (TCC 3000SD). Separation was performed on two mixed bed size exclusion chromatography columns (Polymer Laboratories, Mesopore 250 × 4.6 mm^2, particle diameter 3 µm) with precolumn (Mesopore 50 × 4.6 mm^2) operating at 30 °C. THF at a flow rate of 0.30 mL/min was used as eluent. The mass spectrometer was coupled to the column in parallel to (an UV-Detector (VWD 3400 RS), and) a RI detector (RefractoMax520, ERC, Japan) in a setup described earlier.[397] 0.27 mL/min of the eluent were directed through the RI-detector and 30 µL/min infused into the electrospray source after postcolumn addition of a 100 µM solution of sodium iodide in methanol at 20 µL/min by a micro- flow HPLC syringe pump (Teledyne ISCO, Model 100DM). A 50 µL aliquot of a polymer solution with a concentration of 2 mg/mL was injected onto the HPLC system

Thermogravimetric analysis (TGA)

TGA measurements were performed using a Mettler Toledo TGA/DSC1 instrument. All samples with a mass of 10.0 ± 3 mg were placed in a ceramic crucible where they were kept for 10 min at 30 °C. Specimens were then heated at a rate of 5 K/min in a nitrogen atmosphere (flow rate, 50 mL/min) up to 800 °C and maintained isothermally for 10 min. Mettler-Toledo STARe software V15.00a was used to record all data.

Different Scanning Calorimetry (DSC)

Thermal transitions were investigated by DSC using a Mettler Toledo DSC1 equipped with a sample robot. Measurements were performed with a heating/ cooling rate of 10 K/min in a nitrogen atmosphere (flow rate, 50 mL/min). Samples of about 10.0 ± 5 mg were placed in a 100 µL aluminum crucible and covered using a pierced lid. The DSC thermograms were recorded by heating the samples from -70 °C up to 150 °C (first heating cycle) and isothermally kept for 10 min to erase any thermal history. They were

then cooled to -70 °C and held isothermally for 10 min. In the end, all samples were heated to 250 °C (second heating cycle). The turning point for the second heating cycle was taken as the glass transition temperature. The data were analyzed with Mettler-Toledo STARe software V15.00a.

Dynamic mechanical thermal analysis (DMTA)

The viscoelastic properties were obtained by a TA Instruments DMA Q800 equipped with a gas cooling accessory and tensile film clamps. The rectangular samples were subjected to a strain of 0.1% at 1 Hz with a preload force of 0.01 N (force track 125%). Prior to testing, the samples were cooled and equilibrated at -130 °C. Afterward, they were heated to a temperature of 200 °C at a rate of 3 K/min. The T_α was determined from the maximum of the tan δ signal.

Thermal conductivity measurements of PIR foams

Thermal conductivity measurements were carried out on a HESTO-Lambda-CONTROL A50 using the program Z50148/K according to DIN EN 12667 “Thermal performance of building materials and products - Determination of thermal resistance by means of guarded hot plate and heat flow meter methods - Products of high and medium thermal resistance”, May 2001. The temperature of the heating plate was 36.0 °C and the cooling plate was set to 10.0 °C. The duration for each experiment varied from 28 to 57 minutes.

Mechanical tests of PIR foams

Compressive and tensile strength test were performed on a Zwick/ Roell Z020 according to DIN EN 826 “Thermal insulating products for building applications - Determination of compression behavior”, May 2013.

Procedure for measuring flame behavior of PIR foams

Flame behavior tests were conducted according to DIN 4102 part 1 “Fire behavior of building materials and building components - Part 1: Building materials; concepts, requirements and tests”, May 1998. All foams were categorized and tested as B2: Standard flammable building materials. The inflammability must be in the required range according to the DIN standard.

6.3 Experimental Procedure

6.3.1 Experimental Procedures and Supporting Information of Chapter 4.1

General procedure for the reduction of aliphatic polyester with TMDS

Polyester was placed under inert conditions in a Schlenk-Flask and dissolved in dry DCM. Afterwards $GaBr_3$ was added and stirred at room temperature. Then 1,1,3,3-tetratmethyldisiloxane (TMDS) was added dropwise within one hour *via* syringe pump and stirred at room temperature. After full conversion, the crude product was washed with diluted hydrochloric acid (5%) and water, dried over Na_2SO_4 and concentrated under reduced pressure. The crude mixture was dissolved in a mixture of methanol and water (ratio 10:1) and extracted with petroleum ether (5×) to remove polysiloxane. The methanolic layer was concentrated *in vacuo*, the residue was again dissolved in a mixture of methanol and water (ratio 10:1, 25% v/v as before) and extracted again with petroleum ether (5×, 25% v/v as before). The methanolic layer was dried over Na_2SO_4 and after filtration the solvent was removed *in vacuo.*

General procedure for the reduction of aliphatic polyester with TES

Polyester was placed under inert conditions in a Schlenk-Flask and dissolved in dry DCM. Afterwards $GaBr_3$ was added and stirred at room temperature. Then triethylsilane (TES) was added dropwise within one hour *via* syringe pump and stirred at room temperature. After full conversion, the crude product was washed with diluted hydrochloric acid (5%) and water, dried over Na_2SO_4 and concentrated under reduced pressure. The residue was distilled under reduced pressure (1 mbar) at 130 °C.

General procedure for the reduction of cellulose acetate with TMDS

Cellulose acetate was placed under inert conditions in a Schlenk-Flask and dissolved in dry DCM. Afterwards $GaBr_3$ was added and stirred at room temperature. Then 1,1,3,3-tetratmethyldisiloxane (TMDS) was added dropwise within one hour *via* syringe pump and stirred at room temperature. The obtained gel was filtered and the filtrate was concentrated under reduced pressure.

Polyether 2a

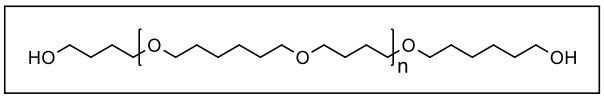

Reduction of polyester 1a with TES

60.0 g polyester **1a** (297 mmol, 1.00 eq.[21]) was placed under inert conditions in a 1 L Schlenk-Flask and 480 mL dry DCM was added until the starting material was totally dissolved. Afterwards 1.84 g $GaBr_3$ (5.93 mmol, 0.02 eq.) was added and stirred at room temperature. Then 209 mL triethylsilane (152 g, 1.31 mol, 4.40 eq.) was added dropwise within one hour *via* syringe pump and stirred at room temperature for 5 days. Then the crude product was washed with hydrochloric acid (5%) and water, dried over Na_2SO_4 and concentrated under reduced pressure. The residue was distilled under reduced pressure (1 mbar) at 130 °C. Polyether **2a** was obtained as a colorless liquid (44.4 g, 86%).

Reduction of polyester 1a with TMDS

40.0 g polyester **1a** (198 mmol, 1.00 eq.) was placed under inert conditions in a 1 L Schlenk-Flask and 800 mL dry DCM was added until the starting material was totally dissolved. Afterwards 1.22 g $GaBr_3$ (3.96 mmol, 0.02 eq.) was added and stirred at room temperature. Then 76.9 mL 1,1,3,3-tetratmethyldisiloxane (TMDS) (58.5 g, 435 mmol, 2.20 eq.) was added dropwise within one hour *via* syringe pump and stirred at room temperature for 7 days. The crude mixture was dissolved in a mixture of methanol (800 mL) and water (80 mL) and extracted with 160 mL petroleum ether (5×) to remove polysiloxane. The methanolic layer was concentrated *in vacuo*, the residue was dissolved in a mixture of methanol (200 mL) and water (20 mL) and extracted again with 40 mL petroleum ether (5×). The methanolic layer was dried over Na_2SO_4 and after filtration the solvent was removed *in vacuo.* Polyether **2a** was obtained as a colorless liquid (14.6 g, 42%).

[21] The stoichiometry was calculated per repeating unit. 1.00 eq is equal to one repeating unit. The same assumptions were applied for the synthesis of polyether **2b-d**.

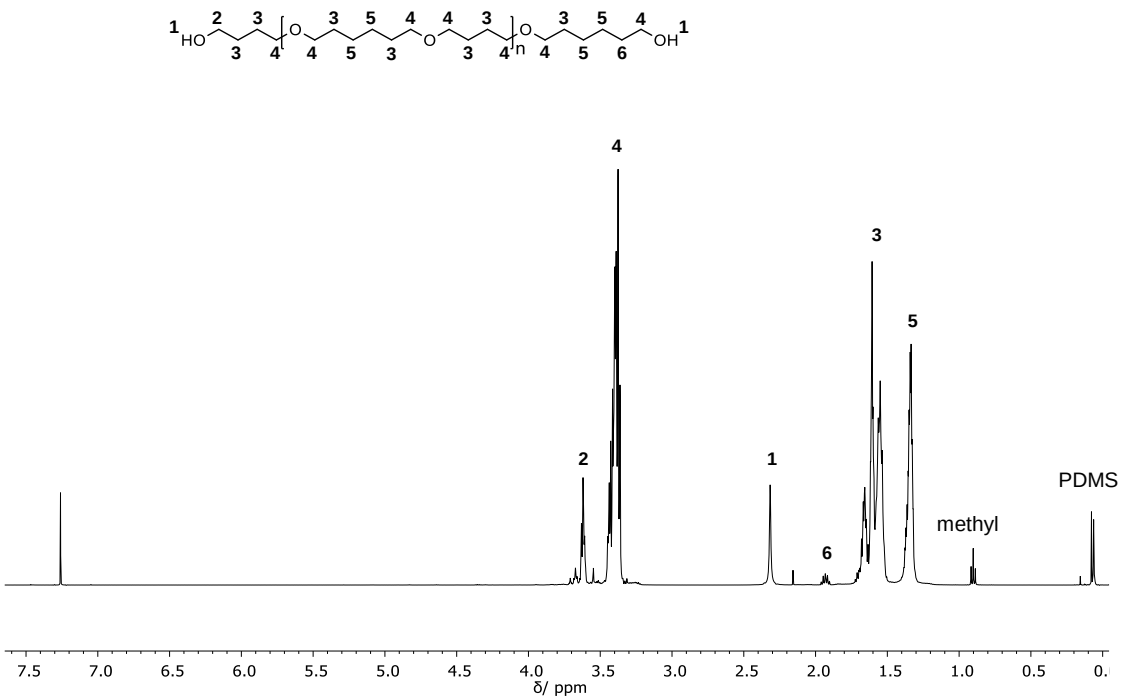

Figure S 1 ^{1}H-NMR spectrum of polyether **2a**, measured in $CDCl_3$.

^{1}H-NMR (500 MHz, DMSO-d_6): ***δ***/ppm = 3.67 (t, C***H₂***OSi, end group), 3.62 (t, C***H₂²***OH, end group), 3.35-3.46 (m, 8H, C***H₂⁴***OC***H₂⁴*** + C***H₂⁴***OH, end group), 2.32 (s, O***H¹***, end group), 1.93 (quint, C***H₂⁶***CH_2OH, end group), 1.50-1.75 (m, 8H, C***H₂³***CH_2OCH_2C***H₂³***), 1.34 (m, 4H, OCH_2CH_2C***H₂⁵***C***H₂⁵***CH_2CH_2O), 0.90 (t, C***H₃***CH_2, end group).

^{13}C-NMR (126 MHz, DMSO-d_6): ***δ***/ppm = 71.17, 70.98, 70.92, 70.75, 62.84, 32.83, 30.52, 29.85, 29.81, 29.69, 27.10, 26.61, 26.21, 26.13, 25.72.

IR (ATR platinum diamond): *ν*/cm^{-1} = 2933, 2859, 2802, 1489, 1465, 1436, 1374, 1244, 1218, 1205, 1113, 1057, 1028, 979, 728, 576, 559, 525, 453.

Polyether 2b

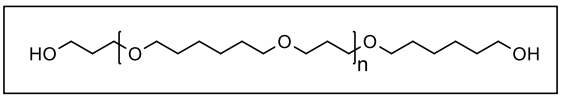

Reduction of polyester 1b with TMDS

40.0 g polyester **1b** (212 mmol, 1.00 eq.) was placed under inert conditions in a 1 L Schlenk-Flask and 800 mL dry DCM was added until the starting material was totally dissolved. Afterwards 1.32 g $GaBr_3$ (4.25 mmol, 0.02 eq.) was added and stirred at room temperature. Then 82.6 mL 1,1,3,3-tetratmethyldisiloxane (TMDS) (62.8 g, 458 mmol, 2.20 eq.) was added dropwise within one hour *via* syringe pump and stirred at room

temperature for 18 hours. Then the crude product was washed with diluted hydrochloric acid (5%) and water, dried over Na_2SO_4 and concentrated under reduced pressure. The crude mixture was dissolved in a mixture of methanol (800 mL) and water (80 mL) and extracted with 160 mL petroleum ether (5×) to remove polysiloxane. The methanolic layer was concentrated *in vacuo*, the residue was dissolved in a mixture of methanol (200 mL) and water (20 mL) and extracted again with 40 mL petroleum ether (5×). The methanolic layer was dried over Na_2SO_4 and after filtration the solvent was removed *in vacuo.* Polyether **2b** was obtained as a colorless liquid (25.5 g, 72%).

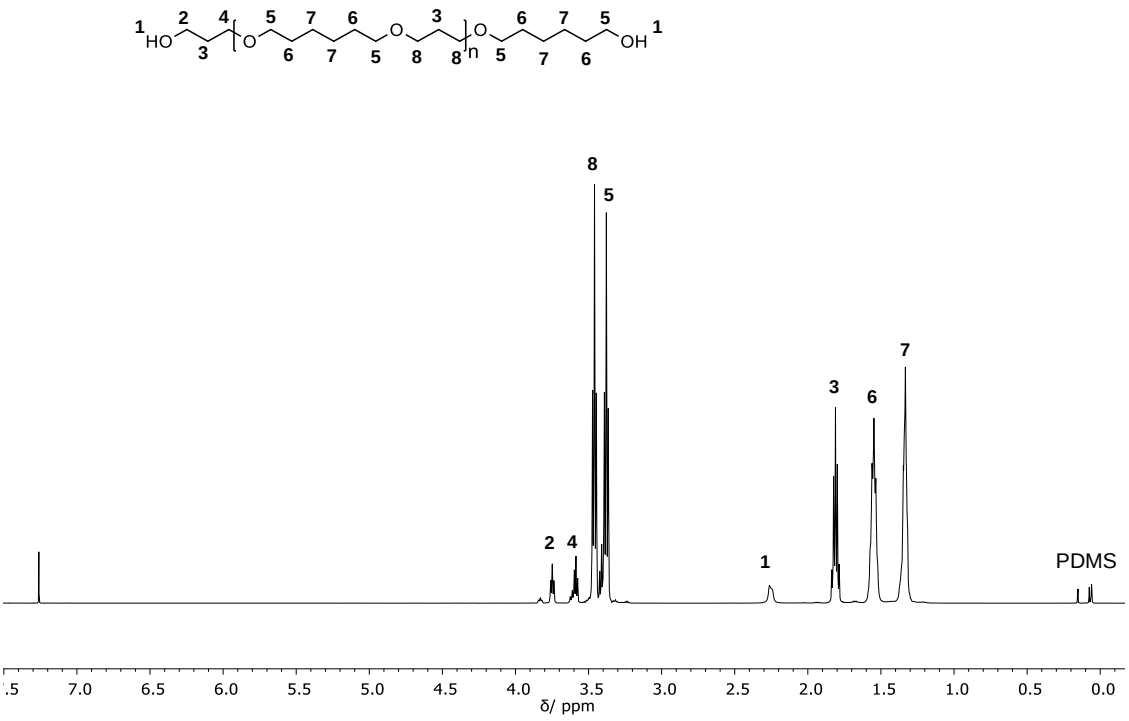

Figure S 2 ^{1}H-NMR spectrum of polyether **2b**, measured in $CDCl_3$.

^{1}H-NMR (500 MHz, DMSO-d_6): *δ*/ppm = 3.75 (t, C***H*₂²**OH, end group), 3.59 (t, OC***H*₂⁴**CH_2CH_2OH, end group), 3.46 (t, 4H, C***H*₂⁸**OC***H*₂⁸**), 3.41 (t, C***H*₂⁵**OH, end group), 3.38 (t, 4H, C***H*₂⁵**OC***H*₂⁵**), 2.26 (s, O***H*¹**, end group), 1.81 (quint, OCH_2C***H*₂³**CH_2O), 1.55 (m, 4H,OCH_2C***H*₂⁶**CH_2CH_2C***H*₂⁶**CH_2O), 1.55 (m, 4H,OCH_2CH_2C***H*₂⁷**C***H*₂⁷**CH_2CH_2O).

^{13}C-NMR (126 MHz, DMSO-d_6): *δ*/ppm = 71.44, 71.07, 71.01, 70.37, 67.93, 62.33, 32.09, 30.27, 29.83, 29.77, 29.75, 26.20, 26.14.

IR (ATR platinum diamond): *ν*/cm^{-1} = 2931, 2854, 2796, 1483, 1462, 1434, 1368, 1316, 1298, 1251, 1217, 1184, 1108, 957, 916, 850, 780, 728, 620, 559.

Polyether 2c

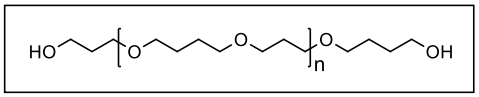

Reduction of polyester 1c with TMDS

40.0 g polyester **1c** (253 mmol, 1.00 eq.) was placed under inert conditions in a 1 L Schlenk-Flask and 800 mL dry DCM was added until the starting material was totally dissolved. Afterwards 1.57 g $GaBr_3$ (1.26 mmol, 0.02 eq.) was added and stirred at room temperature. Then 98.3 mL 1,1,3,3-tetratmethyldisiloxane (TMDS) (74.7 g, 556 mmol, 2.20 eq.) was added dropwise within one hour *via* syringe pump and stirred at room temperature for 4 days. After full conversion, the crude product was washed with diluted hydrochloric acid (5%) and water, dried over Na_2SO_4 and concentrated under reduced pressure. The crude mixture was dissolved in a mixture of methanol (800 mL) and water (80 mL) and extracted with 160 mL petroleum ether (5×) to remove polysiloxane. The methanolic layer was concentrated *in vacuo*, the residue was dissolved in a mixture of methanol (200 mL) and water (20 mL) and extracted again with 40 mL petroleum ether (5×). The methanolic layer was dried over Na_2SO_4 and after filtration the solvent was removed *in vacuo.* Polyether **2c** was obtained as a colorless liquid (33.2 g, 97%).

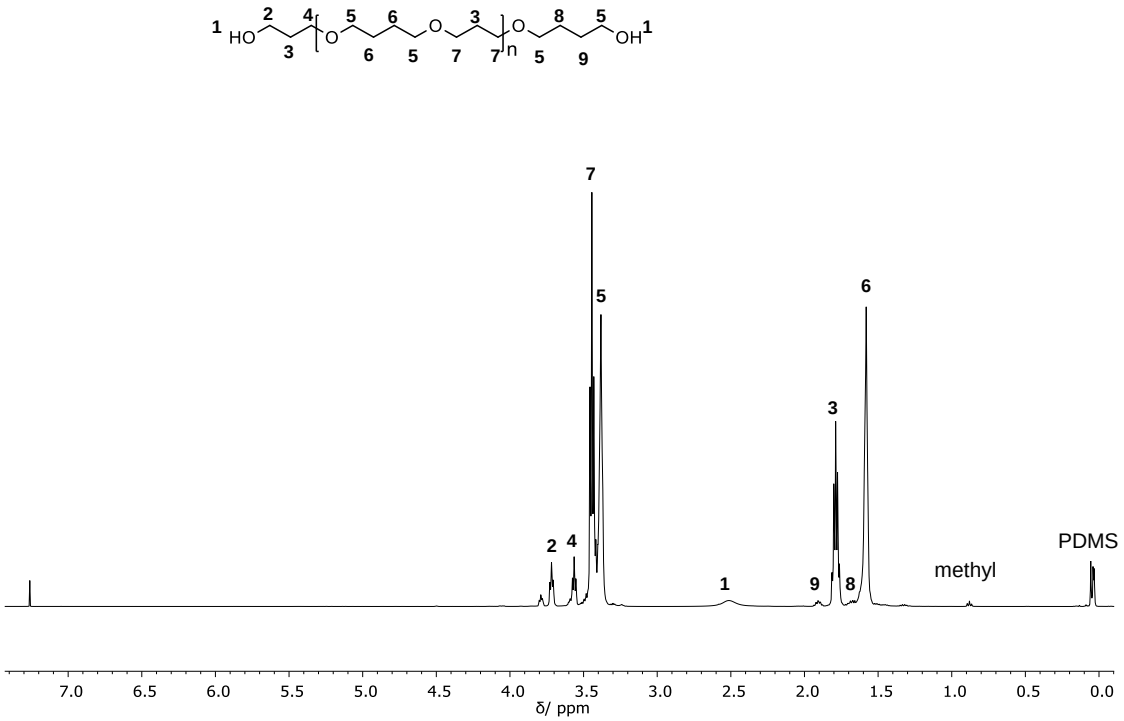

Figure S 3 ^{1}H-NMR spectrum of polyether **2c**, measured in $CDCl_3$.

^{1}H-NMR (500 MHz, DMSO-d_6): *δ*/ppm = 3.79 (t, C***H₂***OSi, end group), 3.72 (t, C***H₂²***OH, end group), 3.56 (t, OC***H₂⁴***CH_2CH_2OH, end group), 3.44 (t, 4H, C***H₂⁷***OC***H₂⁷***), 3.34-3.42 (m, 4H, C***H₂⁵***OC***H₂⁵*** + C***H₂⁵***OH, end group), 2.52 (s, O***H¹***, end group), 1.91 (quint, CH_2CH_2C***H₂⁹***CH_2OH, end group), 1.79 (quint, 2H OCH_2C***H₂³***CH_2O), 1.67 (m, CH_2C***H₂⁸***CH_2CH_2OH, end group), 1.58 (m, 4H,OCH_2C***H₂⁶***C***H₂⁶***CH_2O), 0.90 (t, C***H₃***CH_2, end group).

^{13}C-NMR (126 MHz, DMSO-d_6): *δ*/ppm = 71.13, 71.77, 70.67, 70.00, 69.90, 67.87, 67.85, 67.82, 34.18, 33.83, 32.23, 32.09, 30.21, 30.19, 29.80, 28.38, 26.53, 26.46.

IR (ATR platinum diamond): *ν*/cm^{-1} = 2939, 2859, 2799, 1483, 1469, 1438, 1421, 1368, 1314, 1294, 1259, 1244, 1199, 1172, 1103, 950, 810, 747, 638, 559, 496, 471, 453.

Polyether 2d

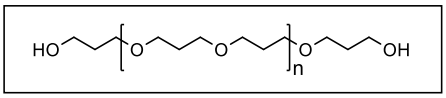

Reduction of polyester 1d with TMDS

40.0 g polyester **1d** (276 mmol, 1.00 eq.) was placed under inert conditions in a 1 L Schlenk-Flask and 800 mL dry DCM was added until the starting material was totally dissolved. Afterwards 1.71 g $GaBr_3$ (5.51 mmol, 0.02 eq.) was added and stirred at room temperature. Then 107 mL 1,1,3,3-tetratmethyldisiloxane (TMDS) (81.5 g, 606 mmol, 2.20 eq.) was added dropwise within one hour *via* syringe pump and stirred at room temperature for 18 hours. Then the crude product was washed with diluted hydrochloric acid (5%) and water, dried over Na_2SO_4 and concentrated under reduced pressure. The crude mixture was dissolved in a mixture of methanol (800 mL) and water (80 mL) and extracted with 160 mL petroleum ether (5×) to remove polysiloxane. The methanolic layer was concentrated *in vacuo*, the residue was dissolved in a mixture of methanol (200 mL) and water (20 mL) and extracted again with 40 mL petroleum ether (5×). The methanolic layer was dried over Na_2SO_4 and after filtration the solvent was removed *in vacuo.* Polyether **2d** was obtained as a colorless liquid (17.0 g, 51%).

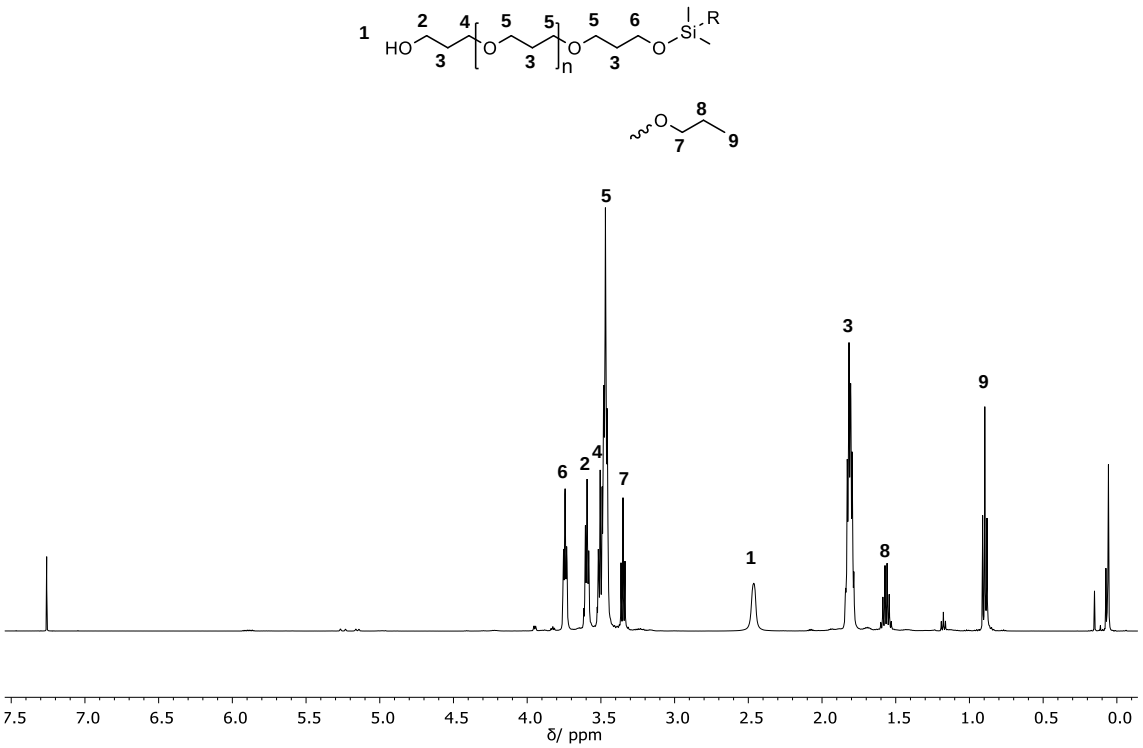

Figure S 4 ^{1}H-NMR spectrum of polyether **2d**, measured in $CDCl_3$.

^{1}H-NMR (500 MHz, DMSO-d_6): *δ*/ppm = 3.74 (t, C***H*₂⁶**OSi, end group), 3.59 (t, C***H*₂²**OH, end group), 3.51 (t, C***H*₂⁴**OH, end group), 3.46 (t, 4H, C***H*₂⁵**OC***H*₂⁵**), 3.35 (t, OC***H*₂⁷**CH_2CH_3), 2.46 (s, O***H*¹**, end group), 1.81 (m, 2H, OCH_2C***H*₂³**CH_2O), 1.55 (sext, OCH_2C***H*₂⁸**CH_3), 0.90 (t, OCH_2CH_2C***H*₃⁹**).

^{13}C-NMR (126 MHz, DMSO-d_6): *δ*/ppm = 72.75, 72.74, 70.33, 68.43, 68.03, 67.99, 67.92, 67.85, 67.80, 67.75, 62.16, 32.20, 32.10, 31.97, 30.18, 30.16, 30.12, 23.00, 10.69.

IR (ATR platinum diamond): *ν*/cm^{-1} = 2933, 2861, 2802, 1730, 1643, 1483, 1467, 1440, 1421, 1370, 1318, 1294, 1261, 1100, 919, 810, 759, 559, 529, 496, 455.

Supporting Information

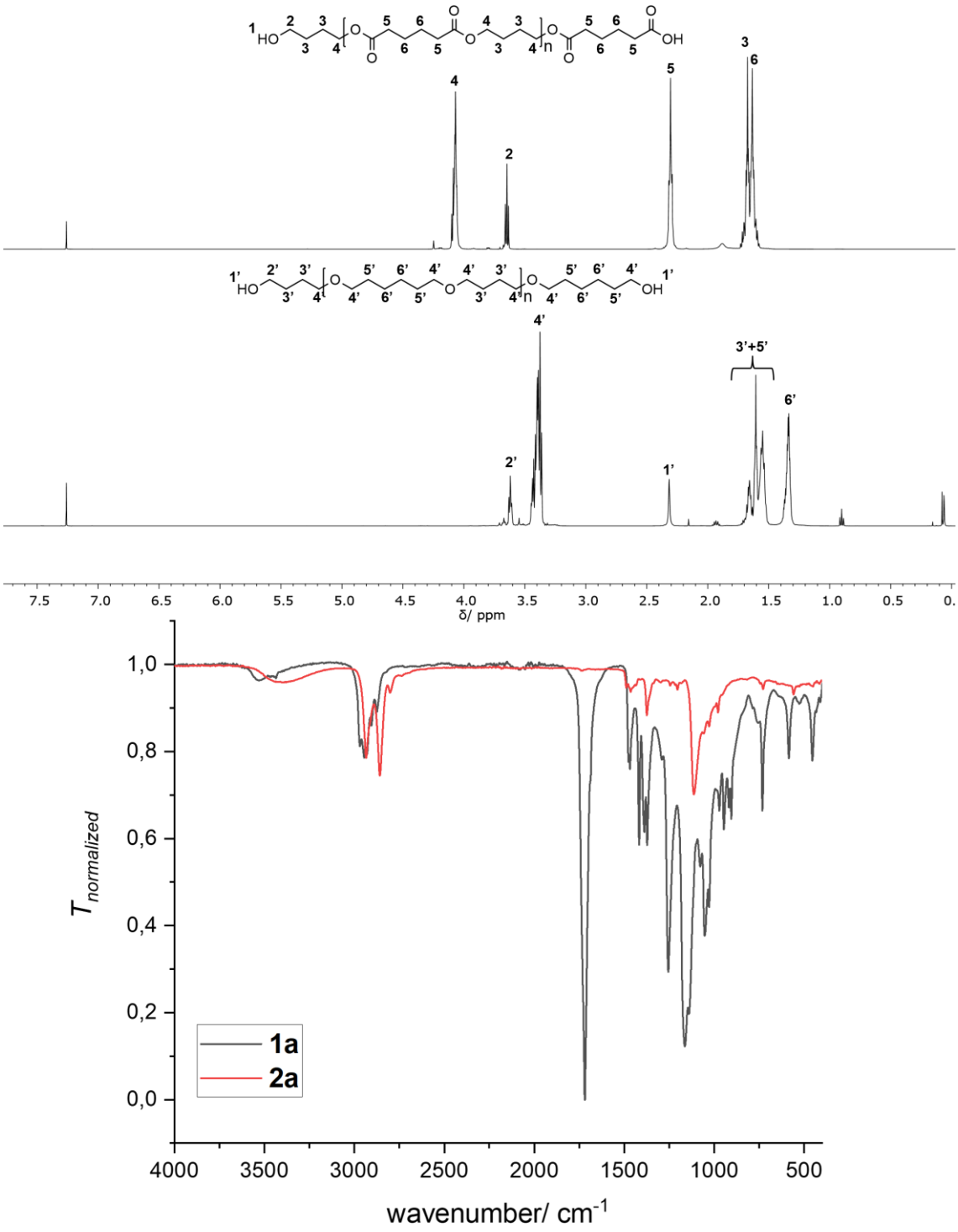

Figure S 5 Top: ^{1}H-NMR analysis of polyester **1a** (top) and polyether **2a** (bottom) measured in $CDCl_3$. Bottom: normalized ATR-IR spectra of polyester **1a** (black) and polyether **2a**, referenced on the CH_2 vibration of **1a** at 2935 cm^{-1} (red).

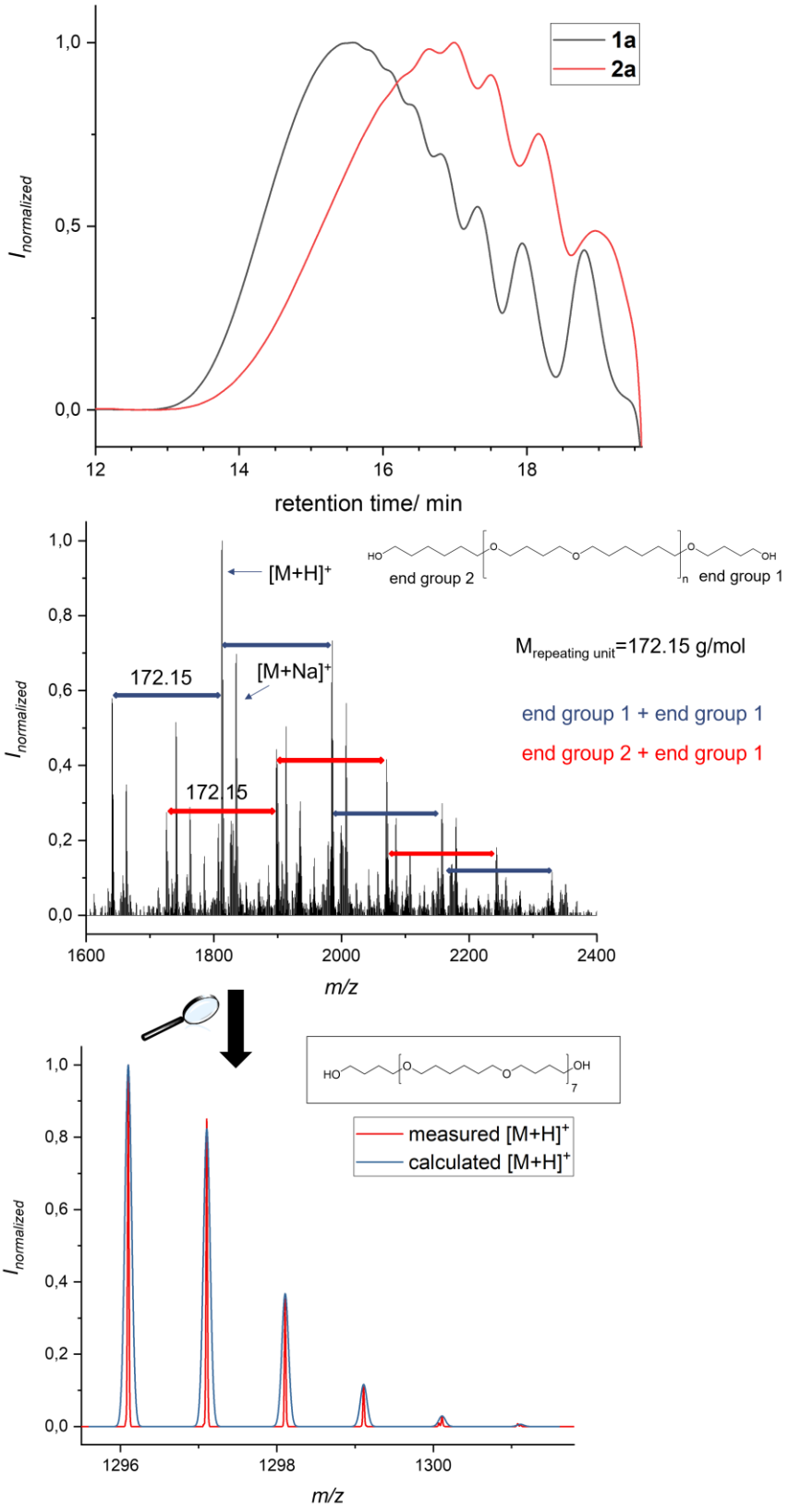

Figure S 6 SEC-ESI measurement of polyester **1a** (black) and polyether **2a** (red) with corresponding ESI spectra of polyether **2a** and high resolution for an exemplarily chosen oligomer.

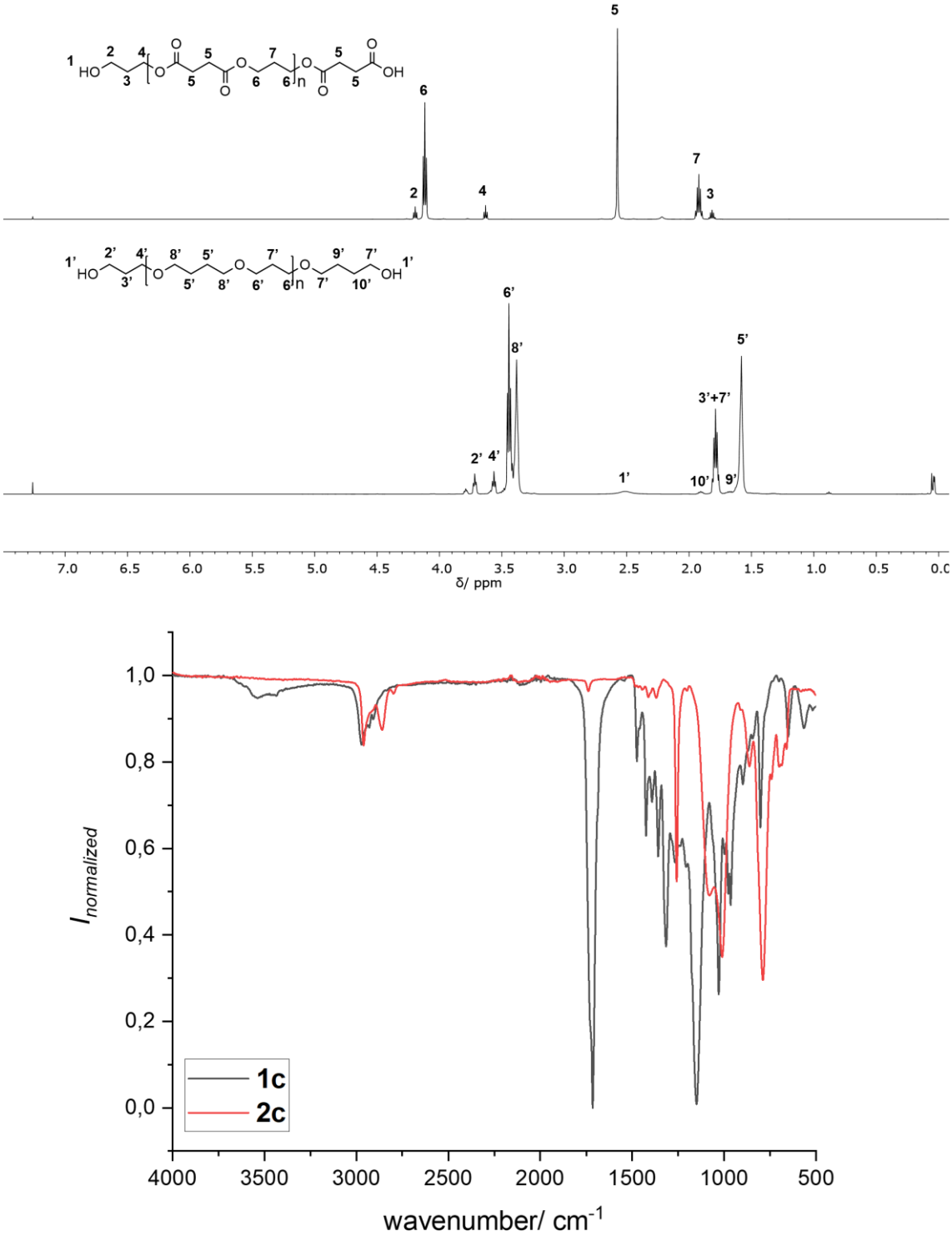

Figure S 7 Top: ^{1}H-NMR analysis of polyester **1c** (top) and polyether **2c** (bottom) measured in $CDCl_3$. Bottom: normalized ATR-IR spectra of polyester **1c** (black) and polyether **2c**, referenced on the CH_2 vibration of **1c** at 2935 cm^{-1} (red).

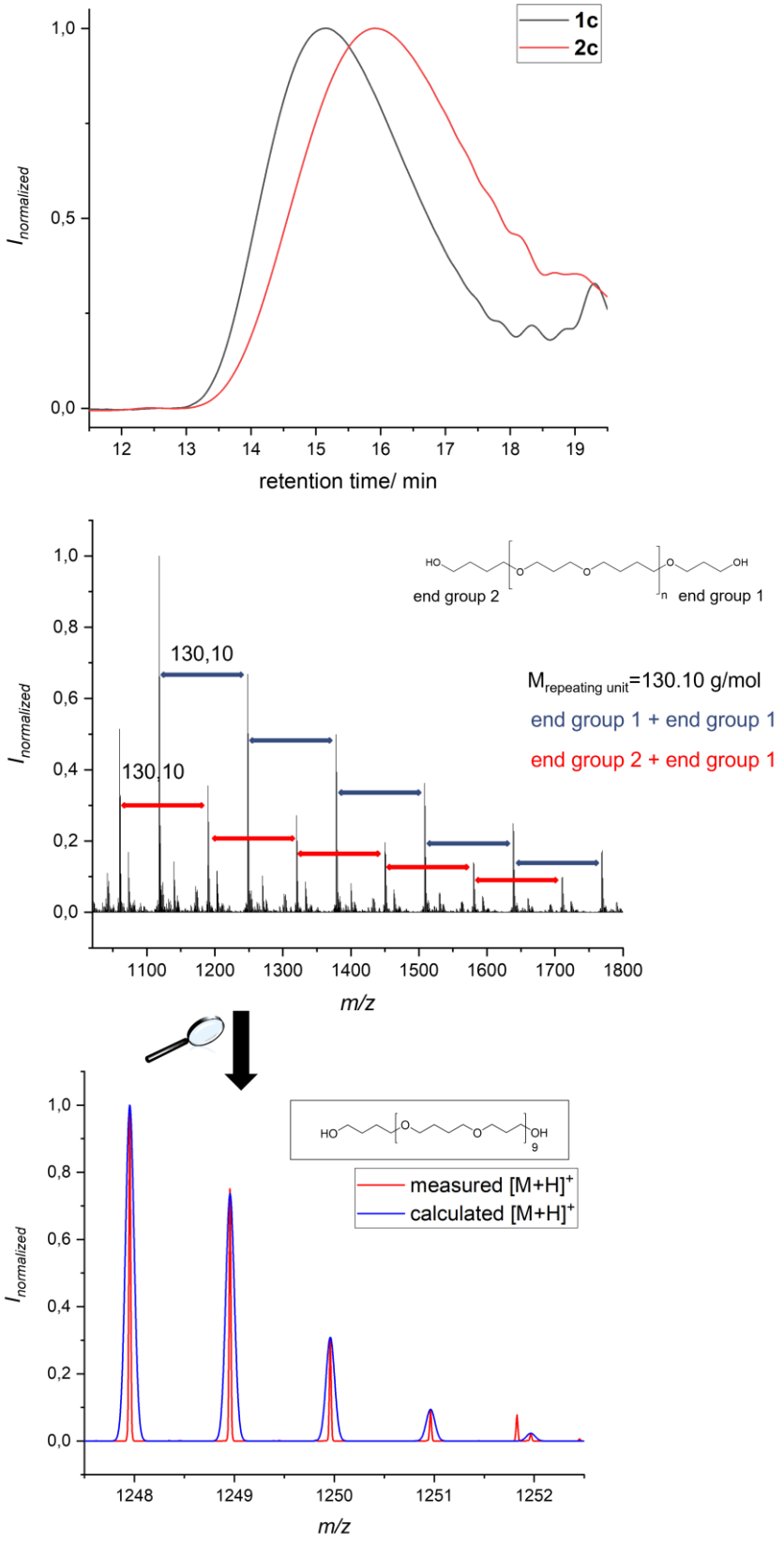

Figure S 8 SEC-ESI measurement of polyester **1c** (black) and polyether **2c** (red) with corresponding ESI spectra of polyether **2c** and high resolution for an exemplarily chosen oligomer.

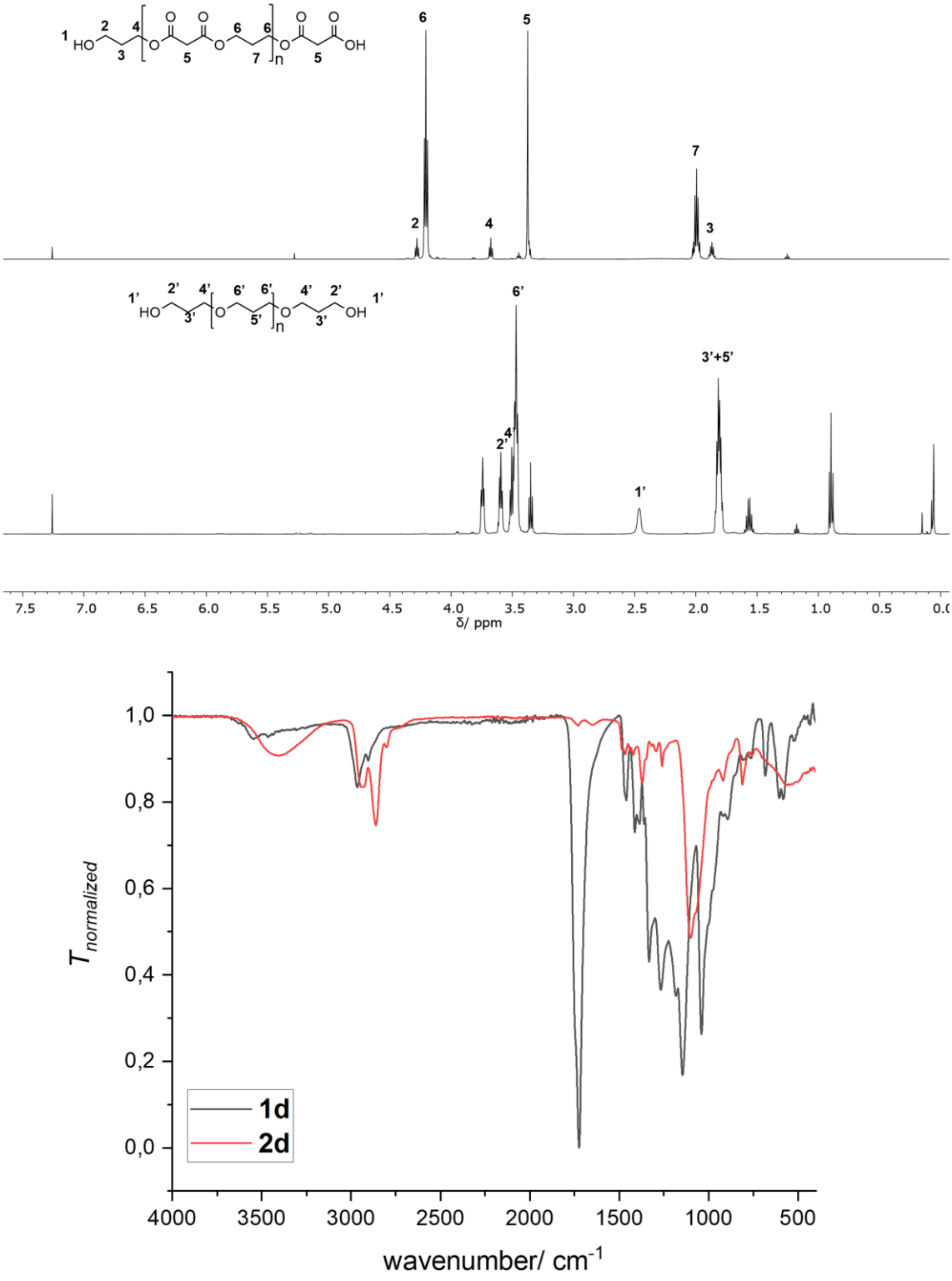

Figure S 9 Top: ^{1}H-NMR analysis of polyester **1d** (top) and polyether **2d** (bottom) measured in $CDCl_3$. Bottom: normalized ATR-IR spectra of polyester **1d** (black) and polyether **2c**, referenced on the CH_2 vibration of **1d** at 2935 cm^{-1} (red).

6.3.2 Experimental Procedures and Supporting Information of Chapter 4.2[22]

General procedure for the polyol synthesis

Glycol and surfactant (here applicable) were placed in three necked flask equipped with a distillation bridge and either a magnetic (< 5.00 g dicarboxylic acid) or a mechanical (> 5.00 g dicarboxylic acid) stirrer. The reaction set-up was preheated for 30 min at 160 °C to remove remaining water from the glycol. Afterwards, catalyst and dicarboxylic acids were added and stirred while the condensate was continuously removed.

General procedure for the PIR foam synthesis

Polyol, flame retardants, catalyst, foam stabilizer and water were placed in a beaker and premixed. Then, pentane was added and mixed again. Afterwards, polyisocyanate was added and stirred for 20 seconds with a “Pendraulik Labormischer Typ L34” at 2000 rpm. The reaction mixture was poured into a lined wooden foam cast (20×20×20 cm^3) and covered with a lid. PIR foams were synthesized by two different procedures. First, a threefold excess of polyisocyanate compared to the polyol was used and 10 mol% of a commercial aliphatic polyether polyol was added. Second, PIR foams were obtained by a stochiometric ratio of isocyanate to polyol of 2:1.

PDEF (polyol 2)

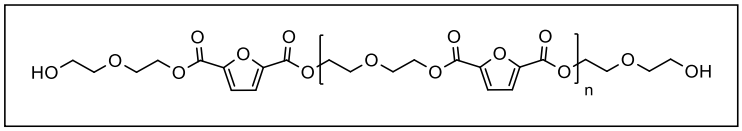

121 mL Diethylene glycol (136 g, 1.28 mol, 2.00 eq.) were placed in a 500 mL three necked flask, equipped with a mechanical stirrer and distillation bridge, and preheated to 160 °C for 30 minutes. Then, 9.48 mL $Ti(O^iPr)_4$ (9.10 g, 32.0 mmol, 0.05 eq.) and 100 g FDCA (641 mmol, 1.00 eq.) were added and the reaction mixture was stirred while the condensate was continuously removed by distillation. The reaction process was followed *via* ^{1}H-NMR and the reaction was stopped when full conversion of FDCA was observed.

[22] Parts of this chapter were submitted as a manuscript to the journal ACS Applied Polymer Materials titled “A fully biobased aromatic polyester polyol for polyisocyanurate rigid foams: poly(diethylene furanoate)”.

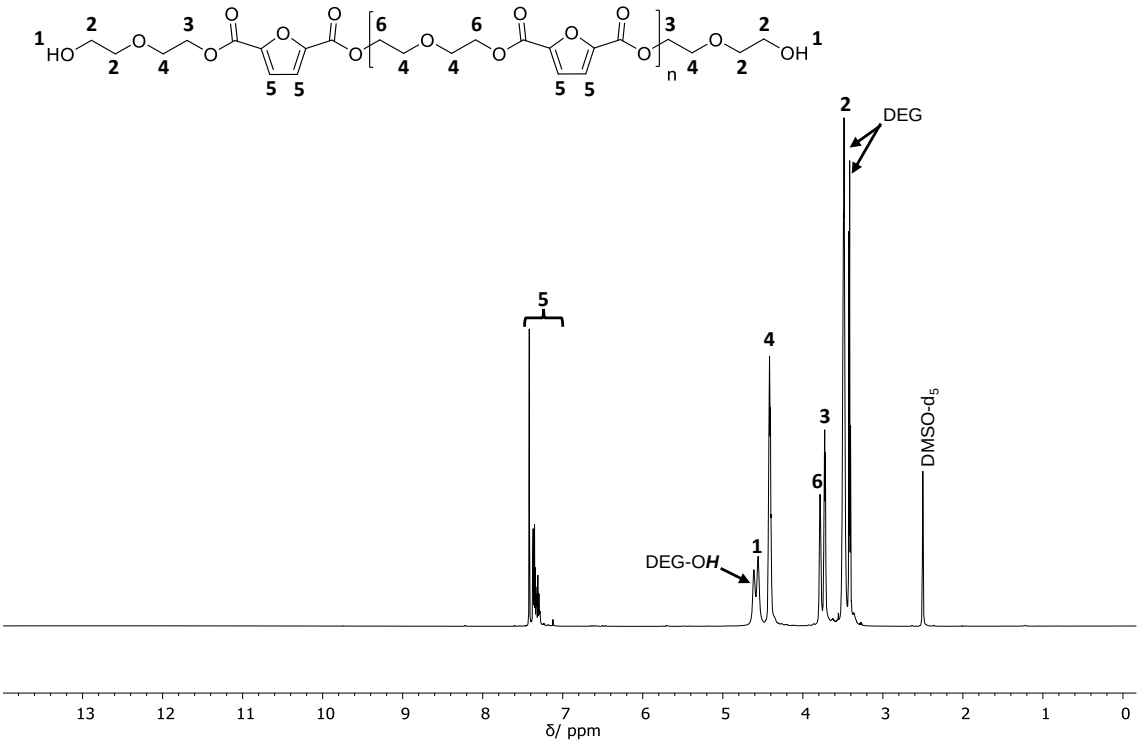

Figure S 10 ^{1}H-NMR spectrum of polyol **2**, measured in DMSO-d_6.

^{1}H-NMR (500 MHz, DMSO-d_6): *δ*/ppm = 7.28-7.44 (m, ***H*^{5}**), 4.61 (s, O(CH_2CH_2O***H***)$_2$), 4.56 (s, OCH_2CH_2O***H*^{1}**, end group), 4.38-4.44 (m, OCH_2C***H*$_2^{4}$**O), 3.76-3.81 (m, OC***H*$_2^{6}$**CH_2OCHO), 3.70-3.75 (m, OC***H*$_2^{3}$**CH_2OCHO), end group, 3.45-3.53 (m, OC***H*$_2^{2}$**C***H*$_2^{2}$**OH, end group + O(CH_2C***H*$_2$**OH)$_2$), 3.38-3.43 (m, O(C***H*$_2$**$CH_2OH)_2$).

^{13}C-NMR (126 MHz, DMSO-d_6): *δ*/ppm = 157.2-157.5, 146.0-146.2, 119.0-119.4, 72.37, 72.33, 64.55-64.65, 64.23-64.33, 60.32, 60.24.

IR (ATR platinum diamond): *ν*/cm^{-1} = 3394, 2873, 1716, 1581, 1509, 1452, 1382, 1271, 1223, 1120, 1060, 1020, 965, 924, 890, 827, 765, 618, 480.

FDCA/ SA copolymer (polyol 3)

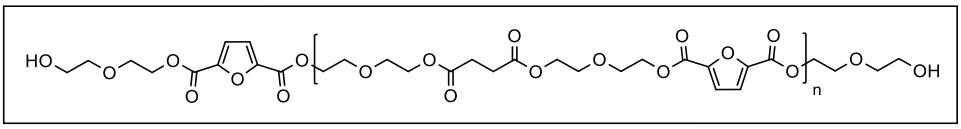

121 mL Diethylene glycol (136 g, 1.28 mol, 2.00 eq.) were placed in a 500 mL three necked flask, equipped with a mechanical stirrer and distillation bridge, and preheated to 160 °C for 30 minutes. Then, 9.48 mL $Ti(O^iPr)_4$ (9.10 g, 32.0 mmol, 0.05 eq.), 90.0 g FDCA (577 mmol, 0.90 eq.) and 7.57 g succinic acid (64.1 mmol, 0.10 eq.) were added and the reaction mixture was stirred while the condensate was continuously removed by distillation. The reaction process was followed *via* ^{1}H-NMR and the reaction was stopped when full conversion of FDCA was observed.

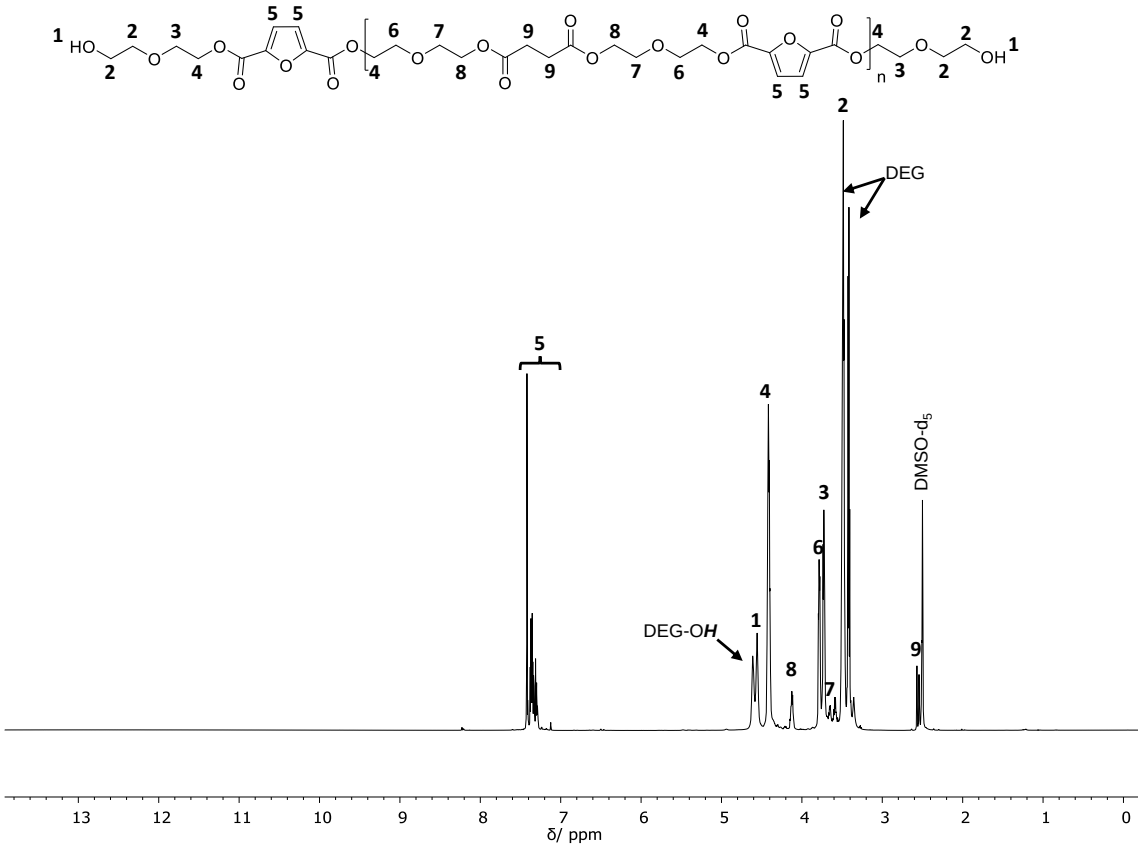

Figure S 11 ^{1}H-NMR spectrum of polyol **3**, measured in DMSO-d_6.

^{1}H-NMR (500 MHz, DMSO-d_6): ***δ***/ppm = 7.28-7.44 (m, ***H*^{5}**), 4.61 (s, $O(CH_2CH_2O\boldsymbol{H})_2$), 4.56 (s, $OCH_2CH_2O\boldsymbol{H}^1$, end group), 4.38-4.44 (m, $OCH_2C\boldsymbol{H_2}^4O$), 4.09-4.16 (m, $OCH_2C\boldsymbol{H_2}^8O$), 3.76-3.81 (m, $OC\boldsymbol{H_2}^6CH_2OCHO$), 3.70-3.75 (m, $OC\boldsymbol{H_2}^3CH_2OCHO$, end group), 3.62-3.68 (m, $OC\boldsymbol{H_2}^7CH_2OCHO$), 3.45-3.53 (m, $OC\boldsymbol{H_2}^2C\boldsymbol{H_2}^2OH$ end group + $O(CH_2C\boldsymbol{H_2}OH)_2$), 3.38-3.43 (m, $O(C\boldsymbol{H_2}CH_2OH)_2$), 2.53-2.57 (m, $OOCC\boldsymbol{H_2}^9C\boldsymbol{H_2}^9COO$).

^{13}C-NMR (126 MHz, DMSO-d_6): δ/ppm = 171.9-172.0, 157.2-157.5, 146.0-146.2, 131.3-131.8, 119.0-119.4, 72.4, 72.3, 68.0-68.2, 64.7-64.8,64.5-64.7, 64.2-64.4, 63.6, 63.4, 62.9, 60.3, 60.2.

IR (ATR platinum diamond): ν/cm^{-1} = 3407, 2874, 1716, 1581, 1509, 1452, 1382, 1271, 1224, 1120, 1062, 1020, 964, 924, 889, 827, 764, 618, 479.

FDCA/ AA copolymer (polyol 4)

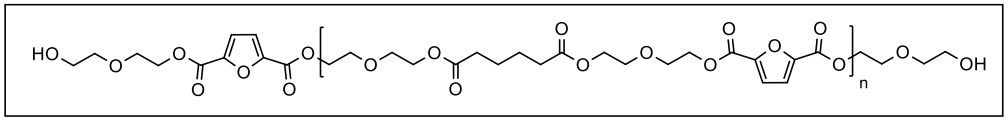

121 mL Diethylene glycol (136 g, 1.28 mol, 2.00 eq.) were placed in a 500 mL three necked flask, equipped with a mechanical stirrer and distillation bridge, and preheated to 160 °C for 30 minutes. Then, 9.48 mL Ti(O^{i}Pr)$_4$ (9.10 g, 32.0 mmol, 0.05 eq.), 90.0 g FDCA (577 mmol, 0.90 eq.) and 9.36 g adipic acid (64.1 mmol, 0.10 eq.) were added and the reaction mixture was stirred while the condensate was continuously removed by distillation. The reaction process was followed *via* ^{1}H-NMR and the reaction was stopped when full conversion of FDCA was observed.

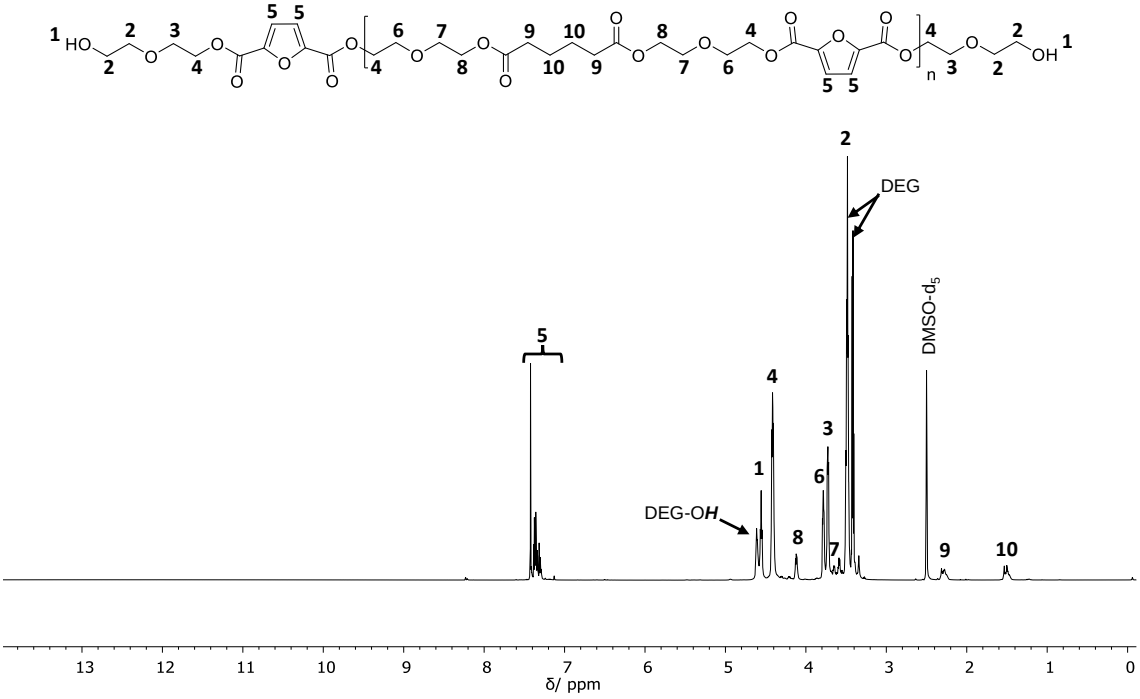

Figure S 12 ^{1}H-NMR spectrum of polyol **4**, measured in DMSO-d_6.

^{1}H-NMR (500 MHz, DMSO-d_6): δ/ppm = 7.28-7.44 (m, ***H*^{5}**), 4.61 (s, O(CH_2CH_2O***H***)$_2$), 4.56 (t, OCH_2CH_2O***H*^{1}**, end group), 4.38-4.44 (m, OCH_2C***H*$_2^{4}$**O), 4.09-4.15 (m, OCH_2C***H*$_2^{8}$**O), 3.76-3.81 (m, OC***H*$_2^{6}$**CH_2OCHO), 3.70-3.75 (m, OC***H*$_2^{3}$**CH_2OCHO, end group), 3.62-3.68 (m, OC***H*$_2^{7}$**CH_2OCHO), 3.45-3.53 (m, OC***H*$_2^{2}$**C***H*$_2^{2}$**OH, end group + O(CH_2C***H*$_2$**OH)$_2$), 3.38-3.43 (m, O(C***H*$_2$**$CH_2OH)_2$), 2.20-2.35 (m, CH_2C***H*$_2^{9}$**COO), 1.40-1.55 (m, CH_2C***H*$_2^{10}$**COO).

^{13}C-NMR (126 MHz, DMSO-d_6): δ/ppm = 172.6-172.8, 157.2-157.5, 145.9-146.2, 131.3-131.8, 119.0-119.4, 72.4, 72.3, 67.9-68.3, 64.6-64.7,64.2-64.4, 62.8-63.2, 60.3, 60.2.

IR (ATR platinum diamond): $\tilde{\nu}$/cm^{-1} = 3402, 2873, 1716, 1581, 1509, 1453, 1382, 1271, 1224, 1220, 1061, 1021, 964, 924, 889, 827, 765, 618, 481.

FDCA/ PA copolymer

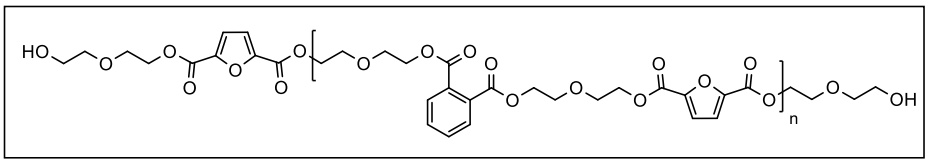

121 mL Diethylene glycol (136 g, 1.28 mol, 2.00 eq.) were placed in a 500 mL three necked flask, equipped with a mechanical stirrer and distillation bridge, and preheated to 160 °C for 30 minutes. Then, 9.48 mL Ti($O^{i}Pr$)$_4$ (9.10 g, 32.0 mmol, 0.05 eq.), 80.0 g FDCA (513 mmol, 0.80 eq.) and 21.3 g phthalic acid (128 mmol, 0.20 eq.) were added and the reaction mixture was stirred while the condensate was continuously removed by distillation. The reaction process was followed *via* ^{1}H-NMR and the reaction was stopped when full conversion of FDCA was observed.

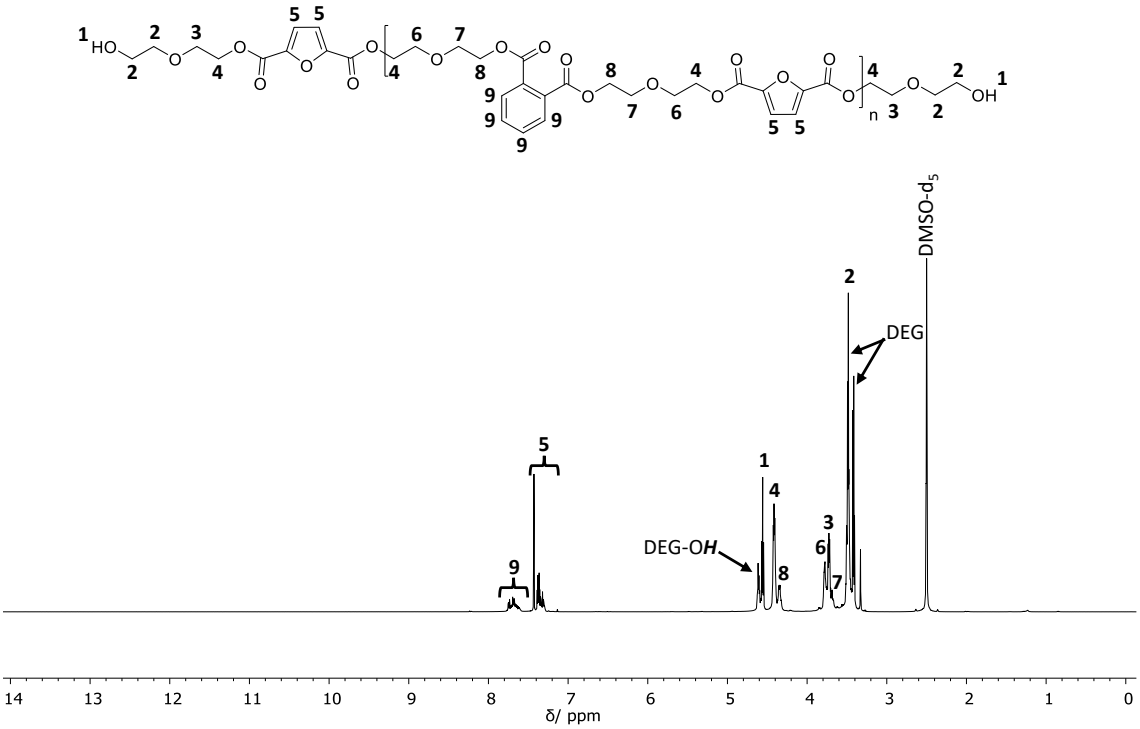

Figure S 13 ^{1}H-NMR spectrum of FDCA/ PA copolymer, measured in DMSO-d_6.

^{1}H-NMR (500 MHz, DMSO-d_6): *δ*/ppm = 7.58-7.78 (m, ***H*^{9}**), 7.28-7.44 (m, ***H*^{5}**), 4.61 (s, O(CH_2CH_2O***H***)$_2$), 4.56 (s, OCH_2CH_2O***H*^{1}**, end group), 4.38-4.44 (m, OCH_2C***H*$_2^{4}$**O), 4.30-4.38 (m, OCH_2C***H*$_2^{8}$**O), 3.76-3.81 (m, O***C*H_2^{6}**CH_2OCHO), 3.70-3.75 (m, O***C*H_2^{3}**CH_2OCHO, end group), 3.65-3.70 (m, O***C*H_2^{7}**CH_2OCHO), 3.45-3.53 (m, O***C*H_2^{2}**C***H*$_2^{2}$**OH, end group + O(CH_2C***H*$_2$**OH)$_2$), 3.38-3.43 (m, O(C***H*$_2CH_2OH)_2$).

^{13}C-NMR (126 MHz, DMSO-d_6): *δ*/ppm = 166.8-167.0, 157.2-157.5, 146.0-146.2, 131.3-131.8, 128.6-128.8, 119.0-119.4, 72.4, 72.3, 68.0-68.2, 64.7-64.8,64.5-64.7, 64.3-64.4, 64.2-64.3, 60.3, 60.2.

IR (ATR platinum diamond): *v*/cm^{-1} = 3402, 2874, 1716, 1581, 1509, 1451, 1381, 1271, 1224, 1119, 1065, 1021, 964, 924, 889, 827, 765, 705, 618, 480.

6.3.3 Experimental Procedures and Supporting Information of Chapter 4.3

Polyester (4)

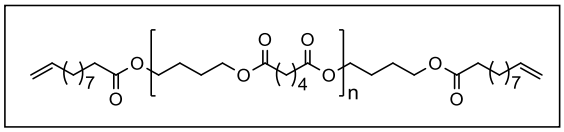

30.0 g adipic acid (205 mmol, 1.00 eq.), 21.8 mL 1,4-butanediol (22.2 g, 246 mmol, 1.20 eq.) and 3.04 mL $Ti(O^iPr)_4$ (2.92 g, 10.3 mmol, 0.05 eq.) were placed in a 250 mL three necked flask equipped with a mechanical stirrer and two outlets. The reaction mixture was heated to 160 °C and stirred for 12 hours. Then, 45.6 g 10-undecenylenic acid was added and stirred at 160 °C for 28 hours. The crude polymer was dissolved in 100 mL DCM, filtered and the filtrate was precipitated in cold *n*-hexane (1.5 L). Polyester **(4)** was dried under reduced pressure and was obtained as a yellowish solid (35.0 g, 72%).

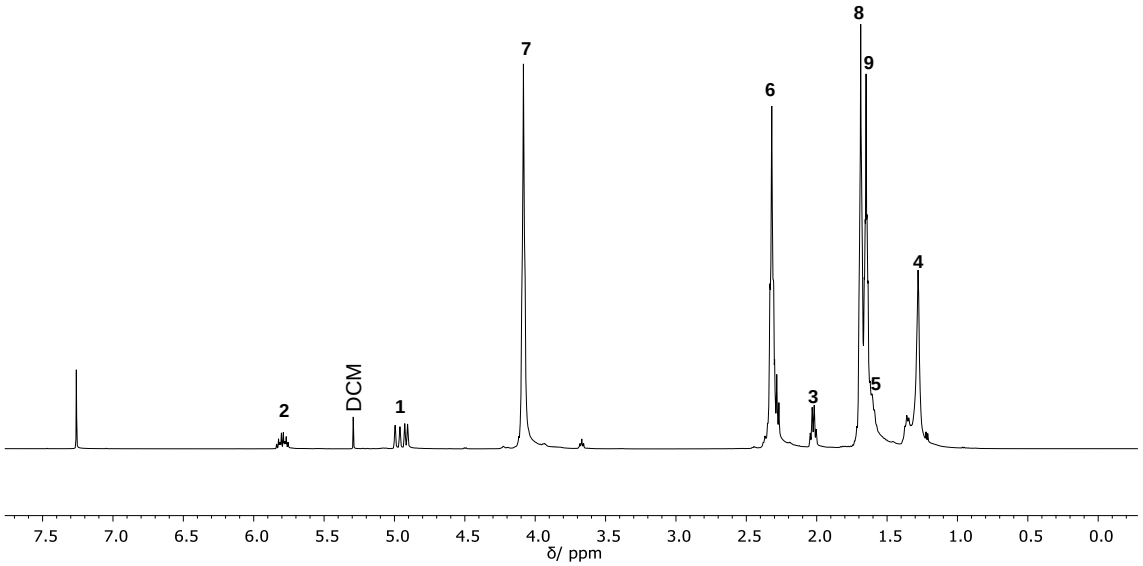

Figure S 14 ^{1}H-NMR spectrum of polyester **(4)**, measured in $CDCl_3$.

^{1}H-NMR (500 MHz, $CDCl_3$): δ/ppm = 5.74-5.85 (m, $CH_2C\boldsymbol{H^2}CH2$, end group), 4.88-5.03 (dd, $C\boldsymbol{H_2^1}CHCH_2$, end group), 4.08 (m, 4H, $COOC\boldsymbol{H_2^7}$), 3.67 (t, $C\boldsymbol{H_2}OH$, end group), 2.25-2.35 (m, 4H, $OOCC\boldsymbol{H_2^6}$), 2.03(q, $CH_2CHC\boldsymbol{H_2^3}CH_2$, end group), 1.69 (m, 4H, $COOCH_2C\boldsymbol{H_2^8}$), 1.65 (quint, 4H, $OOCCH_2C\boldsymbol{H_2^9}$), 1.55-1.60 (m, $C\boldsymbol{H_2^5}CH_2COO$, end group), 1.18-1.40 (m, $C\boldsymbol{H_2^4}$, end group).

^{13}C-NMR (126 MHz, DMSO-d_6): δ/ppm = 178.26, 174.02, 173.44, 139.30, 114.28, 63.97, 63.82, 34.43, 33.98, 33.90, 33.88, 29.41, 29.38, 29.32, 29.30, 29.25, 29.17, 29.16, 29.00, 25.42, 25.08, 24.49.

IR (ATR platinum diamond): $\tilde{\nu}$/cm^{-1} = 2927, 2874, 2855, 1728, 1462, 1417, 1401, 1370, 1318, 1257, 1209, 1164, 1065, 996, 959, 93, 909, 854, 734, 634, 584, 525.

Polyester (5)

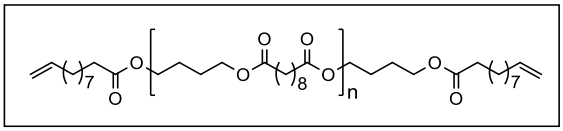

30.0 g sebacic acid (148 mmol, 1.00 eq.), 15.7 mL 1,4-butanediol (16.0 g, 178 mmol, 1.20 eq.) and 2.20 mL $Ti(O^iPr)_4$ (2.11 g, 7.42 mmol, 0.05 eq.) were placed in a 250 mL three necked flask equipped with a mechanical stirrer and two outlets. The reaction mixture was heated to 160 °C and stirred for 15 hours. Then, 27.3 g 10-undecenylenic acid was added and stirred at 160 °C for 34 hours. The crude polymer was dissolved in 100 mL DCM and the insoluble residues were removed *via* centrifugation. Subsequently, the polymer (dissolved in DCM) was precipitated in cold *n*-hexane (1.5 L). Polyester **(5)** was dried under reduced pressure and was obtained as a white solid (23.4 g, 54%).

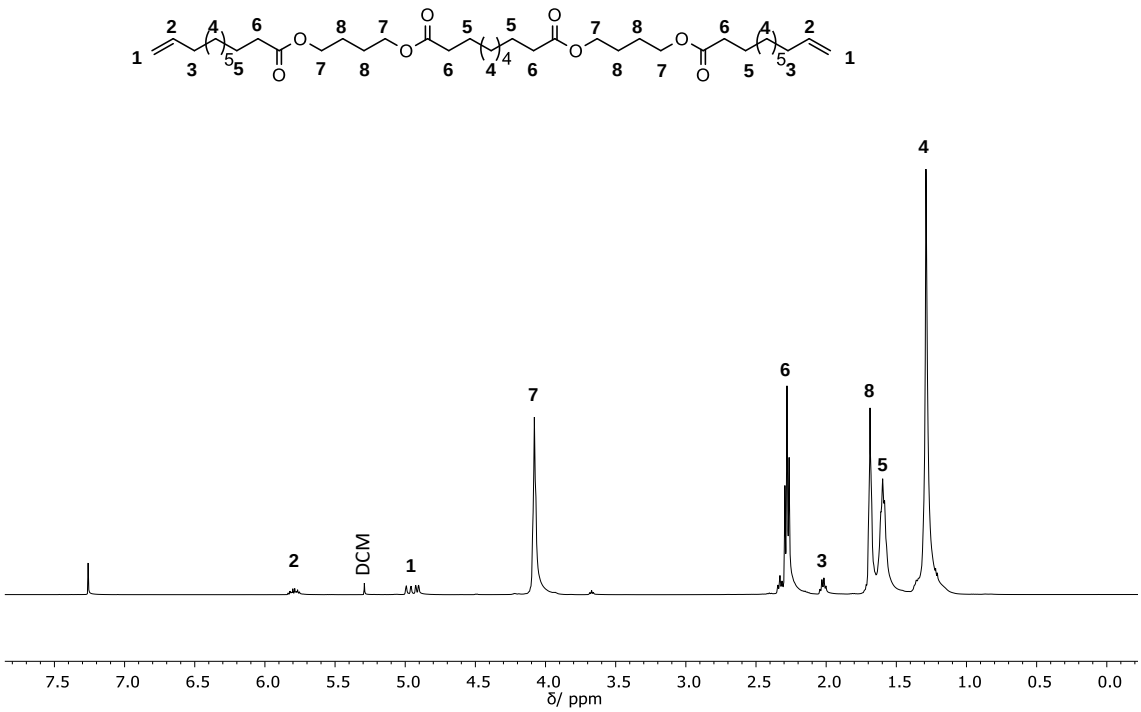

Figure S 15 ^{1}H-NMR spectrum of polyester **(5)**, measured in $CDCl_3$.

^{1}H-NMR (500 MHz, $CDCl_3$): *δ*/ppm = 5.74-5.85 (m, $CH_2C\boldsymbol{H^2}CH2$, end group), 4.88-5.03 (dd, $C\boldsymbol{H_2^1}CHCH_2$, end group), 4.08 (m, 4H, $COOC\boldsymbol{H_2^7}$), 3.67 (t, $C\boldsymbol{H_2}OH$, end group), 2.15-2.35 (m, 4H, $OOCC\boldsymbol{H_2^6}$), 2.03 (q, $CH_2CHC\boldsymbol{H_2^3}CH_2$, end group), 1.69 (m, 4H, $COOCH_2C\boldsymbol{H_2^8}$), 1.60 (m, 4H, $OOCCH_2C\boldsymbol{H_2^5}$), 1.18-1.40 (m, 8H, $C\boldsymbol{H_2^4}$ + $C\boldsymbol{H_2^4}$, end group).

^{13}C-NMR (126 MHz, DMSO-d_6): *δ*/ppm = 174.02, 173.96, 139.29, 114.28, 63.85, 34.43, 34.39, 33.90, 33.86, 29.41, 29.32, 29.21, 29.08, 29.00, 25.46, 25.08, 25.04.

IR (ATR platinum diamond): *v*/cm^{-1} = 2917, 2853, 1736, 1473, 1465, 1450, 1411 1395, 1360, 1302, 1290, 124, 1216, 1164, 1123, 1070, 1055, 1008, 965, 944, 926, 911, 856, 817, 812, 753, 734, 722, 712, 638, 625, 582, 541, 525, 428.

Polyether (6)

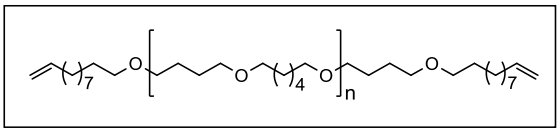

10.0 g polyester **(4)** (1.00 eq./ repeating unit[23]) was placed under inert conditions in a 250 mL Schlenk-Flask and 80 mL dry DCM was added until the starting material was totally dissolved. Afterwards 307 mg $GaBr_3$ (0.989 mmol, 0.02 eq.) was added and stirred at room temperature. Then 34.8 mL triethylsilane (25.3 g, 218 mmol, 4.40 eq.) was added dropwise within one hours *via* syringe pump and stirred at room temperature for 3 days. The crude product was washed with hydrochloric acid (5%) and water, dried over Na_2SO_4 and concentrated under reduced pressure. The residue was distilled under reduced pressure (1 mbar) at 130 °C. Polyether **(6)** was obtained as colorless liquid (7.50 g, 87%).

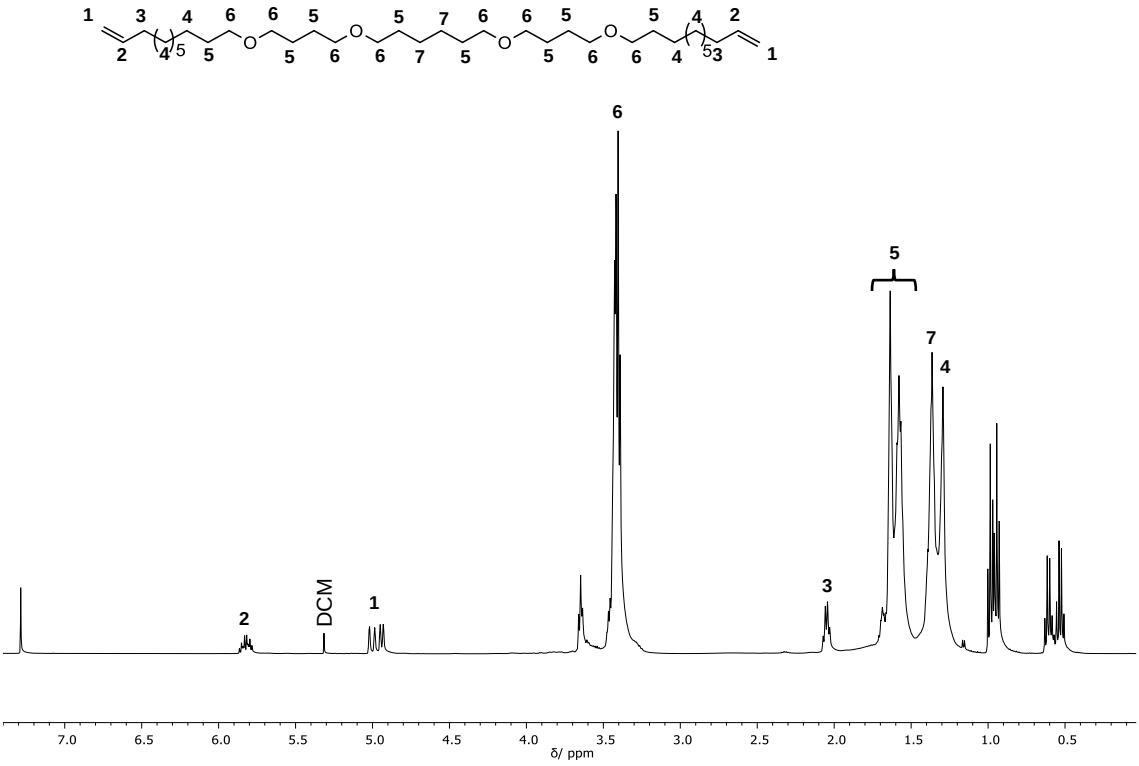

Figure S 16 ^{1}H-NMR spectrum of polyether **(6)**, measured in $CDCl_3$

[23] The stoichiometry was calculated per repeating unit. 1.00 eq is equal to one repeating unit. The same assumptions were applied for the synthesis of polyether **(7)**.

^{1}H-NMR (500 MHz, $CDCl_3$): *δ*/ppm = 5.74-5.85 (m, $CH_2C\boldsymbol{H^2}CH2$, end group), 4.88-5.03 (dd, $C\boldsymbol{H_2^1}CHCH_2$, end group), 3.62 (t, $C\boldsymbol{H_2}OSi$, end group), 3.30-3.45 (m, 8H, $COOC\boldsymbol{H_2^6}$), 2.03 (q, $CH_2CHC\boldsymbol{H_2^3}CH_2$, end group), 1.45-1.70 (m, 8H, $C\boldsymbol{H_2^5}CH_2COO$), 1.30-1.40 (m, 4H, $OCH_2CH_2C\boldsymbol{H_2^7}$),1.18-1.30 (m, $C\boldsymbol{H_2^4}$, end group).

^{13}C-NMR (126 MHz, DMSO-d_6): *δ*/ppm = 139.35, 114.23, 70.99, 70.76, 33.93, 32.92, 32.85, 30.56, 29.87, 29.70, 29.67, 29.61, 29.56, 29.54, 29.25, 29.05, 27.12, 26.62, 26.31, 26.22, 26.16.

IR (ATR platinum diamond): *ν*/cm^{-1} = 2929, 2853, 2795, 1460, 1436, 1413, 1368, 1298, 1238, 1205, 1109, 1014, 1004, 977, 909, 854, 736, 687, 631, 578, 547, 508, 479, 444.

Polyether (7)

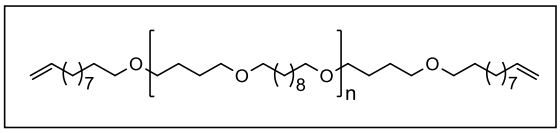

10.0 g polyester **(5)** (1.00 eq./ repeating unit) was placed under inert conditions in a 250 mL Schlenk-Flask and 80 mL dry DCM was added until the starting material was totally dissolved. Afterwards 599 mg $GaBr_3$ (1.94 mmol, 0.05 eq.) was added and stirred at room temperature. Then 27.2 mL triethylsilane (19.8 g, 170 mmol, 4.40 eq.) was added within dropwise one hour *via* syringe pump and stirred at room temperature for 3 days. The crude product was washed with hydrochloric acid (5%) and water, dried over Na_2SO_4 and concentrated under reduced pressure. The residue was distilled under reduced pressure (1 mbar) at 130 °C. Polyether **(7)** was obtained as colorless liquid (7.94 g, 89%).

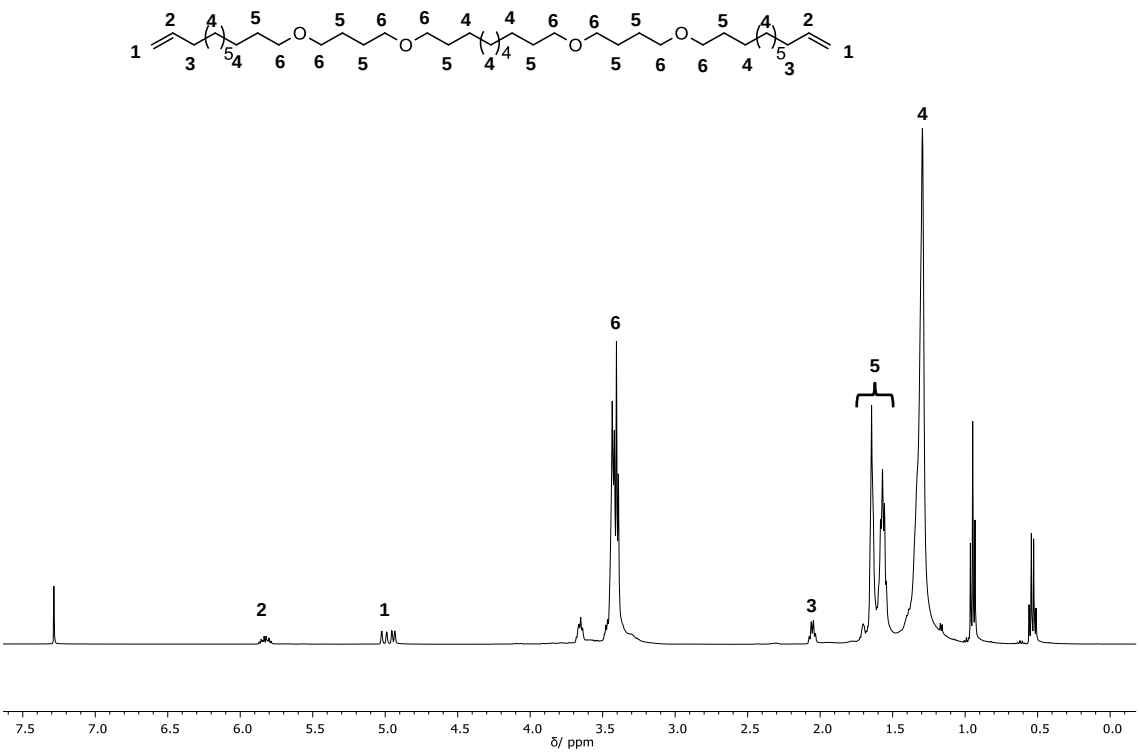

Figure S 17 ^{1}H-NMR spectrum of polyether **(7)**, measured in $CDCl_3$

^{1}H-NMR (500 MHz, $CDCl_3$): *δ*/ppm = 5.74-5.85 (m, $CH_2C\boldsymbol{H^2}CH2$, end group), 4.88-5.03 (dd, $C\boldsymbol{H_2^1}CHCH_2$, end group), 3.62 (t, $C\boldsymbol{H_2}OSi$, end group), 3.30-3.45 (m, 8H, $COOC\boldsymbol{H_2^6}$), 2.03 (q, $CH_2CHC\boldsymbol{H_2^3}CH_2$, end group), 1.45-1.70 (m, 8H, $C\boldsymbol{H_2^5}CH_2COO$), 1.10-1.45 (m, 12H, $C\boldsymbol{H_2^4}$ + $C\boldsymbol{H_2^4}$, end group).

^{13}C-NMR (126 MHz, DMSO-d_6): *δ*/ppm = 139.37, 114.23, 71.38, 71.11, 70.77, 63.18, 33.95, 32.93, 29.92, 29.73, 29.68, 29.58, 2.26, 29.07, 26.64, 26.34, 25.87.

IR (ATR platinum diamond): *ν*/cm^{-1} = 2927, 2921, 2853, 2802, 1485, 1467, 1411, 1372, 1238, 1203, 1115, 1014, 1004, 989, 977, 909, 740, 722, 555.

Polyester diamine (8)

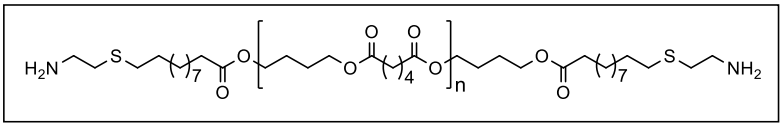

10.0 g polyester **(4)** (6.34 mmol, 1.00 eq.[24]) were dissolved in 150 mL DCM. Then, 2.88 g cysteamine hydrochloride (25.4 mmol, 4.00 eq.) dissolved in 50 mL methanol was slowly added. Afterwards, 162 mg DMPA (0.634 mmol, 0.10 eq.) was added to the mixture and stirred at room temperature under UV-irradiation (365 nm, 15 W) for 15 hours. Subsequently, the crude mixture was washed with saturated sodium carbonate solution (3×) and water (2×), dried over Na_2SO_4 and concentrated under reduced pressure. The polyester diamine **(8)** was obtained as a yellowish, waxy solid (10.0 g, 93%[25]).

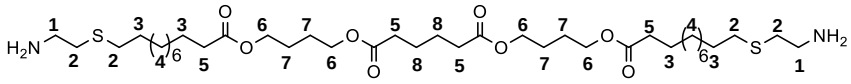

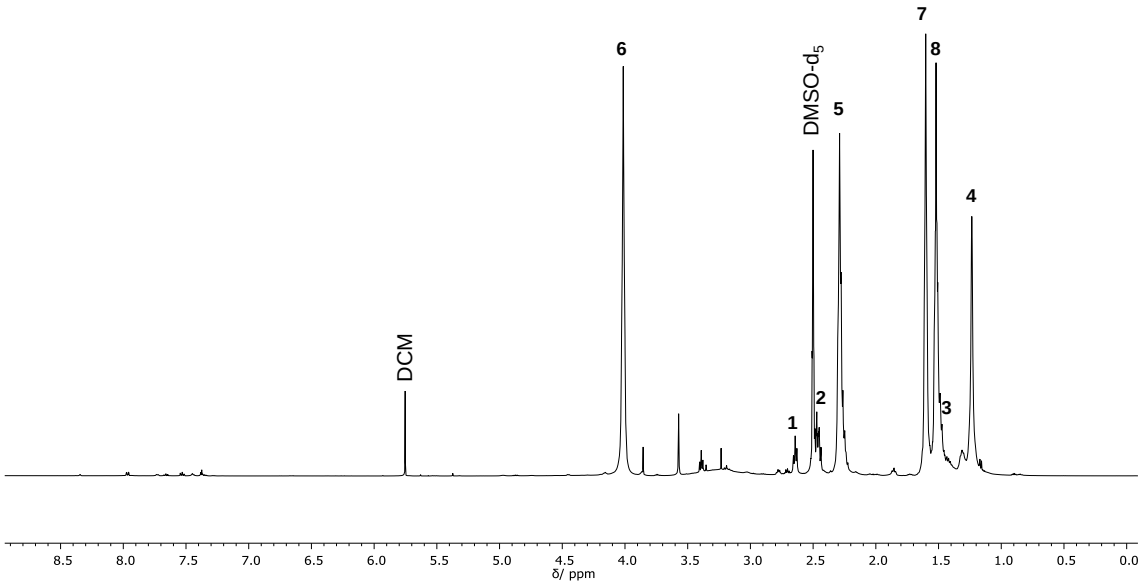

Figure S 18 ^{1}H-NMR spectrum of polyester diamine **(8)**, measured in DMSO-d_6.

[24] Determined *via* M_n(NMR) assuming only double bond end groups. This calculation was transferred to the synthesis of polyester **(9)** as well as of polyethers **(10)** and **(11)**, respectively.
[25] Assuming the same X_n than for polyester **(4)**.

^{1}H-NMR (500 MHz, DMSO-d_6): *δ*/ppm = 4.01 (m, 4H, COOC***H₂⁶***), 3.39 (t, C***H₂***OH, end group), 2.64 (t, C***H₂¹***NH_2, end group), 2.43-2.49 (m, C***H₂²***SC***H₂²***CH_2NH_2, end group), 2.29 (m, 4H, OOCC***H₂⁵***), 1.60 (quint, 4H, $COOCH_2C$***H₂⁷***), 1.52 (quint, 4H, $OOCCH_2C$***H₂⁸***), 1.49 (m, CH_2SCH_2C***H₂³*** + C***H₂³***CH_2COO, end group), 1.18-1.33 (m, C***H₂⁴***, end group).

^{13}C-NMR (126 MHz, DMSO-d_6): *δ*/ppm = 172.88, 272.66, 63.74, 63.31, 63.23, 60.22, 54.91, 51.17, 41.67, 35.42, 33.48, 33.10, 30.96, 29.32, 28.89, 28.84, 28.82, 28.65, 28.60, 28.44, 28.21, 24.81, 24.45, 23.88.

IR (ATR platinum diamond): *ν*/cm^{-1} = 2925, 2873, 2854, 1727, 1566, 1463, 1417, 1401, 1258, 1164, 1143, 1067, 959, 931, 911, 880, 867, 735, 703, 673, 663, 636, 622, 612.

Polyester diamine (9)

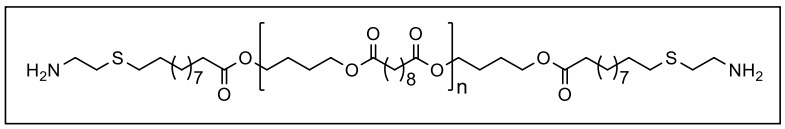

10.0 g polyester **(5)** (4.60 mmol, 1.00 eq.) were dissolved in 150 mL DCM. Then, 2.09 g cysteamine hydrochloride (18.4 mmol, 4.00 eq.) dissolved in 50 mL methanol was slowly added. Afterwards, 118 mg DMPA (0.460 mmol, 0.10 eq.) was added to the mixture and stirred at room temperature under UV-irradiation (365 nm, 15 W) for 14 hours. Subsequently, the crude mixture was washed with saturated sodium carbonate solution (3×) and water (2×), dried over Na_2SO_4 and concentrated under reduced pressure. The polyester diamine **(9)** was obtained as a yellowish, waxy solid (11.3 g, 91%[26]).

[26] Assuming the same X_n than for polyester **(5)**.

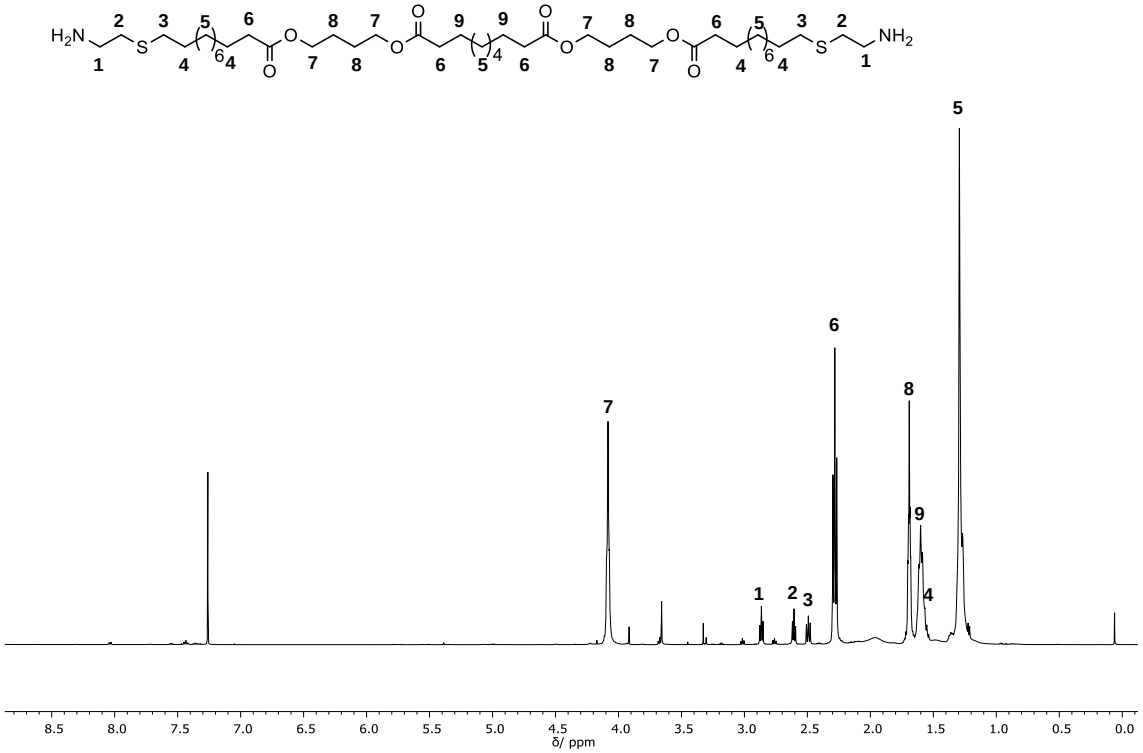

Figure S 19 ^{1}H-NMR spectrum of polyester diamine **(9)**, measured in $CDCl_3$.

^{1}H-NMR (500 MHz, $CDCl_3$): *δ*/ppm = 4.08 (m, 4H, COOC***H₂⁷***), 3.67 (t, C***H₂***OH, end group), 2.86 (t, C***H₂¹***NH_2, end group), 2.61 (t, SC***H₂²***CH_2NH_2, end group), 2.49 (t, C***H₂³***$SCH_2CH_2NH_2$, end group), 2.28 (t, 4H, OOCC***H₂⁶***), 1.69 (quint, 4H, $COOCH_2C$***H₂⁸***), 1.60 (m, 4H, $OOCCH_2C$***H₂⁹***), 1.55 (m, CH_2SCH_2C***H₂⁴*** + C***H₂⁴***CH_2COO, end group), 1.15-1.40 (m, 8H, C***H₂⁵*** + C***H₂⁵***, end group).

^{13}C-NMR (126 MHz, DMSO-d_6): *δ*/ppm = 174.01, 173.96, 63.85, 41.27, 36.47, 34.44, 34.20, 31.98, 29.92, 29.58, 29.51, 29.37, 29.34, 29.23, 29.01, 25.47, 25.09, 25.05.

IR (ATR platinum diamond): *ν*/cm^{-1} = 2917, 2851, 1730, 1566, 1465, 1451, 1412, 1402, 1376, 1361, 1291, 1245, 1217, 1168, 1124, 1105, 1071, 1004, 964, 928, 880, 856, 824, 808, 792, 754, 730, 721, 663, 637, 619.

Polyether diamine (10)

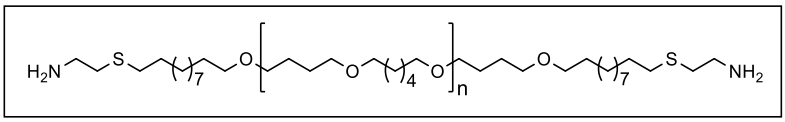

6.00 g polyether **(6)** (3.43 mmol, 1.00 eq.) were dissolved in 100 mL DCM. Then, 1.56 g cysteamine hydrochloride (13.7 mmol, 4.00 eq.) dissolved in 33 mL methanol was slowly added. Afterwards, 87.9 mg DMPA (0.343 mmol, 0.10 eq.) was added to the mixture and stirred at room temperature under UV-irradiation (365 nm, 15 W) for 4 days. Subsequently, the crude mixture was washed with saturated sodium carbonate solution (3x) and water (2x), dried over Na_2SO_4 and concentrated under reduced pressure. The polyether diamine **(10)** was obtained as a yellowish, waxy solid (6.37 g, 86%[27]).

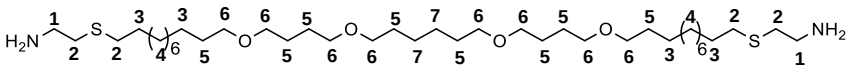

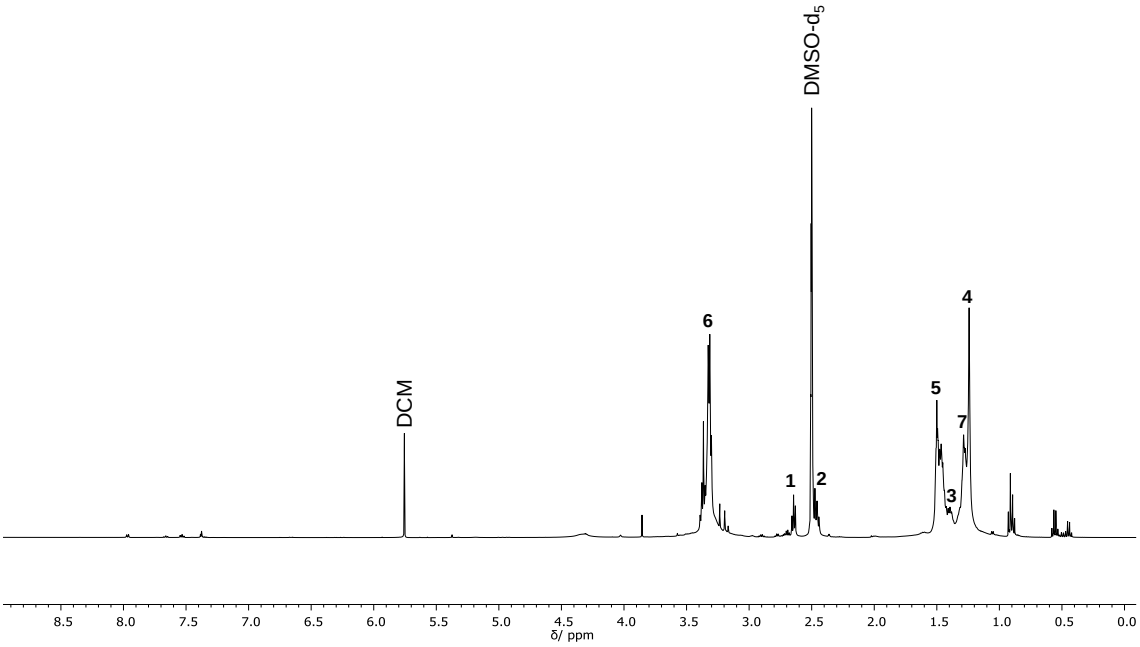

Figure S 20 ^{1}H-NMR spectrum of polyether diamine **(10)**, measured in DMSO-d_6.

[27] Assuming the same X_n than for polyether **(6)**.

^{1}H-NMR (500 MHz, DMSO-d_6): δ/ppm = 3.26-3.40 (m, 8H, OC***H₂⁶***), 2.64 (t, C***H₂¹***NH_2, end group), 2.43-2.49 (m, C***H₂²***SC***H₂²***CH_2NH_2, end group), 1.42-1.54 (m, 8H, OCH_2C***H₂⁵***), 1.36-1.45 (m, CH_2SCH_2C***H₂³*** + C***H₂³***CH_2O, end group), 1.26-1.36 (m, 4H, OCH_2CH_2C***H₂⁷***),1.18-1.26 (m, C***H₂⁴***, end group).

^{13}C-NMR (126 MHz, DMSO-d_6): δ/ppm = 69.90, 69.84, 69.84, 69.74, 60.71, 60.56, 60.55, 54.92, 41.68, 35.41, 32.55, 30.97, 29.23, 29.29, 29.23, 29.08, 28.97, 28.85, 28.63, 28.21, 26.08, 25.92, 25.72, 25.66, 25.58, 25.51, 25.38.

IR (ATR platinum diamond): ν/cm^{-1} = 2929, 2853, 2796, 1483, 1463, 1436, 1413, 1368, 1300, 1276, 1238, 1205, 1183, 1107, 1017, 865, 853, 773, 735, 704, 688, 673, 654, 637, 625, 607.

Polyether diamines (11)

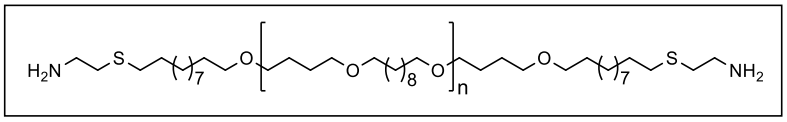

7.85 g polyether **(7)** (3.27 mmol, 1.00 eq.) were dissolved in 140 mL DCM. Then, 1.49 g cysteamine hydrochloride (13.1 mmol, 4.00 eq.) dissolved in 46 mL methanol was slowly added. Afterwards, 83.8 mg DMPA (0.327 mmol, 0.10 eq.) was added to the mixture and stirred at room temperature under UV-irradiation (365 nm, 15 W) for 3 days. Subsequently, the crude mixture was washed with saturated sodium carbonate solution (3x) and water (2x), dried over Na_2SO_4 and concentrated under reduced pressure. The polyether diamine **(11)** was obtained as a yellowish, waxy solid (7.03 g, 84%[28]).

[28] Assuming the same X_n than for polyether **(7)**.

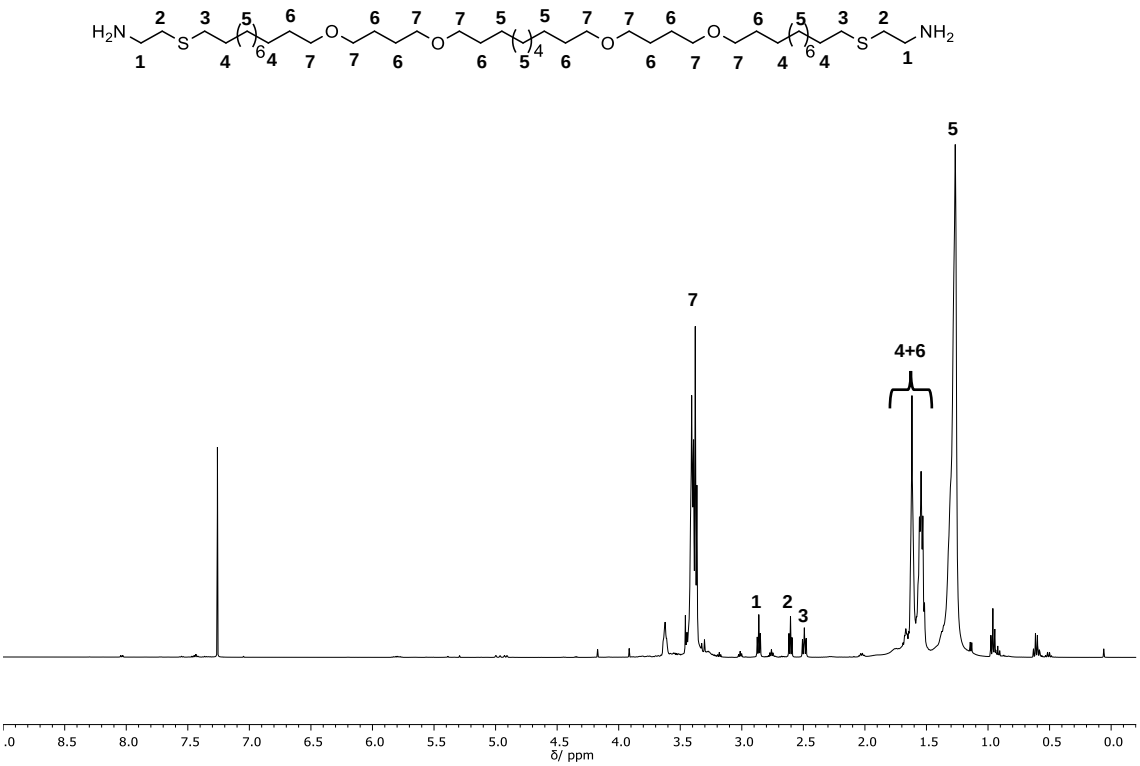

Figure S 21 ^{1}H-NMR spectrum of polyether **(11)**, measured in $CDCl_3$.

^{1}H-NMR (500 MHz, $CDCl_3$): *δ*/ppm = 3.33-3.47 (m, 8H, OC***H₂⁷***), 2.86 (t, C***H₂¹***NH_2, end group), 2.60 (t, SC***H₂²***CH_2NH_2, end group), 2.49 (t, C***H₂³***$SCH_2CH_2NH_2$, end group), 1.49-1.70 (m, 8H, OCH_2C***H₂⁶*** + CH_2SCH_2C***H₂³*** + C***H₂³***CH_2O, end group), 1.20-1.39 (m, 12H, OCH_2CH_2C***H₂⁵*** + C***H₂⁵***, end group).

^{13}C-NMR (126 MHz, DMSO-d_6): *δ*/ppm = 71.11, 70.77, 63.15, 41.30, 36.50, 32.95, 31.99, 29.92, 29.76, 29.70, 29.65, 29.60, 29.57, 29.54, 29.38, 29.04, 27.19, 26.64, 26.34, 26.26, 25.87.

IR (ATR platinum diamond): *ν*/cm^{-1} = 2919, 2852, 2802, 1489, 1468, 1437, 1413, 1374, 1300, 1276, 1242, 1203, 1112, 1030, 986, 977, 908, 878, 866, 808, 776, 742, 720, 702, 687, 672, 637, 613.

General curing procedure

Diamine and epoxide were added in a 5 mL vial equipped with a magnetic stirring bar and dissolved in DCM. The mixture was stirred for 30 minutes and added into a poly(tetrafluoroethylene) (PTFE) mold. The solvent was evaporated at room temperature for 2 hours and cured according to the curing parameters.
For the final films used for thermal and mechanical analysis 400 mg diamine and the respective amount of epoxide were dissolved in 1 mL DCM and stirred at room temperature for 30 minutes. Then, the mixture was added into a poly(tetrafluoroethylene) (PTFE) mold and the solvent was evaporated for 2 hours at room temperature. Finally, the films cured with epoxidized linseed oil were cured at 180 °C for 72 hours, while the epoxidized lignin cured films were cured at 100 °C for 2 hours followed by a post-curing at 125 °C for 3 hours. The film were carefully removed with a spatula from the mold and analyzed.

Supporting Information

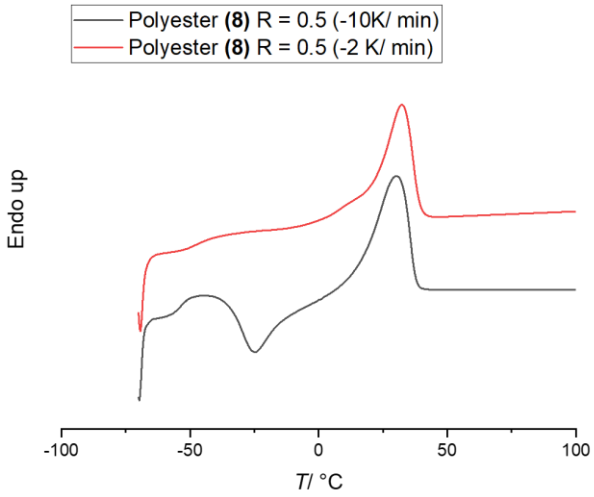

Figure S 22 Second heating cycle of DSC measurements of polyester **(8)** cured ELO with R = 0.5 after two different cooling rates: -10K/min (black) and -2K/min (red).

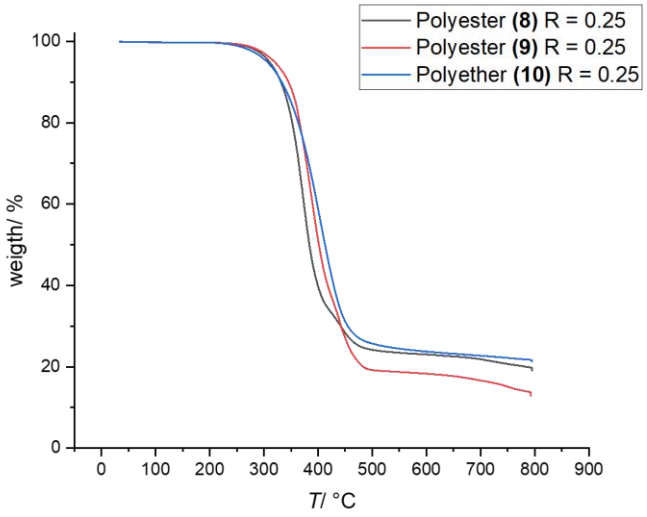

Figure S 23 TGA measurements of the polyester and polyether diamines **(8)**-**(10)** cured films with ELO for R = 0.25.

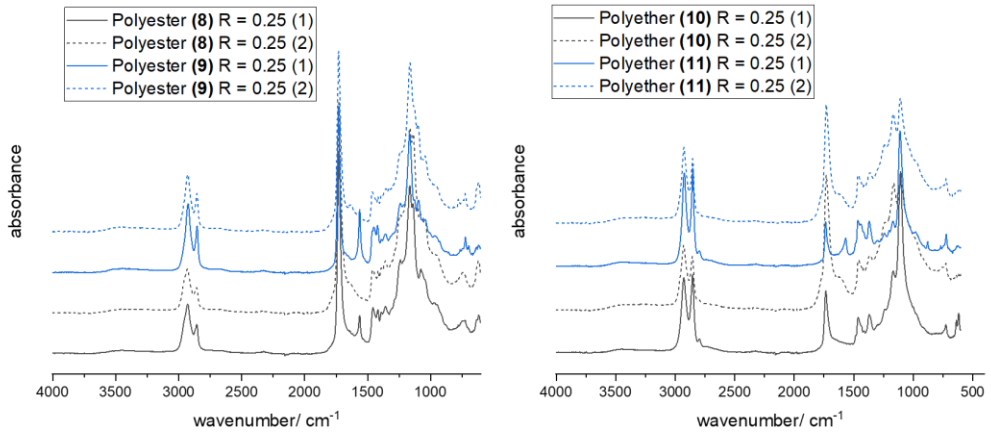

Figure S 24 IR spectra of the diamine films cured with ELO and R = 0.25, measured from the bottom side (1) and the top side (2).

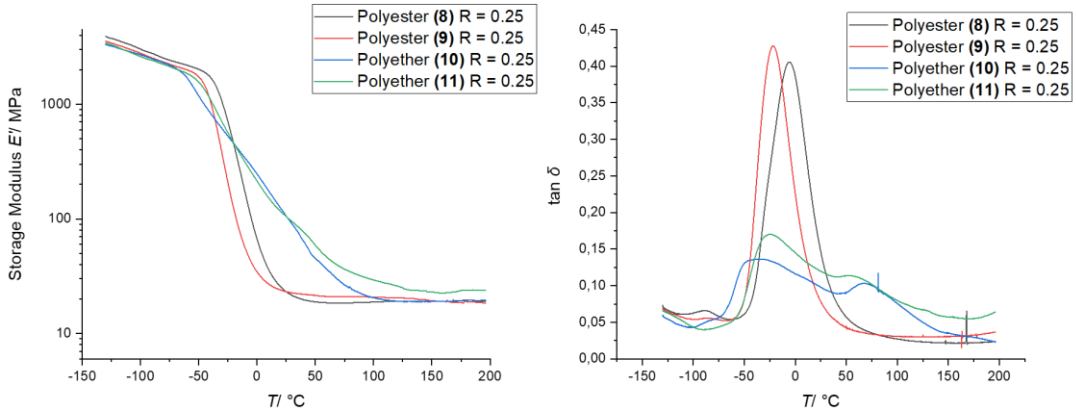

Figure S 25 Storage modulus *E'* (left) and tan *δ* (right), determined *via* DMTA measurements of the diamine films cured with ELO with R = 0.25.

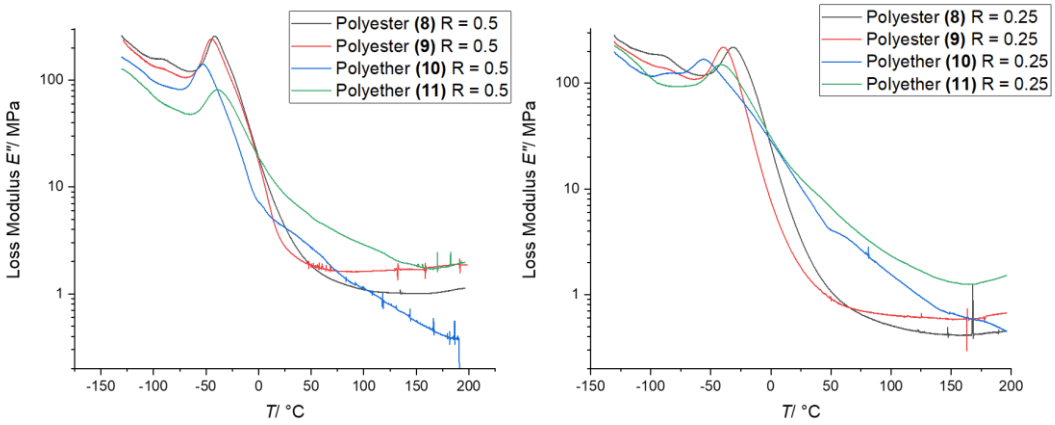

Figure S 26 Loss Modulus *E"*, determined *via* DMTA measurements of the diamine films cured with ELO with R = 0.5 (right) and R = 0.25 (left).

7 Appendix

7.1 Abbreviations

Abbreviation	Explanation
°C	Degree centigrade
AA	Adipic acid
ACE	Activated chain-end mechanism
ADMET	Acyclic diene metathesis
AGU	Anhydroglucose unit
AIBN	Azobis(isobutyronitril)
AM	Activated monomer mechanism
AO	Acros Organics
ATR	Attenuated total reflection
aq	aqueous
b (NMR)	Broad (NMR)
BD	1,4-Butanediol
BO	Butylene oxide
CA	Cellulose acetate
$CDCl_3$	Deuterated chloroform
COSY	Correlated spectroscopy
d	Days
d (NMR)	Doublet
DAF	2,5-Diacetyl furan
DBU	1,8-Diazabicyclo[5.4.0]undec-7-ene
DCM	Dichloromethane
DEA	Diethanol amine
DEG	Diethylene glycol
DIN	Deutsches Institut für Normung
DMFD	Dimethyl 2,5-furandicarboxylate
DMPA	2,2-Dimethoxy-2-phenylacetophenon
DMTA	Dynamic mechanical thermal analysis
DMSO	Dimethyl sulfoxide
DP	Degree of polymerization

DS	Degree of substitution
DSC	Different scanning calorimetry
e.g.	For example
E-Factor	Ecological factor
E‘	Storage modulus
E“	Loss modulus
EC	Ethyl cellulose
EG	Epoxidized lignin
EL	Ethylene glycol
ELO	Epoxidized linseed oil
EO	Ethylene oxide
ESI-MS	Electrospray ionization mass spectrometry
Eq.	Equivalent
Et al.	Et alii, et aliae, et alia. Lat.: and others
FBC	Fluidized bed combustion
FDCA	2,5-furandicarboxylic acid
FTIR	Fourier transform infrared spectroscopy
g	Grams
h	Hours
HDI	Hexamethylene diisocyanate
HEDS	Hexaethyl disiloxane
HFIP	Hexafluoro isopropanol
HMF	Hydroxymethylfurfural
HMBC	Heteronuclear multiple bond correlation
HPLC	High-performance liquid chromatography
HSQC	Heteronuclear single quantum coherence
IPDI	Isophorone diisocyanate
IR	Infrared spectroscopy
K	Kelvin
KHYS	Karlsruhe House of Young Scientists
KIT	Karlsruhe Institute of Technology
KTH	Kungliga Tekniska högskolan
kV	Kilovolt
LO	Linseed oil
M	Molar
m (NMR)	Multiplet
mbar	Millibar

MDI	Methylene diphenyl diisocyanate
MeOH	Methanol
mg	Milligram
MHz	Mega Hertz
Mio.	Million
min	Minutes
mL	Milliliter
mm	Millimeters
M_n	Number average molar mass
mol	Mole
mol%	Mole percent
M_p	Molar mass of the highest peak
MPa	Mega pascal
MS	Mass spectrometry
MSW	Municipal solid waste
M_w	Mass average molar mass
nm	nanometer
NIPU	Non-isocyanate polyurethane
NMR	Nuclear magnetic resonance
OEF	Oligomerized ethylene furanoate
p	Conversion
p.a.	Per annum
PA	Phthalic acid
PBO	Poly(butylene oxide)
PBG	Poly(butylene glycol)
PD	1,3-Propanediol
PDEF	Poly(diethylene furanoate)
PDEP	Poly(diethylene phthalate)
PDMS	Poly(dimethylsiloxane)
PEF	Poly(ethylene furanoate)
PEG	Poly(ethylene glycol)
PEO	Poly(ethylene oxide)
PET	Poly(ethylene terephthalate)
PIR	Polyisocyanurate rigid foam
PMMA	Poly(methyl methacrylate)
PO	Propylene oxide
PPG	Poly(propylene glycol)

PPO	Poly(propylene oxide)
PTFE	Poly(tetrafluoroethylene)
PTHF	Poly(tetrahydrofuran)
PTMO	Poly(tetramethylene oxide)
PU	Polyurethane
PUF	Polyurethane flexible foam
PUI	Polyurethane ionomers
PUR	Polyurethane rigid foam
ppm	Parts per million
q (NMR)	Quartet
Q-TOF	Quadrupole- time of flight
quint. (NMR)	Quintet
r (R)	Stochiometric ratio of reactants
r.t.	Room temperature
RI	Refractive index
ROP	Ring-opening polymerization
s (NMR)	Singlet (NMR)
SA	Succinic acid
SeA	Sebacic acid
SEC	Size exclusion chromatography
sext (NMR)	Sextet (NMR)
SSS	Switchable solvent system
t	Reaction time
t (NMR)	Triplet (NMR)
T	Temperature
T (IR)	Transmittance
T_{α}	Transition temperature
T_{d}	Degradation temperature
$T_{d\ 5\%}$	Temperature after 5% weight loss
TDI	Toluene diisocyanate
TES	Triethylsilane
THF	Tetrahydrofuran
T_{g}	Glass transition temperature
TGA	Thermogravimetric analysis
T_{m}	Melting temperature
TMDS	1,1,3,3-Tetramethyldisiloxane
TMO	Tetramethylene oxide

TPA	Terephthalic acid
TPU	Thermoplastic polyurethane
UC	10-undecylenic acid
UV	Ultraviolet
V	Volt
W	Watt
wt%	Weight percent
X_n	Degree of polymerization
δ (NMR)	Chemical shift
δ (DMTA)	Phase angel
µs	Microsecond

7.2 List of Figures

Figure 1 Usage of raw materials in the German chemical industry in 2019.[18] 8
Figure 2 Share of different renewable resources used in the German chemical industry in 2017.[18] 8
Figure 3 Classification of polyurethanes by their applications. 18
Figure 4 Overview of different recycling methods for PU. 23
Figure 5 SEC traces of polyester **1b** and the precipitation fractions according to **Table 5**, measured in THF..... 51
Figure 6 Top: ^{1}H-NMR analysis of polyester **1b** (top) and polyether **2b** (bottom) measured in $CDCl_3$. Bottom: normalized ATR-IR spectra of polyester **1b** (red) and polyether **2b**, referenced on the CH_2 vibration of **1b** at 2935 cm^{-1} (black). 53
Figure 7 SEC-ESI measurement of polyester **1b** (black) and polyether **2b** (red) with corresponding ESI spectra of polyether **2b** and high resolution for an exemplarily chosen oligomer. 54
Figure 8 Exemplary ^{1}H-NMR spectrum of polyether **2a**, measured in $CDCl_3$. 55
Figure 9 SEC traces of polyester **1a-d** and polyether **2a-d** according to **Table 7** after work-up, measured in THF. 59
Figure 10 SEC trace of polyester **1a** compared to the crude SEC traces of the reduction of polyester **1a** with TES and TMDS after 4 hours, measured in THF. 60
Figure 11 SEC traces of the scale-up reactions of polyester **1a** with TES according to **Table 8**, measured in THF. 62
Figure 12 Pictures of the reduction of cellulose acetate with TMDS catalyzed by $GaBr_3$ in DCM. 65
Figure 13 IR spectra of cellulose acetate (CA), the obtained gel, and commercially available ethyl cellulose (EC) as reference substance. 65
Figure 14 IR spectra of gel and concentrated filtrate for 5 mol% (left) and 20 mol% $GaBr_3$ (right)..... 66
Figure 15 HFIP SEC traces of three different CA obtained from Acros Organics (AO), Sigma Aldrich (SA) and the switchable solvent system (SSS), measured in HFIP..... 67
Figure 16 HFIP SEC traces of CA (SSS), commercially EC and the concentrated filtrate. 69
Figure 17 ^{1}H-NMR spectra of FDCA (top), EG (center) and the reaction mixture according to **Scheme 37** (bottom), measured in DMSO-d_6. 74
Figure 18 ^{1}H-NMR spectrum of the PEF crude mixture after the esterification step, assigning all furane species, measured in DMSO-d_6. 74

Figure 19 Exemplary ^{1}H-NMR spectrum of PEF measured in DMSO-d_6, used to determine the X_n.....78
Figure 20 ^{1}H-NMR spectrum of commercial phthalic acid based polyester polyol (polyol **1**, bottom) and the zoom-in (top), measured in DMSO-d_6.....82
Figure 21 Exemplary ^{1}H-NMR spectrum of PDEF, used to determine the conversion of FDCA, excess of DEG and X_n, measured in DMSO-d_6.....84
Figure 22 SEC traces of the commercial polyester polyol PDEP (polyol **1**) and the final biobased polyester polyols **2-4**, measured in THF.....89
Figure 23 Foaming of polyol **2** with MDI. Left: 25 seconds after addition of MDI, center 30 seconds after addition of MDI, right: final foam 50 seconds after addition of MDI ...90
Figure 24 Exemplary ^{1}H-NMR spectrum of the one-pot polymerization of succinic acid (SA), 1,4-butandiol (BD) and 10-undecylenic acid (UC) after 2 hours, measured in $CDCl_3$. Conversions of the starting materials are highlighted by the shift of the CH_2 groups of SA, the α-carbonyl CH_2 group of UC and BD.....97
Figure 25 SEC trace of polyester **(1)** in THF, showing a "cut off" at lower retention times between 15.0 and 15.5 min as they were not soluble. 98
Figure 26 SEC traces of adipic acid (AA) based polyester **(2)** and **(4)** (left) and the sebacic acid (SeA) based polyester **(3)** and **(5)** (right), before (black) and after (red) end group modification with 10-undecylenic acid (UC) and precipitation in *n*-hexane.....101
Figure 27 Exemplary ^{1}H-NMR spectra of the $GaBr_3$ catalyzed reduction with TES of the adipic acid based polyester **(4)** (top) to the polyether **(6)** (bottom), measured in $CDCl_3$. 103
Figure 28 SEC traces of the adipic acid based polyester **(4)** and polyether **(6)** (left) and the sebacic acid based polyester **(5)** and polyether **(7)** (right), measured in THF. 104
Figure 29 Exemplary ^{1}H-NMR spectra of adipic acid based polyester **(4)** with double bond end groups, measured in $CDCl_3$ (top) and of the diamine polyester **(8)**, measured in DMSO-d_6 (bottom), showing the complete conversion of the double bonds by the applied thiol-ene reaction. 106
Figure 30 SEC traces of adipic acid based polyester **(4)** and polyether **(6)** before and after thiol-ene reaction (left) yielding the corresponding diamines **(8)** and **(10)** and the sebacic acid base polyester **(5)** and polyether **(7)** before and after thiol-ene reaction (right) yielding the corresponding diamines **(9)** and **(11)**, measured in THF.....106
Figure 31 ^{1}H-NMR of polyester **(8)** before (top) and after work-up (bottom), measured in $CDCl_3$. 107
Figure 32 IR spectra of polyester diamines **(8)** and **(9)** (left) as well as of polyether diamines **(10)**, **(11)** and Jeffamine® (right). 108

Appendix

Figure 33 Second heating cycle of the DSC measurement (left) and TGA measurement (right) of the polyester and polyether diamines **(8)**-**(11)**. 109
Figure 34 IR spectra of polyester **(8)**, polyether **(10)**, linseed oil (LO) and epoxidized linseed oil (ELO, left) and the zoom-in (right)..... 112
Figure 35 Second heating cycle of the DSC measurement (left) and IR spectra (center) before and after curing of polyester **(8)** with R = 0.5 at 180 °C for 17 hours as well as the zoom-in (right). 113
Figure 36 Second heating cycle of the DSC measurement (left) and IR spectra (center) of the curing of polyester **(8)** with ELO (R = 0.5) under different temperatures as well as the zoom-in (right). 114
Figure 37 Second heating cycle of the DSC measurement (left) and IR spectra (center) for different R values of polyester **(8)** and ELO cured at 180 °C for 48 hours as well as the zoom-in (right). 115
Figure 38 Second heating cycle of the DSC measurement (left) and IR spectra (center) for different R values of polyester **(8)** and ELO cured at 160 °C for 72 hours as well as the zoom-in (right). 115
Figure 39 Second heating cycle of the DSC measurements of the polyester (left) and polyether diamines (right) cured films with ELO at 180 °C for 72 hours. 117
Figure 40 TGA measurements of the polyester and polyether diamines **(8)**-**(11)** cured films with ELO for R = 0.5..... 118
Figure 41 IR spectra of the diamine films cured with ELO and R = 0.5, measured from the bottom side (1) and the top side (2). 118
Figure 42 Storage modulus *E'* (left) and tan *δ* (right), determined *via* DMTA measurements of the diamine films cured with ELO with R = 0.5. 120
Figure 43 IR spectrum of polyester **(8)** cured epoxidized lignin (EL) with R = 0.5 for 5 hours at 180 °C, compared to the IR spectra of polyester **(8)**, EL and before curing (0 h, left) as well as the zoom-in (right)..... 121
Figure 44 Second heating cycle of the DSC measurements (left) and IR spectra (right) of polyester **(8)** cured with EL for different R values at 180 °C after 7 hours..... 122
Figure 45 Second heating cycle of the DSC measurements (left) and IR spectra (center) of polyester **(8)** cured EL for different R values at 100 °C (125 °C) after 2 h (2 h) as well as the zoom-in (right). 122
Figure 46 DMTA measurement (left) and DSC trace of the second heating cycle (right) of the polyester **(8)** cured film with EL and R = 0.5 at 100 °C for 2 h and subsequently at 125 °C for 3 h. 123

7.3 List of Schemes

Scheme 1 General cellulose structure with cellobiose as repeating unit. 9
Scheme 2 Typical synthesis of EC from alkali cellulose and ethyl chloride. 10
Scheme 3 Synthesis of CA using a CO_2 switchable solvent system of DMSO and DBU. 11
Scheme 4 Phenylpropane building blocks of lignin. 12
Scheme 5 Synthesis of polyurethanes *via* polyaddition of polyisocyanate and polyol. 14
Scheme 6 Most common polyisocyanates for industrial applications. 15
Scheme 7 Structure of most common polyether polyols poly(ethylene oxide) PEO and poly(propylene oxide) PPO as well as the general structure of a polyester polyol. 16
Scheme 8 Different ways to obtain polyfunctional isocyanates. 16
Scheme 9 Different synthesis routes of non-isocyanate polyurethane (NIPU).....17
Scheme 10 Formation of CO_2 as blowing agent through the reaction of isocyanate and H_2O. 18
Scheme 11 Synthesis of polyisocyanate prepolymers. 20
Scheme 12 Chemical recycling methods for PU. 24
Scheme 13 Overview of the main aliphatic polyether polyol representatives.....26
Scheme 14 Mechanism of anionic ROP, exemplarily shown for PO. 27
Scheme 15 Activated monomer mechanism of the anionic ROP, exemplarily shown for PO.....28
Scheme 16 Coordinative insertion ROP mechanism, exemplarily shown for PO. 28
Scheme 17 Active chain-end (ACE) mechanism (top) and active monomer (AM) mechanism (bottom) of cationic ROP, exemplarily shown for EO. 29
Scheme 18 ADMET polymerization (top) and thiol-ene polymerization (bottom) of α,ω-diene ether. 31
Scheme 19 Catalytic reduction of polyester to polyether. 31
Scheme 20 Synthesis of biobased polyester polyols *via* polycondensation of biobased dicarboxylic acids and diols (top) and ROP of ε-caprolactone (bottom). 33
Scheme 21 Thiol-ene reaction of limonene and 1-thioglycerol. 34
Scheme 22 Synthesis of biobased aromatic polyether polyols derived from lignocellulosic biomass. 34
Scheme 23 Synthesis of renewable aromatic polyester polyols *via* glycolysis followed by esterification with biobased aliphatic dicarboxylic acids. 35
Scheme 24 Synthesis of PEF (top) and PET (bottom). 36

Scheme 25 Overview of different FDCA synthesis routes: **a** Oxidation of HMF obtained *via* dehydration of fructose, **b** carbonate-promoted C-H carboxylation of 2-furoic acid, **c** Henkel reaction of 2-furoic acid, **d** Iodoform reaction of DAF. 38
Scheme 26 Typical polycondensation synthesis route of PEF (top) and the ROP route introduced by Morbidelli and coworkers (bottom).[353] 39
Scheme 27 Exemplary reduction of an ester to the corresponding ether on steroids using $LiAlH_4$, introduced by Petitt and coworkers.[367] 40
Scheme 28 First reduction of an ester to an ether using silanes as reducing agents under γ-irradiation, reported by Tsurugi and coworkers.[371] 40
Scheme 29 Indium-catalyzed reduction of esters to ethers using different hydrosilanes and solvents.[388] 41
Scheme 30 Proposed mechanism of the indium catalyzed reduction of esters.[388] 41
Scheme 31 $GaBr_3$ catalyzed reduction of methyl oleate and a triglyceride with TMDS. 42
Scheme 32 Synthesis of renewable polyethers enabled by the $GaBr_3$ catalyzed reduction of aliphatic esters. 42
Scheme 33 $GaBr_3$ catalyzed reduction of renewable polyester. 43
Scheme 34 Overview of the $GaBr_3$ catalyzed reduction of four different polyesters **1a-d** and the studied reducing agents. 49
Scheme 35 Synthesis of ethyl cellulose through reduction of cellulose acetate with TMDS catalyzed by $GaBr_3$. 64
Scheme 36 Synthesis of poly(ethylene furanoate) (PEF). 72
Scheme 37 Esterification of FDCA with 4.00 eq. EG and subsequent antimony(III) oxide catalyzed polycondensation.[362] 72
Scheme 38 Titanium(IV) isopropoxide catalyzed esterification of FDCA with 2.20 eq. EG and subsequent polycondensation.[357] 75
Scheme 39 Hydrochloric acid catalyzed esterification of FDCA with 100 eq. EG.[392] . 75
Scheme 40 Synthesis of poly(diethylene furanoate) (PDEF) from FDCA and diethylene glycol (DEG). 81
Scheme 41 Non-catalyzed synthesis of PDEF with 1.50 eq. DEG at 175 °C for 3 days. 82
Scheme 42 Structural overview of used chemicals for the oligomerization of FDCA. . 87
Scheme 43 Synthesis route towards fully biobased polyether and polyester diamines starting from different dicarboxylic acids and 1,4-butanediol. 95
Scheme 44 One-pot polymerization of succinic acid (SA), 1,4-butanediol (BD) and 10-undecylenic acid (UC). 96

Scheme 45 Pseudo one-pot polymerization of adipic acid (AA) or sebacic acid (SeA) with 1,4-butanediol (BD) and 10-undecylic acid (UC). 99
Scheme 46 $GaBr_3$ catalyzed reduction of the end group modified polyester based on adipic acid (AA) and sebacic acid (SeA) with TES.....102
Scheme 47 Thiol-ene reaction of the adipic acid (AA) and sebacic acid (SeA) based end group modified polyester **(4)** and **(5)** as well as of the corresponding polyether **(6)** and **(7)**. 104
Scheme 48 Schematic overview of the thermoset synthesis from different diamines (blue) with epoxidized linseed oil or epoxidized lignin (red). 111

7.4 List of Tables

Table 1 The Twelve Principles of Green Chemistry.[21] 4
Table 2 Typical E-Factors for different industry segments.[28] 7
Table 3 Overview of different wood types, their lignin content, and the ratio of building blocks.[83] 12
Table 4 Overview of the four different polyesters **1a-d**, their molecular weights as well as OH and acid values. 50
Table 5 Precipitation fractions of polyesters **1a** and **1b** in methanol and *n*-hexane. ... 51
Table 6 Optimization of the reaction conditions for possible scale-up reactions with TMDS. 57
Table 7 Scale-up reactions of polyester **1a-d** with TMDS. 58
Table 8 Scale-up reactions of polyester **1a** with TES. 61
Table 9 Overview of DS and molecular weight of three different CA. 67
Table 10 Solubility study for three different CA, EC, and the obtained gel. 68
Table 11 Investigation of different solvents for the reduction of CA supplied from Sigma Aldrich. 70
Table 12 Esterification of FDCA and EG for different reaction conditions without argon flow. 77
Table 13 Screening of different eq. of EG and catalysts for the polycondensation of FDCA and EG at 175 °C for 6 hours. 80
Table 14 Screening of different temperatures and reaction times without the use of a catalyst. 81
Table 15 Optimization of reactions conditions for the synthesis of PDEF using different eq. of DEG. 86
Table 16 Copolymerization of different dicarboxylic acids with FDCA. 87
Table 17 Scale-up reactions of polyol synthesis using FDCA as well as FDCA with 10 mol% of SA or AA. 88
Table 18 Thermal and mechanical properties of the PIR rigid foams for polyols **1-4**. . 92
Table 19 First test reactions of the one-pot polymerization of succinic acid (SA), 1,4-butanediol (BD), and 10-undecylenic acid (UC) after six days. 97
Table 20 Scale-up reaction of the polycondensation with adipic acid (AA) and sebacic acid (SeA) as well as subsequent end group modification with 10-undecylenic acid (UC). 101
Table 21 $GaBr_3$ catalyzed reduction of adipic acid (AA) and sebacic acid (SeA) based polyester **(6)** and **(7)** after three days showing 13 mol% silyl species per repeating unit, determined *via* ^{1}H-NMR spectroscopy. 103

Table 22 Summary of thiol-ene reactions of polyester **(4)** and **(5)** as well as of polyether **(6)** and **(7)**. 105
Table 23 Summary of M_n and thermal analysis data for all diamines.....109
Table 24 Overview of the thermal analysis of the polyester and polyether diamines cured films with ELO. 117
Table 25 DMTA analysis of the polyester cured films with ELO.....120

7.5 List of Equations

Equation 1 Definition of the atom economy according to Trost.[27] 6
Equation 2 Definition of the E-Factor according to Sheldon.[29] 6
Equation 3 Calculation of FDCA conversion *via* ^{1}H-NMR spectroscopy..... 73
Equation 4 Carothers equation for A-A/B-B systems with p = conversion and r = stochiometric ratio of reactants..... 77
Equation 5 Calculation of M_n (NMR) with X_n determined *via* ^{1}H-NMR spectroscopy, normalized on the four protons of the EG end group ($\delta_{3.66\ ppm}$), measured in DMSO-d_6. 78
Equation 6 Calculation of *Mn*. *z* = functionality of polyol. 83
Equation 7 Calculation of X_n. 83
Equation 8 Determination of X_n *via* ^{1}H-NMR with $X_n = 1$ for $n = 0$. ^{1}H-NMR was normalized to the aromatic protons of the furan repeating unit. 84
Equation 9 Calculation of excess DEG in wt% *via* ^{1}H-NMR. ^{1}H-NMR was normalized to the aromatic protons of the furan repeating unit. 84

7.6 List of Publications

1. F. Rhein, S. Kaiser, **M. Rhein**, H. Nirschl, Agglomerate processing and recycling options in magnetic seeded Filtration, *Chemical Engineering Science* ***2021****, 238,*116577
2. M. von Czapiewski, **M. Rhein**, M. A. R. Meier* Fatty Acid Derived Renewable Platform Chemicals via Selective Oxidation Processes, *ACS Sustainable Chem. Eng.* **2018**, *6*, 15170-15179.

Appendix

8 Bibliography

[1] *Ourworldindata* **2022**, https://ourworldindata.org/world-population-growth 13-01-2022.
[2] J. O. Metzger, A. Hüttermann, *Naturwissenschaften* **2009**, *96*, 279-288
[3] *Ourworldindata* **2022**, https://ourworldindata.org/grapher/crude-oil-prices 13-01-2022.
[4] E. Henrich, N. Dahmen, E. Dinjus, J. Sauer, *Chemie Ingenieur Technik* **2015**, *87*, 1667-1685
[5] *Ourworldindata* **2022**, https://ourworldindata.org/energy-mix 13-01-2022.
[6] *Plastics Europe* **2021**, https://plasticseurope.org/de/knowledge-hub/plastics-the-facts-2019/ 15-11-2021.
[7] *European bioplastics* **2021**, https://www.european-bioplastics.org/market/ 15-11-2021.
[8] G. Brundtland, M. Khalid, S. Agnelli, S. Al-Athel, B. Chidzero, L. Fadika, V. Hauff, I. Lang, M. Shijun, M. Morino de Botero, M. Singh, S. Okita, A. Others, *Our Common Future ('Brundtland report')*, Oxford University Press, USA, **1987**.
[9] U. Nations, *Report of the World Summit on Sustainable Development Johannesburg.* **2002**
[10] D. L. Klass, *Biomass for renewable energy, fuels, and chemicals*, Elsevier, **1998**.
[11] E. Henrich, N. Dahmen, E. Dinjus, J. Sauer, *Chemie Ingenieur Technik* **2015**, *87*, 1667-1685
[12] *FNR* **2022**, https://basisdaten.fnr.de/bioenergie/energiedaten 13-01-2022.
[13] *FNR* **2022**, https://basisdaten.fnr.de/bioenergie/biokraftstoffe 13-01-2022.
[14] A. Muscat, E. M. de Olde, I. J. M. de Boer, R. Ripoll-Bosch, *Global Food Security* **2020**, *25*, 100330
[15] L. C. Over, M. A. R. Meier, *Green Chemistry* **2016**, *18*, 197-207
[16] I. A. Pearl, *The chemistry of lignin.* **1967**
[17] R. A. Sheldon, *Green Chemistry* **2014**, *16*, 950-963
[18] *VCI Verband der Chemischen Industrie e.V.* **2022**, https://www.vci.de/die-branche/zahlen-berichte/vci-statistik-grafiken-energie-klima-rohstoffe-chemie.jsp 13-01-2022.
[19] P. Anastas, N. Eghbali, *Chemical Society Reviews* **2010**, *39*, 301-312
[20] P. T. Anastas, M. M. Kirchhoff, *Accounts of Chemical Research* **2002**, *35*, 686-694
[21] P. Anastas, J. Warner, *Green Chemistry: Theory and Practice; Oxford University Press: New York, NY, USA* **2000**
[22] M. S. Holzwarth, B. Plietker, *ChemCatChem* **2013**, *5*, 1650-1679
[23] R. A. Sheldon, J. M. Woodley, *Chemical Reviews* **2018**, *118*, 801-838
[24] A. Corma, S. Iborra, A. Velty, *Chemical Reviews* **2007**, *107*, 2411-2502
[25] C. J. Clarke, W.-C. Tu, O. Levers, A. Bröhl, J. P. Hallett, *Chemical Reviews* **2018**, *118*, 747-800
[26] H. C. Erythropel, J. B. Zimmerman, T. M. de Winter, L. Petitjean, F. Melnikov, C. H. Lam, A. W. Lounsbury, K. E. Mellor, N. Z. Janković, Q. Tu, L. N. Pincus, M. M. Falinski, W. Shi, P. Coish, D. L. Plata, P. T. Anastas, *Green Chemistry* **2018**, *20*, 1929-1961
[27] B. M. Trost, *Science* **1991**, *254*, 1471-1477
[28] R. A. Sheldon, *Chemical Communications* **2008**, 3352-3365
[29] R. A. Sheldon, *Green Chemistry* **2007**, *9*, 1273-1283
[30] *VCI Verband der Chemischen Industrie e.V.* **2019**, https://www.bayerische-chemieverbaende.de/wp-content/uploads/sites/4/2019/2009/daten-fakten-rohstoffbasis-chemieindustrie-2013.pdf 28-01-2022.

[31] D. Klemm, B. Heublein, H.-P. Fink, A. Bohn, *Angewandte Chemie International Edition* **2005**, *44*, 3358-3393
[32] A. Payen, *Comptes rendus* **1838**, *7*, 1052-1056
[33] W. Ferrier, *Acta Crystallographica* **1963**, *16*, 1023-1031
[34] G. S. Rekhi, S. S. Jambhekar, *Drug Development and Industrial Pharmacy* **1995**, *21*, 61-77
[35] G. Murtaza, *Acta poloniae pharmaceutica* **2012**, *69*, 11-22
[36] R. Rowe, American Pharmaceutical Association: Pharmaceutical Press, **2003**
[37] C. Zhang, J. Tang, D. Liu, X. Li, L. Cheng, X. Tang, *International Journal of Pharmaceutics* **2016**, *503*, 41-55
[38] Y. Zhang, Z. Huang, E. Omari-Siaw, S. Lu, Y. Zhu, D. Jiang, M. Wang, J. Yu, X. Xu, W. Zhang, *AAPS PharmSciTech* **2016**, *17*, 339-349
[39] R. C. Rowe, P. Sheskey, M. Quinn, *Handbook of pharmaceutical excipients*, Libros Digitales-Pharmaceutical Press, **2009**.
[40] S. Muschert, F. Siepmann, B. Leclercq, B. Carlin, J. Siepmann, *European Journal of Pharmaceutics and Biopharmaceutics* **2009**, *72*, 130-137
[41] J. Grund, M. Koerber, M. Walther, R. Bodmeier, *International Journal of Pharmaceutics* **2014**, *469*, 94-101
[42] G. S. Rekhi, R. Mendes, S. Porter, S. Jambhekar, *Pharm. Tech* **1989**, *13*, 112-125
[43] R. Chang, C. Hsiao, J. Robinson, *Pharm. Technol* **1987**, *11*, 56-68
[44] R. C. Rowe, *International Journal of Pharmaceutics* **1986**, *29*, 37-41
[45] M. Emeje, O. Kunle, S. Ofoefule, *AAPS PharmSciTech* **2006**, *7*, 58
[46] M. R. Sanoufi, A. Aljaberi, I. Hamdan, N. Al-Zoubi, *Pharmaceutical Development and Technology* **2020**, *25*, 187-196
[47] N. Follonier, E. Doelker, E. T. Cole, *Journal of Controlled Release* **1995**, *36*, 243-250
[48] C. de Brabander, G. van den Mooter, C. Vervaet, J. P. Remon, *Journal of Pharmaceutical Sciences* **2002**, *91*, 1678-1685
[49] M. M. Crowley, B. Schroeder, A. Fredersdorf, S. Obara, M. Talarico, S. Kucera, J. W. McGinity, *International Journal of Pharmaceutics* **2004**, *269*, 509-522
[50] A. J. Gravelle, A. G. Marangoni, M. Davidovich-Pinhas, in *Edible Oleogels (Second Edition)* (Eds.: A. G. Marangoni, N. Garti), AOCS Press, **2018**, pp. 331-362.
[51] A. Ascherio, M. B. Katan, P. L. Zock, M. J. Stampfer, W. C. Willett, *New England Journal of Medicine* **1999**, *340*, 1994-1998
[52] D. Mozaffarian, M. B. Katan, A. Ascherio, M. J. Stampfer, W. C. Willett, *New England Journal of Medicine* **2006**, *354*, 1601-1613
[53] R. P. Mensink, P. L. Zock, A. D. Kester, M. B. Katan, *The American Journal of Clinical Nutrition* **2003**, *77*, 1146-11553/30/2020.
[54] J. A. Nettleton, I. A. Brouwer, J. M. Geleijnse, G. Hornstra, *Annals of Nutrition and Metabolism* **2017**, *70*, 26-33
[55] J.-M. AIACHE, P. GAUTHIER, S. AIACHE, *International Journal of Cosmetic Science* **1992**, *14*, 228-234
[56] M. Davidovich-Pinhas, S. Barbut, A. G. Marangoni, *Annual Review of Food Science and Technology* **2016**, *7*, 65-91
[57] A. J. Gravelle, S. Barbut, M. Quinton, A. G. Marangoni, *Journal of Food Engineering* **2014**, *143*, 114-122
[58] M. Davidovich-Pinhas, S. Barbut, A. G. Marangoni, *Carbohydrate Polymers* **2015**, *127*, 355-362
[59] Dow, *Dow Chemical Company.* **2016**
[60] W. Koch, *Industrial & Engineering Chemistry* **1937**, *29*, 687-690
[61] M. Davidovich-Pinhas, S. Barbut, A. G. Marangoni, *Cellulose* **2014**, *21*, 3243-3255
[62] R. Mehta, J. Teckoe, C. Schoener, S. Workentine, D. Ferrizzi, A. Rajabi-Siahboomi, *AAPS PharmSciTech* **2016**, *17*, 1366-1375

[63] T. H. E. Moellmann, T. Liebert, S. Koehler, **2008**
[64] R. A. V. Myllymäki, **2005**
[65] C. Goncalves, C. Favre, P. Feuardant, S. Klein, C. Vaca-Garcia, C. Cecutti, S. Thiébaud-Roux, E. Vedrenne, *Carbohydrate Polymers* **2015**, *116*, 51-59
[66] L.-G. Tang, D. N.-S. Hon, Y.-Q. Zhu, *Journal of Applied Polymer Science* **1997**, *64*, 1953-1960
[67] A. Hummel, *Macromolecular Symposia* **2004**, *208*, 61-80
[68] S. Fischer, K. Thümmler, B. Volkert, K. Hettrich, I. Schmidt, K. Fischer, *Macromolecular Symposia* **2008**, *262*, 89-96
[69] J. Wu, J. Zhang, H. Zhang, J. He, Q. Ren, M. Guo, *Biomacromolecules* **2004**, *5*, 266-268
[70] Y. Yang, H. Xie, E. Liu, *Green Chemistry* **2014**, *16*, 3018-3023
[71] J. Wolfs, M. A. R. Meier, *Green Chemistry* **2021**, *23*, 4410-4420
[72] Y. Cao, J. Wu, T. Meng, J. Zhang, J. He, H. Li, Y. Zhang, *Carbohydrate Polymers* **2007**, *69*, 665-672
[73] K. J. Edgar, C. M. Buchanan, J. S. Debenham, P. A. Rundquist, B. D. Seiler, M. C. Shelton, D. Tindall, *Progress in Polymer Science* **2001**, *26*, 1605-1688
[74] T. Heinze, T. Liebert, *Progress in Polymer Science* **2001**, *26*, 1689-1762
[75] H. N. Cheng, M. K. Dowd, R. L. Shogren, A. Biswas, *Carbohydrate Polymers* **2011**, *86*, 1130-1136
[76] R. K. Singh, *Journal of Thermal Analysis and Calorimetry* **2013**, *114*, 809-819
[77] F. Xuli, D. D. L. Chung, *Cement and Concrete Research* **1996**, *26*, 535-538
[78] F. Jia, H.-j. Liu, G.-g. Zhang, *Procedia Environmental Sciences* **2016**, *31*, 98-102
[79] X. He, W. Lu, C. Sun, H. Khalesi, A. Mata, R. Andaleeb, Y. Fang, *Carbohydrate Polymers* **2021**, *255*, 117334
[80] C. O. Tuck, E. Pérez, I. T. Horváth, R. A. Sheldon, M. Poliakoff, *Science* **2012**, *337*, 695-699
[81] J. Zakzeski, P. C. A. Bruijnincx, A. L. Jongerius, B. M. Weckhuysen, *Chemical Reviews* **2010**, *110*, 3552-3599
[82] Y. Zhang, M. Naebe, *ACS Sustainable Chemistry & Engineering* **2021**
[83] P. Azadi, O. R. Inderwildi, R. Farnood, D. A. King, *Renewable and Sustainable Energy Reviews* **2013**, *21*, 506-523
[84] N. Smolarski, *Frost & Sullivan* **2012**, *1*, 1-15
[85] W. Schutyser, T. Renders, S. Van den Bosch, S. F. Koelewijn, G. T. Beckham, B. F. Sels, *Chemical Society Reviews* **2018**, *47*, 852-908
[86] M. Ragnar, G. Henriksson, M. E. Lindström, M. Wimby, J. Blechschmidt, S. Heinemann, *Ullmann's Encyclopedia of Industrial Chemistry* **2000**, 1-92
[87] F. S. Chakar, A. J. Ragauskas, *Industrial Crops and Products* **2004**, *20*, 131-141
[88] B. Saake, R. Lehnen, *Ullmann's Encyclopedia of Industrial Chemistry* **2000**
[89] T. Aro, P. Fatehi, *ChemSusChem* **2017**, *10*, 1861-1877
[90] A. Gandini, T. M. Lacerda, A. J. F. Carvalho, E. Trovatti, *Chemical Reviews* **2016**, *116*, 1637-1669
[91] F. G. Calvo-Flores, J. A. Dobado, J. Isac-García, F. J. Martín-Martínez, *Lignin and lignans as renewable raw materials: chemistry, technology and applications*, John Wiley & Sons, **2015**.
[92] R. Rinaldi, R. Jastrzebski, M. T. Clough, J. Ralph, M. Kennema, P. C. A. Bruijnincx, B. M. Weckhuysen, *Angewandte Chemie International Edition* **2016**, *55*, 8164-8215
[93] F. G. Calvo-Flores, J. A. Dobado, *ChemSusChem* **2010**, *3*, 1227-1235
[94] C. E. Wyman, *Aqueous pretreatment of plant biomass for biological and chemical conversion to fuels and chemicals*, John Wiley & Sons, **2013**.
[95] X. Zhao, K. Cheng, D. Liu, *Applied Microbiology and Biotechnology* **2009**, *82*, 815-827
[96] M.-F. Li, S. Yang, R.-C. Sun, *Bioresource Technology* **2016**, *200*, 971-980
[97] P. Sannigrahi, A. J. Ragauskas, S. J. Miller, *Energy & Fuels* **2010**, *24*, 683-689

[98] M. G. Alriols, A. Tejado, M. Blanco, I. Mondragon, J. Labidi, *Chemical Engineering Journal* **2009**, *148*, 106-114
[99] T. vom Stein, P. M. Grande, H. Kayser, F. Sibilla, W. Leitner, P. Domínguez de María, *Green Chemistry* **2011**, *13*, 1772-1777
[100] R. Katahira, A. Mittal, K. McKinney, P. N. Ciesielski, B. S. Donohoe, S. K. Black, D. K. Johnson, M. J. Biddy, G. T. Beckham, *ACS Sustainable Chemistry & Engineering* **2014**, *2*, 1364-1376
[101] B. M. Upton, A. M. Kasko, *Chemical reviews* **2016**, *116*, 2275-2306
[102] O. Bayer, H. Rinke, W. Siefken, L. Orthner, H. Schild, *Patent DRP* **1937**, *728981*
[103] M. Szycher, *Szycher's handbook of polyurethanes*, CRC press, **1999**.
[104] F. Zafar, E. Sharmin, *Polyurethane*, BoD–Books on Demand, **2012**.
[105] G. Avar, U. Meier-Westhues, H. Casselmann, D. Achten, in *Polymer Science: A Comprehensive Reference* (Eds.: K. Matyjaszewski, M. Möller), Elsevier, Amsterdam, **2012**, pp. 411-441.
[106] D. K. Chattopadhyay, K. V. S. N. Raju, *Progress in Polymer Science* **2007**, *32*, 352-418
[107] P. Vermette, H. J. Griesser, G. Laroche, R. Guidoin, *Biomedical applications of polyurethanes*, Landes Bioscience Georgetown, TX, **2001**.
[108] J. O. Akindoyo, M. D. H. Beg, S. Ghazali, M. R. Islam, N. Jeyaratnam, A. R. Yuvaraj, *RSC Advances* **2016**, *6*, 114453-114482
[109] H.-W. Engels, H.-G. Pirkl, R. Albers, R. W. Albach, J. Krause, A. Hoffmann, H. Casselmann, J. Dormish, *Angewandte Chemie International Edition* **2013**, *52*, 9422-9441
[110] H. Ulrich, *Chemistry and technology of isocyanates*, Wiley-Blackwell, **1996**.
[111] H. Sardon, A. Pascual, D. Mecerreyes, D. Taton, H. Cramail, J. L. Hedrick, *Macromolecules* **2015**, *48*, 3153-3165
[112] M. F. Sonnenschein, *Polyurethanes: science, technology, markets, and trends*, John Wiley & Sons, **2021**.
[113] D. Bello, S. R. Woskie, R. P. Streicher, Y. Liu, M. H. Stowe, E. A. Eisen, M. J. Ellenbecker, J. Sparer, F. Youngs, M. R. Cullen, C. A. Redlich, *American Journal of Industrial Medicine* **2004**, *46*, 480-491
[114] M. Malik, R. Kaur, *Polymer Engineering & Science* **2018**, *58*, 112-117
[115] N. Karak, *Biobased smart polyurethane nanocomposites: from synthesis to applications*, Royal Society of Chemistry, **2017**.
[116] D. Klempner, K. C. Frisch, *Handbook of polymeric foams and foam technology, Vol. 404*, Hanser Munich, **1991**.
[117] Z. S. Petrović, *Polymer Reviews* **2008**, *48*, 109-155
[118] J. H. Saunders, R. J. Slocombe, *Chemical Reviews* **1948**, *43*, 203-218
[119] S. Ozaki, *Chemical Reviews* **1972**, *72*, 457-496
[120] Y. He, X. Zhang, X. Zhang, H. Huang, J. Chang, H. Chen, *Journal of Industrial and Engineering Chemistry* **2012**, *18*, 1620-1627
[121] K. H. Slotta, H. Dressler, *Berichte der deutschen chemischen Gesellschaft (A and B Series)* **1930**, *63*, 888-8982021/11/19.
[122] A. W. Hofmann, *Berichte der deutschen chemischen Gesellschaft* **1870**, *3*, 653-6582021/11/19.
[123] M. Ionescu, *Chemistry and technology of polyols for polyurethanes*, iSmithers Rapra Publishing, **2005**.
[124] O. Kreye, H. Mutlu, M. A. R. Meier, *Green Chemistry* **2013**, *15*, 1431-1455
[125] G. Rokicki, P. G. Parzuchowski, M. Mazurek, *Polymers for Advanced Technologies* **2015**, *26*, 707-761
[126] L. Maisonneuve, O. Lamarzelle, E. Rix, E. Grau, H. Cramail, *Chemical Reviews* **2015**, *115*, 12407-12439
[127] Y. Bienvenu, *Comptes Rendus Physique* **2014**, *15*, 719-730
[128] K. Yasunaga, R. A. Neff, X. D. Zhang, C. W. Macosko, *Journal of Cellular Plastics* **1996**, *32*, 427-448
[129] W. Li, A. J. Ryan, I. K. Meier, *Macromolecules* **2002**, *35*, 6306-6312

[130] S. Adnan, M. T. I. Tuan Noor, N. H. 'Ain, K. P. P. Devi, N. S. Mohd, Y. Shoot Kian, Z. B. Idris, I. Campara, C. M. Schiffman, K. Pietrzyk, V. Sendijarevic, I. Sendijarevic, *Journal of Applied Polymer Science* **2017**, *134*, 45440
[131] G. Beaucage, **2012**
[132] W. W. Reichmann, B. A. Phillips, *Journal of Cellular Plastics* **1988**, *24*, 601-610
[133] E. Dominguez-Rosado, J. J. Liggat, C. E. Snape, B. Eling, J. Pichtel, *Polymer Degradation and Stability* **2002**, *78*, 1-5
[134] E. Endres, J. Kleser, Industrieverband Polyurethan-Hartschaum, IVPU http://www.daemmt-besser.de, **2008**^21-01-2022.
[135] X. Zeng, T. Tang, J. An, X. Liu, H. Xiang, Y. Li, C. Yang, T. Xia, *Polymer Composites* **2021**, *42*, 4549-4559
[136] K. Ashida, *Polyurethane and related foams: chemistry and technology*, CRC press, **2006**.
[137] A. Demharter, *Cryogenics* **1998**, *38*, 113-117
[138] C. Hepburn, *Polyurethane elastomers*, Springer Science & Business Media, **2012**.
[139] U. Šebenik, M. Krajnc, *International Journal of Adhesion and Adhesives* **2007**, *27*, 527-535
[140] B. Claeys, A. Vervaeck, X. K. D. Hillewaere, S. Possemiers, L. Hansen, T. De Beer, J. P. Remon, C. Vervaet, *European Journal of Pharmaceutics and Biopharmaceutics* **2015**, *90*, 44-52
[141] A. S. More, T. Lebarbé, L. Maisonneuve, B. Gadenne, C. Alfos, H. Cramail, *European Polymer Journal* **2013**, *49*, 823-833
[142] M. Unverferth, O. Kreye, A. Prohammer, M. A. R. Meier, *Macromolecular Rapid Communications* **2013**, *34*, 1569-1574
[143] P. Davies, G. Evrard, *Polymer Degradation and Stability* **2007**, *92*, 1455-1464
[144] S.-T. Hsiao, C.-C. M. Ma, W.-H. Liao, Y.-S. Wang, S.-M. Li, Y.-C. Huang, R.-B. Yang, W.-F. Liang, *ACS Applied Materials & Interfaces* **2014**, *6*, 10667-10678
[145] A. Burke, N. Hasirci, Springer US, Boston, MA, **2004**, pp. 83-101
[146] N. Hasirci, *Ohio Science Workbook-Polymers* **1993**, 38-41
[147] T. J. Johnson, K. M. Gupta, J. Fabian, T. H. Albright, P. F. Kiser, *European Journal of Pharmaceutical Sciences* **2010**, *39*, 203-212
[148] O. Jaudouin, J.-J. Robin, J.-M. Lopez-Cuesta, D. Perrin, C. Imbert, *Polymer International* **2012**, *61*, 495-510
[149] D. Fragiadakis, S. Dou, R. H. Colby, J. Runt, *Macromolecules* **2008**, *41*, 5723-5728
[150] E. A. Ismail, A. M. Motawie, E. M. Sadek, *Egyptian Journal of Petroleum* **2011**, *20*, 1-8
[151] M. Szycher, *Szycher's Handbook of Polyurethanes, CRC: Boca Raton, FL, USA* **1999**
[152] R. Pires, H. J. Laas, *Surface Coatings International Part B: Coatings Transactions* **2002**, *85*, 185-190
[153] M. S. Gaikwad, V. V. Gite, P. P. Mahulikar, D. G. Hundiwale, O. S. Yemul, *Progress in Organic Coatings* **2015**, *86*, 164-172
[154] H.-J. Streitberger, K.-F. Dossel, *Automotive paints and coatings*, John Wiley & Sons, **2008**.
[155] C.-W. Chang, K.-T. Lu, *Journal of Applied Polymer Science* **2010**, *115*, 2197-2202
[156] G.-N. Chen, K.-N. Chen, *Journal of Applied Polymer Science* **1997**, *63*, 1609-1623
[157] J. Zhang, X. Y. Zhang, J. B. Dai, W. H. Li, *Chinese Chemical Letters* **2010**, *21*, 143-145
[158] G. Oertel, L. Abele, *Polyurethane handbook: chemistry, raw materials, processing, application, properties*, **1994**.
[159] N. M. Zain, E. N. Roslin, S. Ahmad, *International Journal of Adhesion and Adhesives* **2016**, *71*, 1-9

[160] A. Kemona, M. Piotrowska, *Polymers* **2020**, *12*, 1752
[161] N. Kanari, J. L. Pineau, S. Shallari, *JOM* **2003**, *55*, 15-19
[162] D. Klempner, K. C. Frisch, G. Prentice, *Advances in Plastics Recycling: Recycling of polyurethanes*, Technomic Publishing Company, **1999**.
[163] J. Scheirs, *John! Wiley & Sons Ltd, Journals, Baffins Lane, Chichester, Sussex PO 19 1 UD, UK, 1998. 591* **1998**
[164] C.-H. Wu, C.-Y. Chang, J.-K. Li, *Polymer Degradation and Stability* **2002**, *75*, 413-421
[165] C.-H. Wu, C.-Y. Chang, C.-M. Cheng, H.-C. Huang, *Polymer Degradation and Stability* **2003**, *80*, 103-111
[166] A. R. Galimzianova, I. N. Bakirova, L. A. Zenitova, *International Polymer Science and Technology* **2002**, *29*, 17-19
[167] L. R. Mahoney, S. A. Weiner, F. C. Ferris, *Environmental Science & Technology* **1974**, *8*, 135-139
[168] J. L. Gerlock, J. Braslaw, L. R. Mahoney, F. C. Ferris, *Journal of Polymer Science: Polymer Chemistry Edition* **1980**, *18*, 541-557
[169] G. A. Campbell, W. C. Meluch, *Environmental Science & Technology* **1976**, *10*, 182-185
[170] E. Weigand, *Recycling and recovery of plastics" Branderup, J., Bittner, M., Menges, G., Micheali, W., Hanser, Münich (Germany)* **1996**
[171] K. Frisch, D. Klempner, G. Prentice, Univ. of Detroit Mercy, MI (US), **1999**
[172] R. P. Lattimer, M. J. Polce, C. Wesdemiotis, *Journal of Analytical and Applied Pyrolysis* **1998**, *48*, 1-15
[173] J.-W. Wu, W.-F. Sung, H.-S. Chu, *International Journal of Heat and Mass Transfer* **1999**, *42*, 2211-2217
[174] R. Font, A. Fullana, J. A. Caballero, J. Candela, A. García, *Journal of Analytical and Applied Pyrolysis* **2001**, *58-59*, 63-77
[175] R. P. Lattimer, R. C. Williams, *Journal of Analytical and Applied Pyrolysis* **2002**, *63*, 85-104
[176] J. Troitzsch, *T/C PUBLIC., P. O. BOX 842, EL SEGUNDO, CA 90245, USA. 1983.* **1983**
[177] C. Branca, C. Di Blasi, A. Casu, V. Morone, C. Costa, *Thermochimica Acta* **2003**, *399*, 127-137
[178] L. Gausas, S. K. Kristensen, H. Sun, A. Ahrens, B. S. Donslund, A. T. Lindhardt, T. Skrydstrup, *JACS Au* **2021**, *1*, 517-524
[179] B. C. Levin, *Fire and Materials* **1987**, *11*, 143-157
[180] K. C. Frisch, J. H. Saunders, *Polyurethanes; Chemistry and Technology*, John Wiley & Sons, **1964**.
[181] V. Istratov, H. Kautz, Y.-K. Kim, R. Schubert, H. Frey, *Tetrahedron* **2003**, *59*, 4017-4024
[182] J. Kemptner, M. Marchetti-Deschmann, J. Siekmann, P. L. Turecek, H. P. Schwarz, G. Allmaier, *Journal of Pharmaceutical and Biomedical Analysis* **2010**, *52*, 432-437
[183] S. Fusco, A. Borzacchiello, P. A. Netti, *Journal of Bioactive and Compatible Polymers* **2006**, *21*, 149-164
[184] F. E. Bailey, J. V. Koleske, *Ullmann's Encyclopedia of Industrial Chemistry* **2000**
[185] S. Carlotti, F. Peruch, in *Anionic Polymerization: Principles, Practice, Strength, Consequences and Applications* (Eds.: N. Hadjichristidis, A. Hirao), Springer Japan, Tokyo, **2015**, pp. 191-305.
[186] A. Wurtz, *Ann. Chim. Phys* **1863**, *55*, 317-355
[187] H. Staudinger, H. Lohmann, *Justus Liebigs Annalen der Chemie* **1933**, *505*, 41-51
[188] P. J. Flory, *Journal of the American Chemical Society* **1940**, *62*, 1561-1565
[189] H. F. Mark, J. I. Kroschwitz, *Encyclopedia of polymer science and engineering*, **1985**.
[190] C. C. Price, *Accounts of Chemical Research* **1974**, *7*, 294-301

[191] C. C. Price, D. D. Carmelite, *Journal of the American Chemical Society* **1966**, *88*, 4039-4044
[192] A. Deffieux, S. Carlotti, A. Barrère, in *Polymer Science: A Comprehensive Reference* (Eds.: K. Matyjaszewski, M. Möller), Elsevier, Amsterdam, **2012**, pp. 117-140.
[193] A. Deffieux, S. Boileau, *Polymer* **1977**, *18*, 1047-1050
[194] A. Stolarzewicz, D. Neugebauer, J. Grobelny, *Macromolecular Rapid Communications* **1996**, *17*, 787-793
[195] A. Stolarzewicz, D. Neugebauer, Z. Grobelny, *Macromolecular Chemistry and Physics* **1995**, *196*, 1295-1300
[196] S. Penczek, M. Cypryk, A. Duda, P. Kubisa, S. Słomkowski, *Progress in Polymer Science* **2007**, *32*, 247-282
[197] R. P. Quirk, *Applications of anionic polymerization research*, ACS Publications, **1998**.
[198] K. B. Wagener, C. Thompson, S. Wanigatunga, *Macromolecules* **1988**, *21*, 2668-2672
[199] S. Matsumura, N. Yoda, S. Yoshikawa, *Die Makromolekulare Chemie, Rapid Communications* **1989**, *10*, 63-67
[200] C. Billouard, S. Carlotti, P. Desbois, A. Deffieux, *Macromolecules* **2004**, *37*, 4038-4043
[201] A. Labbé, S. Carlotti, C. Billouard, P. Desbois, A. Deffieux, *Macromolecules* **2007**, *40*, 7842-7847
[202] A. Deffieux, S. Carlotti, P. Desbois, *Macromolecular Symposia* **2005**, *229*, 24-31
[203] S. Carlotti, P. Desbois, C. Billouard, A. Deffieux, *Polymer International* **2006**, *55*, 1126-1131
[204] M. Gervais, A. Labbé, S. Carlotti, A. Deffieux, *Macromolecules* **2009**, *42*, 2395-2400
[205] K. Sakakibara, K. Nakano, K. Nozaki, *Chemical Communications* **2006**, 3334-3336
[206] K. Roos, S. Carlotti, *European Polymer Journal* **2015**, *70*, 240-246
[207] I. Dimitrov, C. B. Tsvetanov, in *Polymer Science: A Comprehensive Reference* (Eds.: K. Matyjaszewski, M. Möller), Elsevier, Amsterdam, **2012**, pp. 551-569.
[208] R. A. Miller, C. C. Price, *Journal of Polymer Science* **1959**, *34*, 161-163
[209] E. J. Vandenberg, *Journal of Polymer Science* **1960**, *47*, 486-489
[210] M. Osgan, P. Teyssie, *Journal of Polymer Science Part B: Polymer Letters* **1967**, *5*, 789-792
[211] H. L. Hsieh, *Journal of Applied Polymer Science* **1971**, *15*, 2425-2438
[212] P. Kubisa, in *Polymer Science: A Comprehensive Reference* (Eds.: K. Matyjaszewski, M. Möller), Elsevier, Amsterdam, **2012**, pp. 141-164.
[213] S. Kobayashi, K. Morikawa, T. Saegusa, *Polymer Journal* **1979**, *11*, 405-412
[214] R. J. Kern, *The Journal of Organic Chemistry* **1968**, *33*, 388-390
[215] J. Kennedy, **1982**
[216] P. H. Plesch, *The chemistry of cationic polymerization*, Elsevier, **2016**.
[217] P. Kubisa, S. Penczek, *Progress in Polymer Science* **1999**, *24*, 1409-1437
[218] S. Penczek, P. Kubisa, R. Szymański, *Makromolekulare Chemie. Macromolecular Symposia* **1986**, *3*, 203-220
[219] P. Dreyfuss, *Poly (tetrahydrofuran), Vol. 8*, CRC Press, **1982**.
[220] R. Kjellander, E. Florin, *Journal of the Chemical Society, Faraday Transactions 1: Physical Chemistry in Condensed Phases* **1981**, *77*, 2053-2077
[221] C. Fruijtier-Pölloth, *Toxicology* **2005**, *214*, 1-38
[222] R. Klein, F. R. Wurm, *Macromolecular Rapid Communications* **2015**, *36*, 1147-1165
[223] A. E. Hargreaves, **2007**
[224] C. Dingels, M. Schömer, H. Frey, *Chemie in unserer Zeit* **2011**, *45*, 338-349
[225] K. Knop, R. Hoogenboom, D. Fischer, U. S. Schubert, *Angewandte Chemie International Edition* **2010**, *49*, 6288-6308

[226] E. M. Pelegri-O'Day, E.-W. Lin, H. D. Maynard, *Journal of the American Chemical Society* **2014**, *136*, 14323-14332
[227] C. Dingels, H. Frey, in *Hierarchical Macromolecular Structures: 60 Years after the Staudinger Nobel Prize II* (Ed.: V. Percec), Springer International Publishing, Cham, **2013**, pp. 167-190.
[228] S. Dai, K. C. Tam, *Langmuir* **2004**, *20*, 2177-2183
[229] B. Obermeier, F. Wurm, C. Mangold, H. Frey, *Angewandte Chemie International Edition* **2011**, *50*, 7988-7997
[230] Y. Koyama, M. Umehara, A. Mizuno, M. Itaba, T. Yasukouchi, K. Natsume, A. Suginaka, K. Watanabe, *Bioconjugate Chemistry* **1996**, *7*, 298-301
[231] S. N. S. Alconcel, A. S. Baas, H. D. Maynard, *Polymer Chemistry* **2011**, *2*, 1442-1448
[232] V. Rejsek, D. Sauvanier, C. Billouard, P. Desbois, A. Deffieux, S. Carlotti, *Macromolecules* **2007**, *40*, 6510-6514
[233] A. Louai, D. Sarazin, G. Pollet, J. François, F. Moreaux, *Polymer* **1991**, *32*, 703-712
[234] K. Schillén, P. M. Claesson, M. Malmsten, P. Linse, C. Booth, *The Journal of Physical Chemistry B* **1997**, *101*, 4238-4252
[235] J. L. Wolk, M. Sprecher, H. Basch, S. Hoz, *Organic & Biomolecular Chemistry* **2004**, *2*, 1065-1069
[236] G. Pruckmayr, P. Dreyfuss, M. P. Dreyfuss, in *Kirk-Othmer Encyclopedia of Chemical Technology*.
[237] E.-M. Christ, S. S. Müller, E. Berger-Nicoletti, H. Frey, *Journal of Polymer Science Part A: Polymer Chemistry* **2014**, *52*, 2850-2859
[238] L. Garrido, E. Riande, J. Guzmán, *Die Makromolekulare Chemie, Rapid Communications* **1983**, *4*, 725-729
[239] Y. Xia, Y. Wang, Y. Wang, D. Wang, H. Deng, Y. Zhuang, D. Yan, B. Zhu, X. Zhu, *Macromolecular Chemistry and Physics* **2011**, *212*, 1056-1062
[240] A. Williamson, *The London, Edinburgh, and Dublin philosophical magazine and journal of science* **1850**, *37*, 350-356
[241] P. A. Gunatillake, G. F. Meijs, R. C. Chatelier, D. M. McIntosh, E. Rizzardo, *Polymer International* **1992**, *27*, 275-283
[242] S. Zhang, A. Féret, H. Lefebvre, M. Tessier, A. Fradet, *Chemical Communications* **2011**, *47*, 11092-11094
[243] A. Basterretxea, E. Gabirondo, C. Jehanno, H. Zhu, I. Flores, A. J. Müller, A. Etxeberria, D. Mecerreyes, O. Coulembier, H. Sardon, *ACS Sustainable Chemistry & Engineering* **2019**, *7*, 4103-4111
[244] K. B. Wagener, K. Brzezinska, C. G. Bauch, *Die Makromolekulare Chemie, Rapid Communications* **1992**, *13*, 75-81
[245] K. Wagener, K. Brzezinska, *Macromolecules* **1991**, *24*, 5273-5277
[246] H. Mutlu, L. M. de Espinosa, M. A. R. Meier, *Chemical Society Reviews* **2011**, *40*, 1404-1445
[247] M. Firdaus, M. A. R. Meier, U. Biermann, J. O. Metzger, *European Journal of Lipid Science and Technology* **2014**, *116*, 31-36
[248] P.-K. Dannecker, U. Biermann, A. Sink, F. R. Bloesser, J. O. Metzger, M. A. R. Meier, *Macromolecular Chemistry and Physics* **2019**, *220*, 1800440
[249] P.-K. Dannecker, U. Biermann, M. von Czapiewski, J. O. Metzger, M. A. R. Meier, *Angewandte Chemie International Edition* **2018**, *57*, 8775-8779
[250] P. Furtwengler, L. Avérous, *Polymer Chemistry* **2018**, *9*, 4258-4287
[251] H. Sardon, D. Mecerreyes, A. Basterretxea, L. Avérous, C. Jehanno, *ACS Sustainable Chemistry & Engineering* **2021**, *9*, 10664-10677
[252] G. D. Soto, N. E. Marcovich, M. A. Mosiewicki, *Journal of Applied Polymer Science* **2016**, *133*
[253] C. S. Carriço, T. Fraga, V. E. Carvalho, V. M. D. Pasa, *Molecules* **2017**, *22*, 1091
[254] C. S. Carriço, T. Fraga, V. M. D. Pasa, *European Polymer Journal* **2016**, *85*, 53-61

[255] X. Luo, S. Hu, X. Zhang, Y. Li, *Bioresource Technology* **2013**, *139*, 323-329
[256] T. Calvo-Correas, M. A. Mosiewicki, M. A. Corcuera, A. Eceiza, M. I. Aranguren, *Journal of Renewable Materials* **2015**, *3*, 3-13
[257] N. Čuk, E. Fabjan, P. Grželj, M. Kunaver, *Journal of Applied Polymer Science* **2015**, *132*
[258] V. Ribeiro da Silva, M. A. Mosiewicki, M. I. Yoshida, M. Coelho da Silva, P. M. Stefani, N. E. Marcovich, *Polymer Testing* **2013**, *32*, 665-672
[259] S. Chuayjuljit, A. Maungchareon, O. Saravari, *Journal of Reinforced Plastics and Composites* **2010**, *29*, 218-225
[260] S. Chuayjuljit, T. Sangpakdee, O. Saravari, *Journal of Metals, Materials and Minerals* **2017**, *17*2021/11/25.
[261] K. H. Badri, S. H. Ahmad, S. Zakaria, *Journal of Applied Polymer Science* **2001**, *82*, 827-832
[262] C. Pavier, A. Gandini, *Industrial Crops and Products* **2000**, *12*, 1-8
[263] C. Pavier, A. Gandini, *Carbohydrate Polymers* **2000**, *42*, 13-17
[264] J. Herzberger, K. Niederer, H. Pohlit, J. Seiwert, M. Worm, F. R. Wurm, H. Frey, *Chemical Reviews* **2016**, *116*, 2170-2243
[265] R. H. Carr, J. Hernalsteen, J. Devos, *Journal of Applied Polymer Science* **1994**, *52*, 1015-1022
[266] B. Rieger, A. Künkel, G. W. Coates, R. Reichardt, E. Dinjus, T. A. Zevaco, *Synthetic biodegradable polymers, Vol. 245*, Springer Science & Business Media, **2012**.
[267] M. Bednarek, *Progress in Polymer Science* **2016**, *58*, 27-58
[268] C. L. Wilson, C. J. Benning, *US2863855A* **1958**
[269] C. A. McAdams, S. Farmer, *Journal of Cellular Plastics* **2003**, *39*, 369-386
[270] C. H. Smith, *I&EC Product Research and Development* **1963**, *2*, 27-31
[271] J. Liszkowska, *Polymer Bulletin* **2017**, *74*, 283-305
[272] P. Furtwengler, R. Perrin, A. Redl, L. Avérous, *European Polymer Journal* **2017**, *97*, 319-327
[273] F. Hostettler, D. M. Young, *US3169945A* **1965**
[274] F. Hostettler, D. M. Young, *US3186971A* **1965**
[275] S. S. Narine, X. Kong, L. Bouzidi, P. Sporns, *Journal of the American Oil Chemists' Society* **2007**, *84*, 65-72
[276] Z. S. Petrović, W. Zhang, I. Javni, *Biomacromolecules* **2005**, *6*, 713-719
[277] M. Zieleniewska, M. K. Leszczyński, M. Kurańska, A. Prociak, L. Szczepkowski, M. Krzyżowska, J. Ryszkowska, *Industrial Crops and Products* **2015**, *74*, 887-897
[278] U. Stirna, A. Fridrihsone, B. Lazdiņa, M. Misāne, D. Vilsone, *Journal of Polymers and the Environment* **2013**, *21*, 952-962
[279] A. A. Septevani, D. A. C. Evans, C. Chaleat, D. J. Martin, P. K. Annamalai, *Industrial Crops and Products* **2015**, *66*, 16-26
[280] M. F. Sonnenschein, B. L. Wendt, *Polymer* **2013**, *54*, 2511-2520
[281] D. Ji, Z. Fang, Z. D. Wan, H. C. Chen, W. He, X. L. Li, K. Guo, *Advanced Materials Research* **2013**, *724-725*, 1681-1684
[282] D. S. Ogunniyi, *Bioresource Technology* **2006**, *97*, 1086-1091
[283] M. Ionescu, D. Radojčić, X. Wan, M. L. Shrestha, Z. S. Petrović, T. A. Upshaw, *European Polymer Journal* **2016**, *84*, 736-749
[284] Q. F. Li, Y. L. Feng, J. W. Wang, N. Yin, Y. H. Zhao, M. Q. Kang, X. W. Wang, *Plastics, Rubber and Composites* **2016**, *45*, 16-21
[285] G. Tibério Cardoso, S. Claro Neto, F. Vecchia, *Frontiers of Architectural Research* **2012**, *1*, 348-356
[286] M. Zhang, H. Pan, L. Zhang, L. Hu, Y. Zhou, *Industrial Crops and Products* **2014**, *59*, 135-143
[287] L. Zhang, M. Zhang, L. Hu, Y. Zhou, *Industrial Crops and Products* **2014**, *52*, 380-388
[288] C. Liu, Y. Long, J. Xie, X. Xie, *Polymer* **2017**, *116*, 240-250

[289] W. S. Ng, C. S. Lee, C. H. Chuah, S.-F. Cheng, *Industrial Crops and Products* **2017**, *97*, 65-78
[290] X. Zhou, M. M. Sain, K. Oksman, *Composites Part A: Applied Science and Manufacturing* **2016**, *83*, 56-62
[291] P. K. S. Pillai, S. Li, L. Bouzidi, S. S. Narine, *Industrial Crops and Products* **2016**, *83*, 568-576
[292] R. Tanaka, S. Hirose, H. Hatakeyama, *Bioresource Technology* **2008**, *99*, 3810-3816
[293] N. E. Marcovich, M. Kurańska, A. Prociak, E. Malewska, K. Kulpa, *Industrial Crops and Products* **2017**, *102*, 88-96
[294] M. S. Pawar, A. S. Kadam, B. S. Dawane, O. S. Yemul, *Polymer Bulletin* **2016**, *73*, 727-741
[295] Z. S. Petrović, X. Wan, O. Bilić, A. Zlatanić, J. Hong, I. Javni, M. Ionescu, J. Milić, D. Degruson, *Journal of the American Oil Chemists' Society* **2013**, *90*, 1073-1078
[296] A. Arbenz, R. Perrin, L. Avérous, *Journal of Polymers and the Environment* **2018**, *26*, 254-262
[297] P. Kosmela, P. Kazimierski, K. Formela, J. Haponiuk, Ł. Piszczyk, *Journal of Industrial and Engineering Chemistry* **2017**, *56*, 399-406
[298] A. Palanisamy, M. S. L. Karuna, T. Satyavani, D. B. Rohini Kumar, *Journal of the American Oil Chemists' Society* **2011**, *88*, 541-549
[299] M. Himabindu, K. Kamalakar, M. Karuna, A. Palanisamy, *Journal of Renewable Materials* **2017**, *5*, 124--131
[300] A. Paruzel, S. Michałowski, J. Hodan, P. Horák, A. Prociak, H. Beneš, *ACS Sustainable Chemistry & Engineering* **2017**, *5*, 6237-6246
[301] M. S. Pawar, A. S. Kadam, P. C. Singh, V. V. Kusumkar, O. S. Yemul, *Iranian Polymer Journal* **2016**, *25*, 59-68
[302] R. K. Gupta, M. Ionescu, D. Radojcic, X. Wan, Z. S. Petrovic, *Journal of Polymers and the Environment* **2014**, *22*, 304-309
[303] N. Elbers, C.-K. Ranaweera, M. Ionescu, X. Wan, P.-K. Kahol, R.-K. Gupta, *Journal of Renewable Materials* **2017**, *5*, 74--83
[304] J. D'Souza, R. Camargo, N. Yan, *Polymer Reviews* **2017**, *57*, 668-694
[305] S. Hu, X. Luo, Y. Li, *ChemSusChem* **2014**, *7*, 66-72
[306] L.-L. Gao, Y.-H. Liu, H. Lei, H. Peng, R. Ruan, *Journal of Applied Polymer Science* **2010**, *116*, 1694-1699
[307] S.-H. Lee, Y. Teramoto, N. Shiraishi, *Journal of Applied Polymer Science* **2002**, *83*, 1482-1489
[308] S.-H. Lee, M. Yoshioka, N. Shiraishi, *Journal of Applied Polymer Science* **2000**, *78*, 319-325
[309] Z.-Q. Zheng, Y. Liu, D. Li, L. j. Wang, B. Adhikari, X. D. Chen, *International Journal of Food Engineering* **2017**, *13*
[310] D. Yue, O. Oribayo, Garry L. Rempel, Q. Pan, *RSC Advances* **2017**, *7*, 30334-30344
[311] G. Huang, P. Wang, *Polymer Testing* **2017**, *60*, 266-273
[312] J. Ge, W. Zhong, Z. Guo, W. Li, K. Sakai, *Journal of Applied Polymer Science* **2000**, *77*, 2575-2580
[313] L. Lin, M. Yoshioka, Y. Yao, N. Shiraishi, *Journal of Applied Polymer Science* **1994**, *52*, 1629-1636
[314] M. H. Alma, M. Yoshioka, Y. Yao, N. Shiraishi, **1996**, *50*, 85-90
[315] M. C. Basso, A. Pizzi, C. Lacoste, L. Delmotte, F. M. Al-Marzouki, S. Abdalla, A. Celzard, *Polymers* **2014**, *6*, 2985-3004
[316] J. Ge, X. Shi, M. Cai, R. Wu, M. Wang, *Journal of Applied Polymer Science* **2003**, *90*, 2756-2763
[317] A. Arshanitsa, L. Vevere, G. Telysheva, T. Dizhbite, R. J. A. Gosselink, O. Bikovens, A. Jablonski, *Holzforschung* **2015**, *69*, 785-793
[318] L. C.-F. Wu, W. G. Glasser, *Journal of Applied Polymer Science* **1984**, *29*, 1111-1123

[319] C. A. Cateto, M. F. Barreiro, A. E. Rodrigues, M. N. Belgacem, *Industrial & Engineering Chemistry Research* **2009**, *48*, 2583-2589
[320] A. Arbenz, A. Frache, F. Cuttica, L. Avérous, *Polymer Degradation and Stability* **2016**, *132*, 62-68
[321] A. Arbenz, L. Avérous, *RSC Advances* **2014**, *4*, 61564-61572
[322] C. A. Cateto, M. F. Barreiro, C. Ottati, M. Lopretti, A. E. Rodrigues, M. N. Belgacem, *Journal of Cellular Plastics* **2014**, *50*, 81-95
[323] H. Nadji, C. Bruzzèse, M. N. Belgacem, A. Benaboura, A. Gandini, *Macromolecular Materials and Engineering* **2005**, *290*, 1009-1016
[324] J. Datta, P. Kopczyńska, *Critical Reviews in Environmental Science and Technology* **2016**, *46*, 905-946
[325] D. E. Nikles, M. S. Farahat, *Macromolecular Materials and Engineering* **2005**, *290*, 13-30
[326] N. George, T. Kurian, *Industrial & Engineering Chemistry Research* **2014**, *53*, 14185-14198
[327] U. R. Vaidya, V. M. Nadkarni, *Journal of Applied Polymer Science* **1988**, *35*, 775-785
[328] *Statistica* **2022**, https://www.statista.com/statistics/1245264/polyethylene-terephthalate-market-volume-worldwide/ 21-01-2022.
[329] *Coca Cola* **2022**, https://www.coca-colacompany.com/news/100-percent-plant-based-plastic-bottle 20-01-2022.
[330] D. I. Collias, A. M. Harris, V. Nagpal, I. W. Cottrell, M. W. Schultheis, *Industrial Biotechnology* **2014**, *10*, 91-105
[331] *C&EN Global Enterprise* **2018**, *96*, 16-16
[332] A. J. J. E. Eerhart, A. P. C. Faaij, M. K. Patel, *Energy & Environmental Science* **2012**, *5*, 6407-6422
[333] J. J. Bozell, G. R. Petersen, *Green Chemistry* **2010**, *12*, 539-554
[334] A. A. Rosatella, S. P. Simeonov, R. F. M. Frade, C. A. M. Afonso, *Green Chemistry* **2011**, *13*, 754-793
[335] S. K. Burgess, J. E. Leisen, B. E. Kraftschik, C. R. Mubarak, R. M. Kriegel, W. J. Koros, *Macromolecules* **2014**, *47*, 1383-1391
[336] Y. Román-Leshkov, J. N. Chheda, J. A. Dumesic, *Science* **2006**, *312*, 1933-1937
[337] G. J. M. Gruter, F. Dautzenberg, *US20110082304A1* **2011**
[338] *Avantium* **2022**, https://www.avantium.com/technologies/ 20-01-2022.
[339] W. Partenheimer, V. V. Grushin, *Advanced Synthesis & Catalysis* **2001**, *343*, 102-111
[340] X. Han, L. Geng, Y. Guo, R. Jia, X. Liu, Y. Zhang, Y. Wang, *Green Chemistry* **2016**, *18*, 1597-1604
[341] X. Han, C. Li, Y. Guo, X. Liu, Y. Zhang, Y. Wang, *Applied Catalysis A: General* **2016**, *526*, 1-8
[342] F. Wang, Z. Yuan, B. Liu, S. Chen, Z. Zhang, *Journal of Industrial and Engineering Chemistry* **2016**, *38*, 181-185
[343] N. K. Gupta, S. Nishimura, A. Takagaki, K. Ebitani, *Green Chemistry* **2011**, *13*, 824-827
[344] S. Albonetti, A. Lolli, V. Morandi, A. Migliori, C. Lucarelli, F. Cavani, *Applied Catalysis B: Environmental* **2015**, *163*, 520-530
[345] W. P. Dijkman, D. E. Groothuis, M. W. Fraaije, *Angewandte Chemie International Edition* **2014**, *53*, 6515-6518
[346] S. M. McKenna, S. Leimkühler, S. Herter, N. J. Turner, A. J. Carnell, *Green Chemistry* **2015**, *17*, 3271-3275
[347] T. Pan, J. Deng, Q. Xu, Y. Zuo, Q.-X. Guo, Y. Fu, *ChemSusChem* **2013**, *6*, 47-50
[348] A. Banerjee, G. R. Dick, T. Yoshino, M. W. Kanan, *Nature* **2016**, *531*, 215-219
[349] J.-G. Wang, X.-Q. Liu, J. Zhu, *Chinese Journal of Polymer Science* **2018**, *36*, 720-727

[350] G. Xu, A. Wang, J. Pang, X. Zhao, J. Xu, N. Lei, J. Wang, M. Zheng, J. Yin, T. Zhang, *ChemSusChem* **2017**, *10*, 1390-1394
[351] P. P. Van Uytvanck, B. Hallmark, G. Haire, P. J. Marshall, J. S. Dennis, *ACS Sustainable Chemistry & Engineering* **2014**, *2*, 1098-1105
[352] J. A. Moore, J. E. Kelly, *Macromolecules* **1978**, *11*, 568-573
[353] J.-G. Rosenboom, D. K. Hohl, P. Fleckenstein, G. Storti, M. Morbidelli, *Nature Communications* **2018**, *9*, 2701
[354] E. Gubbels, L. Jasinska-Walc, B. A. J. Noordover, C. E. Koning, *European Polymer Journal* **2013**, *49*, 3188-3198
[355] E. de Jong, M. A. Dam, L. Sipos, G. J. M. Gruter, in *Biobased Monomers, Polymers, and Materials, Vol. 1105*, American Chemical Society, **2012**, pp. 1-13.
[356] M. G. Gert-Jan, S. Laszlo, D. Matheus Adrianus, *Combinatorial Chemistry & High Throughput Screening* **2012**, *15*, 180-188
[357] Z. Terzopoulou, E. Karakatsianopoulou, N. Kasmi, V. Tsanaktsis, N. Nikolaidis, M. Kostoglou, G. Z. Papageorgiou, D. A. Lambropoulou, D. N. Bikiaris, *Polymer Chemistry* **2017**, *8*, 6895-6908
[358] J. Zhu, J. Cai, W. Xie, P.-H. Chen, M. Gazzano, M. Scandola, R. A. Gross, *Macromolecules* **2013**, *46*, 796-804
[359] Y. Zhu, C. Romain, C. K. Williams, *Nature* **2016**, *540*, 354-362
[360] A. Pellis, K. Haernvall, C. M. Pichler, G. Ghazaryan, R. Breinbauer, G. M. Guebitz, *Journal of Biotechnology* **2016**, *235*, 47-53
[361] R. J. I. Knoop, W. Vogelzang, J. van Haveren, D. S. van Es, *Journal of Polymer Science Part A: Polymer Chemistry* **2013**, *51*, 4191-4199
[362] F. W. Gomes, R. C. Lima, C. R. Piombini, J. F. Sinfitele Jr., F. G. de Souza Jr., P. L. A. Coutinho, J. C. Pinto, *Macromolecular Symposia* **2018**, *381*, 1800129
[363] A. L.T. Brandão, B. F. Oechsler, F. W. Gomes, F. G. Souza Jr., J. Carlos Pinto, *Polymer Engineering & Science* **2018**, *58*, 729-741
[364] S. K. Burgess, R. M. Kriegel, W. J. Koros, *Macromolecules* **2015**, *48*, 2184-2193
[365] S. Burgess, O. Karvan, J. R. Johnson, R. Kriegel, W. Koros, *Polymer* **2014**, *55*, 4748-4756
[366] G. R. Pettit, D. M. Piatak, *The Journal of Organic Chemistry* **1962**, *27*, 2127-2130
[367] G. R. PETTIT, T. Kasturi, *The Journal of Organic Chemistry* **1961**, *26*, 4553-4556
[368] G. Pettit, U. Ghatak, B. Green, T. Kasturi, D. Piatak, *The Journal of Organic Chemistry* **1961**, *26*, 1685-1686
[369] G. Pettit, T. Kasturi, *The Journal of Organic Chemistry* **1960**, *25*, 875-876
[370] R. Nakao, T. Fukumoto, J. Tsurugi, *Journal of Organic Chemistry* **1972**, *37*, 4349-4352
[371] J. Tsurugi, R. Nakao, T. Fukumoto, *Journal of the American Chemical Society* **1969**, *91*, 4587-4588
[372] J. Tsurugi, R. Nakao, T. Fukumoto, *The Journal of Organic Chemistry* **1972**, *37*, 76-78
[373] S. W. Baldwin, S. A. Haut, *The Journal of Organic Chemistry* **1975**, *40*, 3885-3887
[374] Z. Mao, B. T. Gregg, A. R. Cutler, *Journal of the American Chemical Society* **1995**, *117*, 10139-10140
[375] K. Matsubara, T. Iura, T. Maki, H. Nagashima, *The Journal of Organic Chemistry* **2002**, *67*, 4985-4988
[376] S. Hanada, T. Ishida, Y. Motoyama, H. Nagashima, *The Journal of Organic Chemistry* **2007**, *72*, 7551-7559
[377] K. J. Barr, S. C. Berk, S. L. Buchwald, *The Journal of Organic Chemistry* **1994**, *59*, 4323-4326
[378] S. C. Berk, S. L. Buchwald, *The Journal of Organic Chemistry* **1992**, *57*, 3751-3753
[379] S. C. Berk, K. A. Kreutzer, S. L. Buchwald, *Journal of the American Chemical Society* **1991**, *113*, 5093-5095

[380] T. Ohta, M. Kamiya, K. Kusui, T. Michibata, M. Nobutomo, I. Furukawa, *Tetrahedron Letters* **1999**, *40*, 6963-6966
[381] K. Miura, M. Tomita, Y. Yamada, A. Hosomi, *The Journal of Organic Chemistry* **2007**, *72*, 787-792
[382] M. Yasuda, Y. Onishi, M. Ueba, T. Miyai, A. Baba, *The Journal of Organic Chemistry* **2001**, *66*, 7741-7744
[383] T. Miyai, M. Ueba, A. Baba, *Synlett* **1999**, *1999*, 182-184
[384] K. Miura, Y. Yamada, M. Tomita, A. Hosomi, *ChemInform* **2005**, *36*
[385] I. Shibata, H. Kato, T. Ishida, M. Yasuda, A. Baba, *Angewandte Chemie International Edition* **2004**, *43*, 711-714
[386] N. Sakai, M. Hirasawa, T. Konakahara, *Tetrahedron Letters* **2005**, *46*, 6407-6409
[387] H. Nagashima, *Synlett* **2015**, *26*, 866-890
[388] N. Sakai, T. Moriya, T. Konakahara, *The Journal of Organic Chemistry* **2007**, *72*, 5920-5922
[389] U. Biermann, J. O. Metzger, *ChemSusChem* **2014**, *7*, 644-649
[390] U. Biermann, J. O. Metzger, *European Journal of Lipid Science and Technology* **2014**, *116*, 74-79
[391] J. Pesti, G. L. Larson, *Organic Process Research & Development* **2016**, *20*, 1164-1181
[392] A. Gandini, A. J. D. Silvestre, C. P. Neto, A. F. Sousa, M. Gomes, *Journal of Polymer Science Part A: Polymer Chemistry* **2009**, *47*, 295-298
[393] A. Todorovic, K. Resch-Fauster, A. R. Mahendran, G. Oreski, W. Kern, *Journal of Applied Polymer Science* **2021**, *138*, 50239
[394] M. A. Meyers, K. K. Chawla, *Mechanical behavior of materials*, Cambridge university press, **2008**.
[395] Y. Ecochard, R. Auvergne, B. Boutevin, S. Caillol, *European Journal of Lipid Science and Technology* **2020**, *122*, 1900145
[396] P. J. Flory, *Polymer Journal* **1985**, *17*, 1-12
[397] T. Gruendling, M. Guilhaus, C. Barner-Kowollik, *Analytical Chemistry* **2008**, *80*, 6915-6927